Potassium homeostasis during intracellular *Chlamydia* development

Susan C Andrew

Institute of Structural and Molecular Biology

University College London

A thesis submitted for the degree of Doctor of Philosophy

February 2014

Declaration

I, Susan Andrew, confirm that the work presented in this thesis is my own. Where information has derived from other sources, I confirm that this has been indicated in the thesis.

Abstract

Chlamydia trachomatis is an obligate intracellular bacterium, which is the leading cause of acquired blindness and the most prevalent bacterial sexually transmitted infection worldwide. *Chlamydiae* exist in two distinct forms. The infectious spore-like elementary bodies (EBs) that invade host cells differentiate into non-infectious reticulate bodies (RBs) that replicate intracellularly within a modified membrane-bound vacuole called the inclusion. Under stress, *Chlamydiae* can enter a persistent state, in which aberrant bodies (ABs) with reduced metabolic activity are formed. Surprisingly little is known about the mechanisms employed by the bacteria to maintain and manipulate their environment within host cells. This thesis investigates the role of inorganic ions in sustaining the inclusion throughout the *Chlamydia* infection cycle.

Potassium starvation of intracellular RBs either after specific ionophore treatment or inhibition of inward rectifying cellular potassium channels induced the formation of ABs, which no longer differentiated into infectious EBs. These data demonstrate an essential role for potassium during *C.trachomatis* replication. Analysis of live RBs, using a potassium sensitive fluorescent probe, illustrated that potassium is actively scavenged from the host cell. Furthermore, when bacteria undergo RB-EB differentiation accumulated potassium is released prior to inclusion lysis. Experimentally reducing potassium ion concentration at this stage caused cells to expel bacteria in bursts. This event is distinct from previously described extrusion mechanisms, where either the inclusion is released intact or the host cell is lysed.

These data show that RBs actively accumulate potassium during replication, with starvation leading to persistence. Loss of potassium ions during re-differentiation into EBs suggests that potassium efflux has a role in triggering inclusion lysis or bacteria exit from the host cell.

Supporting Information

Publications in preparation:

- Susan Andrew, Navin Kumar, Maud Dumoux, Maria O'Donovan, Christopher Carne, Hamid Jalal, and Richard D Hayward. *Analysing interactions between* Chlamydia trachomatis *and human spermatozoa*
  For submission to The Lancet Infectious Diseases
- Susan Andrew, Maud Dumoux, and Richard D Hayward. *Potassium homeostasis during intracellular* Chlamydia *development*

Presentations

- **Health Protection Agency (HPA) Clinical microbiology Department, Addenbrooke's Hospital January 2011**
  Talk title: *Male Factor Infertility: a role for* Chlamydia trachomatis
- **Society for General Microbiology (SGM) Spring conference 2011**
  Poster title: *Analysing interactions between* Chlamydia trachomatis *and human spermatozoa*
- **Institute of Structural and Molecular Biology Friday Wrap November 2011**
  Talk title: *Up close and personal: analysing interactions between* Chlamydia *and sperm*
- **MRC Laboratory for Molecular Cell Biology November 2012**
  Talk title: *You are what you eat: host ion scavenging by intracellular* Chlamydia trachomatis.
- **Institute of Structural and Molecular Biology Graduate Symposium 2012**
  Talk title: *You are what you eat: host ion scavenging by intracellular* Chlamydia trachomatis.
- **Wellcome Trust Sanger Institute April 2013**
  Talk title: *Host ion scavenging by intracellular* Chlamydia trachomatis.

Prizes

- **UCL Graduate School Research Poster Competition 2012/13**
  Runner up: Brain Sciences & Life Sciences.
  Poster title: *You are what you eat: host ion scavenging by intracellular* Chlamydia trachomatis.

Conference Attendance

- **Society for General Microbiology (SGM) Spring conference 2011 (Harrogate, UK)**
- **Chlamydia Basic Research Society biennial meeting 2013 (San Antonio, TX, USA)**

Acknowledgements

First and foremost I'd like to thank my supervisor, Richard Hayward, for giving me this opportunity and allowing me to follow my instincts on this project. The support, encouragement, and forbearance was greatly appreciated.

My sincerest thanks to Jane Nicklin, for acting as my secondary supervisor, and for so much more throughout my PhD. You went above and beyond for me, and I am so very grateful.

My thanks also go to Maud Dumoux, for providing support, inspiration, and pep talks. I really don't think I would have made it to this point without you. My thanks also to the rest of the Hayward group for their friendship, support, and cups of tea.

I wish to thank Anselm Zdebik at the Royal Free Hospital for allowing me to use his flame photometer.

I would like to thank Mark Turmaine, at UCL, for his help with preparing and imaging EM samples. My thanks also to Helen Saibil and her research group, at the ISMB department of crystallography, for use of the EM suite and help along the way.

I would like to offer my profound gratitude to the BBSRC for funding my research.

I would also like to thank David Walker at the University of Exeter, for his help, guidance, and encouragement throughout my PhD.

My thanks are also due to Chris Holmes, for the generous loan of his MacBook for longer than anyone expected, and for his trust in my ability to look after it!

No one warned me how much moral support a PhD requires. The highs and lows demand that you have a network of people experiencing the same rollercoaster to celebrate with when the data is good, scream at when you've done the same protocol 5 times without success, and drink with at the end of a long week. I am fully aware that I owe my sanity to the support of the people of the 6th floor, but especially to Marta Wojnowska, Louise Gavigan, and Tom Hinson. To Tori, for 11pm dinners and a shoulder to cry on, and to Chris, for lab dates and late night bus company, you have my eternal love and gratitude but I hope you already knew that!

Last, but not least, to that motley crew I call a family. For those that saw me through, and those that aren't here to see the end, this was for you.

Table of Contents

Table of Figures

Chapter 1

Chapter 2

Chapter 3

Chapter 4

Chapter 5

Table of Tables

Chapter 1

Chapter 2

Chapter 3

Chapter 4

List of Abbreviations

AB	aberrent body
AM ester	acetoxymethyl ester
APG-2	Asante potassium green-2
Arp	actin recruitment protein
ATCC	American Type Culture Collection
ATP	adenosine triphosphate
BCECF-AM	2',7'-bis(2-carboxyethyl)-5,6-carboxyfluorescein acetoxymethyl ester
bp	base pair
BSA	bovine serum albumin
Ca^{2+}	calcium ions
CFDA	carboxy fluorescein diacetate
cHSP60	60kDa chlamydial heat shock protein
Cl^-I	chloride ionophore I
COMC	chlamydial outer membrane complex
CPAF	chlamydial protease-like activity factor
CT	*C.trachomatis*
DAMPs	damage-related molecular pattern molecules
DAPI	4',6-diamidine-2'-phenylindole
DMEM	Dulbecco's modified eagle medium
DMEM-PR	Dulbecco's modified eagle medium without phenol red
DMSO	dimethyl sulphoxide
DRAQ-5	1,5-bis{[2-(di-methylamino)ethyl]amino}-4,8-dihydroxyanthracene-9, 10-dione
DTT	dithiothreitol
EB	elementary body
EDTA	ethylenediaminetetraacetic acid
EMS	ethyl methanesulphonate
ER	endoplasmic reticulum
FBS	decomplemented fetal bovine serum
FITC	fluorescein isothiocyanate
FOV	field of view
FRAP	fluorescence recovery after photobleaching
GCIP	grap2 cyclin D-interacting protein
GFP	green fluorescent protein
GTPases	guanosine 5'-triphosphotases
H^+	hydrogen ions
HBSS	Hank's balanced salt solution
HF-12	Ham F-12 nutrient mix

Hoechst	bisbenzimide H 33342 trihydrochloride
hpi	hours post infection
IFN- γ	interferon-γ
IFs	intermediate filaments
IFU	inclusion forming unit
IgG	Immunoglobulin G
K^+	potassium ions
K_{ir}	inwardly rectifying K^+ channels
LAMP	lysosome-associated membrane protein
LGV	lymphogranuloma venereum
LPS	lipopolysaccharide
MOI	multiplicity of infection (per cell)
MOMP	major outer membrane protein
MTOC	microtubule organising centre
MVB	multivesicular bodies
MYPT1	myosin phosphatase target subunit 1
N-WASP	neuronal Wiskott-Aldrich syndrome protein
Na^+	sodium ions
NAATs	nucleic acid amplification tests
NF-κB	nuclear factor-κB
NO_2^-	nitrite ions
Omp	outer membrane protein
ORF	open reading frame
PBFI	potassium binding benzofuran isophthalate
PBS	phosphate buffered saline
PCR	polymerase chain reaction
PFA	paraformaldehyde
PID	pelvic inflammatory disease
PLT	psittacosis-lymphogranuloma venereum-trachoma
Pmps	polymorphic membrane proteins
PRRs	pathogen recognition receptors
RB	reticulate body
RNA	ribonucleic acid
ROI	region of interest
RT	room temperature
SBFI	sodium binding benzofuran isophthalate
SNARE	soluble NSF attachment protein receptor
SPG	sucrose-phosphate-glutamic acid buffer
STI	sexually transmitted infection
SUR	sulphonylurea receptor

T2SS	type II secretion system
T3SS	type III secretion system
TARP	translocated actin recruitment protein
TRIC	trachoma and inclusion conjunctivitis
Tris	tris(hydroxymethyl)aminomethane
U	units
WGA	wheat germ agglutinin AlexaFluor® 594 conjugate
WHO	World Health Organisation

Chapter 1 – Introduction

1.1 Taxonomy

The *Chlamydiaceae* are a family of obligate intracellular bacterial pathogens. The *Chlamydiaceae* share a biphasic developmental cycle that occurs within a unique membrane bound compartment, termed an inclusion, within host cells. First described in 1907 by Halberstaedter and von Prowazek the *Chlamydiaceae* historically comprised a single genus, divided into two species. Bacteria that produced uniformly round inclusions that contained electron dense glycogen, which were known as trachoma and inclusion conjunctivitis (TRIC), were termed *Chlamydia trachomatis*. Bacteria from the species known as psittacosis-lymphogranuloma venereum-trachoma (PLT), which inhabit irregular inclusions that do not contain glycogen, were termed *Chlamydia psittaci* (Gordon and Quan, 1965). Initially the *Chlamydiaceae* were classified as viruses, however as understanding of the developmental cycle progressed, it became apparent that these organisms appeared more like bacteria. For example, cell envelopes were comparable in structure to Gram-negative bacteria (Moulder, 1966), and they reproduce by binary fission, unlike viruses (Higashi, 1965; Moulder, 1966). The *Chlamydiaceae* were then reclassified to the kingdom bacteria.

Phylogenetic comparison of 16S rRNA divided the family *Chlamydiaceae* into two genera (**Figure 1.1**). The *Chlamydia* genus contains all species previously classified as *C.trachomatis*, and the *Chlamydophila* genus contains all *C.psittaci* species (Everett *et al.*, 1999; Bush and Everett, 2001). However this new classification remains controversial. Stephens *et al.* (2009) suggest that the genus demarcation is arbitrary due to the fact that the 16S rRNA homology between the proposed *Chlamydia* and

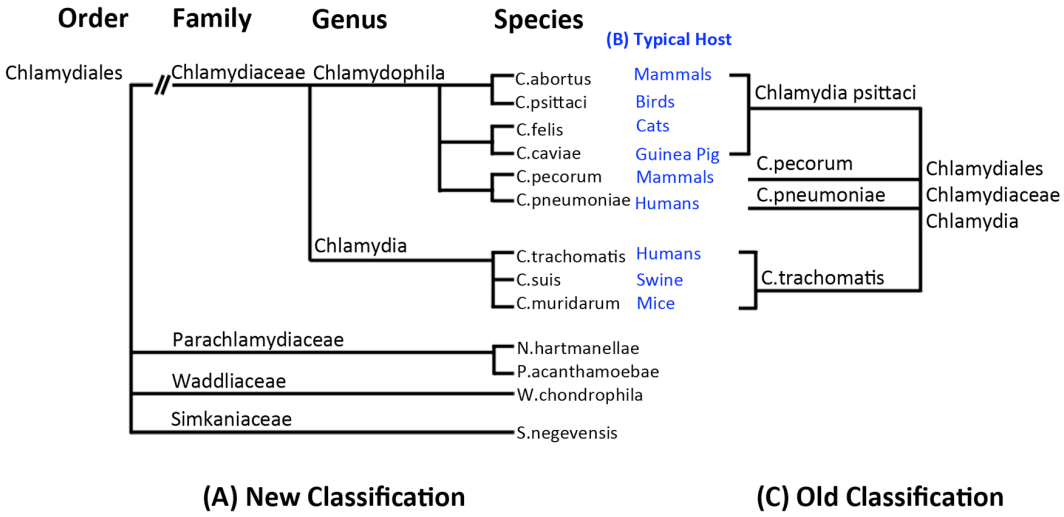
Order
Family
Genus
Species
(B) Typical Host
Chlamydiales
Chlamydiaceae
Chlamydophila
C.abortus
Mammals
C.psittaci
Birds
C.felis
Cats
C.caviae
Guinea Pig
C.pecorum
Mammals
C.pneumoniae
Humans
Chlamydia
C.trachomatis
Humans
C.suis
Swine
C.muridarum
Mice
Parachlamydiaceae
N.hartmanellae
P.acanthamoebae
Waddliaceae
W.chondrophila
Simkaniaceae
S.negevensis
Chlamydia psittaci
C.pecorum
C.pneumoniae
C.trachomatis
Chlamydiales
Chlamydiaceae
Chlamydia
(A) New Classification
(C) Old Classification

Figure 1.1. Bush and Everett taxonomic structure of the order *Chlamydiales*. Adapted from Bush and Everett, 1999. (A) Historical taxonomy including TRIC (*C.trachomatis*) and PLT (*C.psittaci*) pathogens. (B) Typical hosts for *Chlamydiaceae* species. (C) Everett *et al. Chlamydiales* taxonomy.

Chlamydophila genera is 96%, which is the same as homology between both *C.felis* and *C.pecorum,* and *C.pecorum* and *C.pneumoniae*, which are not allocated to separate genera. This viewpoint led them to propose a simplified single genus, multiple species phylogenetic structure (**Figure 1.2**). Like the Everett *et al.* (1999) classification, this single genus phylogeny has yet to be universally accepted, and the current literature remains divided. For the purpose of this introduction the Everett *et al.* (1999) classification system, as depicted in **Figure 1.1**, will be used, as it is the current taxonomic structure of the *Chlamydiales* published in the second edition of *Bergey's Manual of Systematic Bacteriology* (Corsaro *et al.*, 2003).

1.2 Genomics

The *Chlamydiaceae* present a considerable challenge to researchers due to several technical limitations. Firstly, owing to the obligate intracellular nature of the *Chlamydiaceae*, the bacteria must be propagated using suitable cultured eukaryotic cells. HeLa and McCoy cell lines are traditionally used, however these do not perfectly represent the polarised epithelia the bacteria would encounter under physiological conditions (Dautry-Varsat *et al*., 2005), which must be taken into account when interpreting experimental results. Secondly, *Chlamydiae* are intractable to traditional methods of genetic manipulation, such as deletion or inactivation of genes, therefore mutated strains are difficult to obtain. Clinical strains containing natural mutations have been successfully isolated, and subsequent characterisation has provided useful insight into the chlamydial lifecycle. For example, non-fusogenic *C.trachomatis*

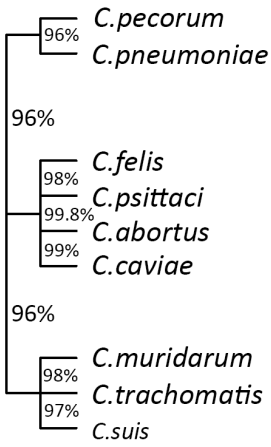
C.pecorum
96%
C.pneumoniae
96%
C.felis
98%
C.psittaci
99.8%
C.abortus
99%
C.caviae
96%
C.muridarum
98%
C.trachomatis
97%
C.suis

Figure 1.2. *Chlamydia* species tree showing percentage homology between 16S rRNA genes. Adapted from Bush *et al.,* 2009.

variants, *i.e.* bacteria that remained in multiple individual inclusions within a host cell, had a variety of mutations within the *IncA* gene (Suchland *et al.,* 2000; Geisler *et al.,* 2001), demonstrating a role for the IncA inclusion protein in vesicle fusion. Transformation of *C.trachomatis* has been demonstrated using shuttle vectors, based on the *C.trachomatis* LGV2 plasmid and *Escherichia coli* plasmid pBR325. This was verified by the production of bacteria expressing green fluorescent protein (GFP) (Wang *et al.,* 2011; Ding *et al.,* 2013; Bauler and Hackstadt, 2014). Chemical mutagenesis, using mutagens such as ethyl methanesulphonate, has been used to create strains with between 3 and 30 mutations per chlamydial genome (Kari *et al.,* 2011; Nguyen and Valdivia, 2012; 2013). Targeted null mutants can be obtained by screening EMS mutagenised strains using CEL 1 digestion to identify single nucleotide polymorphisms in the target gene (Kari *et al.,* 2011). Whole genome sequencing of these strains has enabled phenotype-genotype comparisons and could eventually provide insight into chlamydial gene functions.

The *Chlamydia trachomatis* genome consists of a 1,042,519 base pair (bp) chromosome and a 7493bp plasmid which encodes 894 potential open reading frames (ORFs) (Stephens *et al.,* 1998; Kalman *et al.,* 1999). This is significantly different from the 1,230,230bp *Chlamydophila pneumoniae* genome with 1,073 likely ORFs (Kalman *et al.,* 1999). Analysis of both genomes revealed a number of conserved areas, such as three distinct chromosomal locations encoding a type III secretion system (T3SS) (Hsia *et al.,* 1997; Kalman *et al.,* 1999). In fact, *C.trachomatis* serovar D dedicates almost 10% of the 894 ORFs to encode the components of the T3SS (Betts-Hampkian and Fields, 2010). T3SS is a complex protein transport system common to a number of

pathogenic Gram-negative bacteria including *Salmonella enterica*, *Pseudomonas aeruginosa,* and *Yersinia* spp. (Hueck, 1998; Kubori *et al.,* 1998; Galán and Collmer, 1999). Although core components of the T3SS appear to be conserved among Gram-negative bacteria, the chlamydial T3SS contain distinct features due to the unique chlamydial development cycle (Galán and Collmer, 1999; Büttner, 2012; Mueller *et al.,* 2014).

T3SS systems have evolved to facilitate the translocation of virulence factors and effector proteins across the inner membrane, periplasmic space, and outer membrane of the bacterial cell envelope into either host cells or extracellular space independently of *sec* mediated secretion systems (*i.e.* type II secretion system [T2SS]) (Hueck, 1998; Tseng *et al.,* 2009). The basic components of T3SS apparatus have been well characterised. The apparatus comprises of a membrane-spanning assembly of more than 20 proteins including two upper rings, which interact with the bacterial outer membrane, and two inner rings, which integrate into the cytoplasmic membrane. This is often referred to as the injectisome, and resembles a flagellar basal body (Galán and Collmer, 1999; Büttner, 2012; Mueller *et al.,* 2014). Proteins are transported via a needle-like complex, which is 80nm long and 13nm wide in *Salmonella typhimurium* (Kubori *et al.,* 1998). Rosqvist *et al.* (1995) showed that, although there are no common peptide sequences, proteins transported by T3SS can be exported by pathogens that employ a heterologous T3SS. For example, *Shigella flexneri* IpaB will be translocated by *Yersinia pseudotuberculosis.* Protein secretion is mediated by a diverse range of specific chaperones, which maintain partially unfolded substrates and target them for secretion (Mueller *et.al.,* 2014). Effector protein secretion is regulated by

ATPases (Buttner, 2012). In *C.pneumoniae*, CdsN has been identified as the T3SS ATPase based on sequence similarity to T3SS ATPases and interaction with structural components of the T3SS basal body and T3SS chaperones (Stone *et al.,* 2008). The conservation of T3SS apparatus across the *Chlamydiaceae* genus reinforces the fundamental importance of protein secretion to the intracellular survival of bacteria.

In most Gram-negative bacteria T3SS encoding genes are often located within pathogenicity islands, a set of virulence genes that are unique to pathogenic bacteria (Groisman and Ochman *et al.,* 1996). In chlamydial systems however, T3SS effector genes appear dispersed, and structural components occur in three distinct chromosomal loci (Kalman *et al.,* 1999; Harris *et al.,* 2012; Mueller, 2014). The incorporation of virulence genes into bacterial pathogens by horizontal gene transfer is thought to be an important step in the coevolution of bacteria and their specific hosts (Groisman and Ochman *et al.,* 1996; Harris *et al.,* 2012).

1.3 Pathogenesis

The *Chlamydiaceae* family contains pathogens specifically adapted to a wide range of hosts. This thesis is primarily concerned with species that cause human infection therefore the following section will introduce the most common human pathogens *Chlamydia trachomatis* and *Chlamydophila pneumoniae*, as well as animal pathogens which have been used as model infections.

1.3.1 *Chlamydia trachomatis*

Chlamydia trachomatis serovars comprise two disease biovars: trachoma, which contains both ocular and urogenital serovars, and lymphogranuloma venereum (LGV)(**Table 1.1**).

biovar	serovars	target cells	sequelae
trachoma (ocular)	A, B, Ba, C	conjunctival epithelia	conjunctivitis, conjunctival scarring and fibrosis, trichiasis, and corneal opacity
trachoma (urogenital)	D, E, F, G, H, I, Ia, K	genital epithelia	♂: urethritis, prostatitis, epididymitis, infertility? ♀: salpingitis, cervicitis, urethritis, pelvic inflammatory disease (PID), infertility
LGV	L1, L2, L2a, L3	genital epithelia	genital lesions, lymphadenopathy, proctatitis

Table 1.1. ***Chlamydia trachomatis*** **biovars.** *C.trachomatis* serotypes and consequences of infection for men (♂) and women (♀).

Trachoma is the leading cause of preventable blindness in developing countries. Repeated inflammation of the conjunctiva coupled with trichiasis, the inversion of the eyelashes, leads to corneal scarring and eventual blindness (Hu *et al.*, 2010). In 2011 an estimated 1.2 million individuals were suffering from total blindness and a further 1 million with partial blindness as a result of chronic *C.trachomatis* infection (WHO,

2012). Trachoma is spread by contact and is endemic in countries with limited access to clean water and antibiotics.

C.trachomatis trachoma biovar is also the most common bacterial sexually transmitted infection (STI) globally. Treatment of urogenital *Chlamydia* infections, and all associated conditions, costs as much as $4 billion annually in the USA (Stamm, 1999). In 2005 the World Health Organisation (WHO) reported 101 million new cases of *C.trachomatis* infection worldwide (WHO, 2011), the majority of which were reported in the Indian subcontinent and south east Asia. *C.trachomatis* infections are an increasing global problem. Between 1996 and 2001 cases of genital *Chlamydia* more than doubled and in August 2002 *Chlamydia* diagnoses outnumbered infections associated with any other pathogen (Eley, 2003). It is estimated that urogenital trachoma infections in Europe affect 1-3% of the population aged between 18 and 44 (Howie *et al.*, 2011) however, the majority of genital *C.trachomatis* infections are asymptomatic which makes an exact figure impossible to estimate. The asymptomatic nature of the genital tract infections increases the risk of complications as a result of chronic infection. In women *C.trachomatis* causes salpingitis and cervicitis which can lead to tubal scarring and pelvic inflammatory disease (PID) resulting in ectopic pregnancies and in some cases infertility (Gottlieb *et al.*, 2010; Stamm, 1999). Between 18 and 50% of infants born to mothers infected with genital *Chlamydia* will develop chlamydial conjunctivitis within 6 months of birth, and between 3 and 20% will develop pneumonia (Numazaki *et al.,* 1989). *C.trachomatis* infections have been linked to increased risk of squamous-cell carcinoma of the cervix and have been implicated in facilitated transmission of human immunodeficiency virus 1 and human papilloma

virus (Malhotra *et al.*, 2013). In men up to 50% of reported cases of non-gonococcal urethritis can be attributed to *C.trachomatis* (Oriel, 1992) however a link between *C.trachomatis* infection and male infertility remains controversial. Incubation of human sperm with chlamydial lipopolysaccharide (LPS), an endotoxin found in the bacterial envelope, was shown to cause apoptosis (Eley *et al.,* 2005), however the physiological relevance of this remains disputed.

LGV serovar STIs cause chronic infection of the lymphatic system, characterised by the swelling of lymph nodes. LGV often presents as severe proctitis (White, 2009). LGV was considered rare prior to an outbreak in the Netherlands in 2004. It is now prevalent in industrialised countries amongst homosexual men (White, 2009).

Prior to the introduction of nucleic acid amplification tests (NAATs) chlamydial infections were difficult to diagnose. Clinical diagnosis relied on cell culture methods, which required viable bacteria, and various immunofluorescence techniques, which were insensitive to low titres of infection. There are a number of different NAATs available, with the most common being polymerase chain reaction (PCR) amplification of chlamydial *ompA*. This has also been used to serotype infections (Jalal *et al.,* 2007), however recent comparison of whole genomes from clinical isolates suggest that there is significant intra-serovar recombination and exchange of *ompA,* which renders current serotyping misleading (Harris *et al.,* 2012).

Chronic and repeat ocular and genital *Chlamydia* infections have severe long-term effects as a result of inflammation and immune system activation (Stephens, 2003). As much as 50% of reactive arthritis cases can be attributed to chronic *C.trachomatis*

genital infection (Carter *et al.,* 2012). Literature often cites that PID, and consequent female infertility, is caused by scarring as a result of tissue damage following an inflammatory response to chlamydial infection. However, approximately 80% of women diagnosed with a chlamydial infection will not develop PID, and many will clear an infection without sustaining tissue damage (Taylor *et al.,* 2011). The mechanisms of tissue damage and the immunopathology of chlamydial infections are not fully understood. Histopathological analyses of both natural and experimental chlamydial infections showed cellular infiltration of polymorphonuclear neutrophils and lymphocytes at the site of infection (Stephens, 2003). This chronic inflammatory response causes damage to the epithelium leading to the formation of scars. Chlamydial protease-like activity factor (CPAF), chlamydial protein CT795, and 60kDa chlamydial heat shock protein (cHsp60) can all induce a humoral immune response in samples from patients with inflammatory trachoma (Skwor *et al.,* 2010) and purified cHsp60 can activate nuclear factor-κB (NF-κB), and therefore induce the production of pro-inflammatory cytokines, in non-immune cells (Stephens, 2003). The range of sequelae observed between individuals suggests differences in susceptibility to scarring and fibrosis (Stephens, 2003).

1.3.2 *Chlamydophila pneumoniae*

Chlamydophila pneumoniae is the causative agent of atypical pneumonia, and is linked to asthma, bronchitis, and obstructive pulmonary disease (Honarmand, 2013; Roulis *et al.,* 2013). As observed in *C.trachomatis* infection, chronic *C.pneumoniae* infection has been implicated in reactive arthritis (Carter *et al.,* 2012; Roulis *et al.,* 2013). Another

controversial sequela of *C.pneumoniae* infection is atherosclerosis, and consequently coronary heart disease (Honarmand, 2013; Roulis *et al.,* 2013). *C.pneumoniae* has recently been identified as a zoonotic pathogen infecting amphibians, reptiles, and mammals such as koalas and horses (Roulis *et al.,* 2013).

1.3.3 Animal pathogens

Chlamydia muridarum, the causative agent of mouse pneumonitis, which naturally infects rodents (**Figure 1.1**). *C.muridarum* infection of mice is a useful animal model for exploring *C.trachomatis* pathogenesis (Barron *et al.,* 1981). Similarly, *Chlamydophila caveae* infection of guinea pigs has been used as a model for human genital *C.trachomatis* infections.

Chlamydophila psittaci is predominantly an avian pathogen, however it can be transmitted to humans by exposure to aerosolised bird excreta (Escalante-Ochoa *et al.*, 1998; Moroney *et al.,* 1998). The incidence of psittacosis in humans is relatively rare. Outbreaks can usually be traced back to infected domestic birds or occupational exposure, to ducks and turkeys in particular (Moroney *et al.,* 1998). In humans *C.psittaci* infections present as atypical pneumonias and fevers but vary greatly in severity between individuals (Moroney *et al.,* 1998).

1.4 Prevention and control

Advances in speed and sensitivity of diagnostic techniques following the introduction of NAATs led to the initiation screening programmes to limit the spread of *Chlamydia* infections. However, the efficacy of screening as a tool to restrict the spread of chlamydial infections is disputed (Jamil *et al.,* 2013). Strategies such as SAFE (Surgery, Antibiotics, Facial cleanliness, Environmental improvement) in trachoma endemic countries have been introduced by WHO to treat infected individuals, reduce the reservoir of infection, and prevent the spread of infections. These measures are contributing to achieving the objective of the global WHO alliance for the elimination of blinding trachoma by 2020 (WHO, 2012).

Clinical *C.trachomatis* STIs are treated using tetracycline antibiotics, which bind to 16S rRNA, preventing bacterial protein synthesis (Brodersen *et al.,* 2000). Tetracycline resistance has been observed in a number of bacterial species including *Helicobacter pylori* (Gerrits *et al.,* 2002), which had a mutation in the 16S rRNA gene. Reports of tetracycline resistant strains of *C.trachomatis* from the USA and France have yet to be confirmed *in vitro* (O'Neill *et al.,* 2013), however mutations in the *tetC* gene of *C.suis* has been shown to confer tetracycline resistance (Dugan *et al.,* 2004). Recent whole-genome analysis of a large number of clinical *C.trachomatis* isolates has shown a surprising degree of horizontal gene transfer among bacteria (Harris *et al.,* 2012) which, given the worldwide prevalence of chlamydial infections, could indicate a potential challenge in the control and treatment of chlamydial infections.

The ideal method for controlling *Chlamydia* transmission would be the development of a vaccine. Early studies using inoculation with inactivated bacteria had some success controlling animal infection. However, only short-term protection against ocular infection was observed in humans, and re-infection produced exacerbated disease in some individuals (Longbottom, 2003). Chlamydial major outer membrane protein (MOMP), a major component of the bacterial membrane, was shown to illicit a strong humoral immune response, and has been the focus of a number of vaccine development programmes, along with polymorphic membrane proteins (Pmps) and cHsp60 (reviewed by Longbottom, 2003). A greater understanding of the complex chlamydial lifecycle would increase the likelihood of effective vaccine development.

1.5 Lifecycle

The *Chlamydiaceae* share a unique infection cycle, comprising of two functionally and morphologically distinct developmental forms (Moulder, 1991). It is thought that the two different forms are the result of the differing pressures exerted on the bacteria in the extracellular and intracellular environments encountered during the infection cycle (Liu *et al.,* 2010).

1.5.1. Elementary body (EB)

Extracellular *Chlamydiaceae* exist as elementary bodies (EBs). EBs are the infectious form of the bacteria, which are metabolically inert but capable of surviving outside the host cell. Bacteria exist as EBs both at the beginning of the infection cycle, prior to host

cell invasion, and at the end before bacteria are released to propagate infection. EBs are approximately 0.3μm in diameter and bound by a double membrane (Friis, 1972). Bacterial rigidity is maintained by an *N*-lauroyl sarcosine insoluble 'P-layer', rich in cysteine cross-linked proteins, known as the chlamydial outer membrane complex (COMC). More than 60% of the COMC is comprised of MOMP monomers that form extensive disulphide bonds (Caldwell *et al.,* 1981; Hatch, 1996; Liu *et al.,* 2010). Chlamydial PmpD has also been identified within the COMC, along with other hypothetical *C.trachomatis* (CT) proteins predicted to localise to the EB surface, including CTL0493 and CTL0645 from the outer membrane protein (Omp) 85 superfamily (Liu *et al.,* 2010). This rigid structure appears to protect the bacteria from osmotic lysis during transmission (Kaul *et al.,* 1997; Liu *et al.,* 2010). Ultrastructural observation of EBs revealed spiky projections from the outer membrane (Fields *et al.*, 2003), which are predicted to be preformed T3SS needles necessary for inducing bacterial internalisation by host cells. (**Figure 1.3A/B**). EBs contain an electron dense, condensed nucleoid containing chlamydial histone H1-like proteins Hc1 and Hc2, which have been shown to cause DNA condensation in *Escherichia coli* (Kaul *et al.,* 1997).

1.5.2 Reticulate body (RB)

Intracellular bacteria exist as reticulate bodies (RBs), which are approximately 1μm in diameter (Friis, 1972). RBs are also bound by a double membrane, however, unlike the EB envelope, RB envelopes are sensitive to osmotic pressure. RBs contain a relaxed chromosome without either of the identified chlamydial histone-like proteins present (Kaul *et al.,* 1997). RBs remain in contact with the inclusion membrane during

replication, presumably to enable the translocation of effector proteins from the bacteria through the inclusion membrane into host cells (Matsumoto, 1981; Peterson and de la Maza, 1988; Wilson *et al.*, 2009). Although RBs are metabolically active they are unable to invade host cells and are therefore entirely non-infectious. Bacteria remain in the RB form for the duration of the intracellular replication phase of the infection cycle (**Figure 1.3C/D**).

1.5.3 Infection cycle

The majority of the *Chlamydiaceae* development cycle occurs inside a host cell, within the bacteria-controlled inclusion (**Figure 1.4**). Host cell invasion and inclusion biogenesis mechanisms are of fundamental importance to the bacteria, however these processes are not fully understood.

EB attachment was observed to occur in cholesterol rich microdomains of host cell membranes (Jutras *et al.,* 2003). Bacterial adhesion has been suggested to occur in two stages: a reversible electrostatic interaction between bacterial adhesins, including MOMP (Su *et al.,* 1990; 1996), and host heparan sulphate-like glycosaminoglycans (Zhang and Stephens, 1992; Su *et al.*, 1996; Carabeo and Hackstadt, 2001), followed by a temperature-dependent irreversible attachment event (Carabeo and Hackstadt, 2001).

Once bacteria have adhered to the host cell they actively promote internalisation in a process that is dependent upon host cell actin remodelling (Carabeo *et al.,* 2002). Host

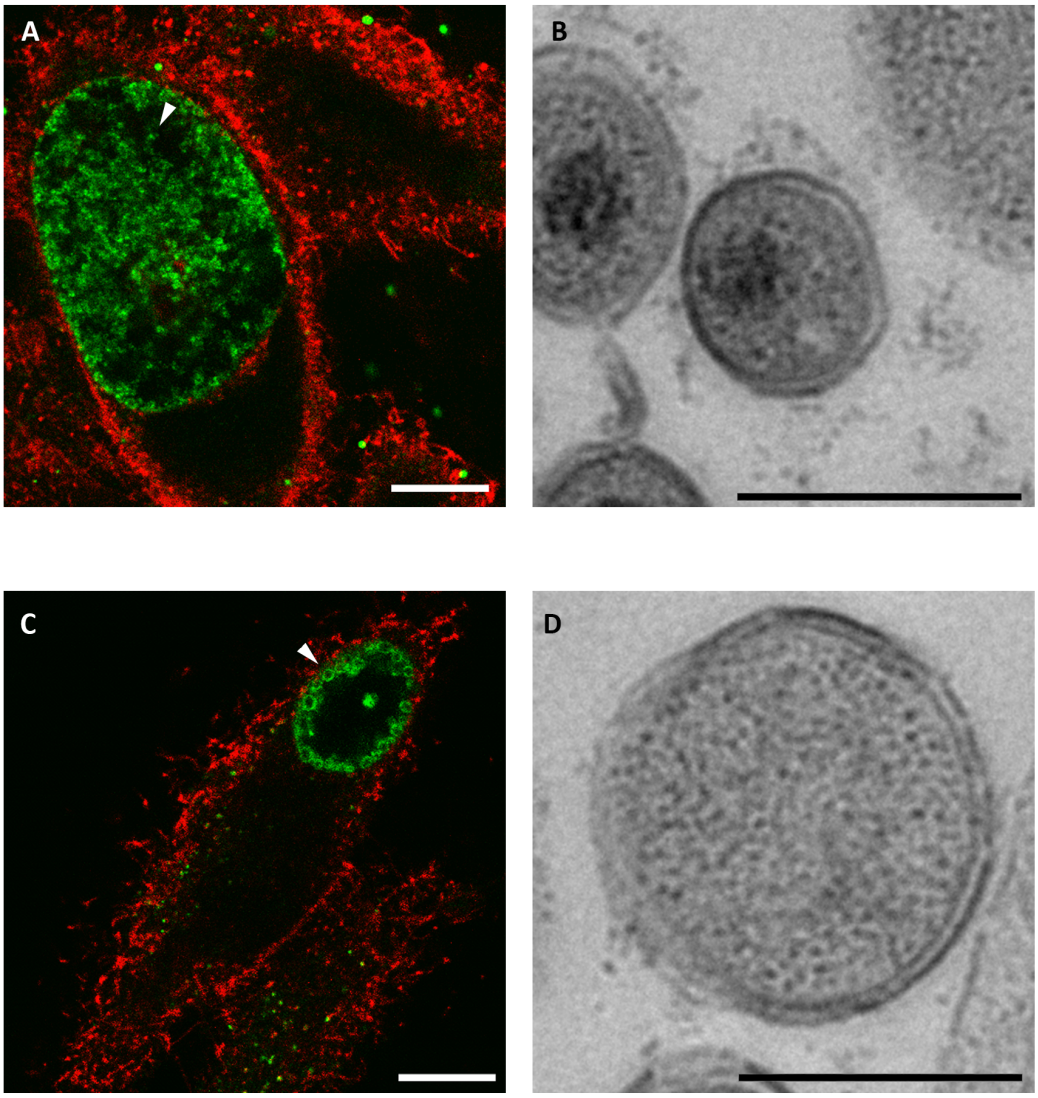
A
B
C
D

Figure 1.3. Two distinct morphological forms of the chlamydial life cycle. (A) Confocal xy-section of a HeLa cell infected with *C.trachomatis* LGV2 when bacteria are present as elementary bodies (EBs) at 36hpi. Plasma membranes were labelled using AlexaFluor®594 conjugated WGA (red) prior to permeabilisation. Bacteria were labelled with *Chlamydia* spp. MOMP/LPS specific primary antibody followed by AlexaFluor®488 conjugated secondary antibody (green). Arrow indicates a single EB within the inclusion. Scale bar, 10μm. (B) A transmission electron micrograph of an EB. Scale bar, 0.5μm. (C) Confocal xy-section of a HeLa cell infected with *C.trachomatis* LGV2 when bacteria are present as reticulate bodies (RBs at 24hpi. Plasma membranes were labelled using AlexaFluor®594 conjugated WGA (red) prior to permeabilisation. Bacteria were labelled with *Chlamydia* spp. MOMP/LPS specific primary antibody followed by AlexaFluor®488 conjugated secondary antibody (green). Arrow indicates a single RB. Scale bar, 10μM. (D) A transmission electron micrograph of an RB. Scale bar, 1μm.

actin recruitment is initiated by translocated actin recruitment protein (TARP), translocated by T3SS into the host during EB entry. TARP nucleates actin filaments and promotes polymerisation (Carabeo *et al.,* 2002; Jewett *et al.*, 2006; 2010). Rho family small guanosine 5'-triphosphotases (GTPases) are recruited to the site of bacterial entry, to interact with host activators of the actin-related protein (Arp) 2/3 complex to initiate actin branching at the site of bacterial attachment (Carabeo *et al.*, 2004; 2007). The GTPases utilised by the bacteria seem to be species specific, for example *C.trachomatis* requires Rac GTPases (Carabeo *et al.*, 2004) whereas *C.caviae* internalisation is inhibited in HeLa cells expressing *cdc42* dominant negative mutants (Subtil *et al.*, 2004). *C.trachomatis* protein CT166, which is conserved in all urogenital serovars, acts as a glucosyltransferase. CT166 is present in EBs, and in infected cell lysate for the first hour after infection (Thalmann *et al.,* 2010). Thalman *et al.* (2010) showed that CT166 glucosylates Rac1, thereby inducing actin reorganisation and mediating EB uptake by host cells. Electron microscopic analysis of EB attachment points at the host cell plasma membrane revealed pedestal-like structures reminiscent of the pedestals observed during enteropathogenic *E.coli* adhesion to host cells (Carabeo *et al.,* 2002) (**Figure 1.4A**).

Once internalised, bacteria modify entry vesicles by inserting a number of serovar specific effector proteins into the membrane. (Grieshaber *et al.*, 2003; Lutter *et al.,* 2012; Mital *et al.,* 2013). Inc proteins are a diverse family of effector proteins that contain a characteristic bi-lobed hydrophobic domain (Li *et al*., 2008; Lutter *et al*., 2012; Mital *et al*., 2013). Inc proteins are predicted to localise to the inclusion membrane (Bannantine *et al.,* 2000), which has been experimentally demonstrated to

be the case for a number of Incs (reviewed by Valdivia, 2008 and Betts *et al.*, 2009). IncB and *C.trachomatis* proteins CT101, CT222, and CT850, spontaneously induce round vesicular structures when expressed in HeLa cells, indicating a role for these Incs in inclusion membrane morphology (Mital *et al.,* 2013). *Chlamydiaceae* encode between 39 and 59 Inc proteins and, although there is very little primary sequence similarity between the Incs (Lutter *et al.,* 2012; Mital *et al.,* 2013), all *Chlamydiaceae* encode homologues of 23 core Incs (Lutter *et al.,* 2012).

Within 2h of internalisation, EB containing entry vesicles are trafficked to the microtubule organising centre (MTOC) along microtubules in a dynein-dependent manner (Clausen *et al.,* 1997; Grieshaber *et al.*, 2003). In cases where multiple bacteria invade a single host cell, entry vesicles will fuse to form a single inclusion (Matsumoto *et al.,* 1991; Van Ooij *et al.,* 1998; Hackstadt *et al.,* 1999), with the exception of *C.caviae* strain GPIC (Van Ooij *et al.,* 1998). Vesicle fusion requires IncA (Hackstadt *et al.,* 1999; Suchland *et al.,* 2000), an Inc protein that is highly conserved among the *Chlamydiaceae* that localises to the cytoplasmic face of the inclusion membrane (Hackstadt *et al.,* 1999; Scidmore-Carlson *et al.,* 1999). IncA, along with other hypothetical *C.trachomatis* proteins including CT223 and CT813, contains a soluble NSF attachment protein receptor (SNARE)-like motif. (Delevoye *et al.*, 2008). These motifs interact with host SNAREs, but full-length IncA was demonstrated to specifically recruit SNAREs involved in endosomal trafficking (Delevoye *et al.*, 2008) (**Figure 1.4B**).

Once a nascent inclusion has been established, bacteria undergo EB-RB differentiation (Moulder, 1991) (**Figure 1.4C**), however the signals and mechanisms involved in this transition are unknown.

A recent study has demonstrated the presence of peptidoglycan in bacteria during reorganisation from EBs to RBs (Liechti *et al.,* 2013). Peptidoglycan is involved in cell division in most Gram-negative bacteria (Egan and Vollmer, 2013), but was previously thought to be absent from *Chlamydiaceae*. The lack of detectable peptidoglycan was considered to be the 'chlamydial anomaly' (Liechti *et al.,* 2013), as *Chlamydiaceae* encode the majority of peptidoglycan biosynthesis machinery and are sensitive to β-lactam antibiotics that inhibit peptidoglycan synthesis, such as penicillin (Ghuysen and Goffin, 1999; Patin *et al.,* 2012). The detection of peptidoglycan during EB-RB differentiation could be a significant step in understanding the mechanism of bacterial reorganisation and consequent replication.

RBs multiply by binary fission (Higashi, 1965; Moulder, 1966) and remain in contact with the inclusion membrane (Matsumoto, 1981; Peterson and de la Maza, 1988; Wilson *et al.*, 2009) (**Figure 1.4D**). RB-inclusion membrane contact sites are rich in IncF, however it is not yet clear which membranes the protein interacts with (Scidmore-Carlson *et al.,* 1999). Inclusions co-opt host RhoA GTPases to form a scaffold of F-actin and intermediate filaments (IFs) to support the inclusion (Kumar and Valdivia, 2008a; 2008b). Disruption of actin structures induces IL-8 chemokine expression, and consequently, activation of an innate immune response. This would suggest that, as well as providing stability to the inclusion, the assembled actin filament cage reduces

the likelihood of pathogen recognition receptors (PRRs) stimulating chemokine and cytokine signalling cascades (Kumar and Valdivia, 2008a; 2008b). As the inclusion expands to accommodate replicating bacteria, IFs are processed by CPAF (Kumar and Valdivia, 2008a; 2008b), which is translocated by the bacteria via T2SS (Chen *et al.,* 2010).

At the end of the infection cycle, RBs redifferentiate into EBs following Hc1 expression, which causes the formation of the condensed nucleoid of EBs (Kaul *et al.,* 1997) (**Figure 1.4E**). EBs are then released from host cells to propagate infection. This is achieved by at least two distinct mechanisms, cell lysis (Perfettini *et al.,* 2003; Hybiske and Stephens, 2007) (**Figure 1.4F**) and extrusion (Todd and Caldwell, 1985; Hybiske and Stephens, 2007) (**Figure 1.4G**). Bacterial exit by host cell lysis appears to be independent of apoptotic mechanisms (Hybiske and Stephens, 2007), but is reliant on proteases, with cysteine protease inhibitor E64 having a dramatic inhibitory effect on lysis mechanisms. Extracellular calcium influx was also demonstrated to be an important factor in the lysis of host cells (Hybiske and Stephens, 2007). Extrusion of intact inclusions requires actin polymerisation, neuronal Wiskott-Aldrich syndrome protein (N-WASP), Rho GTPase, and Myosin II phosphorylation (Hybiske and Stephens, 2007, Lutter *et al.,* 2013). Recent work has implicated interactions between *C.trachomatis* protein CT228 and myosin phosphatase target subunit 1 (MYPT1), along with other subunits of the myosin phosphatase pathway, as regulators of the extrusion pathway of host cell egress (Lutter *et al.,* 2013).

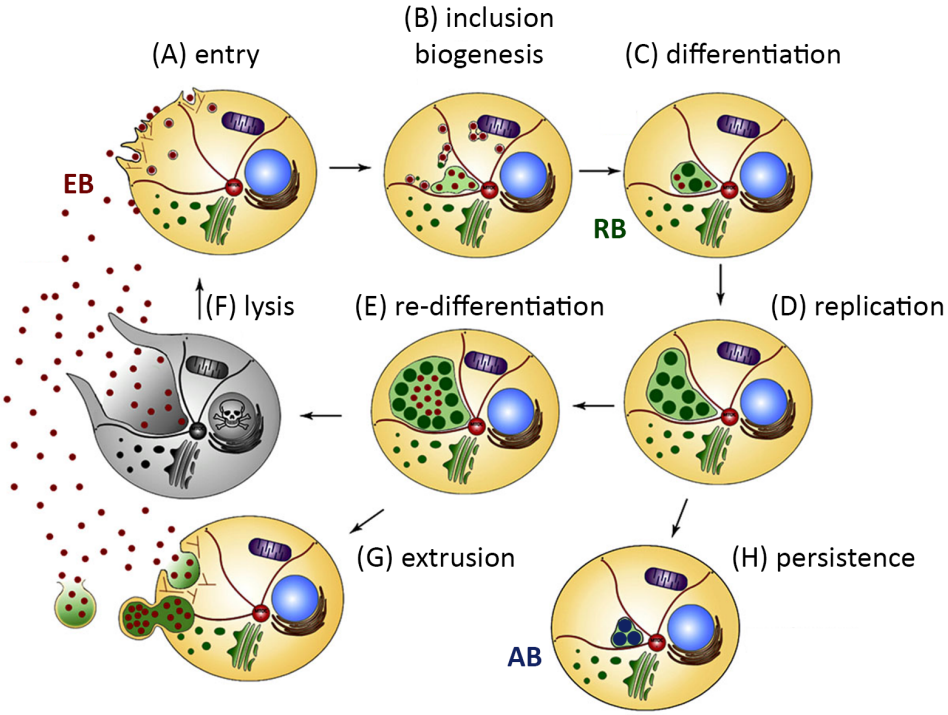
(A) entry
(B) inclusion biogenesis
(C) differentiation
EB
RB
(F) lysis
(E) re-differentiation
(D) replication
(G) extrusion
(H) persistence
AB

Figure 1.4. Schematic representation of the chlamydial infection cycle. (A) Infectious but metabolically inert elementary bodies (EBs; red) invade host cells. (B) Entry vesicles are then trafficked to the microtubule organisation centre (MTOC) where the inclusion is established. (C) EBs differentiate into reticulate bodies (RBs; green) which are non-infectious but metabolically active. (D) RBs replicate by binary fission within the bacteria-controlled inclusion. (E) RBs re-differentiate into EBs, prior to release from host cells either by lysis (F) or extrusion (G). (H) Stressors such as nutrient deficiency or cytokine exposure can induce persistence identified by non-infectious but viable aberrant bodies (ABs; blue).

1.5.4 Intracellular nutrient acquisition

Bacteria interact extensively with the host cells during replication to maintain their intracellular niche and obtain nutrients. The inclusion membrane, characterised by Inc proteins secreted by the bacteria during inclusion biogenesis, is an important mediator of these interactions (Scidmore *et al.,* 2003).

Chlamydial inclusions remain distinct from endosome-lysosome trafficking, unlike many intracellular pathogens. For example, *Salmonella*-containing vesicles will arrest endosome maturation, transiently retaining early endosome markers such as Rab5, and will selectively acquire later maturation markers such as lysosome-associated membrane protein (LAMP)-1 (reviewed by Bakowski *et al.,* 2008). The chlamydial inclusion does not acidify (Grieshaber *et al.*, 2003), and does not acquire any lysosomal markers (Scidmore *et al.,* 2003). However, inclusions will selectively acquire elements from exocytic pathways that are essential to development. For example, inclusions intercept vesicles containing sphingolipids (Hackstadt *et al.,* 1996; Heinzen *et al.*, 1996) and cholesterol (Carabeo *et al.,* 2003) *en route* from the Golgi to the plasma membrane. Sphingomyelin, synthesised using fluorescent C_6-NBD-ceramide, was incorporated into bacterial envelopes (Hackstadt *et al.,* 1996; Heinzen *et al.*, 1996). Sphingolipid delivery to the inclusion, and consequently chlamydial development, was disrupted by chemical inhibition of multivesicular bodies (MVBs) (Beatty, 2006; 2008), organelles involved in sorting proteins and lipids for recycling in the Golgi. This suggests a direct association between MVBs and the chlamydial inclusion, which is reinforced by the observation that an MVB resident protein, CD63, is delivered to the

inclusion (Beatty, 2006). However, CD63 itself is not required for inclusion-MVB interactions (Beatty, 2008). These interactions are mediated by the recruitment of Rab GTPases involved in receptor recycling (Rab4 and Rab11), and endoplasmic reticulum (ER) – Golgi trafficking (Rab1) (Rzomp *et al.,* 2003). Rab recruitment is achieved using chlamydial Inc proteins, for example Rab4 interacts with *C.trachomatis* protein CT229 (Rzomp *et al.,* 2006).

Close association between truncated Golgi mini stacks and the inclusion is necessary for chlamydial acquisition of lipids, as inhibiting cleavage of golgin-84, a Golgi matrix protein, disrupts delivery of lipids to the inclusion (Heuer *et al.* 2009). Cocchiaro *et al.* (2008) observed intact lipid droplets inside the inclusion lumen, indicating that inclusions are capable of engulfing whole organelles, demonstrating another method of nutrient acquisition by *Chlamydiaceae*.

Recent work in our lab has demonstrated that ER is recruited to the cytoplasmic face of the inclusion in a biphasic manner. ER was recruited during bacterial entry and then shed as inclusions developed. ER was once again recruited to mature inclusions. Disruption of ER recruitment during mid-cycle development resulted in bursting of the inclusion (Dumoux *et al.* 2012). The ER-golgi lipid transfer protein CERT is recruited to the chlamydial inclusion membrane via interaction with IncD at inclusion membrane-ER contact sites (Derré *et al.,* 2011). Tomography of ER-inclusion membrane contact sites show that where an RB-ER synapse occurs, an array of T3SS injectisomes can be seen in contact with the inner and outer bacterial membranes, the inclusion membrane and the rough ER (Dumoux *et al.,* 2012).

1.5.5 Bacterial intervention in host cell processes

Chlamydiaceae have developed a number of strategies to modulate various aspects of the cell cycle and protect their intracellular niche. As chlamydial entry vesicles are trafficked to the MTOC, a close association is formed between the inclusion and host centrosomes (Grieshaber *et al.,* 2006). This association causes centrosome amplification and prevents accurate chromosome division (Grieshaber *et.al.,* 2006). Furthermore, chlamydial infection causes defects during mitotic spindle formation (Knowlton *et al.,* 2011).

One of the better-studied aspects of chlamydial infection is the ability of the bacteria to inhibit host cell apoptosis, and therefore maintain intracellular survival. Apoptosis is often triggered in response to damage-related molecular pattern molecules (DAMPs) in response to pathogen invasion. *Chlamydiaceae* prevent apoptotic response to host cell invasion by recruiting signalling molecules and their pro-apoptotic binding partners to the inclusion. For example, IncG sequesters the 14-3-3β signalling protein, and consequently the pro-apoptotic BH3-only protein BAD. This prevents the signalling cascade reaching the mitochondria, thus protecting the host cell from mitochondrial apoptosis induction (Verbeke *et al.,* 2006). Tse *et al.* (2005) showed that, during intracellular replication, diacylglycerol is accumulated around the inclusion. The novel protein kinase PKCδ, which has a diacylglycerol binding site, is therefore sequestered away from the mitochondria, preventing cytochrome c release and downstream pro-apoptotic activity (Tse *et al.,* 2005). The chlamydial protease CPAF also plays an important role in modulating the host response to pathogen invasion, degrading BH3-

only and Bcl-2 pro-apoptotic proteins (Pirbhai *et al.,* 2006), and other factors involved in adaptive immune response including RFX-5 and USF-1, which correlates to the suppression of class I and II MHC antigen expression. However, a recent study by Chen *et al.* (2012) demonstrated that CPAF can survive cell lysis protocols, including exposure to 8M urea, and previously published substrates such as golgin-84 failed to undergo proteolysis when CPAF was inhibited during cell processing. This suggests that, although CPAF might have a variety of functions, the likelihood is that *Chlamydiaceae* have a number of functional proteases. For example, CT441, a tail specific protease that cleaves the p65/RelA subunit of NF-κB, therefore inhibiting NF-κB activation (Lad *et al.,* 2007).

In addition to modulating host apoptosis, the *Chlamydiaceae* also disrupt various housekeeping activities. For example, chlamydial proteins CT868 (*Chla*Dub 1) and CT867 (*Chla*Dub 2), conserved across all *Chlamydia* species except *C.pneumoniae*, have de-ubiquitinating and de-neddylating properties (Misaghi *et al.,* 2006). Although cellular substrates have yet to be determined for these de-ubiquitinases their presence could indicate chlamydial interference in ubiquitin-dependent mechanisms such as protein degradation and signalling pathways. Chlamydial CT847, a T3SS secreted effector protein, interacts with Grap2 cyclin D-interacting protein (GCIP) which is ubiquitously expressed throughout the cell cycle. GCIP is involved in the modulation of eukaryotic cell proliferation, suggesting that *Chlamydiaceae* may also intervene in the host cell cycle (Chellas-Géry *et al.*, 2007).

1.5.6 Persistence

The *Chlamydiaceae* enter a 'persistent' state in response to a number of environmental stressors (**Figure 1.4H**). Persistence in *Chlamydiaceae* has a different meaning to the term used most frequently when describing pathogens. Generally persistence is used to describe chronic active infections. In *Chlamydiaceae* the term persistence is used to describe an aberrant phase in the infection cycle where metabolism slows and RBs fail to either replicate or differentiate into EBs. This is usually characterised by the formation of large abnormal bodies, termed aberrant bodies (ABs), which can revert back to RBs to complete a normal infection cycle (Hogan *et al.,* 2004). Persistence has been demonstrated *in vitro*, however controversy still remains as to whether this state occurs *in vivo*. Persistence can be induced by stressors such as interferon-γ (IFN- γ) (Pantoja *et al.,* 2001), heat shock (Kahane and Friedman, 1992), and nutrient deficiencies such as iron depletion (Roulston, 1997) and amino acid starvation (Coles *et al.,* 1993). Each of these conditions gives rise to different gene expression profiles and AB morphologies, however all are termed persistence (Hogan *et al.,* 2004; Shoborg, 2011).

1.6 Potassium regulation in bacteria

Inorganic ions, such as potassium (K^+), are vital for maintaining osmotic pressure in cells, as well as regulating pH and performing a variety of signalling functions such as activation of cytoplasmic enzymes. Intracellular bacteria such as *C.trachomatis* will

encounter different ionic environments throughout their infection cycle, for example, the concentration of intracellular K^+ is higher than the extracellular milieu, where as intracellular sodium (Na^+) concentrations will be lower. In order to be able to adapt to their changing environments and maintain homeostasis, Gram-negative bacteria have developed three major ion transport systems (Epstein, 2003; Su *et al.,* 2009). The Trk low affinity K^+ transport system is found in the largest number of bacterial species (Liu *et al.,* 2013). Trk rapidly transports K^+ under alkaline or neutral conditions (Liu *et al.,* 2013). Trk K^+ transport regulates secretion of *S.typhimurium* T3SS effector proteins and therefore plays and important role in pathogenesis (Su *et al.,* 2009). Kdp is a high affinity K^+ uptake system that is induced by low K^+ environments or high osmolarity (Frymier *et al.,* 1997; Epstein, 2003; Xue *et al.,* 2011). Kdp activity has an important regulatory effect on virulence gene transcription in *Staphylococcus aureus* (Xue *et al.,* 2011). Kup is induced under acidic conditions (Trchounian and Kobayashi, 1999; Epstein 2003) and is the major K^+ uptake system utilised by *E.coli* under hyper-osmotic stress (Trchounian and Kobayashi, 1999).

Although K+ transport systems have yet to be identified in the *Chlamydiaceae*, the *C.trachomatis* protein CT440 has been shown to localise to the inclusion membrane (Li *et al.,* 2008; 2011) and the predicted structure shows homology to a neurotransmitter-gated ion-channel transmembrane pore (Oliver, Nobeli, and Hayward; personal communication).

1.7 Aims

Due to the complexities of studying the *Chlamydiaceae*, very little is known about the environment within the inclusion. Unlike the vacuoles inhabited by other intracellular bacteria, such as *Coxiella burnetii* (Heinzen *et al.,* 1996), the chlamydial inclusion is not acidified and appears to maintain a similar pH to the host cytosol (Grieshaber *et al.*, 2002). In the same study, Grieshaber *et al.* (2002) demonstrated that the ionic composition; *i.e.* the concentration of calcium (Ca^{2+}), sodium (Na^{+}), and potassium (K^{+}), within inclusion lumen was similar to that of the host cytosol. The aim of this project is to explore any role for inorganic ions in the biphasic development cycle.

Chapter 2 – Materials and Methods

2.1 Cell culture

Unless otherwise stated all cell culture materials were purchased from Gibco (Invitrogen, Carlsband, CA, USA). All sterile plasticware was purchased from VWR International (West Chester, PA, USA).

2.1.1 Cell lines and culture conditions

2.1.1.a HeLa cervical epithelial cells

Stocks of HeLa cells were previously prepared in the laboratory and stored in liquid nitrogen. Cells were grown in high glucose Dulbecco's modified eagle medium (DMEM) + GlutaMAX supplemented with 10% decomplemented fetal bovine serum (FBS) and penicillin (100 units [U]/ml) /streptomycin (100μg/ml) antibiotic mixture, as recommended by the American Type Culture Collection (ATCC). $2x10^6$ cells were grown to 70-90% confluence in T75 vented flasks in a humidified incubator at 37°C with 5% CO_2 before passage every 2-3 days.

2.1.1.b RL95-2 uterine endometrial cells

Stocks of RL95-2 cells were previously prepared in the laboratory and stored in liquid nitrogen. Cells were grown in a 1:1 mixture of Ham F-12 nutrient mix (HF-12) + GlutaMAX and DMEM supplemented with 10% FBS and penicillin (100 U/ml) /streptomycin (100μg/ml) antibiotic mixture, as recommended by the ATCC. $5x10^6$ cells were grown to 70-90% confluence in T75 vented flasks in a humidified incubator at 37°C with 5% CO_2 before passage every 3-4 days.

2.1.2 Passage

Solutions:

- trypsin – 0.05% trypsin, 200μg/ml ethylenediaminetetraacetic acid (EDTA)
- HBSS/FBS – Hank's balanced salt solution (HBSS), 10% FBS

When cells reached a confluence of 70-90% in culture flasks growth medium was removed and cells were washed in HBSS at 37°C to remove excess FBS. Cells were then dissociated from flask using trypsin at 37°C for 5min before collection in HSSS/FBS. Cell suspension was then centrifuged at 1200rpm using a Rotina 420R centrifuge (Hettich Lab, Technology, Tuttlingen, Germany) at 4°C for 10min. Supernatant was discarded and pellet resuspended in HBSS/FBS for counting and seeding.

2.1.3 Coverslip preparation

12mm glass coverslips (VWR, West Chester, PA, USA) were washed in 70% ethanol for 10min then washed twice in excess HBSS prior to transfer into 24-well cell culture plates.

2.1.4 Counting and seeding

Following passage, 5μl cells suspended in HBSS/FBS were added to 5μl 0.4% (w/v) trypan blue solution and added to a KOVA Glasstic counting chamber (Hycor, Indianapolis, IN, USA) and viewed under a light microscope. Viable cells, those non-permeable to trypan blue, were counted and added in appropriate volumes (see **Equation 1**) to sterile cell culture plates (**Table 2.1**) and then left to adhere for 18-24h.

	HeLa	RL95-2
35mm glass bottomed petri dish	$7x10^5$ (30%)	
90mm petri dish	$7x10^6$ (70%)	
4 chamber glass bottomed labtek	$3.5x10^5$ (30%)	
24 well plate	$7x10^5$ (70%) $1x10^4$ (100%)	$1x10^5$ (70%) $1.5x10^5$ (100%)
12 well plate	$1x10^5$ (70%) $1.5x10^5$ (100%)	$2x10^5$ (70%) $3x10^5$ (100%)
6 well plate	$4x10^5$ (70%) $7x10^5$ (100%)	

Table 2.1. Cell Plating. Number of cells added to medium to achieve correct confluence (shown in brackets) of adhered cells after 24h.

$$\text{cells/mL} = C_{count} \times \text{dilution factor} \times 10{,}000$$

Equation 1. Number of cells per ml. Where C_{count} is the number of cells counted in 9 grid squares of KOVA counting chamber.

2.2 Bacteria

2.2.1 *Chlamydia* infection protocol

Solutions:

- HeLa cell infection medium – DMEM, 10% FBS, 25μg/ml gentamicin
- RL95-2 cell infection medium – 45% DMEM, 45% HF-12, 10% FBS, 25μg/ml gentamicin

Adherent cells were infected with between 0.9-1 inclusion-forming units (IFU) of stock bacteria per cell, *i.e.* a multiplicity of infection (MOI) of 1, diluted in appropriate infection medium. Cells were then centrifuged at 900rpm using a Rotina 420R centrifuge (Hettich Lab, Technology, Tuttlingen, Germany) for 10min to ensure synchronised infections. Cells were then incubated in a humidified incubator at 37°C with 5% CO_2 for 90min before medium was replaced with fresh infection medium to remove any cell debris and dead bacteria. This second medium change was considered to be the starting point of the infection (t=0 hours post infection [hpi]).

2.2.2 Quantification of infectivity

Due to the obligate intracellular nature of *Chlamydiae,* quantification of viable bacteria presents a challenge. In order to estimate the quantity of infection forming units (IFUs), a serial dilution of each bacteria stock was added to HeLa cell monolayers. Infected cells were fixed at appropriate times post infection dependent on serovar (see below in **Section 2.2.3**). By assuming that each resultant inclusion was the product of a

single viable bacterium (Azenabor *et al.,* 2007), the concentration of the stock solution (IFU/ml) can be quantified (See **Equation 2**). An IFU 0.9-1 will result in infection of 90-100% of cells.

$$\text{IFU} = \frac{\#\text{ inclusions}}{\#\text{ nuclei}} \text{ x dilution factor x correction factor}$$

where,

$$\text{correction factor} = \frac{\text{area of coverslip}}{\text{area of field of view}}$$

Equation 2. IFU quantification. The average number of inclusions and cells from 10 fields of view (FOVs) can be used to calculate the quantity of infection forming units (IFU) in a sample.

2.2.3 *Chlamydiae* stocks

Solutions:

- sucrose-phosphate-glutamic acid buffer (SPG) – 220mM sucrose, 17.4mM Na_2HPO_4, 2.6mM NaH_2PO_4, 20mM L-glutamic acid

HeLa cell monolayers were infected with *Chlamydiae* stocks (Multiplicity of infection (MOI)=1, *i.e.* 1 bacterium per cell). The duration of initial infection differed depending on serovar. Inclusion development was monitored by light microscopy at late stages of the infection and considered ready for collection once inclusions were full of EBs but before the bacteria were released into the supernatant. Bacteria were collected by scraping into SPG buffer and homogenised by flushing through 23 gauge needle to lyse cells and release the bacteria. Bacterial stocks were checked for *Mycoplasma* contamination by polymerase chain reaction (PCR) following DNA extraction using

QIAamp DNA minikit (Qiagen, Hilden, Germany) according to manufacturer's instructions. For primers see **Appendix 1.** For PCR parameters see **Table 2.6**.

2.2.3.a *Chlamydia trachomatis* serovar LGV2

Stocks of *C.trachomatis* LGV2 were collected at approximately 50hpi, stock IFU concentration was then determined at 24hpi.

2.2.3.b *Chlamydia trachomatis* serovar D

Stocks of *C.trachomatis* D were collected at approximately 96hpi, stock IFU concentration was then determined at 48hpi.

2.2.3.c *Chlamydia muridarum*

Stocks of *C.muridarum* were collected at approximately 30hpi, stock IFU concentration was then determined at 18hpi.

2.2.4 Heat inactivation of *C.trachomatis* LGV2

C.trachomatis LGV2 from frozen stock were diluted in DMEM and incubated at 56°C for 30min. Bacteria were then diluted to the same titre as live bacteria (MOI=1) prior to infection of cell monolayers.

2.3 Drug treatments

2.3.1 Drugs

Unless otherwise stated all compounds were obtained from Sigma Aldrich (St Louis, MO, USA). For ionophore structures see **Appendix 2.**

2.3.1.a Nigericin

5mg nigericin sodium salt was reconstituted in 6.7ml dimethyl sulphoxide (DMSO) to yield a 1mM stock solution.

2.3.1.b Monensin

5mg monensin sodium salt was reconstituted in 7.2ml DMSO to yield a 1mM stock solution.

2.3.1.c Ionomycin

1mg ionomycin calcium salt was reconstituted in 1.3ml DMSO to yield a 1mM stock solution.

2.3.1.d Chloride ionophore I (c) Selectophore

5mg Cl^-I (Fluka, Basel, Switzerland) was reconstituted in 7.1ml DMSO to yield a 1mM stock solution.

2.3.1.e Valinomycin

10mg valinomycin was reconstituted in 9ml DMSO to yield a 1mM stock solution.

2.3.1.f Glibenclamide

200mg glibenclamide was reconstituted in 4ml DMSO to yield 100mM stock solution.

2.3.1.g Doxycycline

1mg doxycycline was reconstituted in 2ml deionised water to yield 1mM stock solution.

2.3.1.h Blebbistatin

1mg blebbistatin was reconstituted in 3.4ml DMSO to yield a 1mM stock solution. Cells were treated with 50μM blebbistatin diluted in HeLa cell infection medium (Hybiske and Stephens, 2007).

2.3.2 Drug concentrations

Optimum concentrations for each treatment were determined by subjecting monolayers of cells at 100% confluence to increasing concentrations of the drugs, diluted in HeLa cell infection medium, for 24h. The number of cells remaining in 10 random FOVs, at 63x magnification, was quantified by epifluorescence. (described in **Section 2.5.3**) A final working concentration, which more than 75% of cells could survive for 24h, was selected and used for treatment of infected cells (**Table 2.2**).

	500nM	1µM	5µM	10µM
chloride ionophore I†	77±12	76±14	66±20	40±10
ionomycin†	84±14	76±24	70±24	54±13
monensin†	78±5	76±7	45±11	30±8
nigericin†	81±14	77±14	72±15	45±10
valinomycin†	76±19	75±12	64±17	38±11
	1µM	**5µM**	**10µM**	**50µM**
glibenclamide†	89±19	77±12	76±13	48±15
doxycycline*	102±4	93±18	83±11	72±13

Table 2.2. Drug titrations. Average percentage of cells from 10 FOVs remaining on a coverslip, as a percentage of an untreated control condition, following 24h of exposure to compounds at given concentrations. * solubilised in dH_2O, † solubilised in DMSO. Shaded figures indicate concentrations used for experiments.

2.3.3 Treatment conditions

Cell monolayers, seeded at appropriate confluence for each experiment (**Table 2.1**), were infected as described in **Section 2.2.1**. At appropriate time points infection medium was removed and cells were treated with working concentration of drugs (**Table 2.2**) diluted in HeLa cell infection medium and, unless otherwise stated, were incubated at 37°C with 5% CO_2 in a humidified incubator for the duration of the experiment.

In experiments that required the removal of drugs from cells, treatment medium was discarded at specified times, monolayers were then washed in excess DMEM and

medium was replaced with HeLa cell infection medium for the remainder of the experiment.

2.4 Labelling for Fluorescence microscopy

2.4.1 Sample preparation for fixed microscopy

Where appropriate cells were fixed using the method established to produce the best images by confocal microscopy. For antibody specific fixation methods see **Table 2.3**.

2.4.1a Paraformaldehyde (PFA) fixation

Solutions:

- phosphate buffered saline (PBS) – 137mM NaCl, 2.7mM KCl, 8mM Na_2HPO_4, 1.46mM KH_2PO_4 in deionised water at pH7.4
- PFA – 4% (w/v) PFA in PBS
- neutralisation buffer – 50mM NH_4Cl in PBS

Growth medium was removed and cells were fixed in PFA for 30min at room temperature (RT) before addition of an equal volume of neutralisation buffer and incubated at 4°C for 1h. Cells were then washed in excess PBS prior to permeabilisation either in a 1:1 (v/v) mix of methanol:ethanol at 4°C for 5min or 0.5% (v/v) Triton X-100 (Sigma Aldrich, St Louis, MO, USA) in PBS for 15min at RT

prior to all antibody labelling (for antibody specific permeabilisation methods see **Table 2.3**).

2.4.1.b Methanol fixation

After removal of growth medium cells were incubated with methanol at -20°C for 10min prior to washing in PBS. Methanol fixed cells do not require a permeabilisation step.

2.4.1.c Methanol:Ethanol fixation

After removal of growth medium cells were incubated with an equal mix of methanol:ethanol (v/v) at 4°C for 5min prior to washing in PBS. Methanol:ethanol fixed cells do not require a permeabilisation step.

2.4.2 Inside/outside labelling of bacteria

To differentiate between internal and external bacteria PFA fixed cells were labelled using fluorescein isothiocyanate (FITC) conjugated anti-*Chlamydia* spp. primary antibody (**Table 2.3**) before permeabilisation using methanol:ethanol. A second round of antibody labelling, using anti-*Chlamydia* spp. antibody (**Table 2.3**) and an appropriate AlexaFluor® secondary antibody (**Table 2.4**) was then carried out.

2.4.3 Sample preparation for live microscopy

Solutions:

- live microscopy medium – high glucose Dulbecco's modified eagle medium without phenol red (DMEM-PR), 1x GlutaMAX supplement, 10% FBS (All from Gibco, Invitrogen, Carlsband, CA, USA)

Following experiments, growth medium was removed from cells that had been seeded in either LabTek chambers or glass bottomed petri dishes. Cells were washed with DMEM-PR to remove any traces of phenol red, which could otherwise interfere with fluorescence emissions. Media was replaced with live microscopy media for all labelling steps.

2.4.4 Antibody labelling

- blocking buffer – 1% (w/v) bovine serum albumin (BSA) (Sigma Aldrich St Louis, MO, USA) in PBS

- washing buffer – 0.1% (w/v) BSA in PBS

All primary antibodies were diluted in blocking buffer and incubated with cells using conditions shown in **Table 2.3**.

target	host	source	fixation/ permeabilisation	stock (mg/ml)	dilution
caspase-1	rabbit	Millipore	4% PFA / Triton X-100	0.2	1:50
Chlamydia* spp.-FITC conjugate	mouse	Argene (Now BioMérieux)	4% PFA / methanol:ethanol	-	1:200
Chlamydia* spp.	mouse	Argene (Now BioMérieux)	4% PFA / methanol:ethanol	-	1:200
giantin	rabbit	Covance	methanol	-	1:500
calreticulin	rabbit	Thermo Scientific	4% PFA / methanol:ethanol	-	1:150

Table 2.3. Primary antibodies. Asterisk (*) indicates antibodies discontinued by the manufacturer.

An antibody isotype control for *Chlamydia* spp. MOMP/LPS antibody was carried out using mouse Immunoglobulin G (IgG) isolated from normal mouse serum (described in **Section 2.4.4**). IgG was diluted in blocking buffer and incubated with infected cells according to the conditions used with anti *Chlamydia* spp antibody, as described in **Table 2.3**. Cells were then washed in PBS followed by washing buffer and incubated with appropriate secondary antibody for 1h at RT, washed in PBS followed by washing buffer and then mounted (**Figure 2.1 A-B**).

Following primary antibody incubation coverslips were washed in PBS followed by washing buffer and allowed to dry before application of secondary antibodies. All AlexaFluor® secondary antibodies were purchased from Molecular Probes (Invitrogen, Carlsband, CA, USA). For fluorescene excitation and emission information see **Table2.4**. All secondary antibodies were checked for cross reactivity by incubating with fixed cells in the absence of any primary antisera (**Figure 2.1 C**).

2.4.5 Isolation of mouse IgG from serum

Solutions:

- binding buffer - 20mM sodium phosphate pH8.0
- elution buffers (at decreasing pH from 7.5 [1] to 3.0 [10] at intervals of 0.5) – 0.1M sodium citrate pH7.5(1) - 3.0 (10)
- neutralisation buffer – 1M Tris(hydroxymethyl)aminomethane (Tris)-HCl pH9.0

Specificity of Argene anti *Chlamydia* spp. for each serovar and cell line used was assayed using IgG isolated from mouse serum. Normal mouse serum (Invitrogen, Carlsbad, CA, USA) was added at a ratio of 2:1 to binding buffer and adjusted to pH8.1. A HiTrap protein A column (GE Healthcare, Buckinghamshire, UK) was prepared by equilibrating the column with 10ml binding buffer at 1ml/minute before loading the serum. The column was then flushed through with 10ml binding buffer until no material was visible in effluent. The column was then washed with 1.5ml of each elution buffer with increasing acidity. Flow through was collected in 250μl fractions

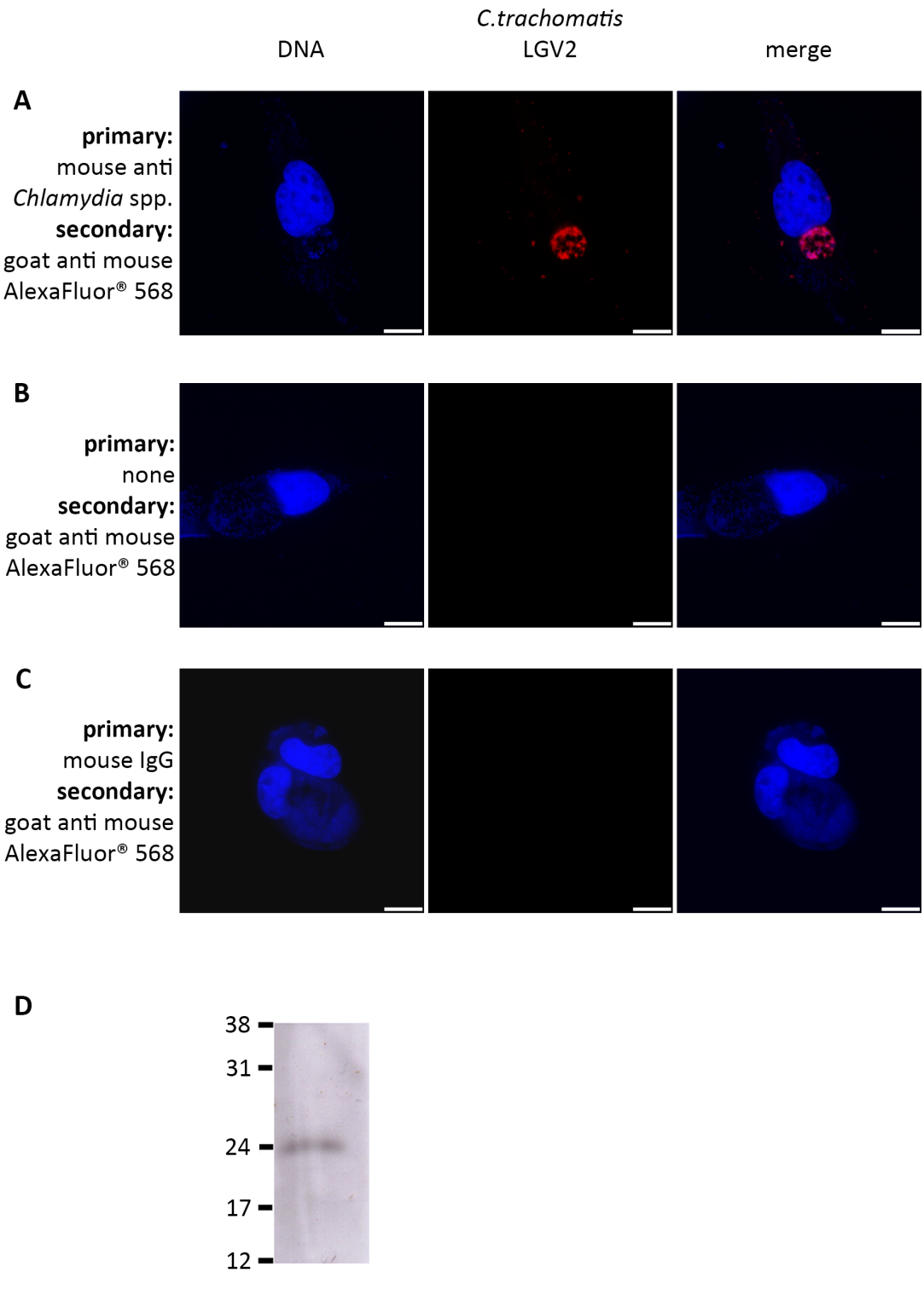
C.trachomatis
DNA
LGV2
merge
A
primary:
mouse anti
Chlamydia spp.
secondary:
goat anti mouse
AlexaFluor® 568
B
primary:
none
secondary:
goat anti mouse
AlexaFluor® 568
C
primary:
mouse IgG
secondary:
goat anti mouse
AlexaFluor® 568
D
38
31
24
17
12

Figure 2.1. Antibody labelling controls. (A-C) Confocal xy-sections of *C.trachomatis* LGV2 infected HeLa cells fixed at 24hpi with methanol:ethanol (v/v) prior to DRAQ-5 DNA labelling (blue) and co-stained with (A) *Chlamydia* spp. MOMP/LPS specific antibody and AlexaFluor®568 conjugated secondary antibody (red) (B) AlexaFluor®568 conjugated secondary antibody only (C) mouse IgG purified from serum followed by AlexaFluor®568 conjugated secondary antibody. Scale bars, 10μm. (D) Mouse IgG purified from normal mouse serum identified by Western blot using goat anti-mouse horseradish peroxidase-conjugated secondary antibody. Molecular weight markers are indicated in kDa.

and neutralised before being assayed for protein content using a Nanodrop 2000 spectrophotometer (Thermo-Fischer, Leicestershire, UK). All immunoglobulin containing samples eluted at the same pH were pooled and all fractions without detectable protein were discarded. IgG eluted at pH 4.5 (elution buffer 7) were pooled and tested for quality using a Western blot (described below in **Section 2.10. Figure 2.1D**).

2.4.6. Mounting fixed samples

Solutions:

- MOWIOL mounting medium (MOWIOL) - PBS, 20% (w/v) MOWIOL 4-88 (Sigma Aldrich, St Louis, MO, USA), 30% (v/v) glycerol

Glass microscope slides were washed in excess ethanol to remove any residual dirt or grease and allowed to dry. Once fixed cells were appropriately labelled, coverslips were washed in PBS and allowed to air dry for 10min. A 10μl drop of MOWIOL per coverslip was applied to clean glass slides and dried coverslips were placed cell side down into the MOWIOL. This was then allowed to polymerise at RT for 30min prior to storage at 4°C.

2.4.7 Fluorescent probes

For emission and excitation wavelengths for each fluorescent probe used see **Table 2.4**.

2.4.7.a Asante potassium green-2 acetoxymethyl ester (AM ester) (APG-2) (TEFLabs, Austin, TX, USA)

50μg of APG-2 was reconstituted in 45μl DMSO to yield a 1M stock solution. A working solution of 1mM was achieved by diluting stock in live microscopy medium before addition to live cells. Cells were then incubated at 37°C for 30min before washing with DMEM-PR. Fresh live microscopy medium was then added for the duration of the imaging experiment.

2.4.7.b BODIPY® Texas Red (TR) Glibenclamide (Molecular Probes, Invitrogen, Carlsband, CA, USA)

100μg of BODIPY TR Glibenclamide was diluted in 110μl DMSO to yield a 1mM stock solution. A working solution of 500nM was achieved by diluting stock in live microscopy medium before addition to live cells. Cells were then incubated at 37°C for 30min before washing with DMEM-PR. Fresh live microscopy medium was then added for the duration of the imaging experiment.

2.4.7.c 4',6-diamidine-2'-phenylindole (DAPI) (Roche, Indianpolis, IN, USA)

10mg of DAPI was diluted in 10ml deionized water to yield a 1mg/ml stock solution. A working solution of 1μg/ml was achieved by diluting stock in PBS before addition to fixed, permeabilised cells, either alone or in combination with antibodies. Cells were incubated for 15min at RT protected from light before washing in excess PBS.

2.4.7.d 1,5-bis{[2-(di-methylamino)ethyl]amino}-4,8-dihydroxyanthracene-9, 10-dione (DRAQ-5) (Abcam, Cambridge, UK)

5mM stock solution of DRAQ-5 was diluted to 5μM working solution in PBS before addition to fixed cells and incubated at RT for 30min before washing in excess PBS. For live microscopy a 25μM working solution was added to live cells. Cells were then incubated at 37°C for 30min before washing with DMEM-PR. Fresh live microscopy medium was then added for the duration of the imaging experiment.

2.4.7.e BisBenzimide H 33342 trihydrochloride (Hoechst) (Sigma-Aldrich, St Louis, MO, USA)

100mg of Hoechst was diluted in 10ml deionised water to yield a stock solution of 10mg/ml. A working solution of 1μg/ml was achieved by diluting stock in live microscopy medium before addition to live cells. Cells were then incubated at 37°C for 30min before washing with DMEM-PR. Fresh live microscopy medium was then added for the duration of the imaging experiment.

2.4.7.f MitoTracker® orange (Molecular probes, Invitrogen, Carlsband, CA, USA)

50μg of Mitotracker Orange was reconstituted in DMSO to yield a 1mM stock solution. A working solution of 50nM was achieved by diluting stock in DMEM before addition to live cells and incubation at 37°C for 45min. Cells were then

washed with DMEM before fixation with warm 4% PFA in DMEM for 20min at 37°C.

2.4.7.g Wheat germ agglutinin AlexaFluor® 594 conjugate (WGA) (Molecular Probes, Invitrogen, Carlsband, CA, USA)

5mg of WGA was diluted in 5ml of PBS to yield a 1mg/ml stock solution. A working concentration of 5μg/ml was achieved by diluting stock in PBS before addition to fixed cells prior to permeabilisation. Cells were incubated at RT for 15min protected from light. Cells were then washed 3 times in excess PBS before permesabilisation and further labelling.

2.4.8 Transfection

Transfection medium was prepared by adding 0.7μl Turbofect (Fermentas, Thermo-Fischer, Leicestershire, UK) to DMEM followed by 150ng DNA (For plasmids see **Appendix 3**). Medium was vortexed thoroughly and incubated at RT for 15min. 50μl transfection medium was added per 500μl media to adherent cells at 70% confluence. When transfecting infected cells, *Chlamydiaceae* infection protocol was carried out, and transfection media was prepared during infection incubation period in order to be added to cells when medium was changed after 90min incubation.

	target	source	excitation (nm)	emission (nm)
AlexaFluor 488		Molecular Probes	499	519
AlexaFluor 568		Molecular Probes	579	603
APG-2	potassium ions	Teflabs	488	540
BODIPY-TR glibenclamide	K_{ir}SUR potassium channels	Molecular Probes	589	615
Chlamydia* spp. FITC conjugate	*Chlamydia*	Argene (Now BioMérieux)	495	519
DAPI	DNA	Roche	345	455
DRAQ-5	DNA	Abcam	647	681-697
GFP			488	507
Hoechst 33342	DNA	Sigma-Aldrich	345	478
MitoTracker orange	mitochondria	Molecular Probes	554	576
mCherry			587	610
WGA Alexafluor 594	plasma membrane	Molecular Probes	591	618

Table 2.4. Fluorescence excitation and emission wavelengths. *indicates products discontinued by manufacturer.

2.5 Microscopy

2.5.1 Fixed confocal microscopy

All confocal microscopy of fixed samples was undertaken using a Leica Sp5 confocal microscope (Leica, Mannheim, Germany) equipped with a 65mW Argon laser, 1mW HeNe 543 laser and a 10mW HeNe 633 laser with Acousto optical beam splitting between 400nm and 800nm. Unless otherwise stated, all images were obtained using a 63x oil emersion objective and z-stack slices were taken at 0.33μm intervals at 1024x1024 resolution with 400Hz scanning speed. All images were obtained from a 3 frame average.

2.5.2 Live confocal microscopy

All live microscopy experiments were undertaken on cells seeded to 30% confluence in 4 well Labtek chambers (Nunc, Thermo-Fischer, Leicestershire, UK) (**Table 2.1**). Images were recorded manually at appropriate timepoints using the Leica Sp5 described above.

2.5.3 Epifluorescence microscopy

DAPI labelled samples were imaged using the Leica Sp5 confocal microscope (described above) using a mercury lamp and an appropriate excitation filter.

2.5.4 Time-lapse microscopy

All time-lapse experiments were imaged using an Olympus Total Internal Reflection 1X81 confocal microscope, which has a UV laser for 405nm excitation and SIM scanner to allow simultaneous excitation and detection with FV10-ASW viewer. Time-lapse experiments were undertaken over 6h periods with images taken every 10min at 63x magnification. Cells, seeded to 30% confluence in 35mm glass bottomed petri dishes (See **Table 2.1**), were maintained at 5% CO_2 on a stage heated to 37°C. The microscope was fitted with vertical drift compensation.

2.5.5 Fluorescence recovery after photobleaching (FRAP)

Cells for FRAP analysis were seeded at 30% confluence in glass bottomed LabTek chambers (Nunc, Thermo-Fischer, Leicestershire, UK). Cells were infected and labelled with APG-2. Using the Leica FRAP wizard, points of interest were bleached with argon and 488 lasers set at 100%. Images were taken at with a scanning speed of 1000Hz for minimised intervals for 10 frames and then at 20s intervals for 20 frames (for FRAP wizard settings see **Appendix 5**). Images were obtained at a resolution of 1024x1024 from a 3 frame average.

2.5.6 Fluorescence intensity comparisons

For timelapse and FRAP experiments fluorescence intensity was measured using ImageJ (for macro used see **Appendix 4**). Average pixel intensities for regions of interest (ROIs) were calculated for each frame and corrected for background

fluorescence using an area within the FOV with no cells present, and photobleaching, using an uninfected cell nucleus from within the FOV (**Equation 3**).

$$\text{fluorescence intensity} = \frac{(\text{average}_{ROI}) - (\text{average}_{\text{background}})}{(\text{average}_{NI}) - (\text{average}_{\text{background}})}$$

Equation 3. Fluorescence intensity calculation. (average_{ROI}) mean pixel intensity of ROI area. ($\text{average}_{background}$) mean pixel intensity of background area. (average_{NI}) mean pixel intensity of non infected cell nucleus.

2.6 Bacteria infectivity assay

Chlamydia is an obligate intracellular bacterium, which makes quantification of infectious bacterial progeny very difficult. Similar to IFU calculations described previously, an approximate IFU/ml value was calculated based on the number of inclusions observed in a monolayer of cells infected with bacteria collected from treated cells at appropriate time points (**Figure 2.2**).

2.6.1 Sample preparation

Cells were plated to 100% confluence and infected following *Chlamydiae* infection protocol (**2.2.1**). Following treatments, infection medium was removed before cells and bacteria were collected by scraping into SPG buffer. Cells were then frozen at -80°C.

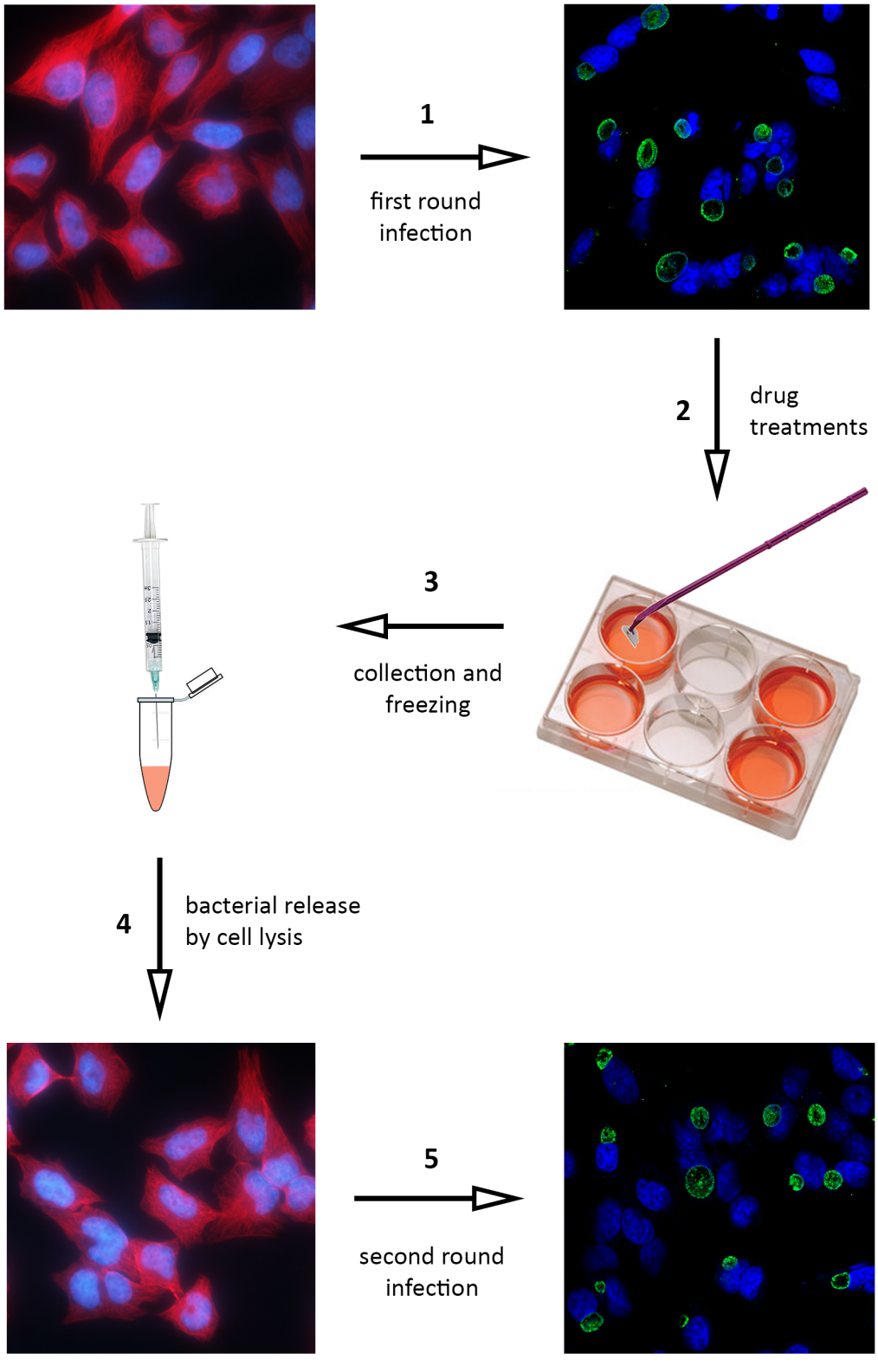
1
first round
infection
2
drug
treatments
3
collection and
freezing
4
bacterial release
by cell lysis
5
second round
infection

Figure 2.2. Schematic representation of bacterial infectivity assay. HeLa cell monolayers were infected (1) prior to drug treatments for appropriate duration (2). Cells were then collected by scraping and frozen at -80°C (3). Cells were then lysed into fresh infection medium, to release bacteria, and used to infect a new monolayer of HeLa cells (4). Second round infection was then allowed to proceed for 24h before cells were fixed and labelled for IFU quantification (5).

2.6.2 Second round infection

HeLa cells were seeded to 70% confluence on glass coverslips. Collected cells were defrosted on ice and diluted 1:100 in HeLa cell infection medium. Bacteria were released by flushing medium repeatedly through a 23g needle. Bacteria were then centrifuged onto cells at 900rpm using a Rotina 420R centrifuge (Hettich Lab, Technology, Tuttlingen, Germany) for 10min. Cells were then incubated at 37°C 5% CO_2 in a humidified incubator for 90min before replacing the infection medium to prevent reinfection. Cells were then incubated for 24h and fixed with 4% PFA.

2.6.3 IFU quantification

Fixed HeLa cells were labelled with DAPI and FITC conjugated anti *Chlamydia* spp. antibody and observed by epifluorescence. IFU/ml was quantified using **Equation 2**. By counting the number of cells and the number of inclusions in 10 FOVs an average number of infections across the coverslip can be calculated. This can be multiplied by the original dilution factor to obtain the IFU/ml from the inclusions collected from the treated inclusions.

2.6.4 Statistical analysis

For each experiment, the IFU was quantified using an average obtained from counting nuclei and inclusions from 10 FOVs. Statistical significance was determined, using the IFU calculated from each individual FOV, using the Mann-Whitney non-parametric *U* test. Each condition (group 2) was compared against an appropriate control condition (group 1). Individual IFU values were ranked (the lowest value was given a ranking of 1,

the next lowest a ranking of 2 *etc.*). Where values were identical, a mean ranking value was given to each. Rank totals for each group were tallied and calculated *U* values were obtained (**Equation 4**). Critical values for *U* are given in **Appendix 6**, and statistical significance was assigned when calculated $U \leq$ critical *U* for 0.05 significance level.

$$U = N_1 \times N_2 + N_x \times \frac{(N_x + 1)}{2} - T_x$$

Equation 4. Mann-Whitney *U* test. (U) calculated *U*. (N_1) Number of values in group 1. (N_2) Number of values in group 2. (N_x) Number of values in the group that gave the largest rank total. (T_x) largest rank total.

2.7 Flame Photometry

2.7.1 Photometer calibration

Changes in intracellular potassium concentrations following drug treatments were determined using flame photometry. Dr Anselm Zdebik (Department of Neuroscience at the Royal Free Hospital, London) kindly allowed us to use his Corning 400 flame photometer (Sherwood Scientific Ltd, Cambridge, UK). To determine the accuracy and range of the flame photometer, calibration solutions of potassium chloride diluted in deionised water were assayed by siphoning the sample into the photometer until the emission intensity at 766nm (Smith and Nesson, 1971) stabilised for 20s. An emission

intensity curve was then constructed and a lower threshold and saturation point established (**Figure 2.3**).

2.7.2 Sample preparation

700,000 HeLa cells were seeded per well of a 6 well plate and allowed to adhere for 24h at 37°C with 5% CO_2 prior to treatment. All drugs were used at the working concentrations shown in **Table 2.2** and incubated with cells for 6h. Following treatment, monolayers were washed in deionised water at 4°C before careful removal of all liquid. Cells were then incubated with 2ml of 0.5% (v/v) Triton X-100 (Sigma, Aldrich, St Louis, MO, USA), diluted in deionized water, on ice for 30min. Supernatants were collected and centrifuged at 13,000rpm using an Eppendorf 5424 benchtop centrifuge (Eppendorf, Hamburg, Germany) for 15min to remove cell debris. For each condition a second well of cells was seeded and treated on order to estimate the number of cells lysed into the samples collected. All samples used were within 1.3 $x10^6$ ± 0.1$x10^6$ cells, to enable appropriate comparison of potassium ion (K^+) concentrations in final samples. K^+ emission intensity was measured as described above and percentage K^+ loss calculated with reference to an untreated control population with a similar number of cells.

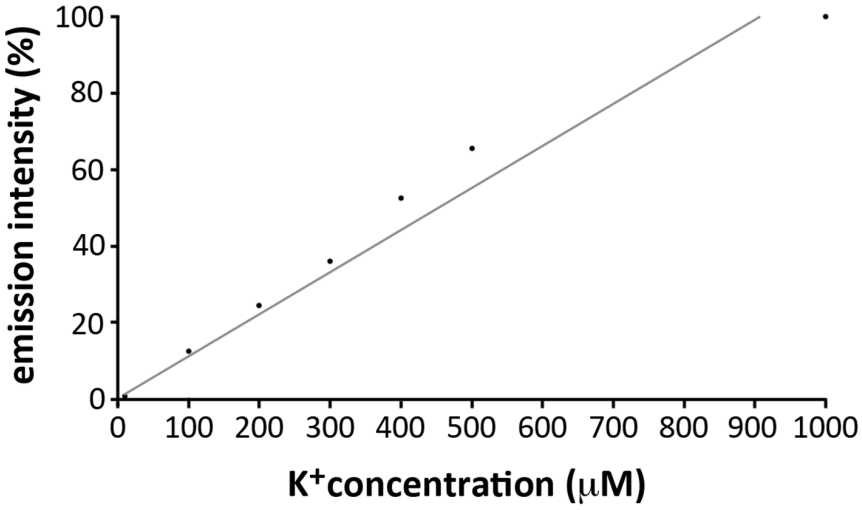
emission intensity (%)
100
80
60
40
20
0
0
100
200
300
400
500
600
700
800
900
1000
K+concentration (μM)

Figure 2.3. K^+ concentration calibration curve. Calibration solutions of KCl from 100-1000μM were assayed using flame photometry. Percentage emission intensity was recorded to determine the sensitivity of the assay and establish a saturation point.

2.8 Electron microscopy

2.8.1 Sample preparation

Solutions:

- fixation buffer – 0.1M sodium cacodylate trihydrate (caco) , 2.5% (w/v) gluteraldehyde, 0.05% malachite green in deionized water
- osmium tetroxide solution – 0.1M caco, 0.5% (w/v) OsO_4, 0.8% (w/v) potassium ferricyanide
- tannic acid – 0.05M caco, 1% (w/v) tannic acid
- uranyl acetate solution – 1% (w/v) uranyl acetate
- resin - agar, DDSA hardener, MNA hardner

HeLa cells were seeded on glass coverslips at 70% confluencey onto glass coverslips. Following *C.trachomatis* infection cells were fixed in fixation buffer for 2h at RT. Fixation buffer was then removed by washing 3 times in 0.1M caco before incubating for 30min with osmium tetroxide to increase contrast of final images. Samples were then post fixed in tannic acid for 1h, with a change of tannic acid solution after 10min in case of osmium precipitation. Samples were then washed twice in 0.1M caco and then twice in deionised water before negative staining with uranyl acetate for 1h, protected from light. Samples were then dehydrated and embedded using ethanol and resin dilution series (see **Table 2.5**) Samples were then incubated at 60°C for the

afternoon. BDHA accelerator was then added and the samples returned to the oven overnight.

dehydration	
EtOH (% in H_2O)	**Incubation**
25%	2x 2m
50%	2x 2m
70%	2x 2m
100%	4x 2m
embedding	
EtOH:resin	**Incubation**
3:1	15m
2:2	15m
1:3	15m
pure resin	overnight

Table 2.5. TEM sample dehydration and embedding dilution series. TEM samples were dehydrated using an increasing concentration of ethanol diluted in water. Samples were then embedded in increasing concentrations of resin diluted in 100% ethanol.

2.8.2 Sectioning

Hardened samples were sectioned using a Leica UC7 microtome. Blocks were trimmed using a cryotrim 45 diamond knife (Diatome, Hatfield, PA, USA) and 100nm ultra thin sections were cut using an Ultra 45° knife (Diatome, Hatfield, PA, USA). Sections were collected using a perfect loop (Diatome, Hatfield, PA, USA) and placed onto 400 square mesh copper grids (Agar scientific, Elektron Technology, Stanstead, UK).

2.8.3 Electron microscopy

Copper grids were imaged using a Tecnai 100kV electron microscope with a charged coupled device (CCD) camera.

2.9 Bacterial viability assay

2.9.1 Sample preparation

700,000 HeLa cells were seeded per well of a 6 well plate and allowed to adhere for 24h at 37°C with 5% CO_2 prior to treatment. All compounds were used at the concentrations shown in **Table 2.2** and incubated with cells for 50h.

2.9.2 Ribonucleic acid (RNA) isolation

RNA was isolated using RNeasy Mini Kit (Qiagen, Hilden, Germany) according to the manufacturers instructions.

Solutions:

- RLT – RNeasy lysis buffer
- RW1 – RNeasy wash buffer 1
- RPE – RNeasy wash buffer 2, 4 volumes ethanol

RNA was collected from cell monolayers using RNeasy mini kit (Qiagen, Hilden, Germany) according to manufacturers instructions. Cells were collected by scraping

into 350μl RLT and homogenized by flushing through a 23 gauge needle. An equal volume of 70% ethanol was added to cell lysate and mixed by pipetting. Lysate was then transferred to RNeasy spin column and centrifuged at 13,000rpm using an Eppendorf 5424 benchtop centrifuge (Eppendorf, Hamburg, Germany) for 15s and flow through was discarded. Column was then washed twice in RPE before RNA was eluted into RNase free water.

2.9.3 DNase treatment

Solutions:

- RDD buffer – DNase 1 Digestion buffer (Quiagen, Hilden, Germany)

RNA samples were treated for DNA contamination using 15 units of DNase 1 in 10% RDD buffer (Quiagen, Hilden, Germany) for 10min at RT before enzyme denaturation at 75°C for 10min. Concentration of samples was then determined using a Nanodrop 2000 spectrophotometer (Thermo-Fischer, Leicestershire, UK), using an absorption wavelength of 260nm.

2.9.4 Reverse transcription

Solutions:

- 10 x AffinityScript reverse transcription buffer (ART buffer) (Agilent Technologies, Santa Clara, CA, USA) – 500mM Tris-HCl pH8.3, 750mM KCl, 30mM $MgCl_2$
- 100mM Dithiothreitol (DTT) (Agilent Technologies, Santa Clara, CA, USA)

- 100mM dNTP mix – 25% dATP, 25% dCTP, 25% dGTP. 25% dTTP (Sigma Aldrich, St Louis, MO, USA)

For each RNA sample, a total of 500ng RNA was added to 300ng random primers (Sigma Aldrich, St Louis, MO, USA) and made up to 14.2μl in RNase/DNase free water (Gibco, Invitrogen, Carlsband, CA, USA). Samples were then incubated at 65°C for 5min then slowly cooled to RT to allow primers to anneal to RNA. Once cooled ART buffer was added, followed by a final concentration of 10mM DTT and 4mM dNTPs, before addition of AffinityScript multiple temperature reverse transcriptase (Agilent Technologies, Santa Clara, CA, USA). Mixture was then incubated at 25°C for 10min before temperature increase to 42°C for 1h. Reaction was then inactivated at 70°C for 15min. DNA templates were then stored at -20°C until PCR amplification.

2.9.5 PCR amplification

Solutions:

- 10x PCR buffer (Sigma Aldrich, St. Louis, MO, USA) – 10mM Tris-HCl pH 8.3, 500mM KCl
- 10mM dNTP mix – 10% dATP, 10% dCTP, 10% dGTP, 10% dTTP (Sigma Aldrich, St. Louis, MO, USA)
- Tris-Borate-EDTA (TBE) – 90mM Tris-base, 90mM boric acid, 2mM EDTA
- 2% agarose gel – TBE, 2% (w/v) agarose, 0.002% (v/v) ethidium bromide

- DNA loading buffer (New England BioLabs, Ipswich, MA, USA) - 2.5% Ficoll-400, 11mM EDTA, 3.3mM Tris-HCl pH8.0, 0.017% SDS, 0.015% bromophenol blue

For *C.trachomatis* 16SFW/ *C.trachomatis* 16SRV and Eukaryotic 18SFW/Eukaryotic 18SRV primers see **Appendix 1**. RNA samples were checked for cellular DNA contamination before and after DNase treatment using the 16S forward and reverse primers along side the DNA templates created by reverse transcription. For each condition 5μl DNA template was added to PCR buffer, 3mM $MgCl_2$ (Sigma Aldrich, St. Louis, MO, USA), 200μM dNTP mix, 2μl of both *C.trachomatis* 16SFW and *C.trachomatis* 16SRV primers and made up to 25μl with RNase/DNase free water (Gibco, Invitrogen, Carlsband, CA, USA) before addition of 0.25 units *Taq* DNA polymerase (Sigma Aldrich, St. Louis, MO, USA). For PCR conditions see **Table 2.6**. This was repeated for each of the samples using Eukaryotic 18SFW and Eukaryotic 18SRV primers. Resultant DNA samples were loaded into 2% agarose gels with a 2:1 ratio of sample to DNA loading buffer. 1.5μg 100bp DNA ladder (New England BioLabs, Ipswich, MA, USA) with a range of 100-1,500 base pairs was also added to the gels in DNA loading buffer. Gels were run in TBE at 100v for 45min. Gels were then imaged using the Gene Genius bioimaging system (Syngene, Cambridge, UK).

Initial denaturation:	95°C	10min
40 cycles:		
Denaturation	95°C	30s
Annealing	60°C	45s
Extension	72°C	45s
Final extension:	72°C	10min
Hold:	4°C	∞

Table 2.6. PCR amplification parameters. DNA was amplified using a GeneAmp PCR system 9700 thermal cycler (Applied Biosystems, Invitrogen, Carlsband, CA, USA) using the parameters described.

2.10 Western Blot

2.10.1 Sample preparation

Solutions:

- Laemmli buffer (x2) – 125mM Tris-HCl pH6.8, 20% (v/v) glycerol, 4% (w/v) sodium dodecyl sulphate (SDS), 20% (v/v) β-mercaptoethanol, 0.02% (w/v) bromophenol blue

700,000 HeLa cells were seeded per well of a 6 well plate and allowed to adhere for 24h at 37°C with 5% CO_2. Cells were then collected in 750µl versene (Gibco, Invitrogen) and counted before centrifugation at 13,000rpm for 15min using an Eppendorf 5424 benchtop centrifuge (Eppendorf, Hamburg, Germany). Pellets were then resuspended in 50µL Laemmli buffer per million cells and boiled at 100°C for 10min.

2.10.2 SDS- polyacrylamide gel electrophoresis (SDS-PAGE)

Solutions:

- 14% resolving gel – 14% (v/v) acrylamide, 0.375mM Tris-HCl pH8.8, 0.01% (w/v) SDS, 0.15% (v/v) ammonium persulphate (APS), 0.06% (v/v) tetramethylethylenediamine (TEMED)
- 5% stacking gel – 5% acrylamide, 0.25mM Tris-HCl pH6.8, 0.02% (w/v) SDS, 0.15% (w/v) APS, 0.1% (v/v) TEMED
- migration buffer – 25mM Tris-base, 192mM glycine, 0.1% (w/v) SDS

4.5ml resolving gel mixture was pipetted into a clean gel caster with 1.5mm spacers, covered with isopropanol and allowed to polymerise for 20min at RT. Isopropanol was then removed and any excess allowed to evaporate whilst stacking gel was prepared. Stacking gel was then layered on top of the resolving gel and a 15 well comb was inserted. Gel was then allowed to polymerise for 30min at RT. Samples were centrifuged for 15min at 13,000rpm using an Eppendorf 5424 benchtop centrifuge (Eppendorf, Hamburg, Germany) prior to loading 12μl of each sample into well of the polymerised gel. 3μL of 2mg/ml full range (12-225 kDa) rainbow weight marker (GE Healthcare, Buckinghamshire, UK) was loaded into the first well of each gel. Gels were run in migration buffer for approximately 2h at 30mA per gel.

2.10.3 Transfer

Solutions:

- transfer buffer – 3.7mM Tris base, 192mM glycine, 20% (v/v) ethanol
- Ponceau red - 0.1% (w/v) ponceau S, 20% acetic acid

Gels were incubated in transfer buffer with 6 sheets of 0.34mm Whatman blotting paper (Fisher Scientific, Leicestershire, UK) and a piece of nitrocellulose membrane at 4°C for 15min to equilibrate osmolarity and buffer temperature. Transfer cassettes were assembled with a sponge followed by three sheets of blotting paper then the gel, the membrane and another sheet of blotting paper. Air bubbles were removed by rolling a falcon tube across the top sheet of paper. Another two sheets of blotting paper were placed on top and rolled again to ensure there were no bubbles between the gel and the membrane. The second sponge was placed on top of the stack and the sandwich enclosed in the cassette. Protein was then transferred from the gel to the membrane overnight at 1.2W per cassette at 4°C. Following transfer the membrane was checked for protein bands with Ponceau red staining for 5min at RT and then destained using deionized water.

2.10.4 Development

Solutions:

- Tris buffered saline 0.05% (v/v) tween (TBST) – 20mM Tris HCl, 150mM NaCl, 0.05% tween

- blocking buffer – TBST with 5% (w/v) powdered milk
- ECL Solution A – luminol solution
- ECL Solution B – peroxide solution

Membranes were blocked in blocking buffer for 1h at RT. Antibodies were diluted in blocking buffer and incubated with membranes for 1h at room RT. Membranes were then washed for 1h in TBST before preparation for detection using Amersham ECL prime western blotting reagent (GE Healthcare, Buckinghamshire, UK) according to the manufacturer's instruction, briefly membranes were incubated with a 1:1 mixture of solution A and solution B for 2min at RT then dried thoroughly. Membranes were then exposed to Amersham ECL Hyperfilm (GE Healthcare, Buckinghamshire, UK) for appropriate time and film was developed using Xograph Compact X4 film developer (Xograph Healthcare, Stonehouse, UK).

Chapter 3 – Results

K^+ starvation during chlamydial replication induces persistence

3.1 Introduction

Replicating *Chlamydiae* actively control the environment within their membrane bound intracellular niche, termed the inclusion. The inclusion lumen is separated from the eukaryotic cytosol by a host-derived membrane, which is modified by the insertion of bacterial proteins (Scidmore *et al.,* 2003). Little is known about the composition of the intra-inclusion environment or the methods by which the bacteria maintain optimal growth conditions. Experiments using small molecule probes demonstrated that the inclusion membrane is apparently impermeable to molecules larger that 520 Da (Heinzen *et al.,* 1997). This is in contrast to the vacuoles of other intracellular pathogens, for example, the parasitophorus vacuole of the intracellular protozoa *Toxoplasma gondii*, which contains pores to allow the exchange of small molecules from 1300-1900 Da between the host and the parasite (Schwab *et al.,* 1994). Many other intracellular organisms, such as *Coxiella burnetii* (Heinzen *et al.,* 1996) and members of the *Mycobacterium* genus (Clemens and Horwitz, 1996; Halaas *et al.,* 2010), inhabit phagosomes and acquire nutrients from their host by interacting with recycling endosomes. Chlamydial inclusions remain largely segregated from endocytic compartments (Friis, 1972; Scidmore *et al.*, 2003). Nevertheless, inclusions actively intercept vesicles containing cholesterol and sphingomyelin (Carabeo *et al.,* 2003; Hackstadt *et al.,* 1996), *en route* from the Golgi apparatus to the plasma membrane, and have species-specific requirements for lysosomes as a method of amino acid uptake (Ouellette *et al.,* 2011).

Although numerous studies have investigated chlamydial nutrient acquisition from the host cell, very little data exists on the physical conditions within the inclusion and the methods of bacteria-host communication. A study by Grieshaber *et al.* (2002) used fluorescent ratiometric probes to determine both the pH and the cationic composition of the *C.trachomatis* LGV2 inclusion lumen 20h into the infection cycle. This was calculated to be pH7.25±0.19 using carboxy fluorescein diacetate (CFDA) and 7.25±0.26 using 2',7'-bis(2-carboxyethyl)-5,6-carboxyfluorescein acetoxymethyl ester (BCECF-AM), in both cases this was equivalent to the pH of the cytoplasm, calculated at 7.29±0.07 and 7.28±0.11 respectively. Similarly, the concentrations of the ions tested within the inclusion lumen were not significantly different from those in the host cytoplasm. Inclusion potassium ion (K^+) concentration was calculated at 148±9mM using potassium-binding benzofuran isophthalate (PBFI) potassium sensitive dye, only 2mM more than the calculated cytoplasmic K^+. Sodium ion (Na^+) concentration was determined to be 14±9mM within the inclusion and 21±4mM in the host cell cytoplasm using sodium-binding benzofuran isophthalate (SBFI). Fura-PE3-AM was used to determine calcium (Ca^{2+}) ion concentrations at 34±4nM within the inclusion and 42±3nM in the host cell. The similarity of the ionic composition of the inclusion lumen and host cell cytoplasm led the authors to suggest that the lack of a discernable ionic gradient across the inclusion membrane, and distortions of the inclusion during incubation with hypertonic sucrose solution, would indicate that inclusion turgor is maintained by osmotic pressure.

In eukaryotic cells inorganic ions not only maintain membrane potentials and pH but also act as signalling molecules. For example, K^+ efflux from cells in response to

pathogens such as *Bacillus anthracis* (Pétrilli *et al.,* 2007) and *Pseudomonas aeruginosa* (Lindestam Arlehamn *et al.,* 2010) activates inflammasomes, a protein complex responsible for initiation of an inflammatory response via caspase-1 processing of interleukin 1β. In prokaryotes, intracellular ions perform a diverse array of functions, for example, Hybiske and Stephens (2007) demonstrated that inhibition of Ca^{2+} fluxes at the end of the *C.trachomatis* infection cycle caused a significant delay in the rupture of the plasma membrane and consequent release of bacteria. The bacterial K^+ transport system Trk is necessary for host cell invasion by *Salmonella enterica*, indicating a role for K^+ in bacterial virulence (Su *et al.,* 2009). Other intracellular pathogens have been shown to utilise the relatively high intracellular K^+ concentrations to their advantage, for example, exposing *Plasmodium* sporozites to intracellular K^+ concentrations has been shown to increase infectivity between 4 and 10-fold depending on species (Kumar *et al.,* 2007).

The aim of this chapter is to determine the importance of inorganic ions in the *Chlamydia* inclusion, and to identify any role for these ions during the bacteria development cycle.

The *C.trachomatis* inclusion is easily damaged by physical manipulation, which has prevented comprehensive characterisation of the inclusion environment (Greishaber *et al.,* 2002). Instead, to further our understanding of the ionic environment within the inclusion, the impact of altering important ions during the *Chlamydia* infection cycle was assessed using compounds to specifically alter selected ion concentrations.

Ionophores are a class of lipid soluble molecules, some naturally occurring and others synthetic, which transport charged ions across membranes. There are two classes of ionophore; mobile ion carriers (**Figure 3.1 A**), which transport specific ions across membranes, and channel formers, which create pores in membranes to allow the movement of ions (**Figure 3.1 B**). Due to the need for specificity, mobile ion carriers will be used in this project. Mobile ion carriers are either cyclic peptides, or form cyclic complexes when bound to an ion, and are arranged with polar side chains directed inwards, generating a hydrophilic core. The size of the hydrophilic core lends binding selectivity to the ionophore, creating a ligand pocket sterically suited to a particular ion. Outwardly, the ionophore complex presents a hydrophobic surface in order to partition into biological membranes. Mobile ionophores will diffuse within a lipid bilayer and sequester an ion at a hydrophilic interface, simultaneously removing water molecules and forming a stable, hydrogen bonded ionophore-ion complex. This complex diffuses across the membrane to a second interface where the ion becomes rehydrated and the ionophore diffuses back into the membrane (Pressman, 1976) (**Figure 3.1 A**). Membrane potential electrophoretically drives ionophore diffusion to equilibrate ion concentrations across membranes (Pressman, 1976; Mollenhauer, 1990).

A

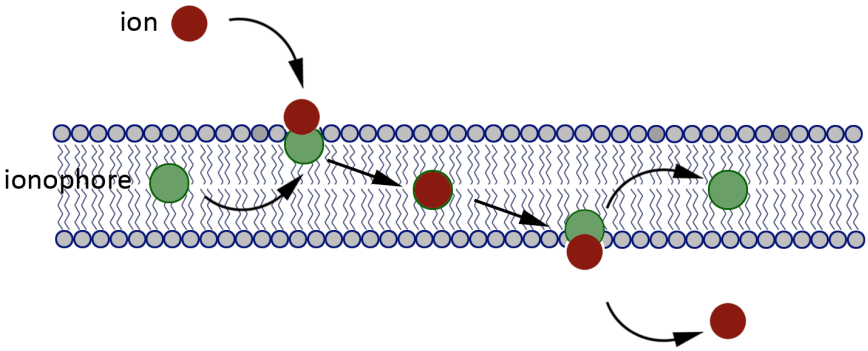

B

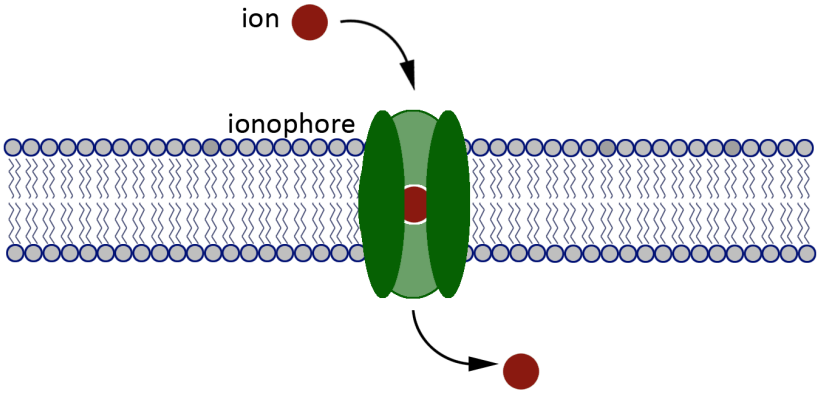

Figure 3.1. Schematic of ionophore mechanisms. (A) *Mobile ion carrier* – Lipid soluble ionophore (green) sequesters an ion (red) at a hydrophilic interface. The ion is hydrogen bonded to the hydrophilic core of the ionophore, which presents a hydrophobic exterior to allow diffusion through the membrane. At the second interface ion is re-hydrated ad released from the ionophore complex. (B) *Channel forming ionophore* – Ionophore (green) inserts a hydrophilic pore into membranes to allow diffusion of charged ions (red) through the hydrophobic membrane interior.

3.2 Reconstituting *Chlamydia trachomatis* serovar LGV2 infection *in vitro* using HeLa cells

Chlamydiae share a unique, biphasic infection cycle, much of which takes place within the inclusion, a parasitophorous vacuole established by the bacteria within host cells. The infection cycle, from bacteria entry to cell lysis, varies between serovars from 36 to 72h, and is dependent on cell line and culture conditions. Before experiments designed to assay alterations in the infection cycle could begin, the *C.trachomatis* LGV2 infection was reconstituted in cultured HeLa cells to observe the serovar specific cycle under the infection conditions that will be used for the remainder of the experiments (**2.2.1**). These data will establish a 'reference' infection cycle.

The progression of *C.trachomatis* LGV2 infection was visualised in fixed cells by fluorescence microscopy at 6h intervals from 1-66 hours post infection (hpi). Infected cells were incubated with AlexaFluor® conjugated wheat germ agglutinin (WGA) that selectively binds to N-acetylneuraminic acid and N-acetylglucosamine residues, which prior to cell permeabilisation labels the plasma membrane (**Figure 3.2A**). Following permeabilisation the bacteria were labelled with an antibody raised against *Chlamydia*-specific major outer membrane protein (MOMP)/lipopolysaccharide (LPS) and an AlexaFluor®-conjugated secondary antibody (**Figure 3.2A**). Elementary bodies (EBs), the infectious form of the bacteria, are approximately 0.3μm in diameter. At the resolution achievable by light microscopy, EBs can be distinguished from the replicative reticulate bodies (RBs) by size. RBs are approximately 1μm in diameter and exhibit a distinctive halo of MOMP and LPS staining, as indicated by the arrow in **Figure**

3.2A 12h. At the start of the infection EBs were observed in association with the HeLa cell plasma membrane (**Figure 3.2A** 1h). Following host cell invasion, bacterial entry vesicles are trafficked the perinuclear region of the host cell (Grieshaber *et al.,* 2003), and by 12hpi RBs are observed within an established inclusion (indicated in **Figure 3.2A** 12h). RBs can be seen clustered in a ring formation within the infected cell from 12-18hpi (**Figure 3.2A** 12h and 18h panels). This configuration of bacteria is consistent with previous observations that RBs replicate in contact with the inclusion membrane (Matsumoto, 1981; Wilson *et al*., 2009). From 30h onwards the RBs remain in a ring, but EBs are present within the inclusion lumen (indicated by the arrow in **Figure 3.2A** 30h), indicating that re-differentiation has initiated. At 48hpi the inclusion contains a higher proportion of EBs, however some RBs remain (**Figure 3.2A** 48h). Once the majority of the bacteria have differentiated into EBs, as shown in **Figure 3.2A** (60h), the bacteria are released from the host cell either by lysis or extrusion (Hybiske and Stephens, 2007) to propagate infection in new cells.

The point at which RB-EB re-differentiation begins to occur is difficult to determine by fluorescence microscopy alone. Instead, using the fact that EBs infect host cells and RBs do not, the number of EBs in a sample can be quantified by scoring the relative number of inclusions observed in a second monolayer of cells following infection with bacteria collected at the time of interest. The number of inclusions observed is directly proportional to the number of infection forming units (IFUs) (*i.e.* EBs) that were added to the monolayer (for a schematic of IFU quantification refer to **Figure 2.2**).

Bacteria collected at timepoints from 1 to 66hpi were used to illustrate the stages at which EBs were present in the sample and consequently to derive the time at which both EB-RB and RB-EB differentiation occurred. At 1hpi IFUs were recovered from cells, indicating that EBs were still present in the sample, and therefore that EB-RB differentiation was yet to be completed (**Figure 3.2B**). By 6hpi there were no inclusions observable in the cell monolayer, indicating that the bacteria present in samples at this time point were exclusively differentiated into the non-infectious RB form, and therefore EB-RB differentiation was complete by 6hpi under these assay conditions. From 6-24hpi there were no IFUs collected from cell monolayers, consistent with the bacteria replicating as RBs during this period. Recovery of IFUs at 30hpi indicated that RB-EB differentiation had begun, and therefore some of the bacteria in the inclusions had re-differentiated from RBs to EBs. This was consistent with the images obtained by fluorescence, in which RBs could be observed around the periphery of the inclusion and EBs within the inclusion lumen (**Figure 3.2A,** 30h). The titre of IFUs recovered from cells increased between 30-54hpi as differentiation continued. Peak infectivity was reached at 54hpi when the bacteria existed predominantly in the EB form but had yet to be released. IFU recovery from cells began to decrease from 60hpi onwards as EBs were released from mature inclusions into the extracellular medium to infect nearby cells.

These experiments demonstrate that the *C.trachomatis* LGV2 infection cycle in HeLa cells lasts approximately 54h. The inclusion was established and EB-RB differentiation was complete by 6hpi. RB replication continued for 24h until 30hpi, when RB-EB differentiation began to occur. Differentiation continues for a further 24h before

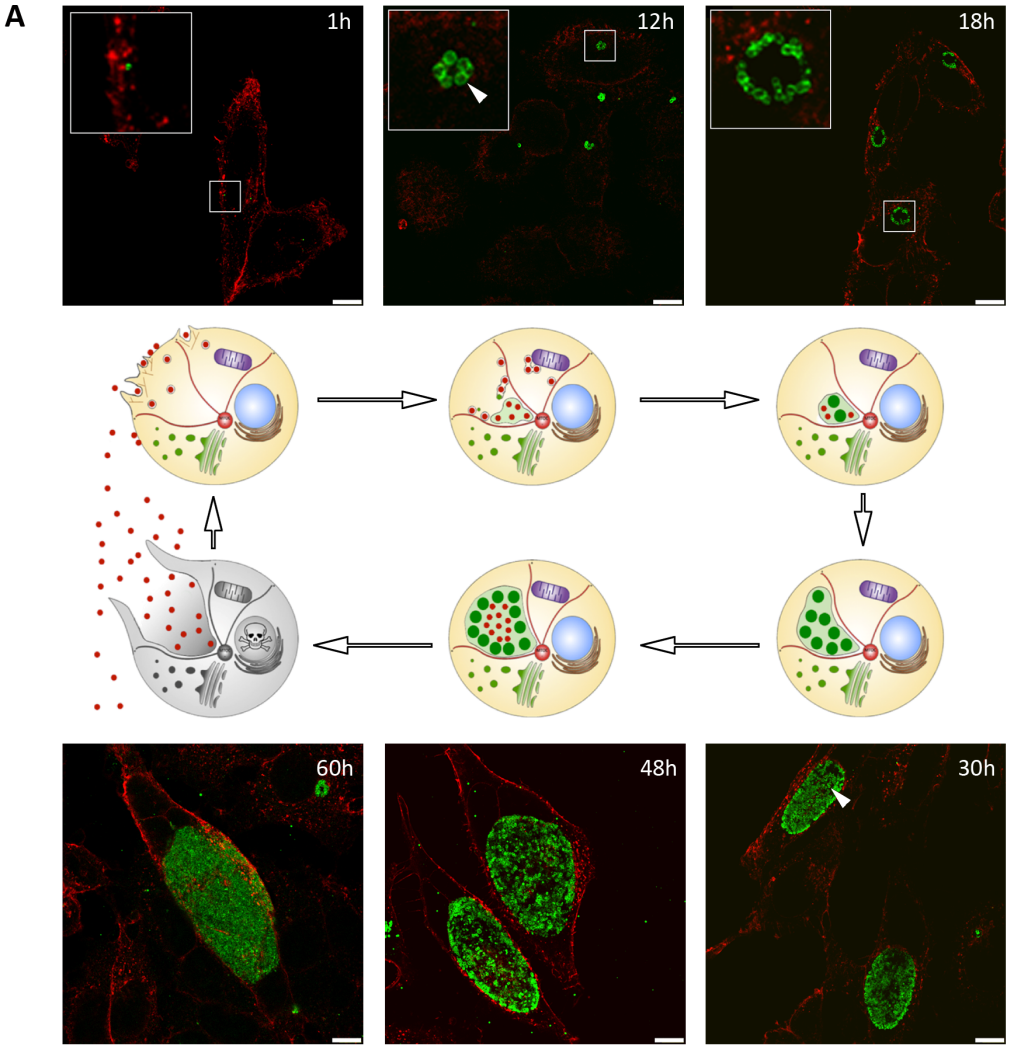
A
1h
12h
18h
60h
48h
30h

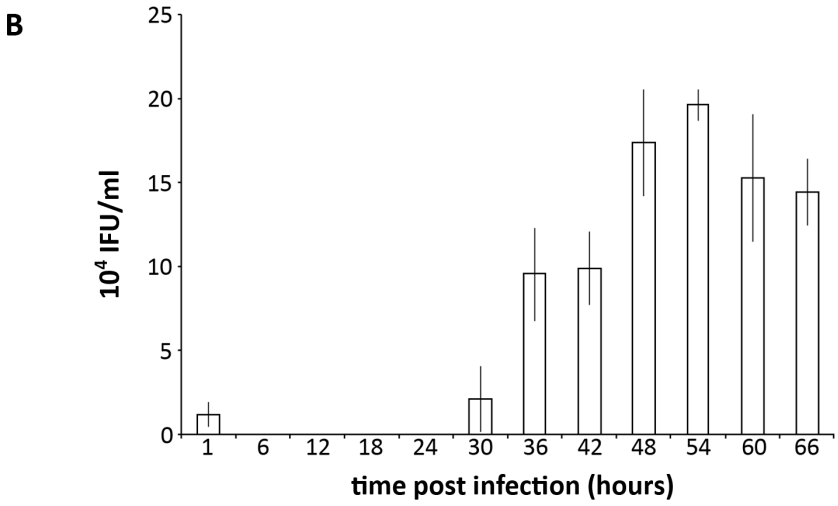
B
25
20
15
10
5
0
10^4 IFU/ml
1
6
12
18
24
30
36
42
48
54
60
66
time post infection (hours)

Figure 3.2. Reconstitution of *C.trachomatis* LGV2 infection cycle in HeLa cells. (A) The infection progression of *C.trachomatis* LGV2 was observed in HeLa cells (multiplicity of infection (MOI=1)). Confocal xy-sections (6h-48h) or confocal xyz-projection (60h) of the infection progression in cells fixed 1-66hpi, as indicated. Plasma membranes were labelled using AlexaFluor®594 conjugated WGA (red) prior to permeabilisation. Bacteria were labelled with *Chlamydia* spp. MOMP/LPS specific primary antibody followed by AlexaFluor®488 conjugated secondary antibody (green). White arrows indicate an RB (12h) and an EB (30h). Scale bar, 10μm. Insets show indicated areas at higher magnification. Schematic diagrams of the phases of the infection cycle are shown for comparison. EBs are shown in red, RBs are shown in green (see **Figure 1.4**). (B) Cell layers collected at appropriate time points after infection were diluted in fresh medium to infect a new layer of cells. After 24h, infected cells were fixed and labelled using anti-*Chlamydia* spp. fluorescein isothiocyanate (FITC)-conjugated antibody and 4', 6-diamidino-2-phenylindole (DAPI) DNA stain. Inclusion-forming units (IFUs) were then quantified (IFU/ml). Error bars show standard deviation.

bacteria began to be released from host cells. These approaches allow both quantitative and qualitative analysis of the infection cycle in the subsequent experiments.

3.3 Ionophore treatment of HeLa cells infected with *C.trachomatis* LGV2 implies a critical role for Na^+ and K^+ cations in bacterial development

Having characterised the *C.trachomatis* LGV2 development cycle in HeLa cells, conditions for the treatment of uninfected HeLa cells with ionophores were established and optimised. Loss of cells during treatment was minimised by titrating ionophore dilutions in growth medium to a concentration that could be tolerated by the majority of a population of cells (≥75%).

Ionophores, dissolved in dimethyl sulphoxide (DMSO), were added to confluent monolayers of HeLa cells at increasing concentrations from 500nM to 10μM. Cell loss after 24h of treatment was determined by counting the cells in 10 random fields of view (FOVs). The average number of cells remaining after each treatment, expressed as a percentage of the untreated control, are presented in **Table 3.1**. As incubation with a 1:1000 dilution of DMSO in growth medium (v/v) for 24h caused a loss of 23±8% of cells, DMSO-diluted ionophores did not exceed 0.1% to prevent excessive cell loss as a result of solvent exposure. Although these data do not reflect the activity of the compounds it is important that the treatments can be tolerated by the majority of cells. The ionophore working dilutions chosen for all subsequent investigations was the

highest that could be tolerated by at least 75% of cells, for chloride ionophore I (Cl^-I), ionomycin, monensin, and nigericin this was 1μM (for ionophore structures see **Appendix 2**). To ensure the working dilutions had limited adverse effects on the cells, nuclei were labelled using 4'6-diamino-2-phenylindole (DAPI), a DNA intercalating fluorescent dye (**Figure 3.3**). The morphology of cell nuclei was assessed to ensure that ionophores introduced at this concentration did not damage host cells by inducing apoptosis, indicated by condensation of the nucleus (as shown in **Figure 3.3** 10μM nigericin panel). Following 24h incubation with 1μM of each ionophore there was no significant morphological changes in the nuclei of HeLa cells, suggesting that the cells can tolerate ionophore treatment for 24h (**Figure 3.3**).

Titrating ionophore concentrations to a working dilution that can be tolerated by more than 75% of host cells ensures that any changes observed during the *C.trachomatis* LGV2 infection cycle in subsequent experiments are the result of alterations in ion concentrations.

Once these working concentrations had been established, the effect of ion disruption on the *C.trachomatis* infection cycle could be assayed, both qualitatively using microscopy, and by quantifying IFU recovery from infected cells.

HeLa cells were treated with ionophores at 12hpi, during the replication phase of the infection cycle, then fixed at 24hpi prior to labelling with anti *Chlamydia* antibody and an AlexaFluor® conjugated secondary antibody. DNA was then labelled using 1,5-bis {[2-(di-methylamino) ethyl] amino}-4,8-dihydroxyanthracene-9, 10-dione (DRAQ-5) a far-red fluorescent DNA-intercalating dye. Initially, infected cells were left untreated,

	500nM	1μM	5μM	10μM
chloride ionophore I	77±12	76±14	66±20	40±10
ionomycin	84±14	76±24	70±24	54±13
monensin	78±5	76±7	45±11	30±8
nigericin	81±14	77±14	72±15	45±10

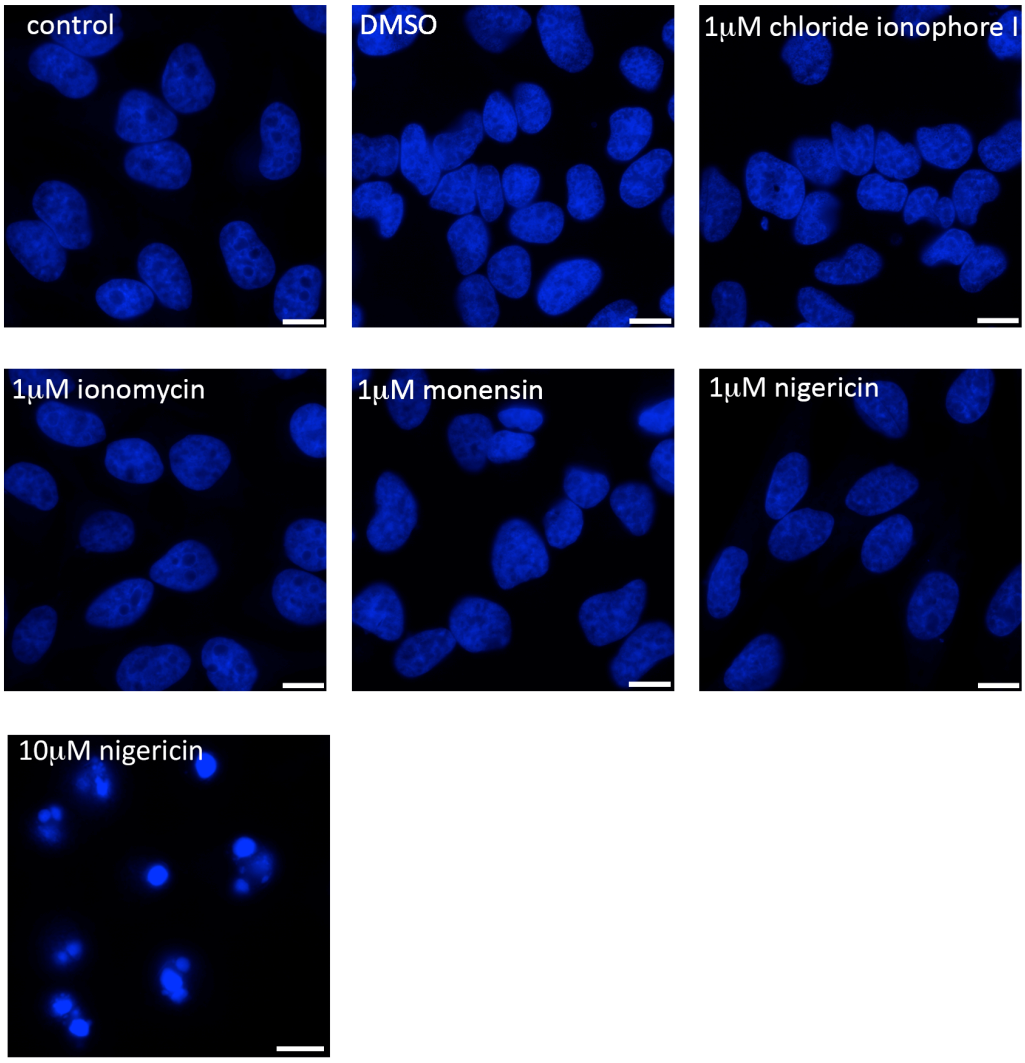

Table 3.1. Titrating ionophores to non-toxic working concentrations. HeLa cells were seeded at 100% confluence and treated with increasing concentration of ionophores. Toxicity was assessed by quantifying the average number of cells per coverslip as a percentage of an untreated control condition. Selected working concentrations are shaded in grey.

Figure 3.3. Assessment of cell nuclei following ionophore treatments. Fluorescence micrographs of untreated HeLa cells (control), and HeLa cells treated with either 1:1000 dilution of DMSO, 1μM chloride ionophore I (Cl^-I), 1μM ionomycin, 1μM monensin, 1μM or 10μM nigericin, as indicated, and fixed after 24h of treatment. Cells were then labelled with 4',6-diamidine-2'-phenylindole (DAPI) DNA stain. Scale bars, 7.5μm.

or incubated with a 1:1000 dilution of DMSO from 12hpi. When untreated and DMSO treated *Chlamydia*-infected cells were compared at 24hpi intracellular bacteria were evident within an inclusion adjacent to the host cell nucleus. Bacteria exhibit the distinctive halo of MOMP/LPS labelling associated with RBs, which is consistent with the replicative phase of the infection cycle (**Figure 3.4** compare control, and DMSO panels). This confirms that the solvent alone does not have a detectable effect on the *C.trachomatis* development cycle.

Cl^-I, a synthetic chloride ion (Cl^-) selective Mn(III) metalloporphyrin, which has a high affinity for chloride ions over nitrite (NO_2^-) and other monovalent anions (Huser *et al.,* 1990), causes the translocation of Cl^- ions across biological membranes (Garber *et al.,* 2005). When HeLa cells infected with *C.trachomatis* LGV2 were treated with Cl^-I at 12hpi, no effect on the morphology of the bacteria was evident when fixed cells were observed at 24hpi, when compared to the control conditions (**Figure 3.4** Cl^- panel). When infected cells were equivalently treated with ionomycin, a calcium (Ca^{2+}) ion specific ionophore produced by *Streptomyces conglobatus* (Liu and Hermann, 1978), RBs were observed within an inclusion indistinguishable to those present under control conditions (**Figure 3.4** Ca^{2+} panel). These data show that perturbation of the concentration of intracellular Cl^- or Ca^{2+} using ionophores at these concentrations during *C.trachomatis* LGV2 replication in HeLa cells has no discernible effect on bacteria or inclusion morphology.

Conversely, when HeLa cells infected with *C.trachomat*is LGV2 were treated with monensin at 12hpi, a Na^+ ionophore from *Streptomyces cinnamonensis* (Mollenhaur

1990), a dramatic effect on the bacteria was clearly evident. The LPS/MOMP antibody labelled abnormally shaped, large chlamydial bodies in fixed cells (**Figure 3.4** Na^+ panel). These bodies, which resemble aberrant bodies (ABs) observed during chlamydial persistence (reviewed by Hogan *et al.,* 2004), retained DRAQ-5 DNA labelling and remained perinuclear, but no longer consistently appeared in the ring formation characteristic of RBs replicating within the inclusion. Equivalent treatment with nigericin, an ionophore from *Streptomyces hygroscopicus* (Heisey and Putnam, 1986) selective for K^+ over Na^+ (Stern, 1977), also induced the formation of similar ABs (**Figure 3.4** K^+ panel). As with monensin treatment, the anti-*Chlamydia* antibody labelled bacterial bodies adjacent to the host cell nucleus, however they no longer formed the distinctive spherical inclusions expected at 24hpi. There were also fewer bodies within inclusions following K^+ and Na^+ ionophore treatments, suggesting replication had slowed or arrested. These data indicate that disruption of Na^+ or K^+ ion gradients during the replicative phase of the *C.trachomatis* LGV2 infection cycle has a profound effect on the bacteria.

The morphological changes in *C.trachomatis* LGV2 were observed during the replicative phase of the infection cycle, when the bacteria are exclusively in the non-infectious RB state. This means that the effect on the number or infectivity of bacterial progeny following ionophore treatment could not be assessed by IFU quantification at an equivalent timepoint. Instead, IFU quantification was undertaken at the end of the infection cycle, once RB-EB re-differentiation was complete. As described previously, during *C.trachomatis* LGV2 infection of HeLa cells RB-EB differentiation begins

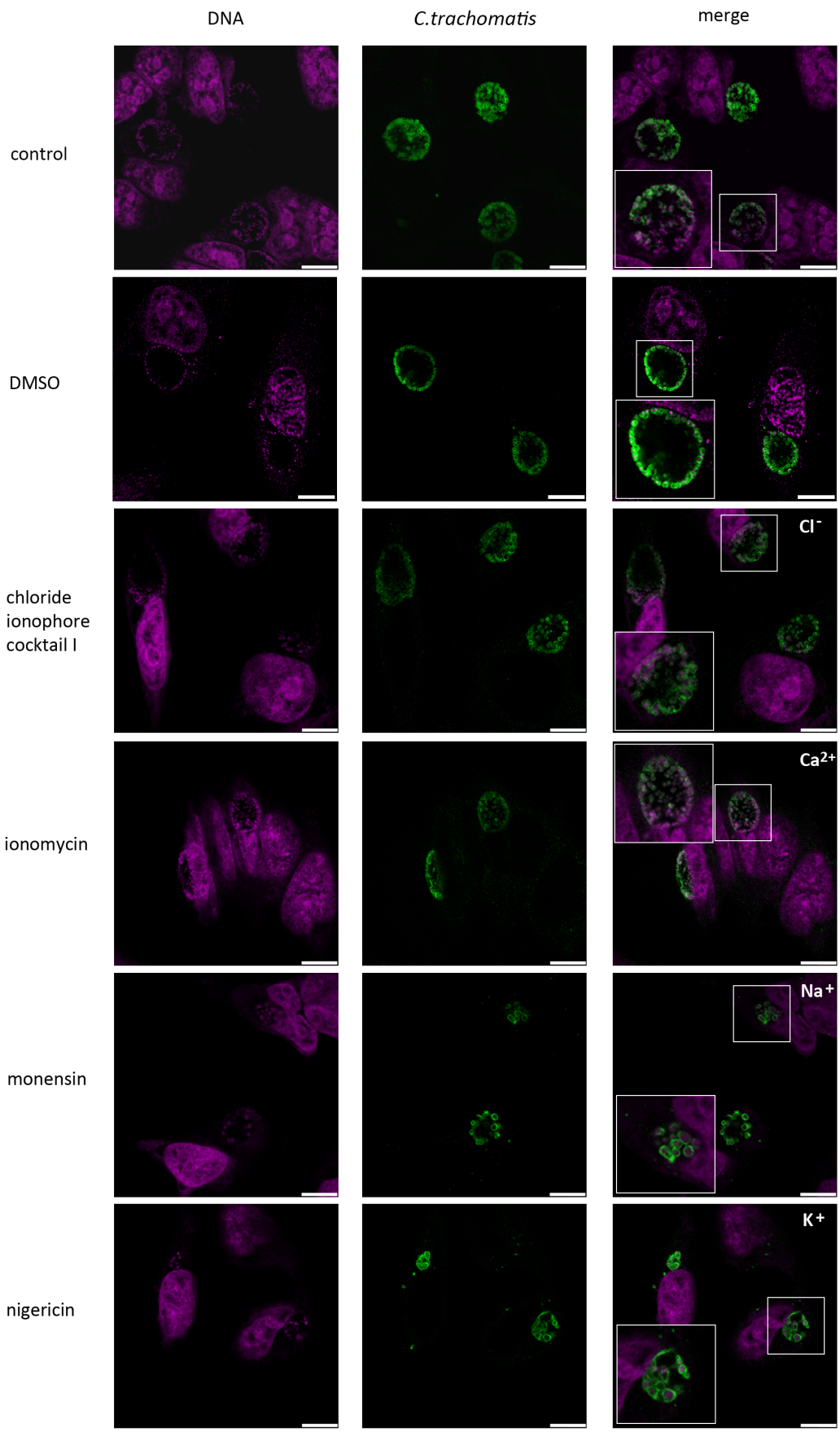
DNA
C.trachomatis
merge
control
DMSO
chloride ionophore cocktail I
ionomycin
monensin
nigericin
Cl⁻
Ca2+
Na+
K+

Figure 3.4. Monovalent cation specific ionophores dramatically alter intracellular *C.trachomatis* LGV2 morphology. Confocal xy-sections of *C.trachomatis* LGV2 infected HeLa cells (MOI=1) either untreated (control) or treated 12hpi with either 1:1000 DMSO, 1μM Cl^-I, 1μM ionomycin, 1μM monensin, or 1μM nigericin, as indicated. Cells were then fixed at 24hpi. Bacteria were labelled with *Chlamydia* spp. MOMP/LPS specific primary antibody followed by AlexaFluor®488 conjugated secondary antibody (green) and 1, 5-bis {[2-(di-methylamino) ethyl] amino}- 4, 8-dihydroxyanthracene-9, 10-dione (DRAQ-5) DNA label (magenta). Scale bars, 10μm. Insets show indicated areas at higher magnification.

approximately 30hpi and is completed by 54hpi. To ensure that samples contained predominantly EBs, bacteria were collected for quantification at 50hpi.

HeLa cells infected with *C.trachomatis* LGV2 were treated with Cl^-I, ionomycin, monensin, nigericin, or DMSO, each at 12hpi. Infection was allowed to progress until 50hpi when infected monolayers were collected (see **Figure 3.5A** for a schematic of the first round infection and collection stage of IFU quantification). IFUs were quantified for each sample following infection of a second cell monolayer and expressed as a percentage of the IFU/ml collected from untreated cells equivalently infected with *C.trachomatis* (**Figure 3.5B**).

Disruption of monovalent cations Na^+ or K^+ had a dramatic effect on the IFU titre. Treatment with either monensin or nigericin eliminated all the IFU from the samples (**Figure 3.5B** Na+ and K+). This loss of IFU suggests that the ABs observed by fluorescence microscopy following monensin or nigericin treatment are either non-viable or incapable of maturing into infectious EBs, either because re-differentiation is arrested, or because released progeny are incapable of establishing subsequent infections.

96±14% of control IFU was collected from Cl^-I treated cells, suggesting that disruption of Cl^- gradients from 12hpi until the end of RB-EB differentiation does not significantly impact the number of infectious progeny (**Figure 3.5B** Cl^-). These data suggest that the majority of *C.trachomatis* infections can tolerate Cl^- gradient disruptions, which is consistent with observations that bacterial morphology is unaffected by Cl^-I treatment during the replicative phase of the infection cycle.

Similarly, more than 92±13% of the control IFU was obtained following equivalent ionomycin treatment (**Figure 3.5B** Ca^{2+}). The relatively unchanged IFU value together with the normal inclusion morphology observed in fluorescent micrographs demonstrates that ionomycin treatment during the replicative phase of *C.trachomatis* LGV2 infection has an insignificant effect on the developmental cycle of the bacteria.

Following DMSO treatment there was no loss of IFUs collected from cells, confirming that prolonged exposure to the solvent did not cause excessive loss of cells (**Figure 3.5B** DMSO). This verifies that any observed decrease in IFU from ionophore treated conditions were the result of the treatment, and not cell loss due to exposure to the solvent.

As both monensin and nigericin collapse gradients of monovalent cations, the observed alteration of bacterial morphology and the development cycle could result from osmotic disruption or pH variation. However, this seems unlikely as perturbation of either Ca^{2+} or Cl^{-} ion concentrations had little effect on bacterial morphology or infectivity, suggesting that bacteria can withstand generic fluctuations in osmotic pressure and membrane potential. This implies that replicating *Chlamydia* have specific requirements for monovalent cations during the developmental cycle, however the data collected following nigericin or monensin treatments is insufficient to determine whether the alterations observed in bacterial morphology and development are the result of altering monovalent cation concentrations or if each specific ion has a distinct role during chlamydial development.

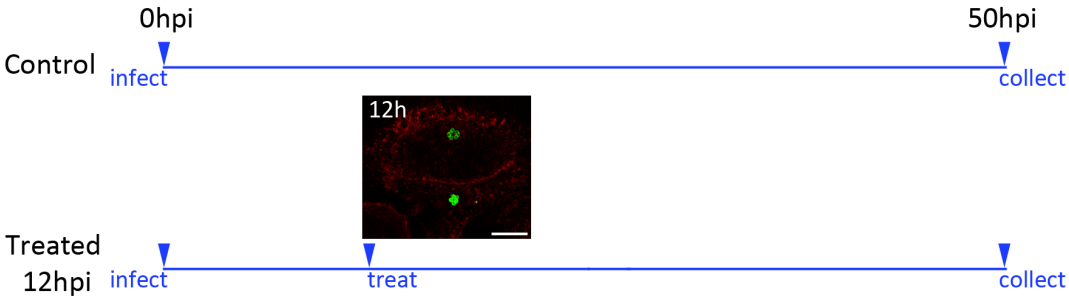
0hpi
50hpi
Control
infect
collect
12h
Treated
12hpi
infect
treat
collect

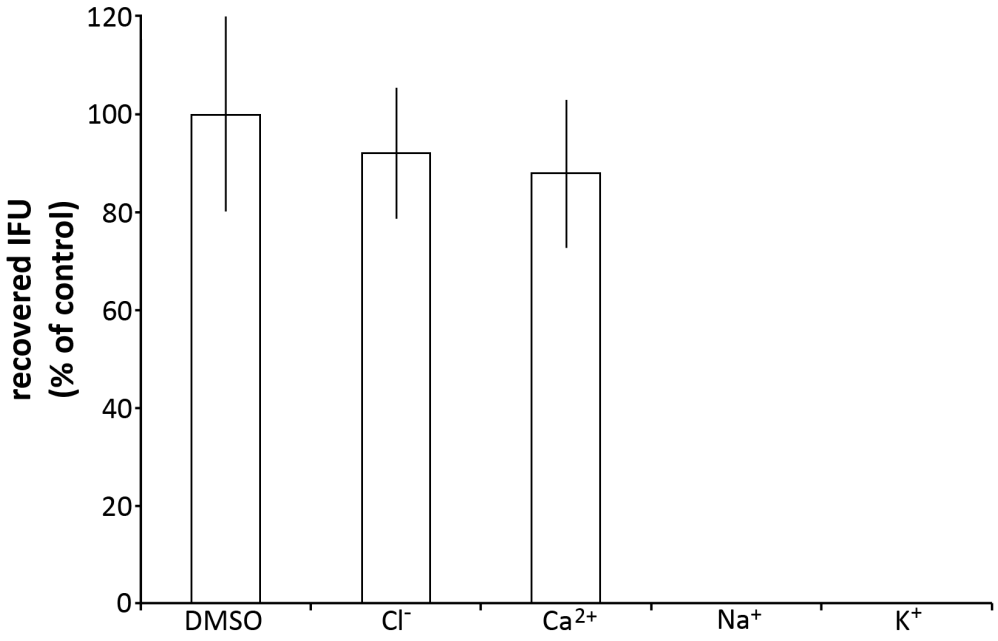
recovered IFU
(% of control)
120
100
80
60
40
20
0
DMSO
Cl-
Ca2+
Na+
K+

Figure 3.5. Treatment of *C.trachomatis* LGV2 infected HeLa cells with monovalent cation specific ionophores significantly reduces the titre of infectious bacteria. (A) Schematic representation of experiment timelines, showing a confocal xy-section of *C.trachomatis* (green) infection of HeLa cells (red) at the time of ionophore treatment. (B) *C.trachomatis* LGV2 infected HeLa cell layers (MOI=1), were treated at 12hpi and bacteria collected 50hpi. Recovered bacteria were diluted in fresh medium to infect a new layer of cells. After 24h, infected cells were fixed and labelled using anti-*Chlamydia* spp. FITC-conjugated antibody and 4', 6-diamidino-2-phenylindole (DAPI) DNA stain. IFUs were then quantified (IFU/ml) IFU/ml for each treatment is compared as a percentage of appropriate control conditions. Experiments were repeated a minimum of three times, and the data presented are representative of each iteration. Error bars show standard deviation. (* = $p \leq 0.05$).

3.4 Intracellular K^+ concentrations are reduced by treatment with either nigericin or monensin

To identify specific triggers for the abnormal development observed in both nigericin and monensin treated conditions, the effect of each of the treatments on host cells, at the concentrations used in the previous experiments, must be examined. Eukaryotic cells maintain a K^+ concentration of approximately 100mM, dependent on cell type, whereas the concentration of the extracellular milieu is much lower, usually 10mM or less (Su *et al.,* 2009). Consequently, using K^+ ionophores such as nigericin to equilibrate gradients across membranes reduces the concentration of available K^+ within cells. Conversely, intracellular Na^+ is normally maintained between 4-16mM compared to extracellular concentrations of approximately 140mM (Bers *et al.,* 2003), therefore Na^+ ionophore treatment causes an influx of Na^+ into the cell.

Selectivity of an ionophore for a specific ion is dependent on a number of factors, the most important being the respective sizes of the ion and the ion-binding site in the ionophore. Both sodium and potassium belong to the alkali metal group, meaning their ions behave in a very similar manner. Sodium is smaller than potassium, with dehydrated ionic radii of 0.95Å and 1.33Å respectively (Hille *et al.,* 1999). Therefore, the positively charged nucleus of a sodium ion has less shielding electron shells than that of a potassium ion. Consequently, the dehydration of Na^+ requires a much higher energy input, and generally Na^+ remains hydrated, increasing the ionic radius to similar dimensions to K^+, decreasing selectivity between Na^+ and K^+. As a result, monensin is only 10-fold more selective for Na^+ over K^+ (Mollenhauer *et al.,* 1990). Given that

nigericin is specific for K^+, but monensin is much less selective for Na^+, the effect of both treatments on intracellular K^+ concentration was assayed.

Flame photometry detects K^+ concentrations from 0.1-1mM in solution (for photometer calibration refer to **Figure 2.3**). Determining the K^+ concentration of a sample is achieved by measuring the emission intensity of a sample at 766.5nm (Smith and Nesson, 1971), the characteristic emission wavelength of K^+ as it is excited by being drawn through a flame. The emission intensity is directly proportional to the K^+ concentration of the sample (Smith and Nesson, 1971). This method was applied to analyse the intracellular K^+ concentration of HeLa cells treated with monensin or nigericin. $1.3 \times 10^6 \pm 0.1 \times 10^6$ cells were incubated with or without 1μM of monensin or nigericin as previously, and K^+ concentration was assayed using the flame photometer. Since equivalent cell numbers were lysed into equal volumes, the K^+ concentrations of the final solutions are comparable to one another. However, because the lysates must be diluted to assay K^+ within the detection range of the flame photometer (0.1-1mM K^+), an exact intracellular K^+ concentration is difficult to obtain without knowing the initial volume of the cellular contents. Relative K^+ concentrations are therefore presented in comparison to untreated cells (**Figure 3.6**). Monensin treatment reduced intracellular K^+ by 25%, compared to a 50% reduction following nigericin treatment. This shows that, due to poor selectivity for Na^+ over K^+, K^+ concentrations are also affected in monensin treated samples.

To identify the ionic alteration responsible for abnormal *C.trachomatis* LGV2 development, ionophores with greater affinities for Na^+ and K^+ should be used.

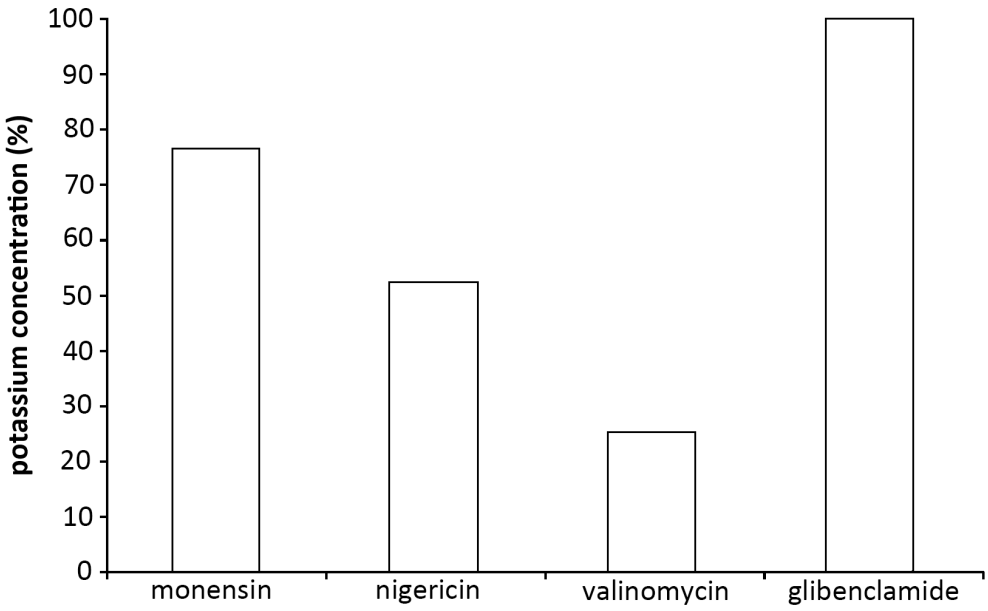
potassium concentration (%)
100
90
80
70
60
50
40
30
20
10
0
monensin
nigericin
valinomycin
glibenclamide

Figure 3.6. Quantification of intracellular K^+ following monensin, nigericin, valinomycin, and glibenclamide treatments. $1.3x10^6$ $\pm 0.1x10^6$ HeLa cells were treated for 12h with either 1μM monensin, 1μM nigericin, 1μM valinomycin (**Section 3.5**), or 10μM glibenclamide (**Section 3.7**). Cells were than lysed and K^+ concentrations were measured using flame photometer (emission intensity at 766.5nm). K^+ concentration is presented as a percentage of the emission intensity of an untreated control population of cells and is representative of each of the three iterations undertaken.

Unfortunately there are currently no Na^+ specific ionophores that would not perturb K^+ gradients to some extent. Nigericin is a K^+/H^+ exchange ionophore, which means that as K^+ is removed it is replaced with a hydrogen ion (H^+) (Nicholls, 2006). To ascertain whether aberrant *C.trachomatis* LGV2 development is the result of a K^+ efflux, and not due to an increase in either cytosolic or luminal pH, *C.trachomatis* LGV2 infected HeLa cells were treated with valinomycin, a K^+ uniporter that induces a K^+ efflux but does not affect H^+ (Nicholls, 2006).

3.5 Depletion of intracellular K^+ concentration disrupts *C.trachomatis* LGV2 development

The experiments presented so far have revealed a correlation between intracellular K^+ depletion and abnormal *C.trachomatis* LGV2 development. Nigericin treatment of HeLa cells 12hpi with *C.trachomatis* LGV2 induced the formation of ABs, which failed to produce infectious progeny at the end of the infection cycle.

Nigericin is a K^+/H^+ antiporter, and will therefore equilibrate both K^+ and H^+ concentrations across membranes. Valinomycin, which only alters K^+ concentrations without altering cellular H^+ concentrations, was used to assess whether K^+ depletion alone has an equivalent impact on *C.trachomatis* LGV2 development. Valinomycin is a cyclic dodecadepsipeptide produced by *Streptomyces fulvissimus* (Ristow *et al.,* 1974), which is 400 times more selective for K^+ over H^+ and Na^+ (Mueller and Rudin, 1967) (For chemical structure see **Appendix 2**).

A working concentration of valinomycin was obtained by treating confluent monolayers of HeLa cells with a range of valinomycin concentrations from 500nM-10μM and comparing cell numbers to an equivalent control monolayer. Following 1μM valinomycin treatment 75% of cells remained on coverslips (**Table 2.2**), therefore 1μM was selected as a working concentration. This concentration, when assayed using flame photometry, reduced intracellular K^+ by more than 70% when compared to an equivalent control sample (**Figure 3.6**), demonstrating that, at the concentrations used in these assays, it is more efficient at reducing intracellular K^+ than either monensin or nigericin.

HeLa cells were infected with *C.trachomatis* LGV2 and treated with valinomycin at 12hpi, a timepoint at which bacterial replication is occurring. When these cells were fixed at 24hpi, large perinuclear bodies were observed. These bodies were recognised by *Chlamydia* specific MOMP/LPS antibody, and were much larger than RBs in the equivalent control this time point (**Figure 3.7A** compare control and valinomycin panels). ABs were universally observed in all *C.trachomatis* LGV2 infected HeLa cells treated with 1μM valinomycin at this timepoint. These ABs were similar to the phenotype previously observed in HeLa cells infected with *C.trachomatis* LGV2 following equivalent treatment with nigericin. These data show that abnormal development occurs as a result of K^+ efflux, independently of an associated H^+ influx.

HeLa cells that were infected with *C.trachomatis* LGV2 and treated 12hpi with valinomycin were collected 50hpi for IFU quantification. No infectivity was recovered from valinomycin treated cells, which demonstrates that valinomycin-induced ABs

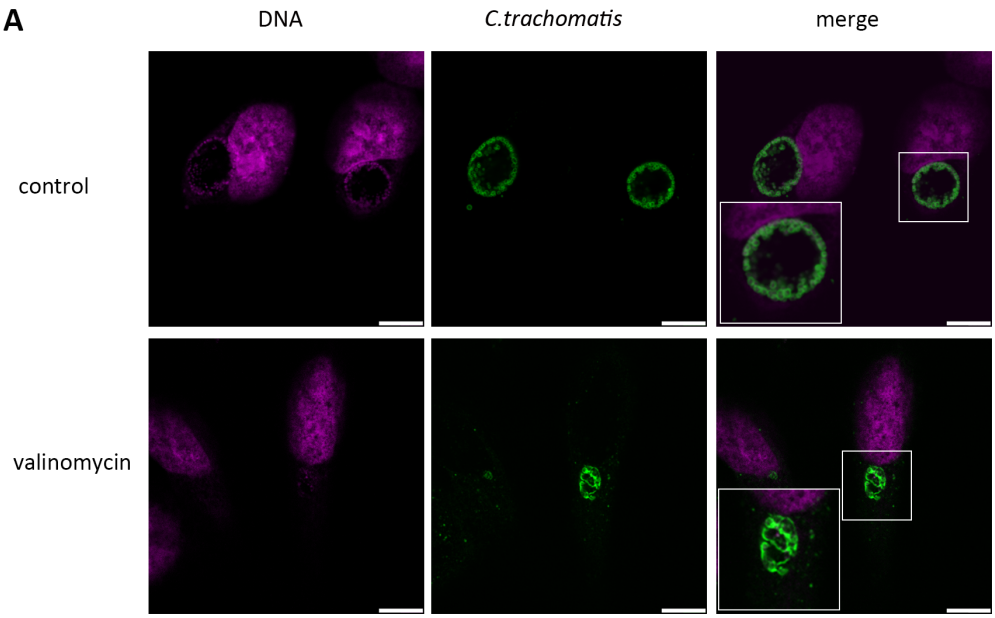
A
DNA
C.trachomatis
merge
control
valinomycin

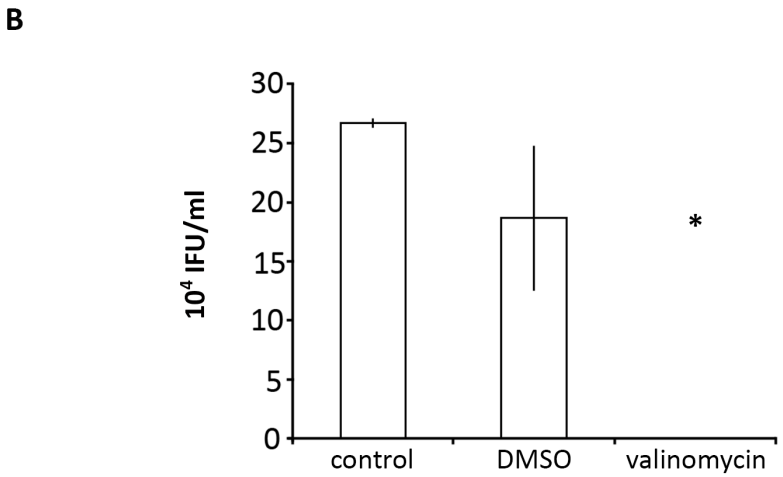
B
30
25
20
15
10
5
0
10^4 IFU/ml
*
control
DMSO
valinomycin

Figure 3.7. Valinomycin induced K^+ efflux during *C.trachomatis* LGV2 replication in HeLa cells causes persistence-like non-infectious ABs. (A) Confocal xy-sections of *C.trachomatis* LGV2 infected HeLa cells (MOI=1) treated with 1μM valinomycin at 12hpi and fixed at 24hpi. Bacteria were labelled with *Chlamydia* spp. MOMP/LPS specific primary antibody followed by AlexaFluor®488 conjugated secondary antibody (green) and DRAQ-5 DNA label (magenta). Scale bars, 10μm. Insets show indicated areas at higher magnification. (B) Cell layers treated with 1μM valinomycin at 12hpi and collected at 50hpi were diluted in fresh media to infect a new layer of cells. After 24h, infected cells were fixed and labelled using anti-*Chlamydia* spp. FITC-conjugated antibody and DAPI DNA stain. IFUs were then quantified (IFU/ml). Each experiment was repeated a minimum of three times, and the data presented are representative of each iteration. Error bars show standard deviation (*$p \leq 0.05$).

were subsequently unable to form infectious EBs (**Figure 3.7B**). Again, this is analogous to the non-infectious nigericin-induced ABs. These data demonstrate that treatment of HeLa cells infected with *C.trachomatis* LGV2 with K^+ ionophores during RB replication has an adverse effect on the bacterial development cycle, which shows that K^+ has a critical role in the *C.trachomatis* lifecycle.

Although ionophore concentrations were titrated to reduce cell loss, K^+ performs many vital functions within eukaryotic cells, which would be interrupted by ionophore treatment. This could potentially cause stress to the eukaryotic cell without resulting in cell death. To further understand the impact of ionophore treatment during *C.trachomatis* development, the potential consequences of cellular K^+ depletion require further investigation.

3.6 K^+ ionophore treatment disrupts mitochondria but not Golgi stacks or endoplasmic reticulum

Both valinomycin and nigericin concentrations were titrated to concentrations that had a minimal impact on host cells, however a significant decrease in intracellular K^+ can still be observed following treatment (**Figure 3.6**). The cellular implications of this efflux must be explored to determine the cause of the abnormal *C.trachomatis* LGV2 development observed in HeLa cells treated with K^+ ionophores. To assess the physiological changes in cellular components due to K^+ efflux, the morphology of mitrochondria, which are sensitive to K^+ fluctuations (Nicholls, 2006), was assessed.

Additionally the effect of nigericin treatment on endoplasmic reticulum (ER) and Golgi, which are both known to participate in the *C.trachomatis* infection cycle, will be evaluated.

Although the mitochondrial outer membrane is freely permeable to ions, the inner membrane is rich in potassium channels (Shi *et al.,* 2005; Szabò *et al.,* 2012). Nigericin causes mitochondrial hyperpolarisation (Nicholls, 2006), presumably due to the high K^+ concentration within the mitochondrial matrix, which in some cell types is thought to be as high as 180mM (Kozoriz *et al.,* 2010). Mitotracker orange, a probe that accumulates in active mitochondria in live cells, was used to label both nigericin treated and untreated HeLa cells. Control cells contain an interconnected network of mitochondria throughout the cell. In contrast, mitochondria in cells treated for 12h with nigericin are less evenly distributed throughout the cell and form a less organised network. (**Figure 3.8A**). Although nigericin-induced K^+ efflux appears to alter the morphology of the mitochondrial network, the remaining mitochondria continue to be active, as demonstrated by the uptake of the mitotracker probe.

C.trachomatis sequesters vesicles from the host secretory pathway to obtain important nutrients such as cholesterol and sphingolipids (Carabeo *et al.,* 2003). The uptake of these nutrients is dependent on functioning Golgi apparatus (Carabeo *et al.,* 2003) and *C.trachomatis* inclusions co-opt Golgi stacks, presumably to facilitate this nutrient uptake (Heuer *et al.,* 2009). To establish whether nigericin induced K^+ efflux disrupts the Golgi apparatus, a specific antibody against giantin, a Golgi membrane protein (Sonnichsen *et al.,* 1998), was used to label *cis*- and medial Golgi. Nigericin-

induced K^+ efflux did not induce any significant morphological changes in Golgi stacks (**Figure 3.8B**), and therefore it seems unlikely that the ABs observed following K^+ ionophore treatment are generated as a result of disrupted *cis*- or medial Golgi stacks.

Recently in our lab, Dumoux *et al.* (2012) showed that ER is recruited to the chlamydial inclusion. This interaction is critical for early inclusion biogenesis, but was unaffected by ionophore treatment (Dumoux *et al.,* 2012), however, K^+ efflux induced by pore-forming toxin, aerolysin, was shown to cause vacuolation of the ER (Abrami *et al.,* 1998). Morphology of the ER in HeLa cells following 12h of nigericin treatment was assessed using a specific antibody against calreticulin, a glycoprotein chaperone in the ER (Molinari *et al.*, 2004). Consistent with the findings of Dumoux *et al.,* there appears to be no difference between nigericin treated and control ER, which indicates that abnormal *C.trachomatis* LGV2 development following nigericin treatment was not the result of disrupted ER (**Figure 3.8C**).

These data show that the only significant disruption of observed organelles following nigericin-induced K^+ efflux is alteration of the active mitochondria network in treated HeLa cells. This could imply that mitochondrial hyperpolarization has a detrimental effect on *C.trachomatis* LGV2 infection of HeLa cells. However, this could just be a side effect of the nigericin treatment, and not the cause of disrupted bacterial development. To determine if this is the case, cells infected with *C.trachomatis* will be observed following K^+ depletion using a method that does not directly affect mitochondrial activity.

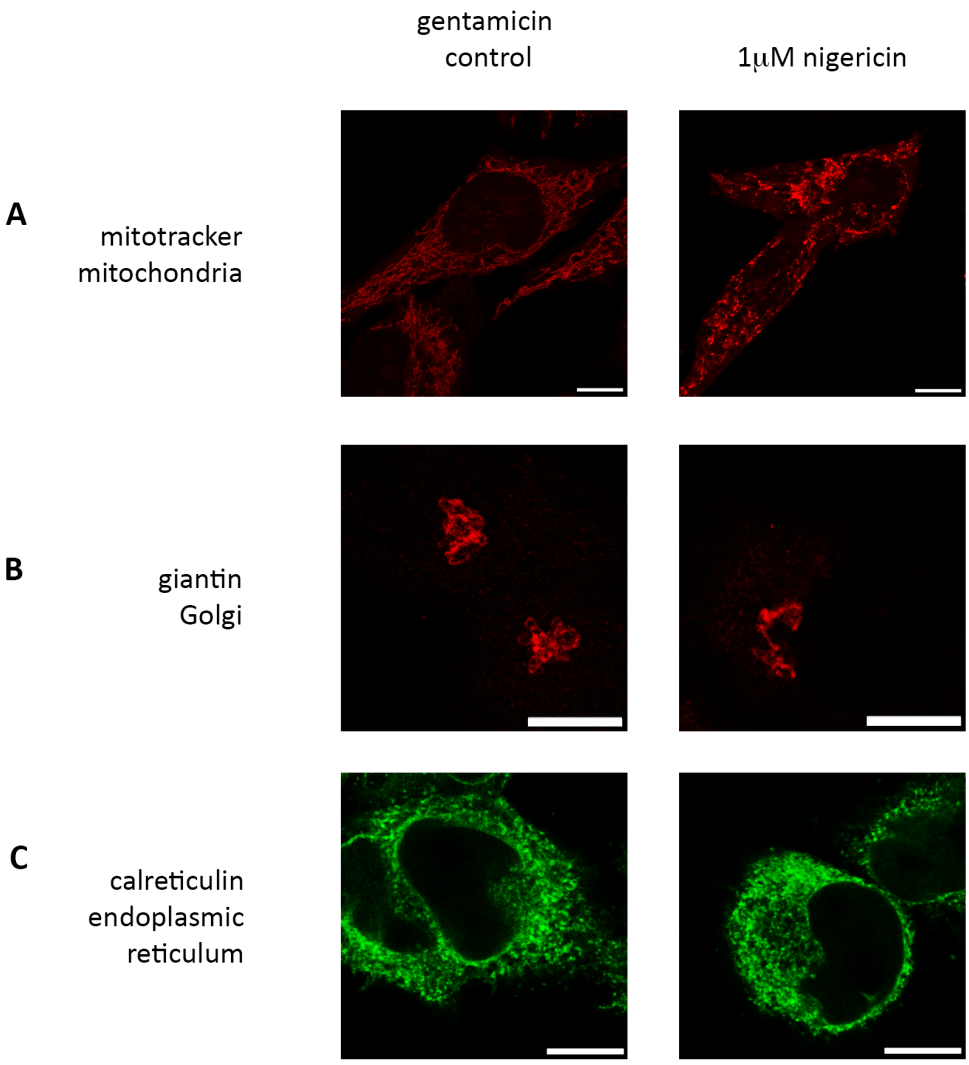
gentamicin
control
1μM nigericin
A
mitotracker
mitochondria
B
giantin
Golgi
C
calreticulin
endoplasmic
reticulum

Figure 3.8. Ionophore induced K^+ efflux disrupts HeLa mitochondria but not Golgi or endoplasmic reticulum. Confocal xy-sections of HeLa cells treated with 1μM nigericin for 24h. (A) Live cells were labelled using mitotracker orange (red) prior to fixation. (B) Fixed cells were labelled using anti-giantin antibody and AlexaFluor®568 conjugated secondary antibody (red). (C) Fixed cells were labelled using anti-calreticulin antibody and AlexaFluor®488 conjugated secondary antibody (green). Scale bars, 10μm.

3.7 Restriction of cellular K^+ uptake has a detrimental effect on *C.trachomatis* LGV2 infection

Nigericin-induced AB formation could imply that replicating bacteria have a nutritional requirement for K^+, however other contributing factors must also be considered. For example, mitochondria in nigericin treated cells appear to be disrupted by the K^+ efflux, which could have an impact on *C.trachomatis* development. Equally, nigericin treatment could activate cellular signalling pathways, usually triggered by a decrease in intracellular K^+. For example, K^+ efflux from eukaryotic cells has been shown to stimulate the production of reactive oxygen species and consequently acts as a trigger for the $NLRP_3$ inflammasome leading to caspase-1 cytokine production to initiate an innate immune response (Muñoz-Planillo *et al.,* 2013). Restricting K^+ concentrations without inducing an efflux or disrupting mitochondria, by inhibiting inwardly rectifying K^+ channels (K_{ir}), will illustrate whether replicating bacteria require a constant influx of K^+ for successful intracellular development. Adenosine triphosphate (ATP)-sensitive K_{ir} channels are located in both the plasma membrane and organelles, including the inner mitochondrial membrane (Shi *et al.,* 2005). K_{ir} channels are comprised of two distinct subunits, a pore forming subunit of the $K_{ir}6.x$ family and an ATP binding sulphonylurea receptor (SUR) subunit (Bryan and Aguilar-Bryan, 1999). SUR domains are sensitive to glibenclamide, which reduces K_{ir} activity by 50-60% (Bryan and Aguilar-Bryan, 1999).

Glibenclamide concentration was titrated to a level that could be tolerated by more that 75% of HeLa cells. Treatment of cells with 10μM glibenclamide caused the loss

less than 25% of HeLa cells (**Table 2.2**), and did not reduce the initial K^+ concentration within the cells, as verified using flame photometry (**Figure 3.6**).

When HeLa cells infected with *C.trachomatis* LGV2 were treated with glibenclamide at 12hpi, ABs morphologically similar to those generated following K^+ ionophore treatment were observed at 24hpi (**Figure 3.9A**). When bacterial infectivity was quantified at 50hpi, following treatment of the cells with glibenclamide from 12hpi, only 33% of the bacteria had differentiated into EBs in comparison to control conditions. The infectious titre was significantly reduced ($p \leq 0.05$) when compared to the control (**Figure 3.9B**). These data would suggest that ABs, induced following glibenclamide treatment, were unable to differentiate into EBs, but the bacteria observed with normal RB morphology successfully completed RB-EB differentiation and were unaffected by glibenclamide inhibition of K_{ir} channels.

Interestingly, glibenclamide treated cells contained a mixed population of inclusions containing either RBs (**Figure 3.10** glibenclamide panel, indicated by *) or ABs (**Figure 3.10** glibenclamide panel, indicated by †), whereas treatment with nigericin induced ABs in every observed inclusion (**Figure 3.10** nigericin panel). This is consistent with infectivity data, where nigericin treatment prevented the formation of any infectious EBs (**Figure 3.5B**) but approximately 30% of bacteria in glibenclamide treated cells successfully completed RB-EB redifferentiation (**Figure 3.9B**). These data could appear contradictory to the hypothesis that a decrease in intracellular K^+ during *C.trachomatis* replication induces the formation of ABs. Quantification of intracellular K^+ using flame photometry showed that glibenclamide treatment did not reduce intracellular K^+,

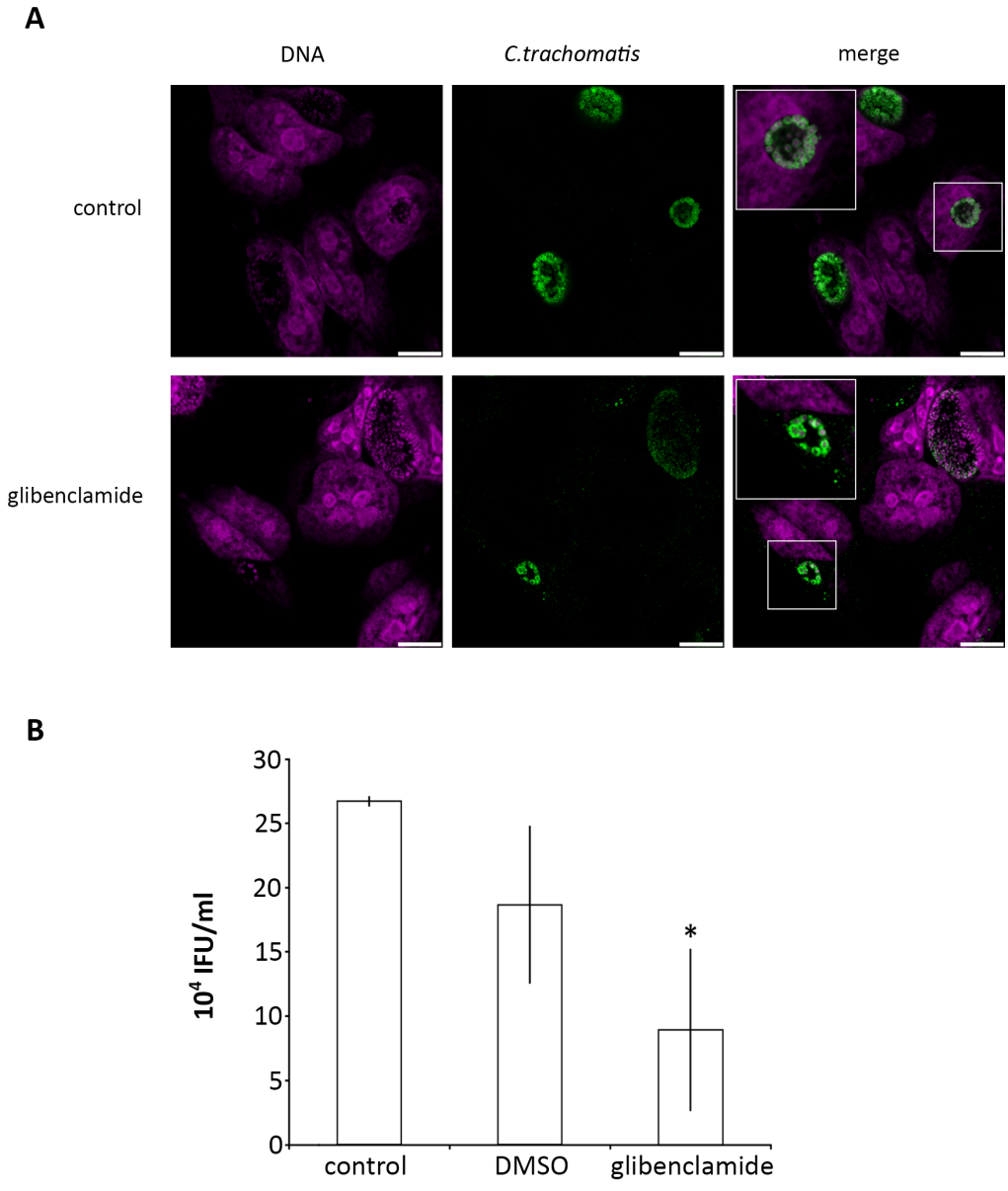
A
DNA
C.trachomatis
merge
control
glibenclamide
B
30
25
20
15
10
5
0
10^4 IFU/ml
*
control
DMSO
glibenclamide

Figure 3.9. Restricting K^+ uptake by HeLa cells causes persistence-like development during *C.trachomatis* LGV2 replication. (A) Confocal xy-sections of *C.trachomatis* LGV2 infected HeLa cells (MOI=1) treated with 10μM glibenclamide at 12hpi and fixed at 24hpi. Bacteria were labelled with *Chlamydia* spp. MOMP/LPS specific primary antibody followed by AlexaFluor®488 conjugated secondary antibody (green) and DRAQ-5 DNA label (magenta). Scale bars, 10μm. Insets show indicated areas at higher magnification. (B) *C.trachomatis* LGV2 infected cell layers treated with 10μM glibenclamide at 12hpi and collected at 50hpi were diluted in fresh media to infect a new layer of cells. After 24h, infected cells were fixed and labelled using anti-*Chlamydia* spp. FITC-conjugated antibody and DAPI DNA stain. IFUs were quantified (IFU/ml). Each experiment was repeated a minimum of three times, and the data presented are representative of each iteration. Error bars show standard deviation (*=p≤0.05).

A gentamicin control

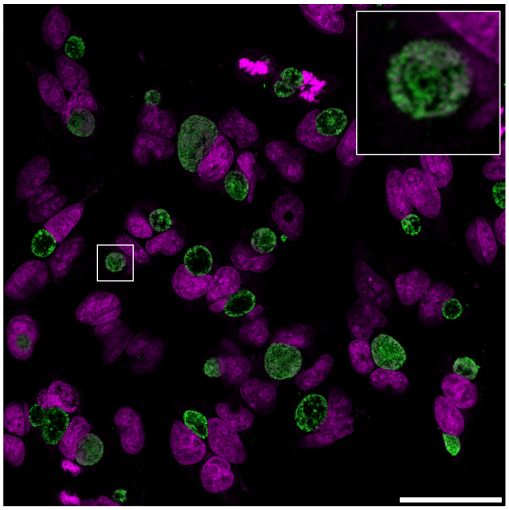

B nigericin

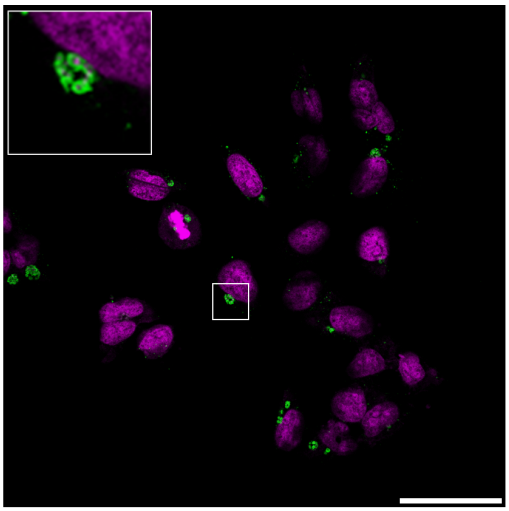

C glibenclamide

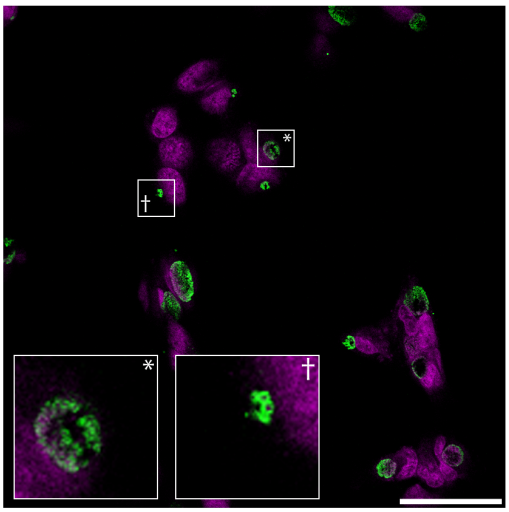

Figure 3.10. Glibenclamide inhibition of K_{ir} channels induces ABs in most, but not all, *C.trachomatis* LGV2 infected HeLa cells. Confocal xy-sections of *C.trachomatis* LGV2 infected HeLa cells either (A) untreated, (B) treated with 1μM nigericin at 12hpi, or (C) treated with 10μM glibenclamide at 12hpi. Cells were fixed at 24hpi. Bacteria were labelled with *Chlamydia* spp. MOMP/LPS specific primary antibody followed by AlexaFluor®488 conjugated secondary antibody (green) and DRAQ-5 DNA label (magenta). Asterisk (*) indicates inclusions that appear to contain RBs. Dagger (†) indicates inclusions that appear to contain ABs. Scale bars, 50μm. Insets show indicated areas at higher magnification.

compared to control cells (**Figure 3.6**), and yet AB formation was still induced in a significant number of glibenclamide treated cells. When analysing intracellular K^+ concentration using a potassium specific ratiometric fluorescent dye, Grieshaber *et al.* (2002) demonstrated a deviation of 28mM in K^+ concentration across 24 Vero cells, which would suggest a natural variation in K^+ concentrations between cells. This variation could indicate that the cells containing RBs following glibenclamide treatment contained sufficient intracellular K^+ to support *C.trachomatis* replication, without the need for inwardly rectifying K^+ channels.

These data show that AB formation is induced in intracellular *C.trachomatis* LGV2 in K^+ restricted environments without the need for a K^+ efflux. This suggests that AB formation is not the result of a host-induced response to intracellular bacteria, and instead, demonstrates a link between K^+ availability during RB replication and abnormal bacterial development. The significant proportion of bacteria disrupted following glibenclamide treatment suggests that replicating *C.trachomatis* LGV2, in the majority of HeLa cells, require more K^+ than is readily available in intracellular K^+ stores.

K^+ starvation from 12hpi, during *C.trachomatis* LGV2 replication, is characterised by the formation of ABs with reduced capacity to produce infectious EBs. The large, non-infectious bodies observed in K^+ ionophore treated cells and K_{ir} inhibited cells are consistent with previously described persistence phenotypes, induced during *in vitro* chlamydial infections in response to a number of environmental stressors (reviewed by Hogan *et al.,* 2004). *C.trachomatis* persistence is defined by enlarged ABs, which are

transcriptionally active but non-replicative, that will resume their development cycle on restoration of favourable conditions (Hogan *et al.,* 2004; Schoborg, 2011). To conclude that restriction of K^+ during *C.trachomatis* replication results in persistence, ultrastructural observation of K^+ starvation-induced ABs was undertaken, and continued transcription and AB recovery investigated.

3.8 Restriction of K^+ during *C.trachomatis* LGV2 replication induces persistence

C.trachomatis can enter a persistent state in response to a number of stressors, including exposure to cytokines, such as interferon-γ (Pantoja *et al.,* 2001), heat shock (Kahane and Friedman, 1992), and various nutrient deficiencies, for example iron starvation (Raulston, 1997) and amino acid deprivation (Coles *et al.,* 1993). Each trigger produces slightly different persistence phenotypes, but share certain identifying features.

Restriction of intracellular K^+ during *C.trachomatis* LGV2 replication appears to induce the formation of ABs, similar to those observed during recognised persistence conditions. These ABs are situated in the perinuclear region of the cell, however fluorescence microscopy images do not provide any structural detail on the effects of K^+ starvation on bacterial morphology. Transmission electron microscopy (TEM) of thin sections of *C.trachomatis* LGV infected HeLa cells allowed ultrastructural comparison of nigericin treatment-induced ABs and RBs under normal infection conditions.

HeLa cells infected with *C.trachomatis* LGV2 were treated with nigericin 12hpi and fixed at 24hpi, prior to embedding and preparation for transmission electron microscopy. Electron micrographs of K^+ starved inclusions contain large bodies, consistent with the morphology of the bacteria observed by fluorescence microscopy. The ABs contain several membrane fragments, which possibly result from arrested replication (**Figure 3.11** nigericin panel, indicated by *). After nigericin treatment the inclusion membrane remains intact as a distinction can clearly be made between the host cell cytosol and the inclusion lumen, and ABs still appear to contact the inclusion membrane. There is also an increase in electron-dense material within the inclusion (indicated by arrows in **Figure 3.11**), which resembles glycogen (Gordon and Quan, 1965; Chiappino *et al.,*1995). These data show that the ABs, observed following K^+ efflux during *C.trachomatis* LGV2 replication, remain inside an intact inclusion but are morphologically distinct from RBs observed in untreated cells. To establish persistence in K^+ deficient bacteria, ABs must be shown to be viable and capable of recovery once optimal K^+ conditions have been restored.

Expression of bacterial 16S rRNA was used to assay the viability of K^+ deficient ABs. Ribosomal RNA precursors are essential to bacteria; therefore the absence of 16S rRNA transcription is a strong indication that bacterial cells are non-viable. To establish a negative control for this assay, conditions that will eliminate bacteria, but are non-toxic to host cells are required. Chlamydial infections are sensitive to tetracycline antibiotics, with doxycycline being one of the most common therapeutic agents (Senn *et al.,* 2005). Doxycycline concentrations were titrated using HeLa cells, and 5μM was selected as a working concentration (**Table 2.2**). HeLa cells infected with *C.trachomatis*

control

nigericin treated
12hpi

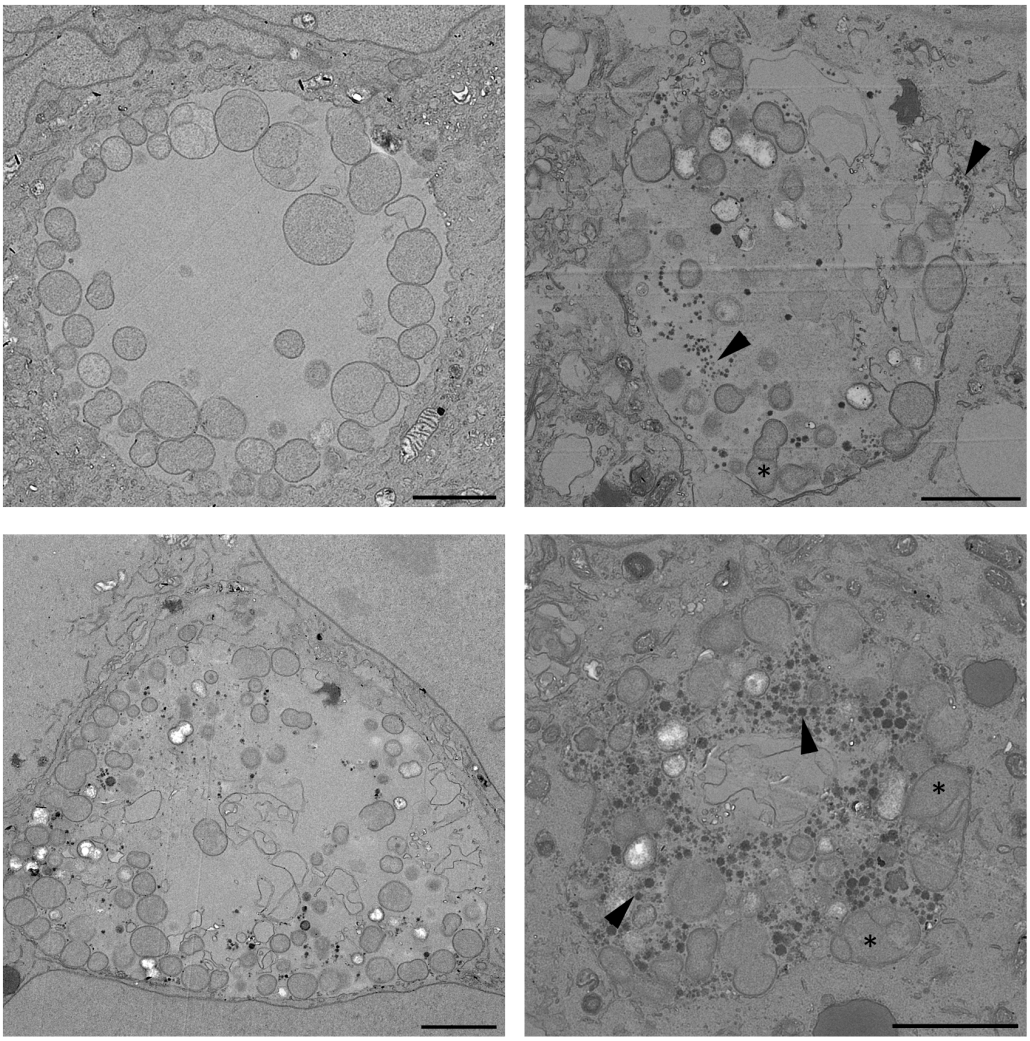

Figure 3.11. Ultrastructure of K^+ starved ABs in HeLa cells. HeLa cells infected with *C.trachomatis* LGV2 (MOI=1) were either left untreated (control) or treated 12hpi with 1μM nigericin (nigericin). Cells were fixed at 24hpi prior to embedding. Asterisk (*) indicates ABs that contain a number of membrane fragments. Arrows indicate areas containing electron dense material within nigericin treated inclusions. Scale bars, 2μm.

LGV2 were treated with 5μM doxycycline at 12hpi. At 24hpi individual bacteria were no longer visible and anti *Chlamydia* MOMP/LPS antibody labelling became diffuse throughout the host cell (**Figure 3.12A**). Infectivity collected from HeLa cells infected with *C.trachomatis* LGV2 and treated with 5μM doxycycline at 12hpi, was quantified 50hpi after either incubation with doxycycline for the duration of the experiment or having had the doxycycline washed out after 1h (for schematic representation of the experiment see **Figure 3.12B**). The infectivity assay confirmed that that doxycycline treatment had prevented the formation of infectious EBs (**Figure 3.12C**), and bacterial infectivity could not be recovered when doxycycline was removed after 1h of treatment (**Figure 3.12C**). This absence of bacterial recovery following doxycycline removal indicates that the bacteria are no longer viable, which demonstrates that doxycycline treatment is effective at killing *C.trachomatis* LGV2, and is therefore an appropriate control treatment for 16S rRNA viability assays.

HeLa cells infected with *C.trachomatis* LGV2 for 12h were either treated with 5μM doxycycline to clear bacterial infection, 1μM nigericin to induce K^+ deficient AB formation, or left untreated, before RNA isolation at 50hpi. RNA samples were treated with DNase I to remove DNA contaminants prior to reverse transcription and PCR to amplify prokaryotic 16S (product 207bp, for primers see **Appendix 1**), and eukaryotic 18S (product 217bp, for primers see **Appendix 1**). For each condition RNA, both before (**Figure 3.13A** -DNase) and after (**Figure 3.13A** +DNase) DNase treatment, was used for PCR, employing 16S primers to ensure that any cellular DNA contamination had been removed. Untreated controls showed amplification of both prokaryotic 16S and

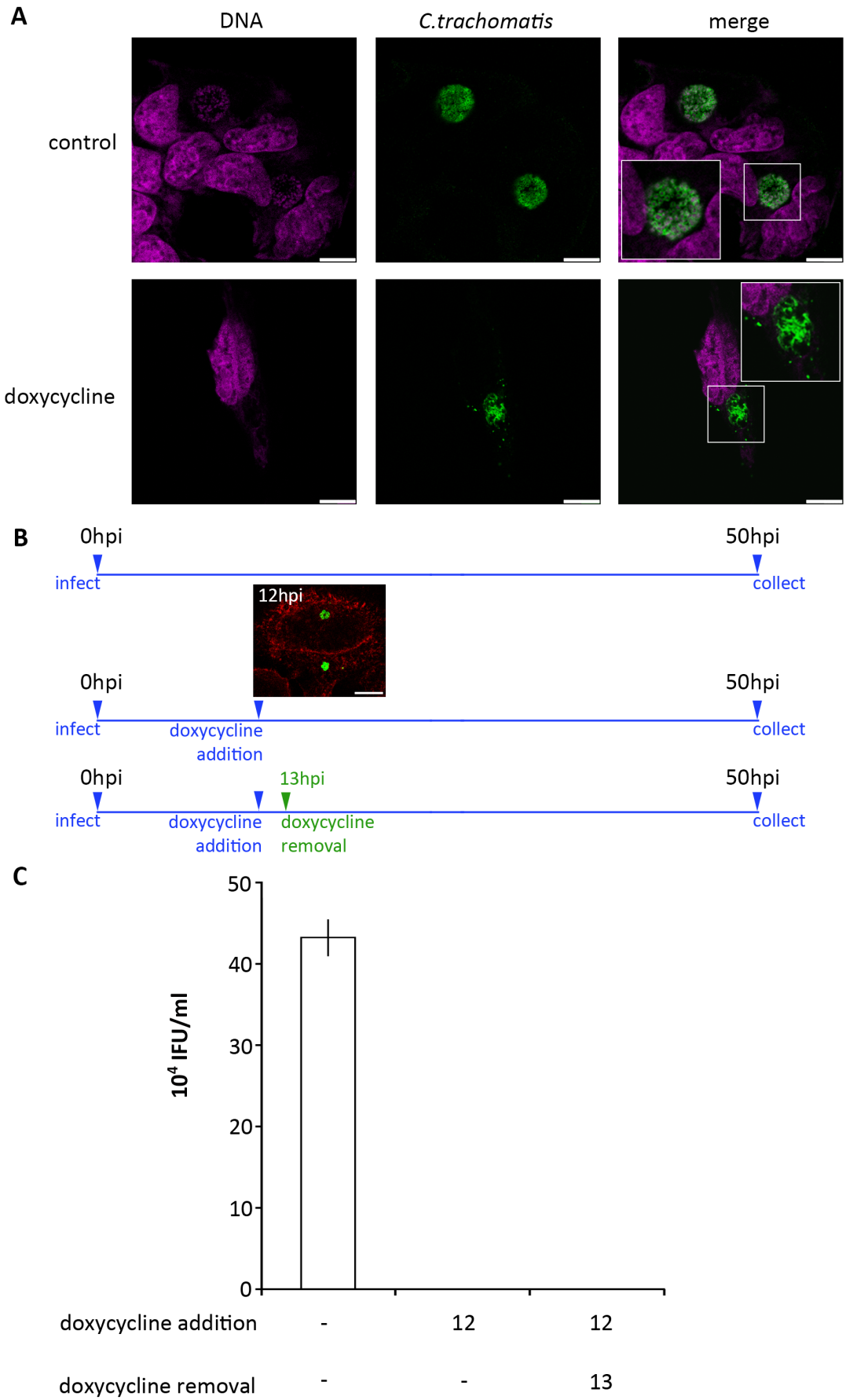
A
DNA
C.trachomatis
merge
control
doxycycline
B
0hpi
50hpi
infect
collect
12hpi
0hpi
50hpi
infect
doxycycline addition
collect
0hpi
13hpi
50hpi
infect
doxycycline addition
doxycycline removal
collect
C
50
40
30
20
10
0
10⁴ IFU/ml
doxycycline addition
-
12
12
doxycycline removal
-
-
13

Figure 3.12. Doxycycline clears *C.trachomatis* LGV2 infection from HeLa cells. (A) Confocal xy-sections of *C.trachomatis* LGV2 infected HeLa cells (MOI=1) either untreated (control), or treated with 5μM doxycycline at 12hpi (doxycycline), were fixed at 24hpi. Bacteria were labelled with *Chlamydia* spp. MOMP/LPS specific primary antibody followed by AlexaFluor®488 conjugated secondary antibody (green) and DRAQ-5 DNA label (magenta). Scale bars, 10μm. Insets show indicated areas at higher magnification. (B) Schematic representation of experiment timelines, showing confocal xy-section of *C.trachomatis* (green) infection of HeLa cells (red) at the time of doxycycline treatment and indicating when treatment was washed out, where appropriate. (C) *C.trachomatis* LGV2 infected HeLa cell layers either untreated, treated 12hpi with 5μM doxycycline for the duration of the experiment, or treated 12hpi with 5μM doxycycline for 1h before doxycycline media was replaced with fresh growth media, were collected at 50hpi and diluted in fresh media to infect a new layer of cells. After 24h, infected cells were fixed and labelled using anti-*Chlamydia* spp. FITC-conjugated antibody and DAPI DNA stain. IFUs were then quantified. Each experiment was repeated a minimum of three times, and the data presented are representative of each iteration. Error bars show standard deviation. (* = $p \leq 0.05$).

eukaryotic 18S complementary DNA (**Figure 3.13A** control panel), indicating viability of both bacteria and host cells respectively. 18S products were still amplified from doxycycline treated cells after bacterial infection, but no amplification of 16S product was observed, confirming that the host cell is viable but the bacteria were not (**Figure 3.13A** doxycycline panel). K^+ starved bacteria, resulting from nigericin treatment of infected cells, show amplification of 18S product at a comparable level to the untreated control and a feint band of amplified 16S product (**Figure 3.13A** nigericin panel). The presence of the 16S product illustrates that bacteria remain viable after nigericin treatment. As this assay was not undertaken using quantitative PCR it is difficult to assess the levels of 16S product, but the amplification of 18S product in each sample allows semi-quantitative analysis. By measuring the mean pixel intensities from the fluorescent bands produced following ethidium bromide intercalation of the DNA present in gels, the quantity of 16S product in relation to the 18S product was obtained. In control conditions the 16S pixel intensity was 76% of the 18S, whereas the intensity of the 16S band obtained from nigericin treated cells was 29% of the corresponding 18S band (**Figure 3.13B**). This difference could be the result of either reduced transcription, or fewer bacteria present in the sample, which would be consistent with disrupted replication following the induction of ABs.

Having established that K^+ deficient *C.trachomatis* ABs are capable of transcription, despite being non-cultivable, recovery upon restoration of optimal K^+ concentrations must be demonstrated before persistence can be confirmed.

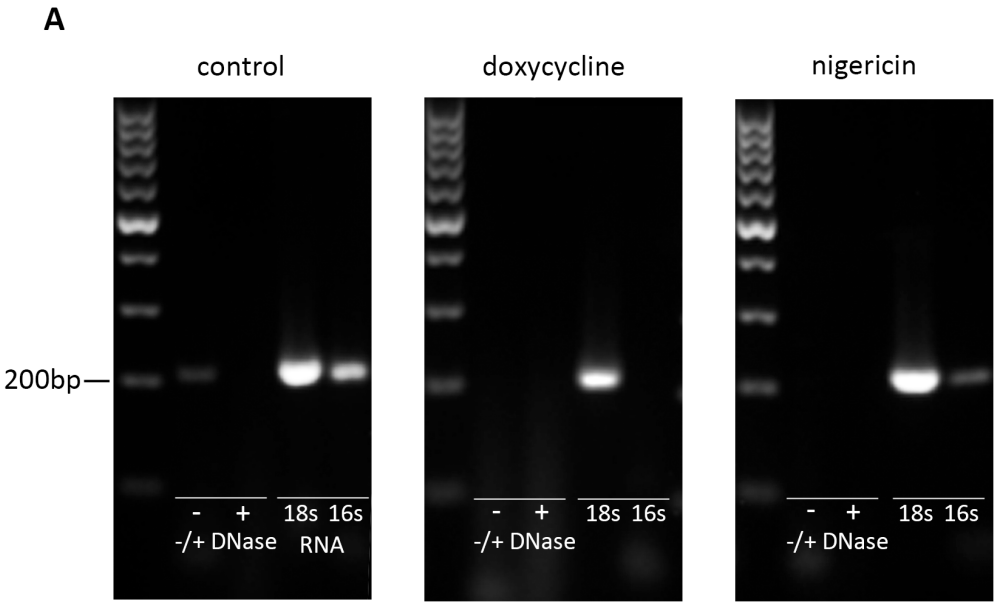
A
control
doxycycline
nigericin
200bp
- + 18s 16s
-/+ DNase RNA
- + 18s 16s
-/+ DNase
- + 18s 16s
-/+ DNase

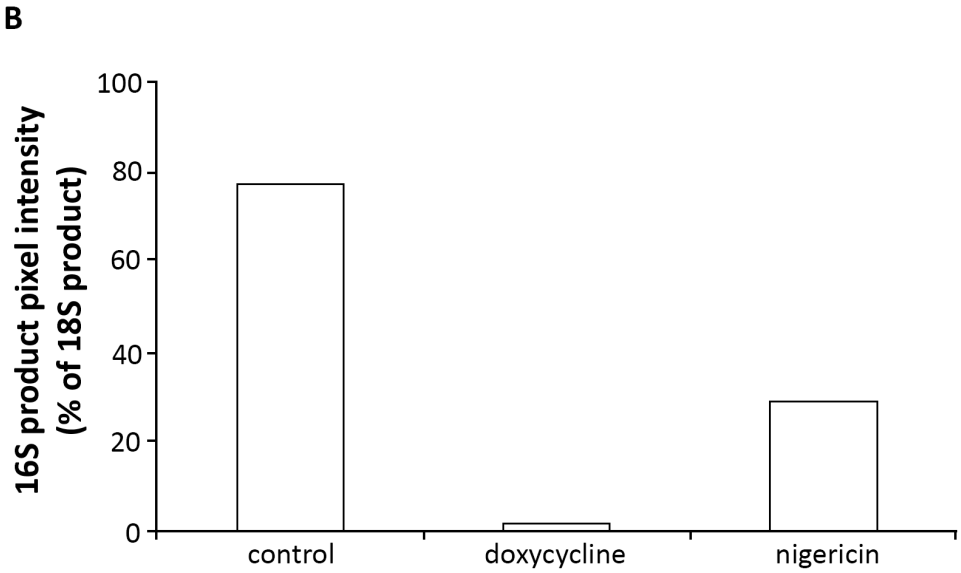
B
16S product pixel intensity
(% of 18S product)
100
80
60
40
20
0
control
doxycycline
nigericin

Figure 3.13. K^+ starved ABs remain viable but non-infectious. (A) HeLa cells were infected with *C.trachomatis* LGV2 (MOI=1) and were either untreated (control), treated at 12hpi with 5μM doxycycline (doxycycline), or treated at 12hpi with 1μM nigericin (nigericin). RNA was then collected at 50hpi prior to reverse transcription before PCR using specific primers for *C.trachomatis* 16S (16S) or eukaryotic 18S (18S) complementary DNA. RNA samples were shown to be free from cellular DNA contamination before (-DNase) or after (+DNase) DNase treatment. (B) Mean pixel intensity of 16S product expressed as a percentage of the equivalent 18S product.

HeLa cells were treated with nigericin 12hpi, and remained in nigericin-containing medium for the duration of the experiment or had the nigericin-containing medium removed either after 1h or 12h of treatment to allow K^+ gradients to be restored (for a schematic of infection, treatment and washing-out times for each condition see **Figure 3.14A**). At 50hpi, a timepoint when bacteria under control conditions had differentiated into EBs, bacteria were collected and infectivity quantified. When nigericin was present for the duration of the experiment no infection was recovered. Strikingly, nigericin removal allowed bacteria to recover infectivity irrespective of the duration of nigericin treatment (**Figure 3.14B**).

These data confirm that K^+ starvation during the replicative phase of the *C.trachomatis* infection cycle induces classical persistence. Persistent ABs remained viable and the infection cycle recovered to complete RB-EB differentiation when physiological K^+ concentrations were restored. This demonstrates an essential role for K^+ during *C.trachomatis* LGV2 replication in HeLa cells. However, due to the wide-ranging tissue tropism of the *Chlamydiaceae*, and the close relationship between these different hosts and the specific pathogenic species, the essential role for K^+ during *C.trachomatis* LGV2 infection of HeLa cells could be unique to this cell line-serovar combination. To assess the wider implications of these observations, different host-*Chlamydiae* combinations were assayed to ascertain whether K^+ is critical to all *Chlamydiae* irrespective of host cell line.

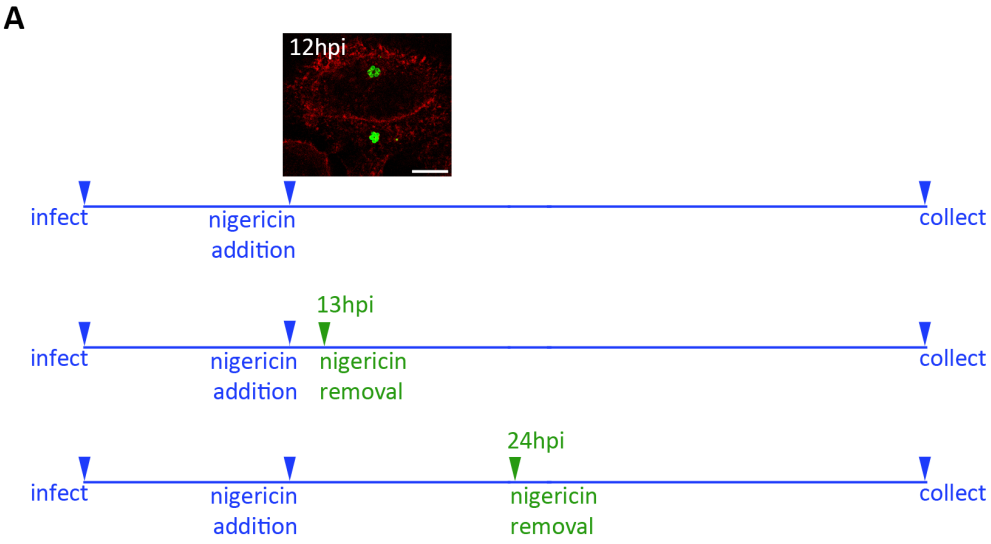
A
12hpi
infect
nigericin addition
collect
13hpi
infect
nigericin addition
nigericin removal
collect
24hpi
infect
nigericin addition
nigericin removal
collect

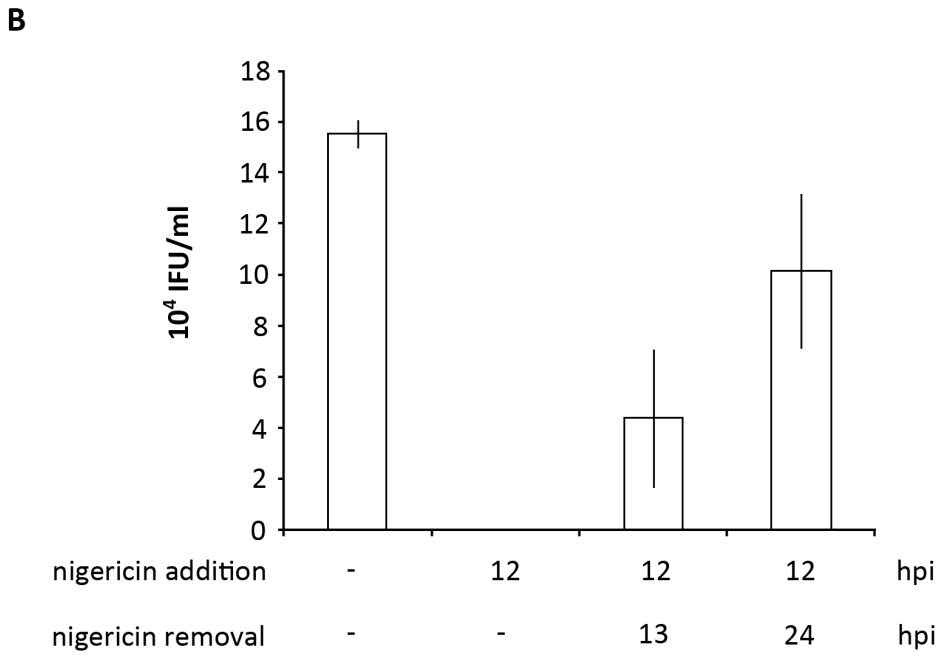
B
10^4 IFU/ml
18
16
14
12
10
8
6
4
2
0
nigericin addition - 12 12 12 hpi
nigericin removal - - 13 24 hpi

Figure 3.14. K^+ starvation-induced *C.trachomatis* LGV2 ABs can recover to complete the infection cycle when K^+ concentrations are restored. (A) Schematic representation of experiment timelines, showing confocal xy-sections of *C.trachomatis* (green) infection of HeLa cells (red) at the time of nigericin treatment, and indicating when treatment was washed out where appropriate. (B) *C.trachomatis* LGV2 infected HeLa cell layers (MOI=1) either untreated, treated at 12hpi with 1μM nigericin for the duration of the experiment, treated at 12hpi with 1μM nigericin for 1h before nigericin media was replaced with fresh growth media, or treated at 12hpi with 1μM nigericin for 1h before nigericin media was replaced with fresh growth media. Cells were collected at 50hpi and diluted in fresh media to infect a new layer of cells. After 24h, infected cells were fixed and labelled using anti-*Chlamydia* spp. FITC-conjugated antibody and DAPI DNA stain. IFUs were then quantified (IFU/ml). Each experiment was repeated a minimum of three times, and the data presented are representative of each iteration. Error bars show standard deviation.

3.9 K^+ starvation of *Chlamydiae* during replication induces persistence, regardless of serovar, species or host

This chapter has demonstrated that reducing intracellular K^+, either by inducing efflux using ionophores or inhibiting K_{ir} channels, causes persistence during *C.trachomatis* LGV2 replication in HeLa cells. It is important to ascertain whether bacterial dependence on K^+ is unique to this serovar-cell line combination, or if K^+ starvation will induce persistence in other *Chlamydiae* strains or *C.trachomatis* serovars in other host cell lines.

Bacteria from the *Chlamydiaceae* family infect a wide range of hosts, and demonstrate diverse tissue tropism (**Figure 1.1**) (Everett *et al,* 2000; Abdelsamed *et al.,* 2013). Due to the obligate intracellular nature of the *Chlamydiaceae* each strain has evolved closely with its host, and will therefore encounter differing environmental pressures and have different nutritional requirements. For example, *C.suis* strain S-45 infection of swine differentiated luminal epithelial cells displayed an active infection cycle, however infection of swine glandular epithelial cells with the same bacteria resulted in persistent infection (Guseva *et al.,* 2003). Allan and Pearce (1983) investigated the differing amino acid requirements of *Chlamydiae* strains and serovars and found that four strains of *C.psittaci* did not require histidine for successful infection development, however intracellular development of eleven serovars of *C.trachomatis*, including ocular, LGV, and genital biovars, was inhibited by omission of histidine from the growth medium. Furthermore, only ocular serovars A-C were shown to require

tryptophan, and LGV2 was shown to require methionine, unlike ocular and genital biovars (Allan and Pearce, 1983).

RL95-2 cells, first immortalized and characterised by Way *et al.* (1983), are human endometrial carcinoma cells, and are therefore physiologically relevant to chlamydial infection. RL95-2 cells were used to observe the effect of K^+ starvation during *C.trachomatis* LGV2 replication in an alternative cell line. As the infection cycle is cell line specific, the normal development cycle of *C.trachomatis* LGV2 in RL95-2 cells was initially reconstituted.

RL95-2 cells infected with *C.trachomatis* LGV2 contained EB-filled inclusions 6hpi (**Figure 3.15A/B** 6h), which begin to differentiate into RBs at 12hpi, (**Figure 3.15A/B** 12h). Mature inclusions began to lyse at 48hpi, demonstrated by a decrease in infectivity collected from cells from 48 to 60hpi (**Figure 3.15A** 48h). These data show that *C.trachomatis* LGV2 development occurs more rapidly in RL95-2 cells than in HeLa cells, and therefore, to investigate the effects of K^+ starvation during replication, cells were treated with nigericin 6hpi and fixed 18hpi. Nigericin induced K^+ efflux during *C.trachomatis* LGV2 infection caused the formation of ABs in RL95-2 cells (**Figure 3.15C**). RL95-2 cells infected with *C.trachomatis* LGV2 were treated 12hpi with either nigericin, to induce a K^+ efflux, glibenclamide, to restrict host cell K^+ uptake, or chloride ionophore I, to disrupt Cl^- gradients and act as a control for disrupted pH, osmolarity, and membrane potentials, before IFU quantification 48hpi. Nigericin treatment prevented bacteria differentiation into infectious EBs at the end of the infection cycle, as demonstrated by the lack of infectivity (**Figure 3.15D**). Glibenclamide treatment also

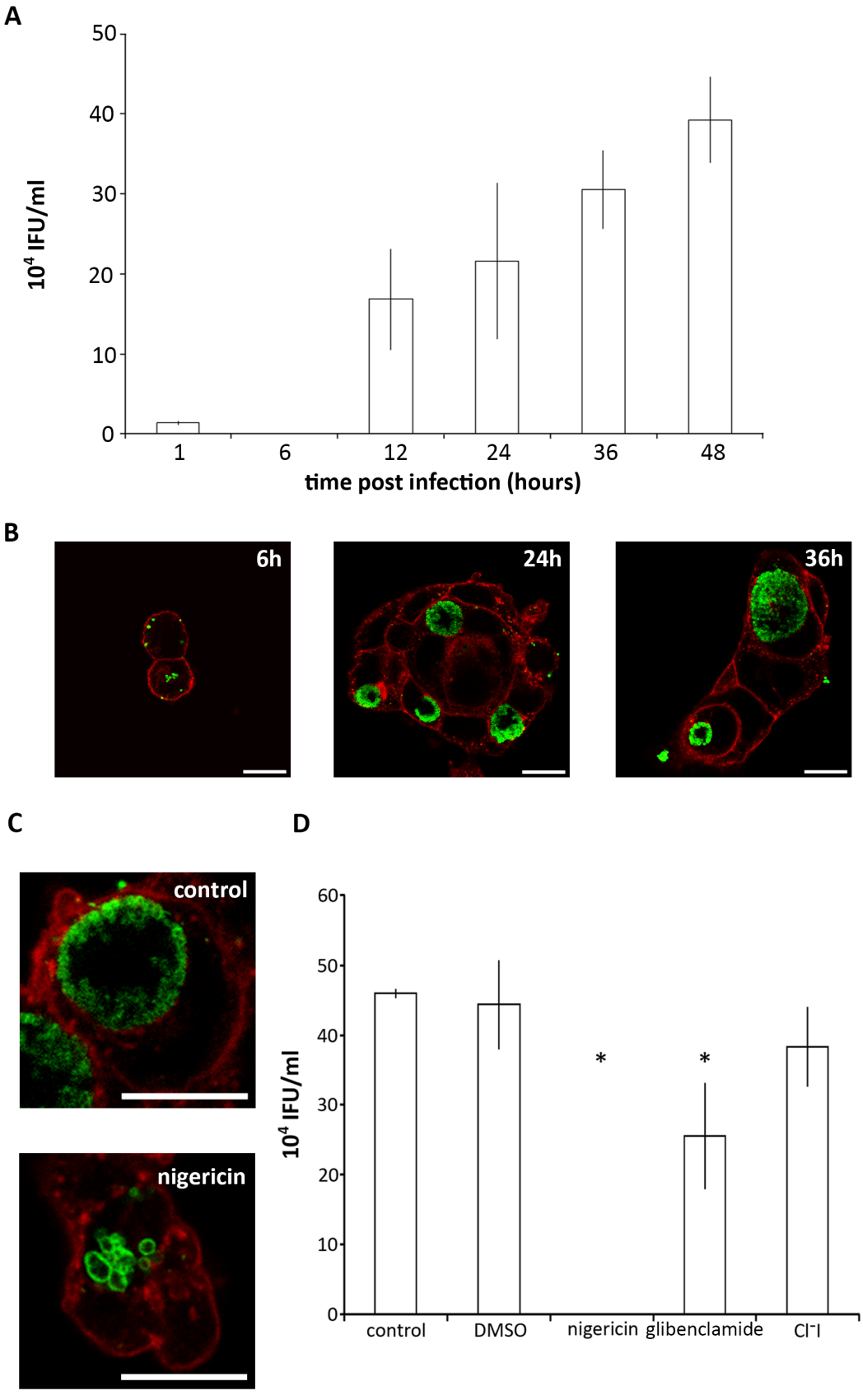
A
50
40
30
20
10
0
10^4 IFU/ml
1
6
12
24
36
48
time post infection (hours)
B
6h
24h
36h
C
control
nigericin
D
60
50
40
30
20
10
0
10^4 IFU/ml
*
*
control
DMSO
nigericin
glibenclamide
Cl^-I

Figure 3.15. K^+ starvation induces persistence during *C.trachomatis* LGV2 replication in RL95-2 cells. (A) The infection progression of *C.trachomatis* LGV2 was observed in RL95-2 cells (MOI=1). Cell layers collected at appropriate time points from 1-60hpi were diluted in fresh media to infect a new layer of cells. At appropriate timepoints secondary infected cells were fixed and labelled using anti-*Chlamydia* spp. FITC-conjugated antibody and DAPI DNA stain. IFUs were then quantified (IFU/ml). Error bars show standard deviation. (B) Confocal xy-sections of the infection progression in cells fixed 6, 24, or 36hpi, as indicated. Plasma membranes were labelled using AlexaFluor®594 conjugated WGA (red) prior to permeabilisation. Bacteria were labelled with *Chlamydia* spp. MOMP/LPS specific primary antibody followed by AlexaFluor®488 conjugated secondary antibody (green). Scale bars, 10μm. (C) Confocal xy-sections of *C.trachomatis* LGV2 infected RL95-2 cells (MOI=1) either untreated (control), or treated with 1μM nigericin at 6hpi (nigericin), and fixed at 18hpi. Plasma membranes were labelled using AlexaFluor®594 conjugated WGA (red) prior to permeabilisation. Bacteria were labelled with *Chlamydia* spp. MOMP/LPS specific primary antibody followed by AlexaFluor®488 conjugated secondary antibody (green). Scale bars, 10μm. (D) *C.trachomatis* LGV2 infected RL95-2 cell layers were either left untreated or treated with either 1:1000 DMSO, 1μM nigericin, 10μM glibenclamide, or 1μM chloride ionophore I, at 6hpi and collected at 48hpi were diluted in fresh media to infect a new layer of cells. After 24h, infected cells were fixed and labelled using anti-*Chlamydia* spp. FITC-conjugated antibody and DAPI DNA stain. Inclusion-forming units (IFUs) were quantified (*$p \leq 0.05$).

significantly reduced infectivity at the end of the infection cycle. This suggests that, similar to the effects observed during *C.trachomatis* LGV2 infection of HeLa cells, bacteria require a ready supply of K^+, above that which is available within most resting host cells. Chloride ionophore I treatment had very little impact on the infectious EBs recoverable when compared to control conditions, indicating that disrupting chloride ion gradients during RB replication does not affect the progression of *C.trachomatis* LGV2 infection (**Figure 3.15D**). These data demonstrate that K^+ starvation induces persistence in *C.trachomatis* LGV2, irrespective of host cell type.

C.trachomatis serovar D infection of HeLa cells was used to determine whether K^+ starvation induced persistence is serovar specific. Reconstitution of the infection cycle in HeLa cells showed that RB replication occurred between 6 and 30h (**Figure 3.16A/B**). RB-EB differentiation began 42hpi and continued until 78hpi when inclusions began to lyse, as infectivity began to decrease. This demonstrates that the intracellular development of *C.trachomatis* D in HeLa cells is much slower than that of *C.trachomatis* LGV2.

HeLa cells infected with *C.trachomatis* D were treated with nigericin at 12hpi. This resulted in ABs similar to those observed during K^+ starvation-induced *C.trachomatis* LGV2 persistence (**Figure 3.16C**). When infectivity was quantified at 78hpi, following nigericin treatment at 12hpi, the induced ABs were observed to be non-infectious (**Figure 3.16D**). Interestingly, glibenclamide treatment during RB replication eliminated the infectivity of *C.trachomatis* D released from HeLa cells. This would suggest that *C.trachomatis* D has a greater requirement for K^+ during development than the LGV2

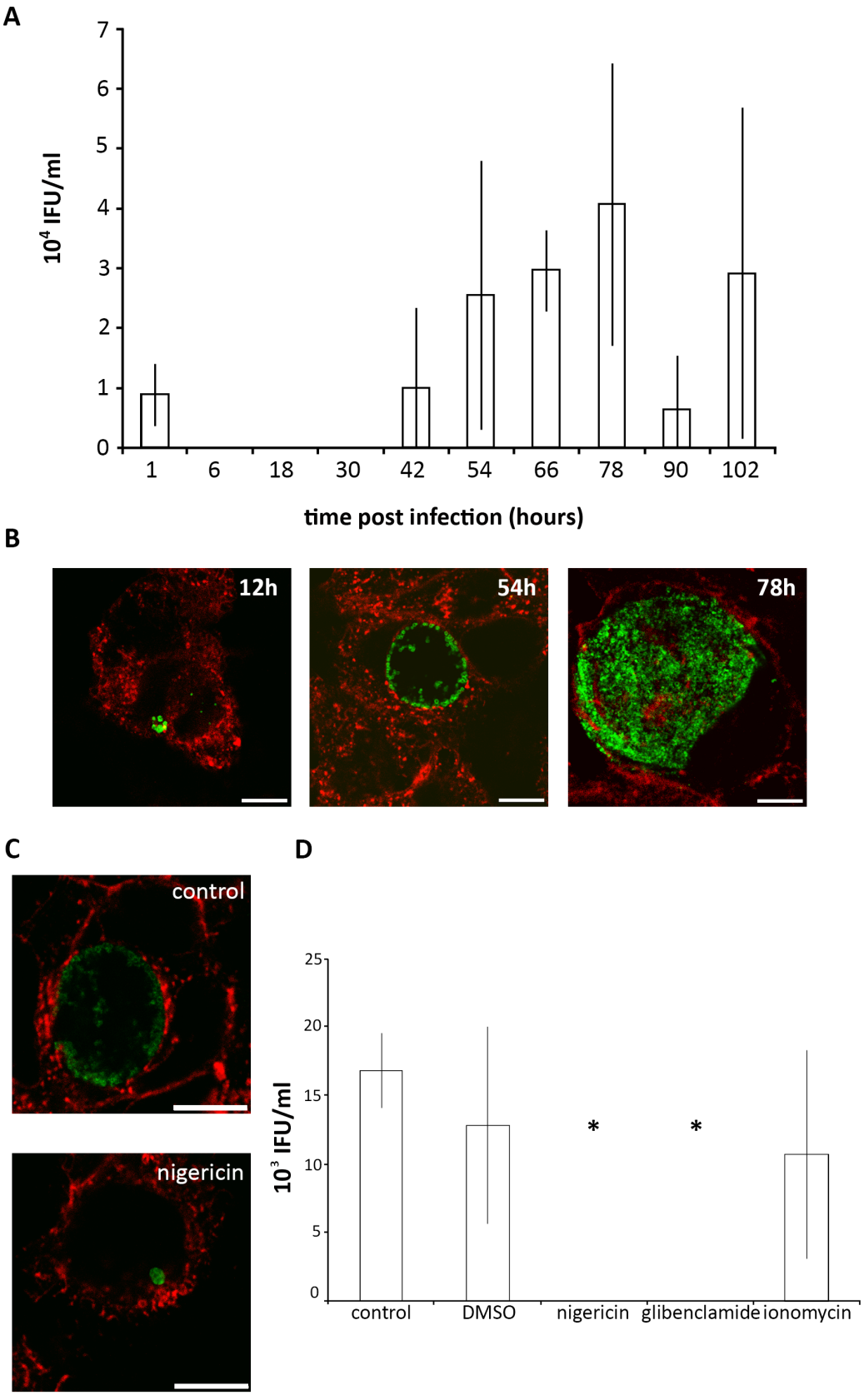
A
10^4 IFU/ml
0
1
2
3
4
5
6
7
1
6
18
30
42
54
66
78
90
102
time post infection (hours)
B
12h
54h
78h
C
control
nigericin
D
10^3 IFU/ml
0
5
10
15
20
25
*
*
control
DMSO
nigericin
glibenclamide
ionomycin

Figure 3.16. K^+ starvation induces persistence during *C.trachomatis* D replication in HeLa cells. (A) The infection progression of *C.trachomatis* D was observed in HeLa cells (MOI=1). Cell layers collected at appropriate time points from 1-102hpi were diluted in fresh media to infect a new layer of cells. At appropriate timepoints secondary infected cells were fixed and labelled using anti-*Chlamydia* spp. FITC-conjugated antibody and DAPI DNA stain. IFUs were then quantified (IFU/ml). Error bars show standard deviation. (B) Confocal xy-sections of the infection progression in cells fixed 12, 54, or 78hpi, as indicated. Plasma membranes were labelled using AlexaFluor®594 conjugated WGA (red) prior to permeabilisation. Bacteria were labelled with *Chlamydia* spp. MOMP/LPS specific primary antibody followed by AlexaFluor®488 conjugated secondary antibody (green). Scale bars, 10μm. (C) Confocal xy-sections of *C.trachomatis* D infected HeLa cells (MOI=1) either untreated (control), or treated with 1μM nigericin 12hpi (nigericin), and fixed 30hpi. Plasma membranes were labelled using AlexaFluor®594 conjugated WGA (red) prior to permeabilisation. Bacteria were labelled with *Chlamydia* spp. MOMP/LPS specific primary antibody followed by AlexaFluor®488 conjugated secondary antibody (green). Scale bars, 10μm. (D) *C.trachomatis* D infected HeLa cell layers were either left untreated or treated with either 1:1000 DMSO, 1μM nigericin, 10μM glibenclamide, or 1μM ionomycin, at 12hpi and collected at 78hpi were diluted in fresh media to infect a new layer of cells. After 30h, infected cells were fixed and labelled using anti-*Chlamydia* spp. FITC-conjugated antibody and DAPI DNA stain. IFUs were quantified (*$p \leq 0.05$).

strain, possibly due to the fact that the replicative phase of *C.trachomatis* D lasts longer. Equivalent ionomycin treatment during *C.trachomatis* D replication had no significant impact on infectivity, indicating that persistence is induced by K^+ starvation specifically, and is not limited to *C.trachomatis* LGV2 serovar.

To determine whether K^+ starvation-induced persistence is unique to *C.trachomatis* the effects of an ionophore-induced K^+ efflux and inhibition of K_{ir} channels were tested on *C.muridarum* infected HeLa cells.

Reconstitution of the *C.muridarum* infection in HeLa cells demonstrated that bacteria exist in the RB form between 6 and 12hpi (**Figure 3.17A/B**), RB-EB differentiation began to occur 18hpi and continued until 30hpi when less infectivity is recoverable from cells, demonstrating that inclusions have begun to lyse. This indicates that the infection cycle of *C.muridarum* in HeLa cells is faster than that of *C.trachomatis* LGV2.

When *C.muridarum* infected HeLa cells were treated with nigericin at 12hpi, large ABs were formed within inclusions when samples were fixed 24hpi (**Figure 3.17C**), suggesting persistence was again induced following K^+ efflux. Bacteria collected at the end of the infection cycle, 30hpi, from nigericin treated conditions were completely non-infectious, and a significantly reduced number of infectious EBs were collected from glibenclamide treated cells, indicating that *Chlamydiae* require K^+ for successful infection. Using ionomycin as a control for other ion-disrupted conditions demonstrated that disruption of Ca^{2+} gradients during replication of *C.muridarum* did not have a significant effect on resultant infectivity, and therefore shows that ionic

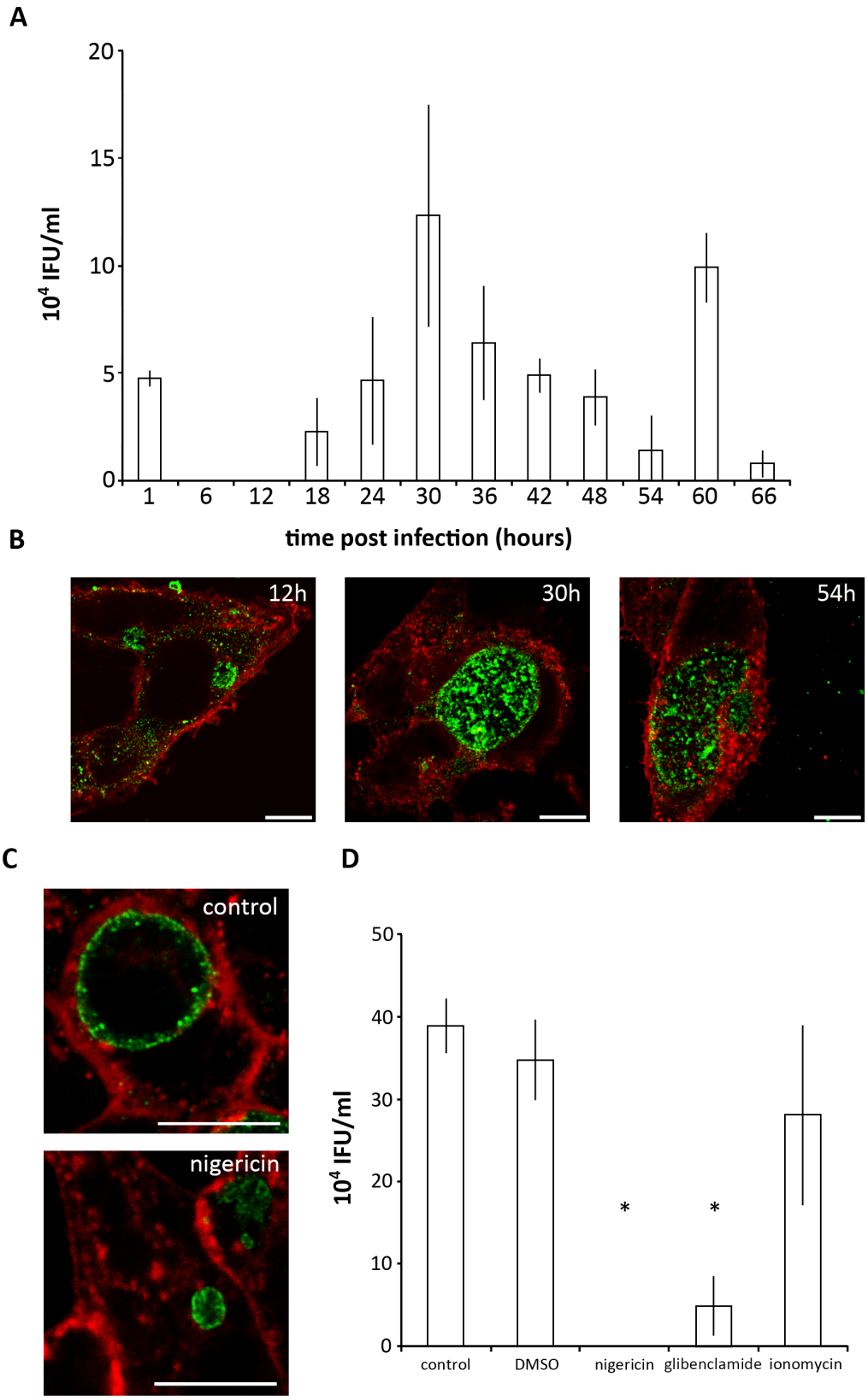
A
20
15
10
5
0
10^4 IFU/ml
1
6
12
18
24
30
36
42
48
54
60
66
time post infection (hours)
B
12h
30h
54h
C
control
nigericin
D
50
40
30
20
10
0
10^4 IFU/ml
*
*
control
DMSO
nigericin
glibenclamide
ionomycin

Figure 3.17. K^+ starvation induces persistence during *C.muridarum* replication in HeLa cells. (A) The infection progression of *C.muridarum* was observed in HeLa cells (MOI=1). Cell layers collected at appropriate time points from 1-66hpi were diluted in fresh media to infect a new layer of cells. At appropriate timepoints secondary infected cells were fixed and labelled using anti-*Chlamydia* spp. FITC-conjugated antibody and DAPI DNA stain. IFUs were then quantified (IFU/ml). Error bars show standard deviation. (B) Confocal xy-sections of the infection progression in cells fixed at 12, 30, or 54hpi, as indicated. Plasma membranes were labelled using AlexaFluor®594 conjugated WGA (red) prior to permeabilisation. Bacteria were labelled with *Chlamydia* spp. MOMP/LPS specific primary antibody followed by AlexaFluor®488 conjugated secondary antibody (green). Scale bars, 10μm. (C) Confocal xy-sections of *C.muridarum* infected HeLa cells (MOI=1) either untreated (control), or treated with 1μM nigericin 12hpi (nigericin), and fixed at 24hpi. Plasma membranes were labelled using AlexaFluor®594 conjugated WGA (red) prior to permeabilisation. Bacteria were labelled with *Chlamydia* spp. MOMP/LPS specific primary antibody followed by AlexaFluor®488 conjugated secondary antibody (green). Scale bars, 10μm. (D) *C.muridarum* infected HeLa cell layers were either left untreated or treated with either 1:1000 DMSO, 1μM nigericin, 10μM glibenclamide, or 1μM ionomycin, at 12hpi and collected at 30hpi were diluted in fresh media to infect a new layer of cells. After 24h, infected cells were fixed and labelled using anti-*Chlamydia* spp. FITC-conjugated antibody and DAPI DNA stain. IFUs were then quantified (*p≤0.05).

balance during *C.muridarum* infection does not generally induce persistence (**Figure 3.17D**).

These data show that K^+ starvation during replication, either as a result of an ionophore-induced efflux or by inhibiting inwardly rectifying K^+ channels, induces persistence in *Chlamydiae*, independent of host, serovar, or species. This also supports the theory that replicating bacteria require a supply of K^+, beyond that which is available in the host cell, as persistence appears to be induced in a significant number of bacteria following inhibition of inwardly rectifying potassium channels.

3.10 Discussion

The data presented in this chapter establish a clear and novel link between intracellular K^+ concentration during chlamydial replication and infection progression. It has been shown that reducing intracellular K^+, either by inducing an efflux or inhibiting K_{ir} channels, causes persistence in *Chlamydiae*.

Using ionophores to selectively disrupt Ca^{2+} or Cl^- gradients in HeLa cells infected with *C.trachomatis* LGV2 during replication at 12hpi, had no effect on bacterial morphology and an insignificant impact on the quantity of infectious bacteria produced at the end of the infection cycle. Treatment with nigericin, to equilibrate K^+ gradients, induced aberrant bodies (ABs) within the *C.trachomatis* inclusion and prevented the formation of infectious EBs when bacteria were collected 50hpi. A similar infection phenotype was observed following treatment with monensin, intended to disrupt Na^+ gradients (**Figures 3.4, 3.5**). As Na^+ retain water molecules they are very similar in size to K^+,

which reduces the steric selectivity of sodium ionophores. As a result, monensin ionophore treatment disrupts K^+ as well as Na^+ concentrations (**Figure 3.6**). In the absence of a higher specificity Na^+ ionophore infected cells were treated with valinomycin, a high affinity K^+ uniport ionophore (Nicholls, 2006), to verify a link between abnormal development and disrupted K^+ gradients (**Figure 3.6**). As eukaryotic cells maintain a high K^+ concentration, compared to the extracellular environment, treatment with nigericin, which equilibrates K^+ concentration across biological membranes, will effectively reduce the concentration of K^+ available within a cell. To determine whether this abnormal bacteria development was the result of K^+ starvation of bacteria, and not a due to any side effects of ionophore treatment, host cell K^+ uptake was restricted. Glibenclamide, a specific inhibitor of SUR in K_{ir} channels, prevents K^+ influx into host cells (Bryan and Aguilar-Bryan, 1999), effectively fixing the K^+ concentration within the cells. Glibenclamide treatment of *C.trachomatis* LGV2 infected HeLa cells caused the formation of ABs during replication, similar to those observed during nigericin-induced K^+ starvation (**Figure 3.9**). This effect was not universal, unlike in ionophore treated conditions (**Figure 3.10**), which is reflected in the infectivity recovered from glibenclamide treated cells. Although the IFUs recovered were significantly less than could be collected under control conditions, infectivity was not entirely eradicated (**Figure 3.9**). This suggests that bacteria scavenge host K^+ during replication and, in a significant number of infections, bacteria require inward rectification of K^+ concentrations to supplement host cell K^+ stores.

Development of ABs within chlamydial inclusions is considered a characteristic hallmark of persistent infection (Hogan *et al*., 2004). Persistence is a term applied to

changes in the progression of chlamydial infection in response to a wide range of external pressures, including heat shock (Kahanne and Friedman, 1992), amino acid starvation (Coles *et al.,* 1993), and interferon-γ treatment (Pantoja *et al.,* 2001). Persistent states are identified by ABs that are viable but non-replicating, and are capable of recovery once favourable conditions have been restored. Observing K^+ starvation-induced ABs at a higher resolution using transmission electron microscopy showed a significant increase in dense, granular material within the inclusion. The large ABs observed by fluorescence in K^+-starved conditions appear to contain a number of different membranes, suggestive of bacteria that have either aggregated together or failed to separate during replication (**Figure 3.11**). Following nigericin treatment the inclusion lumen remains clearly distinguishable from the host cell cytosol. This indicates that nigericin treatment does not permeabilise the inclusion membrane, and that persistence is the result of K^+ deficiency specifically, and not the result of a loss of inclusion integrity.

Persistence was established in K^+ starved ABs using bacterial 16S RNA transcription as a marker for viability. K^+ starved ABs, treated with nigericin during replication, remained viable although they were non infectious (**Figure 3.13**). Abnormal bodies were shown to be capable of recovering the normal infection cycle, once K^+ gradients were restored, irrespective of how long the bacteria had been starved of K^+ (**Figure 3.14**). These data demonstrate that K^+ starvation of *C.trachomatis* during RB replication induces persistence, and that ABs are capable of completing the normal infection cycle once sufficient K^+ is available to them.

Persistence was observed following K^+ starvation, both by restricting K^+ uptake by inhibiting K_{ir} channels, and inducing an efflux with K^+ ionophores, in *C.trachomatis* LGV2 infection of RL95-2 endometrial cells and in HeLa cells infected with *C.trachomatis* D and *C.muridarum*. This demonstrates that *Chlamydiae* are dependent on K^+, beyond that which is available in host cells, during RB replication independent of host, serovar, or species.

These data clearly demonstrate an essential role for K^+ during *Chlamydiae* replication, as restricting K^+ during the RB phase of the infection cycle induces persistence. Persistence inducers can be used to explore *Chlamydia*-host interactions (Schoborg, 2011). Observing changes to bacteria and inclusion morphology, cellular response to the bacteria, and changes to the bacterial cell cycle following persistence induction can provide insight into the biochemistry of chlamydial infection. Identifying the function of K^+ during replication could provide insight into intracellular survival techniques of *C.trachomatis*.

K^+ efflux has been implicated in host responses to pathogen invasion by activation of the $NLRP_3$ inflammasome and consequently caspase-1 production (Muñoz-Planillo *et al.,* 2013). The data presented in this chapter demonstrate that a K^+ efflux in response to chlamydial infection would cause persistence, which would suggest that the bacteria must have some strategy in place to prevent this efflux. Indeed, the inhibition of $NLRP_3$ activation is a strategy employed by pathogens such as *Pseudomonas aeruginosa* (Galle *et al.,* 2008) and *Yersinia* (Schotte, 2004) to avoid detection by host cells. Chang and Moulder (1978) reported that infection of L-cells with high

multiplicities of *C.psittaci* (multiplicity of infection (MOI)=100 or higher) caused a significant loss of K^+, determined using flame photometry of lysed cells. However both HeLa and L-cells infected with more physiological bacterial titres (MOI=10) lost little intracellular K+ until 48hpi, when a significant loss was demonstrated. These observations would appear to conflict with results from two studies by Abdul-Sater *et al.* (2010a; 2010b) which show that K^+ efflux-induced reactive oxygen species (ROS) production and consequent caspase-1 production, via $NLRP_3$ activation, is essential for *Chlamydiae* infection of THP-1 cells. However, ROS production appeared to increase as infection progressed, with the most significant increase between 20-24hpi. This could suggest that, although a K^+ efflux during replication induces persistence, *Chlamydiae* have differing requirements for K^+ as the infection cycle progresses.

Chapter 4 – Results

A novel K^+ cycle during chlamydial development

4.1 Introduction

The data presented in chapter 3 demonstrate that reducing the concentration of intracellular potassium ions (K^+), either by inducing an efflux using K^+ specific ionophores or inhibiting inward rectifying K^+ (K_{ir}) channels, during bacterial replication induces persistence. These data would suggest that high intracellular K^+ concentration plays an essential role in the chlamydial infection cycle.

K^+ efflux from cells in response to bacterial invasion is a common trigger of an innate immune response (Franchi *et al.,* 2012; Muñoz-Planillo *et al.,* 2013). Our data indicate that, if this were to occur during chlamydial invasion, the bacteria would enter a persistent state and infection would not progress. This could suggest that *Chlamydiae* have some strategy in place to sidestep this K^+ efflux. For example, some intracellular pathogens, such as *Pseudomonas aeruginosa* (Galle *et al.,* 2008) and *Yersinia* (Schotte, 2004), inhibit the activation of inflammasomes during cell entry to avoid detection by the host. Host cell response to chlamydial infection via the NLRP3 inflammasome, a complex responsible for caspase-1 activation and interleukin-1β production, has been extensively studied, and caspase-1 has been shown to be activated during *C.trachomatis* infection (Lu *et al.,* 2000; Gervassi *et al.,* 2004; Cheng *et al.,* 2008; Prantner *et al.,* 2009; and Abdul-Sater *et al.,* 2009; 2010a; 2010b). Interestingly, the activation of caspase-1 following *C.trachomatis* LGV2 infection appears to occur later in the infection cycle, from 36-48 hours post infection (hpi) (Lu *et al.,* 2000), as opposed to an immediate response to bacterial invasion. This would suggest that, if a

K^+ efflux is the trigger for caspase-1 activation in this instance, then the efflux occurs later in the infection cycle than we have so far observed.

Our data have established that a K^+ efflux is detrimental to bacteria during replication (12hpi in HeLa cells). As *Chlamydiae* exist in two different forms, with distinct nutritional and metabolic requirements, the effect of a K^+ efflux at different points during the bacterial development cycle was assayed.

4.2 An induced K^+ efflux after RB-EB differentiation does not affect chlamydial infectivity

To determine whether *Chlamydiae* have differing requirements for K^+ throughout the development cycle, intracellular K^+ was depleted using nigericin at different phases of the infection cycle.

C.trachomatis LGV2 inclusions in HeLa cells contain RBs between 6 and 24hpi (**Figure 3.3B**), after which RB-EB differentiation occurs and the inclusion lumen fills with a mixed population of RBs and EBs. At approximately 50hpi, the EBs are released. To determine whether K^+ availability is vital throughout the cycle, or just during replication of RBs, nigericin was used to treat inclusions at different timepoints during *C.trachomatis* LGV2 infection of HeLa cells. Infectivity was quantified at the end of the development cycle, when the bacteria should have undergone RB-EB re-differentiation (as described in **Figure 3.2**).

Infected cells were treated with 1μM nigericin before inclusion formation (1hpi), during RB replication (12hpi), as re-differentiation begins to occur (24hpi), once the inclusion contains a mixed population of EBs and RBs (36hpi), and prior to cell lysis when the inclusion contains predominantly EBs (48hpi) (**Figure 4.1A**). All infections were then allowed to progress until 50hpi before cells were collected. Infectivity was then quantified, as inclusion-forming units (IFUs), following the infection of a new monolayer of cells. No infectious bacteria were collected from cells treated with nigericin prior to RB-EB differentiation, from 1-12hpi. Infectivity was recovered when K^+ concentrations were disrupted at and subsequent to 24hpi (**Figure 4.1B**). Limited infectivity was evident when cells were treated 24hpi, a timepoint at which the RB-EB differentiation had begun. This suggests that intracellular K^+ depletion causes persistence in RBs, as described in **Section 3.8**, but that EBs are unaffected. This is supported by the observation that the later in the *C.trachomatis* LGV2 infection cycle HeLa cells are treated with nigericin, and consequently the greater the number of bacteria that were present as EBs at the time of K^+ efflux, the greater the titre of infectious bacteria. However, treatment of EBs at the beginning of the infection cycle, *i.e.* at 1hpi, abolished detectable infectivity at the end of the infection cycle, 50hpi (**Figure 4.1B**). This could indicate that an ionophore induced K^+ efflux disrupts early events in the infection cycle, or alternatively, could reflect early EB differentiation into K^+ starvation-sensitive RBs.

To monitor any changes in early inclusion biogenesis, HeLa cells infected with *C.trachomatis* LGV2 were treated with nigericin 1hpi, fixed at 24hpi and labelled using anti-*Chlamydia* antibodies. The bacteria were not arranged in the conventional

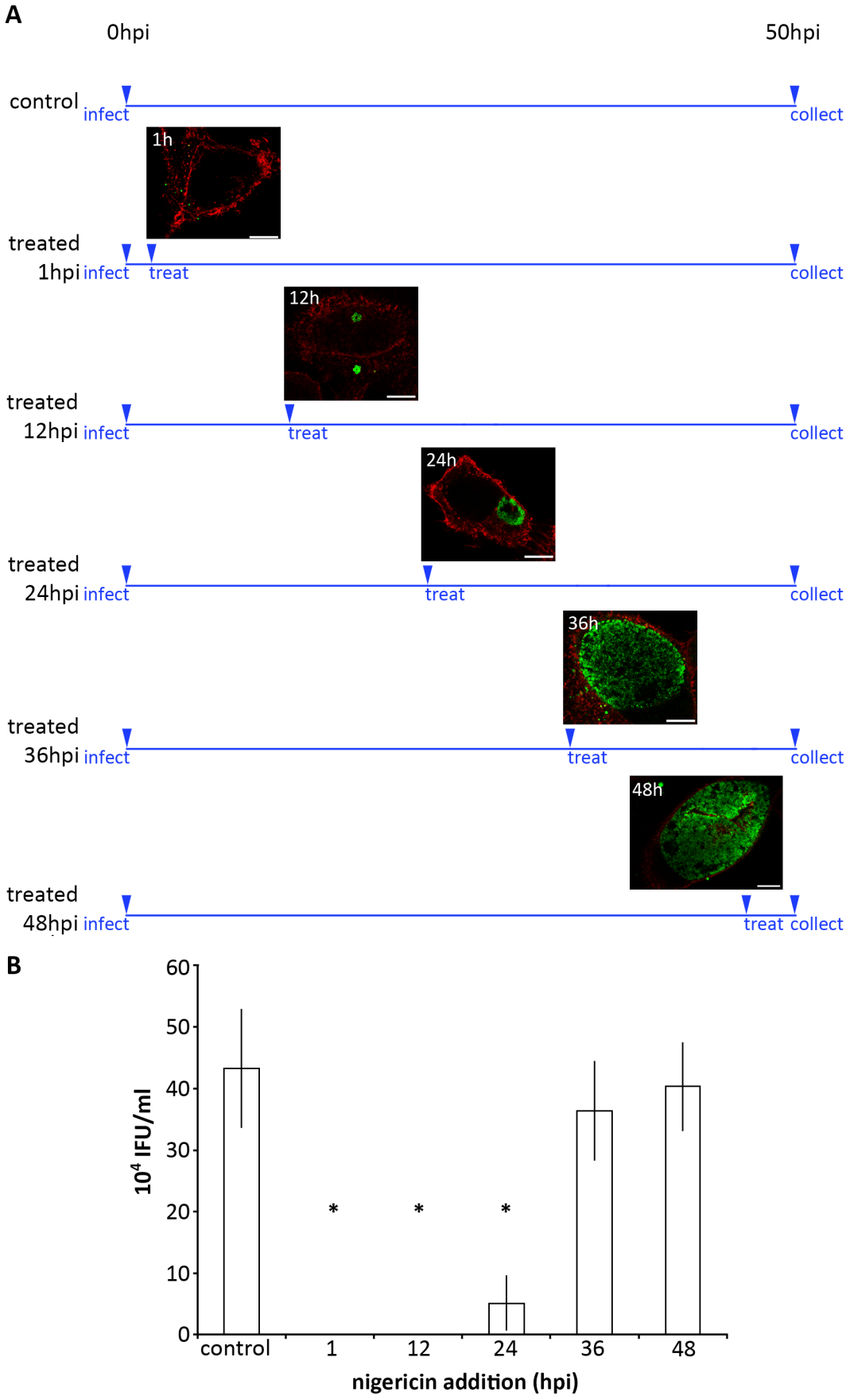
A
0hpi
50hpi
control
infect
collect
1h
treated
1hpi
infect
treat
collect
12h
treated
12hpi
infect
treat
collect
24h
treated
24hpi
infect
treat
collect
36h
treated
36hpi
infect
treat
collect
48h
treated
48hpi
infect
treat
collect
B
60
50
40
30
20
10
0
10^4 IFU/ml
*
*
*
control
1
12
24
36
48
nigericin addition (hpi)

Figure 4.1. Ionophore-induced K^+ efflux causes persistence in *C.trachomatis* LGV2 RBs, however EBs are unaffected. (A) Schematic representation of experiment timelines, showing confocal xy-sections of *C.trachomatis* (green) infected HeLa cells (red) at the time of nigericin treatment. (B) HeLa cell layers were infected with *C.trachomatis* LGV2 (multiplicity of infection (MOI) =1) and either left untreated or treated with 1μM nigericin at either 1hpi, 12hpi, 24hpi, 36hpi, or 48hpi. Cells were collected at 50hpi and diluted in fresh media to infect a new layer of cells. After 24h, the second layer of infected cells were fixed and labelled using anti-*Chlamydia* spp. FITC-conjugated antibody and DAPI DNA stain. Inclusion-forming units (IFUs) were then quantified (IFU/ml). Each experiment was repeated a minimum of three times, and the data presented are representative of each iteration. Error bars show standard deviation. (* = $p \leq 0.05$).

inclusion structure, as observed in the control condition (**Figure 4.2A**). The resolution of confocal xy-sections is insufficient to differentiate between internalised bacteria and those at the cell periphery. Differentiation between internal and external bacteria can nevertheless be achieved by immunolabelling. To determine if the dispersed bacteria observed in cells treated 1hpi with nigericin were intracellular, or if they remain on the cell periphery, cells were labelled both before and after permeabilisation using two different fluorophores. External bacteria were labelled prior to permeabilisation then, following permeabilisation, both intracellular and extracellular bacteria were labelled. Under these conditions, intracellular bacteria are labelled by a single fluorophore, whereas extracellular bacteria are dual labelled. HeLa cells infected with *C.trachomatis* LGV2 exclusively contained singly labelled bacteria at 24hpi, arranged in a ring consistent with a normal inclusion at this time point, demonstrating that they are intracellular (**Figure 4.2B** control). Heat inactivated bacteria, which were introduced to HeLa cells as a control for external bacteria, were dual labelled at 24hpi (**Figure 4.2B** heat inactivated bacteria). In HeLa cells infected with *C.trachomatis* LGV2 and treated at 1hpi with nigericin, bacteria were larger than EBs at 24hpi, the majority of which were single labelled and therefore intracellular (**Figure 4.2B** nigericin. Intracellular bacteria indicated by white arrows in increased zoom panel). However, replication did not appear to have occurred under K^+-starved conditions and the bacteria were dispersed throughout the cell, and are maybe even cytosolic, as opposed to contained within a single inclusion. This demonstrates that when K^+ efflux is induced at 1hpi, bacteria remain inside the host cell, but initial steps in inclusion biogenesis and chlamydial replication are apparently disrupted.

A

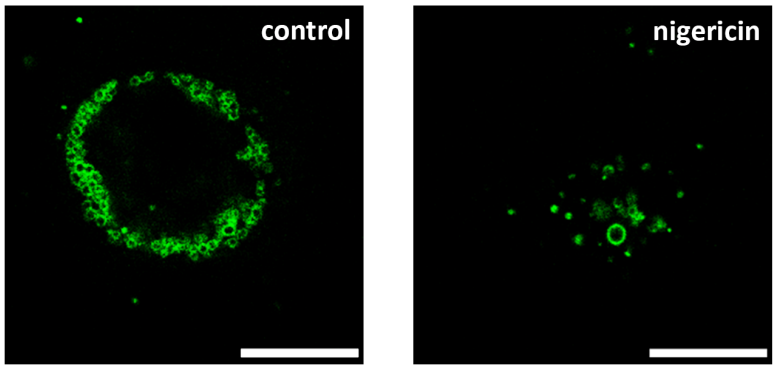
control
nigericin

B

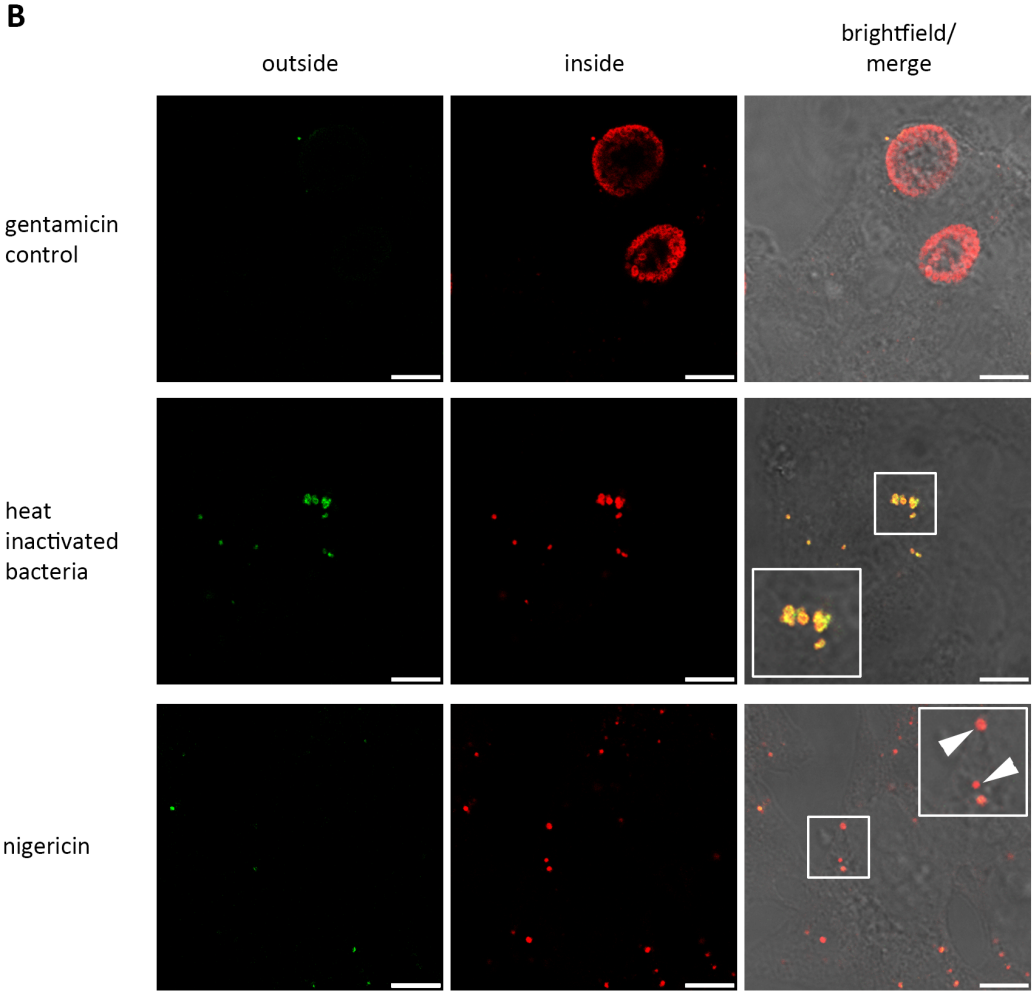
outside
inside
brightfield/
merge
gentamicin
control
heat
inactivated
bacteria
nigericin

Figure 4.2. Ionophore-induced K^+ efflux disrupts early inclusion biogenesis. (A) Confocal xy-sections of HeLa cells infected with *C.trachomatis* LGV2 (MOI=1) either untreated or treated 1hpi with 1μM nigericin. Cells were then fixed 24hpi. Bacteria were labelled with anti-*Chlamydia* spp. MOMP/LPS specific primary antibody followed by AlexaFluor®488 conjugated secondary antibody (green). Scale bars, 10μm. (B) Confocal xy-sections, and bright-field micrographs of HeLa cells infected with either heat inactivated *C.trachomatis* LGV2 (MOI=1), or infected with *C.trachomatis* LGV2 (MOI=1) and left untreated, or infected with *C.trachomatis* LGV2 (MOI=1) and treated at 1hpi with 1μM nigericin. Cells were then fixed at 24hpi. Bacteria were labelled with fluorescein isothiocyanate (FITC) conjugated anti-*Chlamydia* spp. MOMP/LPS specific antibody (green) prior to methanol/ethanol permeabilization, anti-*Chlamydia* spp. MOMP/LPS primary antibody and AlexaFluor®568 conjugated secondary antibody (red). Bacteria labelled with AlexaFluor®568 only were inside the cell, and those that dual labelled (yellow) were external. Scale bars, 10μm. Insets show indicated areas at higher magnification.

Chlamydial infections progress at different rates, dependent on host, serovar and strain. If nigericin treatment at similar points in the development cycle has a similar effect *i.e.* there is a significant impact of K^+ starvation on RBs, but progressively less of an effect as RB-EB differentiation advances, then a clearer link between K^+ availability and the infection cycle can be established.

RL95-2 cells infected with *C.trachomatis* LGV2 and HeLa cells infected with either *C.trachomatis* D or *C.muridarum* were treated with nigericin at specific phases in the infection cycle *i.e.* following internalisation, during RB replication, as RB-EB differentiation began to occur, or once the majority of the bacteria had differentiated into EBs (see **Table 4.1** for treatment times for each bacteria-host combination).

Species	Host	Nigericin treatment			
		after cell invasion	RB replication	RB-EB differentiat-ion	EB prior to release
C.trachomatis LGV2	RL95-2	1hpi	6hpi	12hpi	24hpi
C.trachomatis D	HeLa	1hpi	24hpi	48hpi	72hpi
C.muridarum	HeLa	1hpi	12hpi	24hpi	36hpi

Table 4.1. Time of nigericin addition to target specific phases in the infection cycle for each bacteria-host interaction. Phases of the infection cycle were determined using the data collected in chapter 3 (**Section 3.9**).

RL95-2 cells were infected with *C.trachomatis* LGV2 and treated with nigericin at appropriate timepoints during the infection cycle (**Table 4.1**). Infectivity was

monitored at the end of the infection cycle at 40hpi. By 40hpi bacteria in control cells are present as infectious EBs (**Figure 4.3A** control), therefore a decrease in infectivity at this point as a result of an ionophore-induced K^+ efflux indicates disruption in RB-EB re-differentiation, resulting in non-infectious bacteria. No infectivity was recovered from cells treated prior to RB-EB differentiation, however cells treated at 12hpi and later contained infectious bacteria despite the nigericin-induced K+ efflux (**Figure 4.3A**). Cells treated early in the RB-EB transition contained fewer infectious EBs than those treated later, when a greater proportion of the bacteria were present as EBs. This shows that K^+ starvation only disrupts RBs irrespective of the host cell line.

HeLa cells infected with *C.trachomatis* D contained EBs at 90hpi (**Figure 4.3B**). HeLa cells infected with *C.trachomatis* D, treated at similar phases of the infection cycle (**Table 4.1**), were collected for quantification of infectivity at 90hpi. Bacteria collected from cells treated before RB-EB differentiation had begun were non-infectious (**Figure 4.3B**), but infectivity could be recovered from cells treated after RB-EB differentiation, suggesting that K^+ availability is essential during the period of RB replication only, regardless of serovar.

Finally, HeLa cells infected with *C.muridarum* contained infectious EBs 36hpi (**Figure 4.3C** control). HeLa cells infected with *C.muridarum* and equivalently treated with nigericin (**Table 4.1**) were assayed for infectivity at 40hpi. Once again, K^+ efflux prevented infectivity in cells treated before RB-EB differentiation but had progressively less of an effect as treatment occurred at later timepoints (**Figure 4.3C**). This shows that *Chlamydiae* are only sensitive to K^+ starvation during RB replication.

A

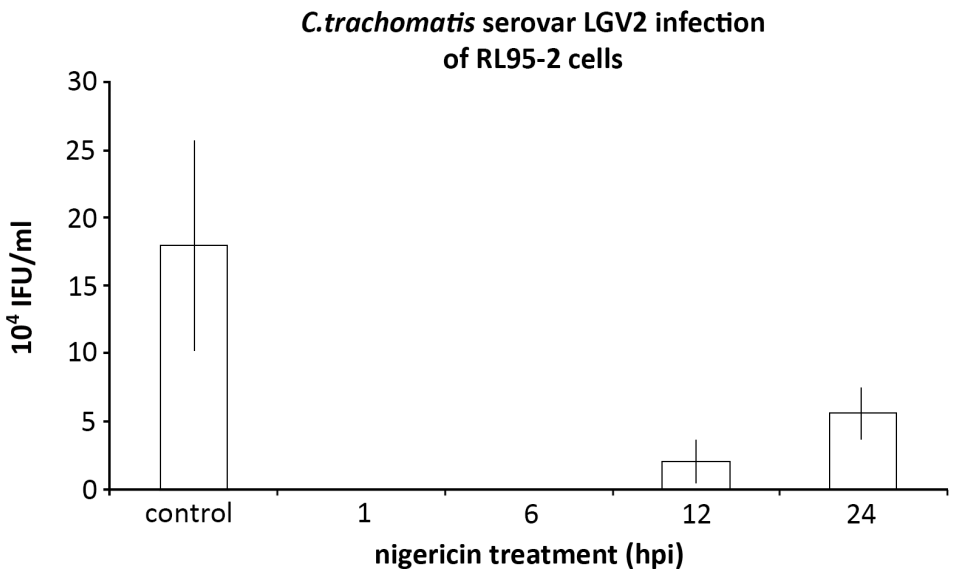
C.trachomatis serovar LGV2 infection
of RL95-2 cells
30
25
20
15
10
5
0
10^4 IFU/ml
control
1
6
12
24
nigericin treatment (hpi)

B

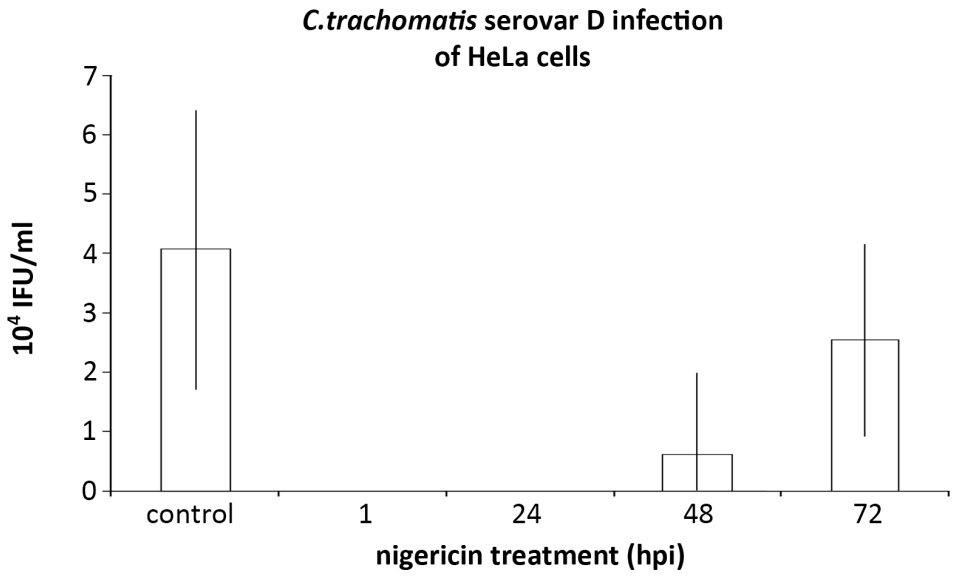
C.trachomatis serovar D infection
of HeLa cells
7
6
5
4
3
2
1
0
10^4 IFU/ml
control
1
24
48
72
nigericin treatment (hpi)

C

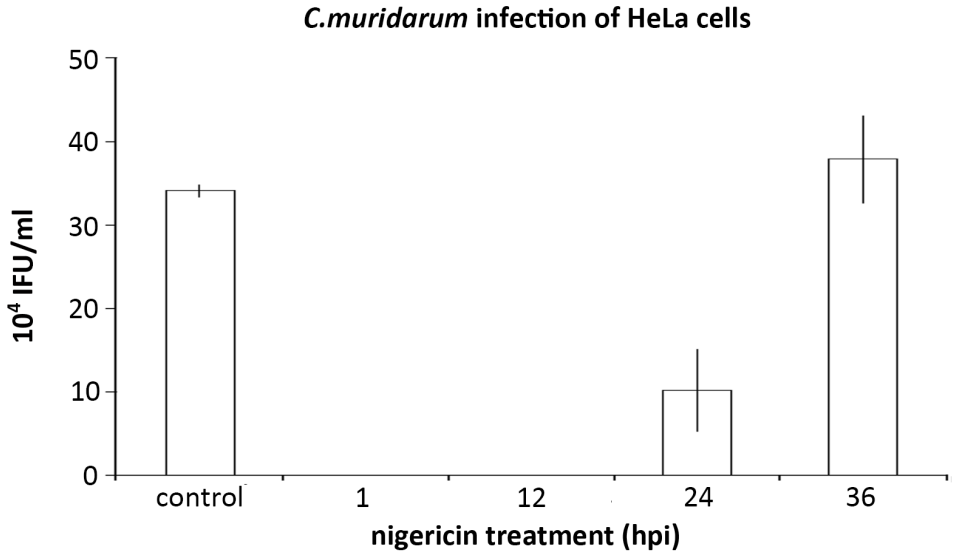
C.muridarum infection of HeLa cells
50
40
30
20
10
0
10^4 IFU/ml
control
1
12
24
36
nigericin treatment (hpi)

Figure 4.3. K^+ efflux during RB phase of the infection cycle induces persistence irrespective of serovar, species or host. (A) *C.trachomatis* LGV2 infected RL95-2 cells (MOI=1) were either untreated or treated with 1μM nigericin at either 1hpi, 6hpi, 12hpi, or 24hpi, prior to collection at 40hpi and diluted in fresh media to infect a new layer of cells. (B) *C.trachomatis* serovar D infected HeLa cells (MOI=1) were either untreated or treated with 1μM nigericin at either 1hpi, 24hpi, 48hpi, or 72hpi, prior to collection at 90hpi and diluted in fresh media to infect a new layer of cells. (C) *C.muridarum* infected HeLa cells (MOI=1) were either untreated or treated with 1μM nigericin either 1hpi, 12hpi, 24hpi, or 36hpi, prior to collection 40hpi and diluted in fresh media to infect a layer of cells HeLa. In all cases the second monolayer of cells was fixed at 24hpi and labelled using anti-*Chlamydia* spp. FITC-conjugated antibody and DAPI DNA stain. IFUs were then quantified (IFU/ml). Error bars show standard deviation.

These data demonstrate that nigericin-induced K^+ efflux disrupts inclusion biogenesis early in the infection cycle, and causes persistence during RB replication, but a K^+ efflux following RB-EB differentiation does not affect bacterial infectivity. This is demonstrated by a progressive increase in infectious bacteria that can be collected from cells the later in the infection cycle the K^+ efflux occurs. This would suggest that the different bacterial forms have different K^+ requirements.

4.3 Chlamydial RBs are enriched with K^+

Asante potassium green 2 (APG-2) is a recently developed K^+-specific fluorescent probe for use in live cells. As there is no published data to validate the use of APG-2 for observing K^+ distribution within cells, a labelling protocol had to be optimised in HeLa cells. APG-2 labelled HeLa cells have diffuse cytosolic labelling with more intense fluorescence within the mitochondria (**Figure 4.4A**). The difference in fluorescence intensity is consistent with differing K^+ concentrations in the cytosol and within the mitochondria, approximately 148mM (Grieshaber *et al.,* 2002) and 180mM (Kozoriz *et al.,* 2010) respectively.

To ensure that differences in fluorescence intensity are indicative of differing K^+ concentrations, live HeLa cells were labelled with APG-2 and treated with 1μM nigericin, which was shown to reduce intracellular K^+ by half when assayed using flame photometry (**Figure 3.6**). Confocal xy-images were taken every 10 minutes for 90 minutes following nigericin addition. Mean pixel intensity measurements were taken

for three regions of interest (ROIs) within the cells using ImageJ (for macro see **Appendix 4**). Measurements were corrected for background fluorescence using equivalent pixel intensity measurements from a ROI that contained no cells. Fluorescence intensity decreased rapidly in the 30 minutes following nigericin addition, and plateaued at approximately half the initial intensity for the remaining 60 minutes (**Figure 4.4B**). It was not possible to correct for photobleaching in the sample because all the cells within the sample were subjected to nigericin treatment. However, APG-2 labelled live HeLa cells were equivalently imaged without the addition of nigericin. Over the same period, three ROIs from the cytosol of APG-2 labelled HeLa cells, corrected for background fluorescence using an ROI from an area containing no cells, were assayed. Fluorescence intensity remained relatively constant throughout the timecourse (**Figure 4.4C**). These data show that, whilst APG-2 is subject to limited photobleaching, K^+ efflux as a result of nigericin treatment reduced APG-2 fluorescence intensity. This verifies that decreased fluorescence intensity in APG-2 labelled micrographs corresponds to lower K^+ concentration. In addition, these data show that APG-2 is an appropriate tool for observing K^+ distribution in *C.trachomatis* infected cells.

HeLa cells infected with *C.trachomatis* LGV2 were labelled with APG-2 at 12hpi. Live confocal observation of xy-sections showed that RBs were intensely labelled with APG-2 probe, indicative of a high K^+ concentration (**Figure 4.5A** 12hpi). There also appeared to be a decrease in fluorescence in both the host cell cytosol and mitochondria, despite being imaged using equivalent confocal settings. HeLa cells infected with *C.trachomatis* LGV2 were APG-2 labelled and observed later in the infection cycle. At

A

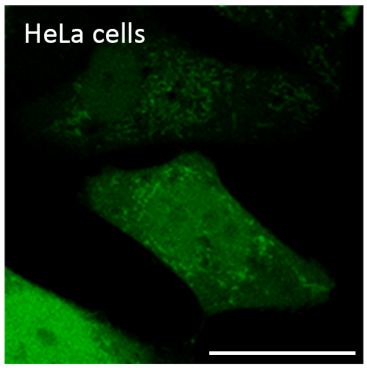
HeLa cells

B

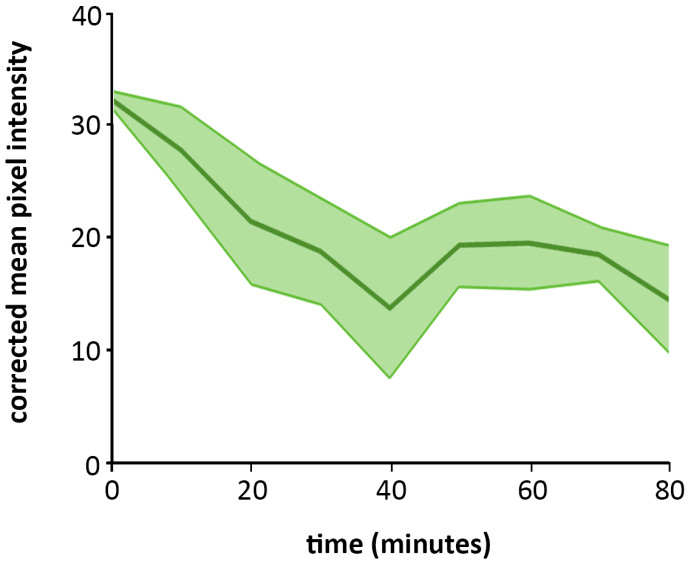
corrected mean pixel intensity
0
10
20
30
40
0
20
40
60
80
time (minutes)

C

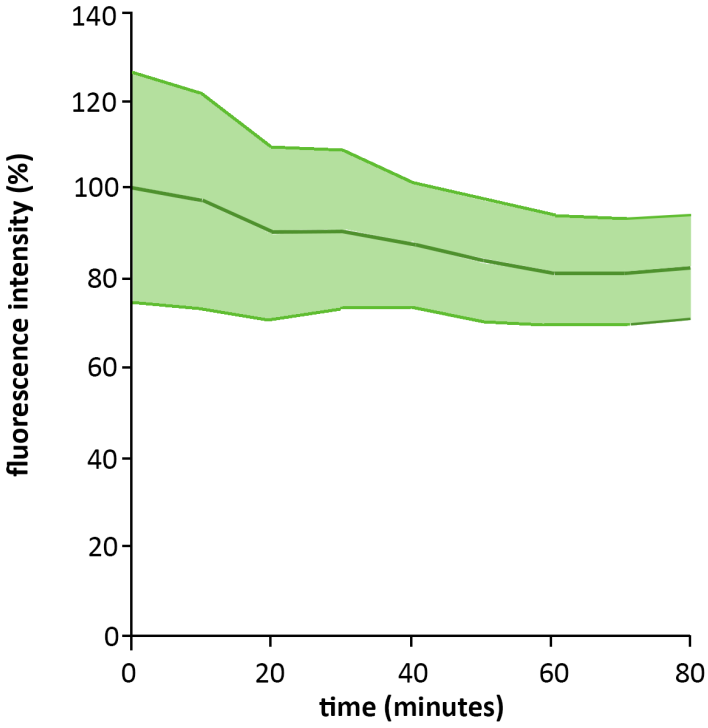
fluorescence intensity (%)
0
20
40
60
80
100
120
140
0
20
40
60
80
time (minutes)

Figure 4.4. Nigericin treatment reduces APG-2 fluorescence by half within 30 minutes. (A) Live confocal xy-sections of HeLa cells labelled using APG-2 (green). Scale bar, 25μm. (B) Mean pixel intensity, corrected for background fluorescence, for 3 regions of interest (ROIs) from HeLa cells treated with 1μM nigericin. Images were taken every 10 minutes for 80 minutes. Shaded area represents standard deviation. (C) Mean pixel intensity from 3 ROIs, presented as a percentage of initial pixel intensity, from HeLa cells labelled with APG-2 and imaged every 10 minutes for 80 minutes to observe photobleaching, presented as a percentage of the average intensity of the initial frame. Shaded area represents standard deviation.

24hpi the infected cells contained intensely labelled RBs. APG-2 fluorescence had reduced in the host cell cytosol and mitochondria as the infection progressed (**Figure 4.5A** 24hpi). This implies that the bacteria use the host cell as a source of K^+ during replication. By 36hpi, once RB-EB differentiation has initiated, APG-2 labelled RBs were observed around the perimeter of the inclusion, however there was very little APG-2 labelling deeper into the lumen of the inclusion (**Figure 4.5A** 36hpi). Confocal xy-sections of equivalently infected cells, fixed at 36hpi and labelled with anti-*Chlamydia* spp. specific MOMP/LPS antibody, showed that the inclusion lumen is filled with bacteria at this timepoint (**Figure 4.5B** MOMP/LPS). However, APG-2 only labelled bacteria around the periphery of the inclusion (**Figure 4.5B** K^+), indicating that the bacteria that are not in contact with the inclusion membrane have a much lower K^+ content.

These data suggest that *Chlamydiaceae* accumulate K^+ during replication, however this K^+ seems to be lost once RB-EB differentiation occurs. Having shown that K^+ fluctuations can be observed using variation in APG-2 fluorescence intensity, this probe can now be applied to follow K^+ fluxes during the *C.trachomatis* infection cycle.

A

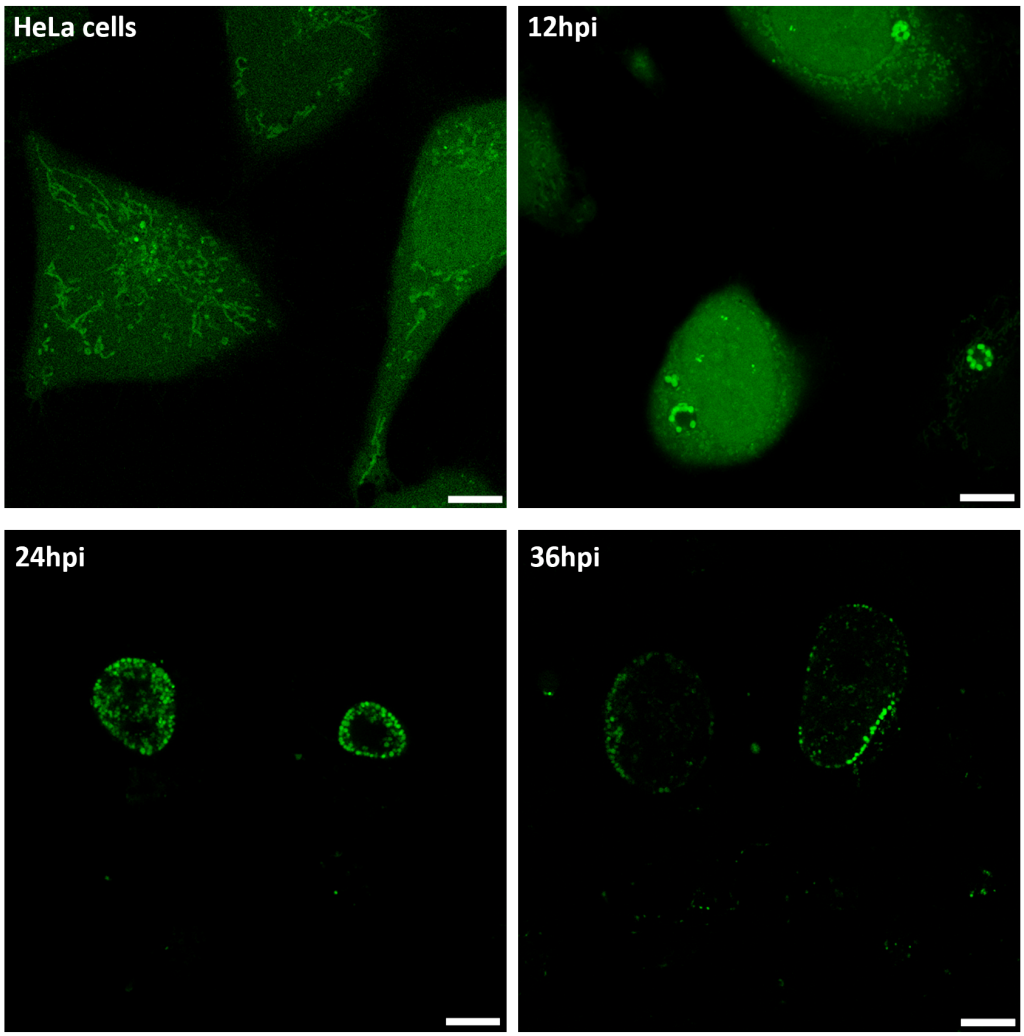
HeLa cells
12hpi
24hpi
36hpi

B

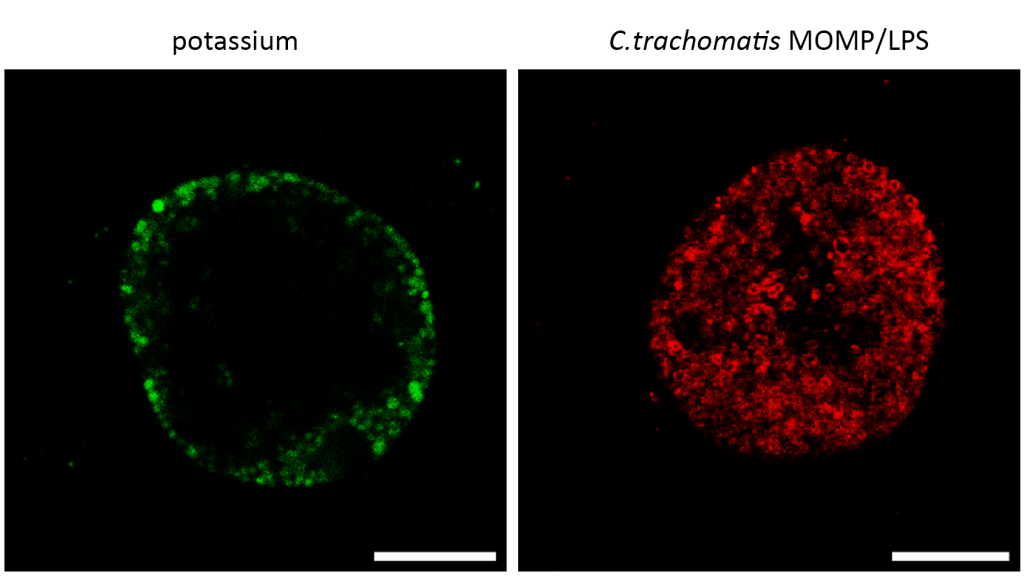
potassium
C.trachomatis MOMP/LPS

Figure 4.5. K^+ sensitive fluorescent probe illustrates high K^+ concentration in RBs but lower K^+ in EBs. (A) Confocal xy-sections of live HeLa cells labelled using APG-2 K+ sensitive probe (green) either uninfected (panel 1), or infected *C.trachomatis* LGV2 (MO=1) after 12hpi, 24hpi, or 36hpi (as indicated). Scale bars, 10μm. (B) Confocal xy-section of *C.trachomatis* LGV2 infected HeLa cells 36hpi either labelled live with APG-2 (green; potassium) or fixed and labelled using *Chlamydia* spp. MOMP/LPS primary antibody followed by AlexaFluor®568 conjugated secondary antibody (red; MOMP/LPS). Scale bars, 10μm.

4.4 RBs scavenge host cell K^+

Having shown that APG-2 can be used to detect changes in K^+ levels, fluorescence recovery after photobleaching (FRAP) analysis was then undertaken to observe K^+ dynamics within the infected cell and the inclusion. HeLa cells were infected with *C.trachomatis* LGV2 and labelled with APG-2 at 24hpi. These cells were then subjected to photobleaching, followed by image capture every 8 seconds for 10 frames, followed by 10 frames every 20 seconds (for Leica FRAP wizard settings see **Appendix 5**). Mean pixel intensities from ROIs within the bacteria, the inclusion lumen, and the host cell cytosol were measured using ImageJ (for macro see **Appendix 4**). Mean pixel intensities were compared before and after photobleaching for ROIs (**Figure 4.6A**). Bacteria partially recover fluorescence very quickly after photobleaching, however they do not appear to recover to the original level over the observed time window (**Figure 4.6B**). The inclusion lumen shows a delay in fluorescence recovery, but fluorescence does recover to some extent. The host cell cytosol shows no decrease in fluorescence, suggesting that the molecules in the cytosol are moving around so rapidly that the bleached fluorophores are replaced almost instantly.

These data show that bacteria continually accumulate K^+ during intracellular replication. We have previously shown that while RBs are high in K^+, EBs do not exhibit any APG-2 fluorescence and therefore are much lower in K^+. This would indicate that K^+ is lost at some point during RB-EB differentiation. Determining when this K^+ efflux occurs could provide some insight into the function of K^+ during the infection cycle.

A

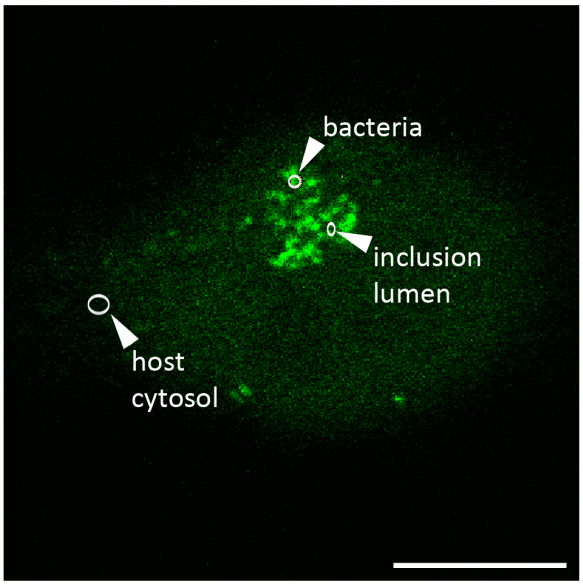
bacteria
inclusion
lumen
host
cytosol

B

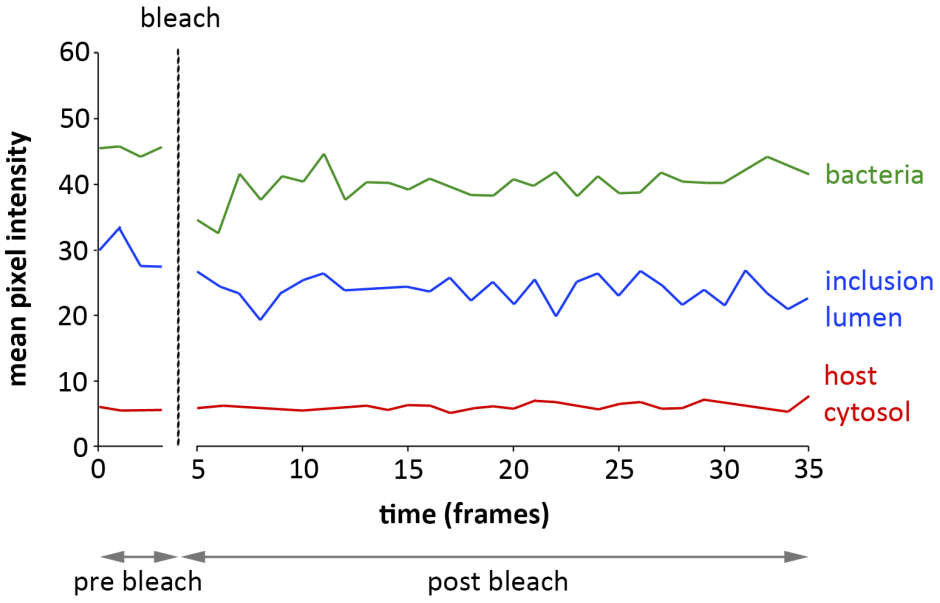
bleach
mean pixel intensity
60
50
40
30
20
10
0
0
5
10
15
20
25
30
35
time (frames)
bacteria
inclusion
lumen
host
cytosol
pre bleach
post bleach

Figure 4.6. Bacteria recover APG-2 fluorescence following photobleaching. (A) Confocal xy-section of *C.trachomatis* LGV2 infected HeLa cells (MOI=1) labelled with APG-2 24hpi prior to bleaching. Bacteria, inclusion lumen, and cytosol ROIs circled and indicated using white arrows. Scale bar, 10μm. (B) Mean pixel intensity for ROIs taken at minimized intervals, with a scanning speed of 400Hz, for 10 frames the every 20 seconds for 20 frames.

4.5 K^+ are lost from the bacteria prior to inclusion expansion

C.trachomatis LGV2 accumulate K^+ during replication. In contrast, EBs were shown to contain less K^+, and infectivity was unaffected by K^+ starvation. These observations suggest that K^+ is lost from the bacteria during the transition from RB to EB.

To observe K^+ fluctuations during RB-EB differentiation, HeLa cells infected with *C.trachomatis* LGV2 were labelled with APG-2 and Hoechst 33342, a fluorescent DNA intercalating agent suitable for imaging live cells, then observed by fluorescence microscopy in a heat-controlled chamber at 5% CO_2. Confocal xyz-stacks were taken every 10 minutes for 6h starting at 30hpi. Maximum intensity z-projections at each time point were compiled for the field of view (FOV) imaged. Changes in fluorescence intensity throughout the time course were assayed for three infected cells within the field of view (numbered in **Figure 4.7A**). For each inclusion mean pixel intensity measurements, in both Hoechst and APG-2 channels, were obtained from an ROI that remained within the inclusion for the duration of the time course (ROI used for **Figure 4.7** inclusion 1 is illustrated in white in each frame in **Figure 4.8**). (For ImageJ macro used to obtain pixel intensity values see **Appendix 4**). Each value was corrected for background fluorescence by subtracting equivalent intensity measurements from an ROI that did not contain any cells. Similarly, pixel intensity measurements obtained from an ROI in an uninfected cell, from the same FOV, were used to correct each value for photobleaching (see **Section 2.5.6, Equation 3**). Bacteria within a chlamydial inclusion remain in constant motion during live imaging, which is problematic when attempting to compare measurements over a time course. Comparison of fluorescence

intensity is further complicated by the continued replication of the bacteria and consequent growth of the inclusion. At confocal resolution it is not possible to follow a single bacteria throughout the time course therefore the risk when comparing ROI averages over time is that the quantity of bacteria within that ROI can fluctuate and impact the values. To monitor the effect of bacterial movement within the ROI throughout the time course, equivalent Hoechst (DNA) pixel intensities were compared along with APG-2 (K^+) values. Variation in DNA pixel intensity measurements should correspond to fluctuations in the number of bacteria within the ROI, *i.e.* increased pixel intensity indicates more bacteria and vice versa. Comparison of corrected mean pixel intensities throughout the time course showed a dramatic increase in APG-2 fluorescence intensity over the first 30 minutes of image capture, which was independent of any increase in Hoechst fluorescence intensity (**Figure 4.7 B**). Between 30 and 110 minutes, *i.e.* from 30h 30m to 31h 50m post infection, APG-2 fluorescence intensity decreases, indicating decreasing K^+ concentrations within the ROIs assayed (**Figure 4.7 B**).

Observing a single cell throughout this time course, as shown in **Figure 4.8** (also see supplementary movie **S1**), shows that from 30-36hpi the *C.trachomatis* LGV2 inclusion undergoes a number of interesting changes. Initially the chlamydial inclusion (outlined in yellow in **Figure 4.8** panel 0), appears tightly packed with bacteria and remains perinuclear for the first 100 minutes of image capture (**Figure 4.8** panels 0-100). By 110 minutes the inclusion appears to have expanded dramatically and the bacteria appear more diffuse within the inclusion (**Figure 4.8** panel 110). Using Hoechst DNA labelling of bacteria to identify the inclusion area, an estimate of the inclusion area, at

A

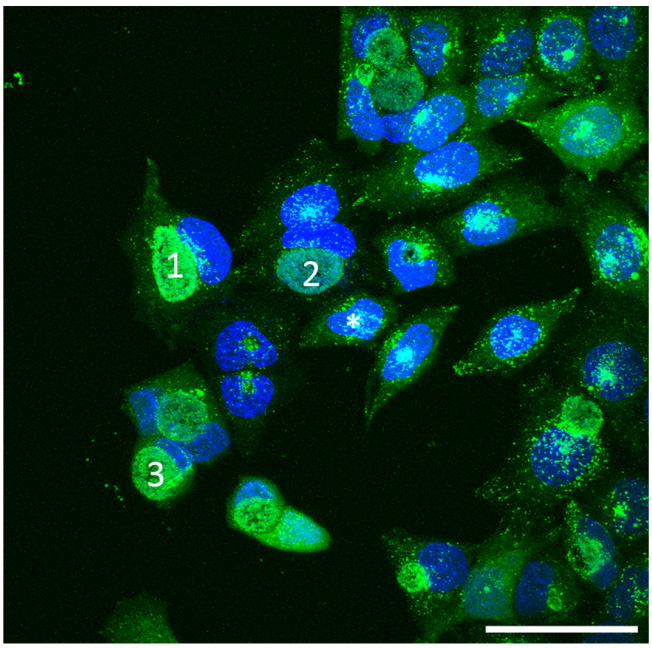
1
2
*
3

B

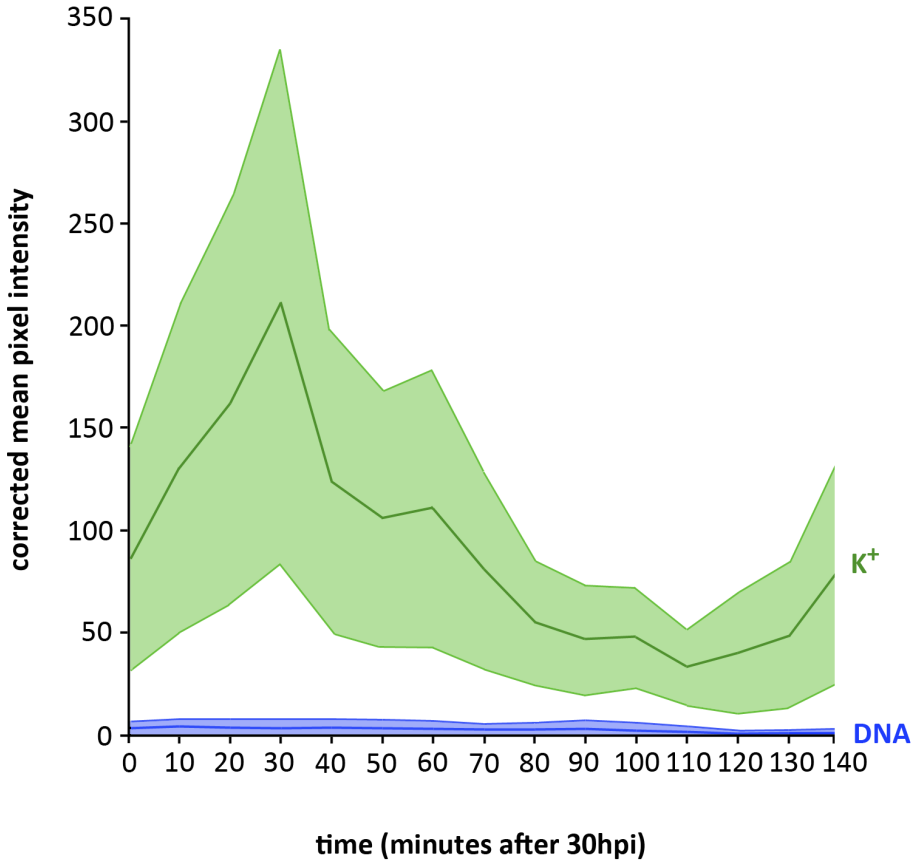
corrected mean pixel intensity
350
300
250
200
150
100
50
0
0 10 20 30 40 50 60 70 80 90 100 110 120 130 140
time (minutes after 30hpi)
K+
DNA

Figure 4.7. Inclusion K^+ concentration reaches a peak and is then steadily lost, with the lowest point corresponding with a dramatic increase in inclusion size. (A) Live confocal xyz-projection of HeLa cells infected with *C.trachomatis* LGV2 (MOI=1) and labelled using APG-2 K^+ probe (green) and Hoechst DNA stain (blue). Confocal xyz-stacks were obtained every 10 minutes from 30h to 32h 20m post infection (0-140 minutes after the beginning of image capture). Numbers indicate inclusions assayed for fluorescence intensity throughout the timecourse. Scale bar, 50μm. (B) Mean fluorescence intensity, corrected for photo-bleaching (using an uninfected cell indicated by * in A) and background fluorescence, over the time-course was assayed in both the DNA and K^+ channels and averaged for three inclusions in the field of view (ROI for the first inclusion illustrated in white in **Figure 4.8**). Shaded areas indicate standard deviation.

the largest point in the z-projections, was calculated for each frame throughout the time course (inclusion areas for frames before {100} and after {110} the inclusion expansion outlined in yellow in **Figure 4.9 A**). The inclusion area in the xy-plane, more than doubled from 100-110 minutes, *i.e.* from 31h 50m to 32hpi, for this inclusion (**Figure 4.9 B**), a change which is all the more evident in the supplementary movie **S1**. Interestingly, this dramatic change in the size of the inclusion appears to coincide with the point of lowest K^+ concentration.

The speed of the inclusion expansion, which occurs between frames and therefore takes less than 10 minutes, could indicate lysis of the inclusion membrane, however the bacteria appear to remain constrained within the host cell membrane beyond the end of image capture in this experiment (**Figure 4.8**).

These data show that the loss of K^+ from bacteria occurs gradually in the build up to inclusion expansion, which coincides with the point of lowest K^+ concentration within the inclusion. Inclusion membrane lysis has been illustrated using cytosolic GFP, which is excluded from intact inclusions (Heinzen *et al.,* 1997; Hybiske and Stevens, 2007). This method can be used to determine if K^+ loss corresponds to inclusion membrane lysis.

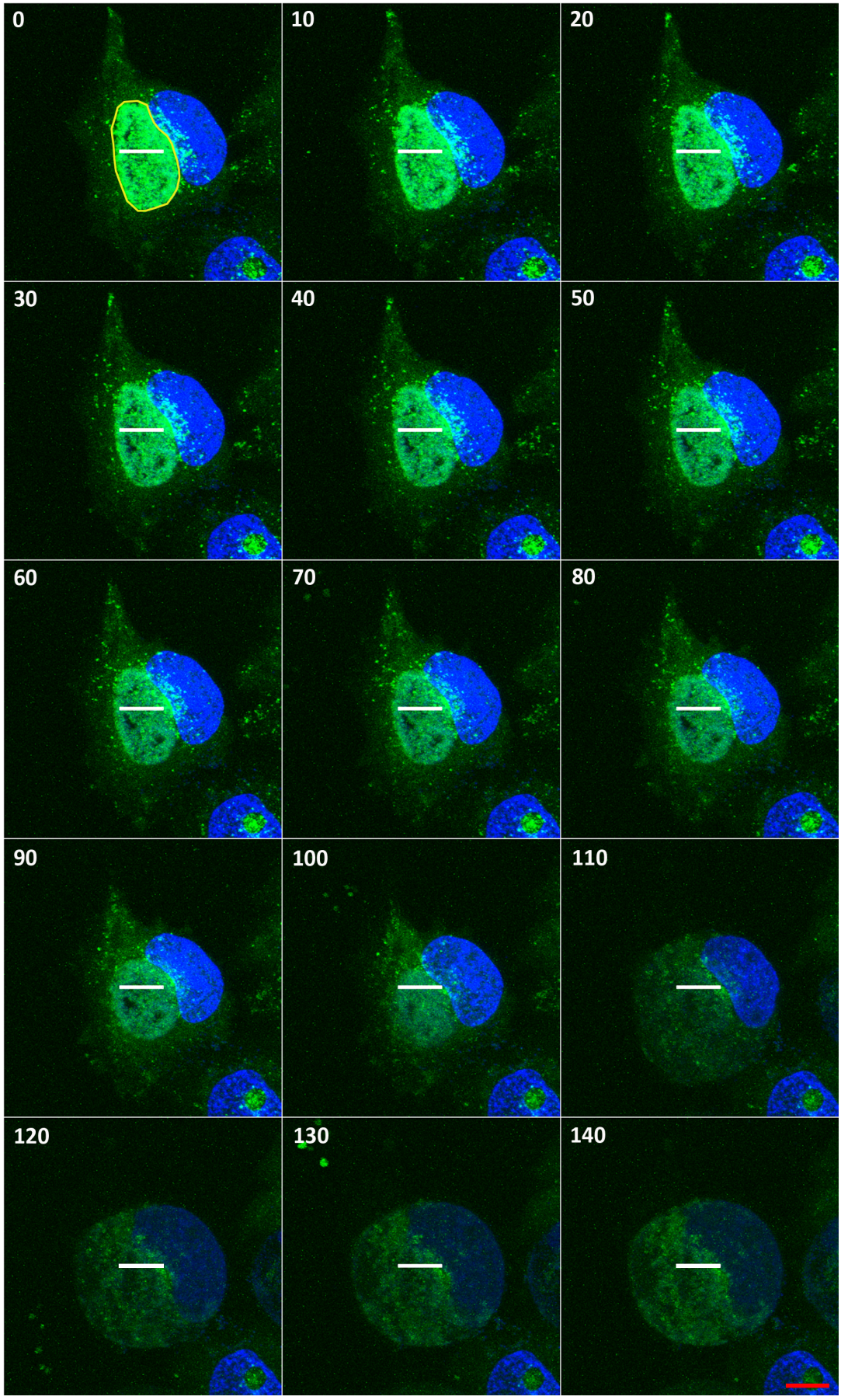
0
10
20
30
40
50
60
70
80
90
100
110
120
130
140

Figure 4.8. Time-lapse microscopy of *C.trachomatis* LGV2 infected HeLa cells from 30hpi shows a dramatic increase in inclusion size. Live confocal xyz-projections of *C.trachomatis* LGV2 infected HeLa cells (MOI=1) labelled using APG-2 K^+ probe (green) and Hoechst DNA stain (blue). Confocal xyz-stacks were obtained every 10 minutes from 30h to 32h 20m post infection (0-140 minutes after the beginning of image capture). White line indicates the ROI analysed for this inclusion (**Figure 4.7** inclusion 1). Scale bar (shown in red), 10μm.

A

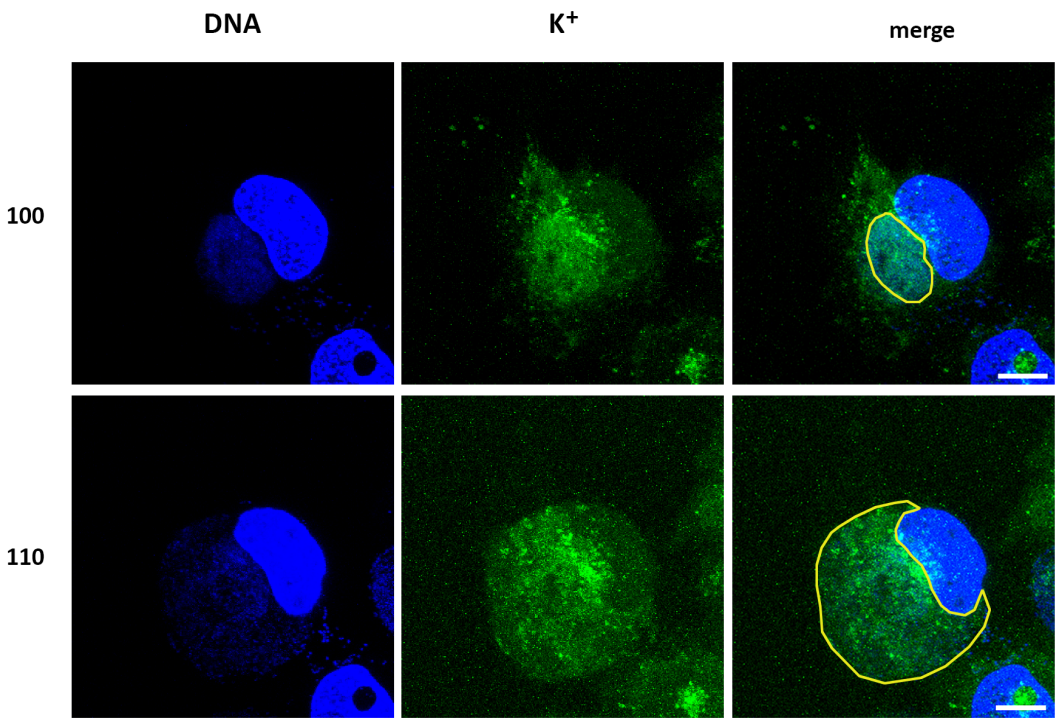
DNA
K+
merge
100
110

B

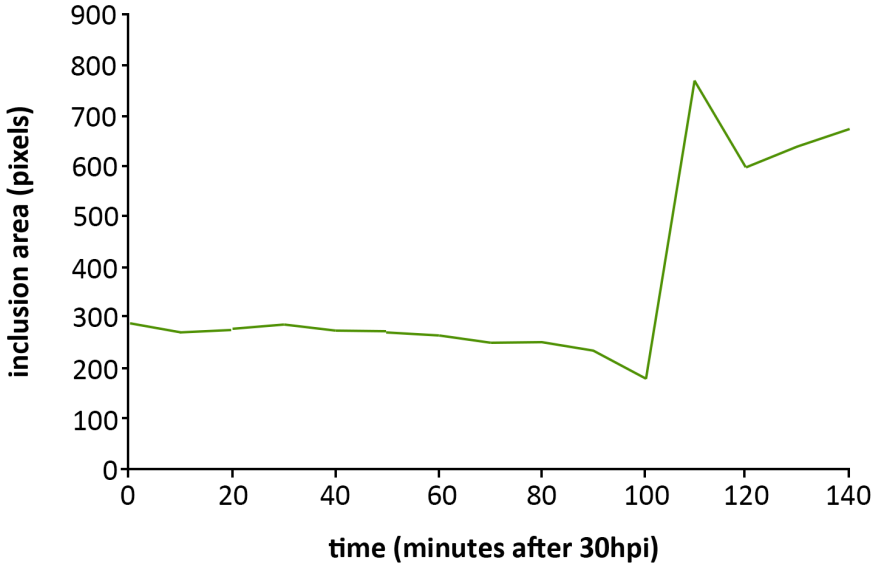
inclusion area (pixels)
900
800
700
600
500
400
300
200
100
0
0
20
40
60
80
100
120
140
time (minutes after 30hpi)

Figure 4.9. Inclusion area more than doubles 31h 50m after infection. (A) Confocal xyz-projections of live HeLa cells infected with *C.trachomatis* LGV2 (MOI-1) labelled with APG-2 K^+ probe (green) and DAPI DNA label (blue) and imaged at 31h 40 m after infection (100) and 31h 50m after infection (110). Inclusions outlined in yellow. Scale bars, 10μm. (B) Inclusion area (in pixels) measured for inclusion 1 (**Figure 4.7**) for the duration of the timecourse (0-140 minutes after the beginning of image capture).

4.6 The chlamydial inclusion membrane ruptures following a decrease in K^+ concentration

Cytosolic green fluorescent protein (GFP) (26.9kDa) is excluded from the inclusion in cells infected with *C.trachomatis* (Hybiske and Stephens, 2007), however GFP cannot be used in conjunction with the APG-2, as they have similar emission wavelengths. mCherry fluorescent protein, at 28.8kDa, should be unable to cross an intact inclusion membrane, and can be used with APG-2. HeLa cells were infected with *C.trachomatis* LGV2 and transiently transfected with either GFP or mCherry and fixed 30hpi. Inclusions (outlined in yellow in **Figure 4.10**) excluded both GFP (**Figure 4.10A**) and mCherry (**Figure 4.10B**) at 30hpi, demonstrating that mCherry can be used alongside APG-2 in order to assess the integrity of the inclusion membrane.

HeLa cells expressing mCherry were infected with *C.trachomatis* LGV2 and labelled 30hpi with Hoechst and APG-2 probes. Cells were then observed by live confocal microscopy at 37°C and 5% CO_2. Confocal xyz stacks were captured every 10 minutes to observe changes in K^+ concentration and inclusion membrane integrity simultaneously. Following a single cell from 31-32hpi shows that initially mCherry is excluded from the inclusion, where bacteria can be seen labelled with Hoechst (inclusion outlined in yellow in 31hpi panels in **Figure 4.11**). Between 40-50 minutes after the start of image capture, *i.e.* between 30h 40m and 30h 50m post infection, mCherry was no longer excluded from the inclusion (**Figure 4.11** +50 minutes panels).

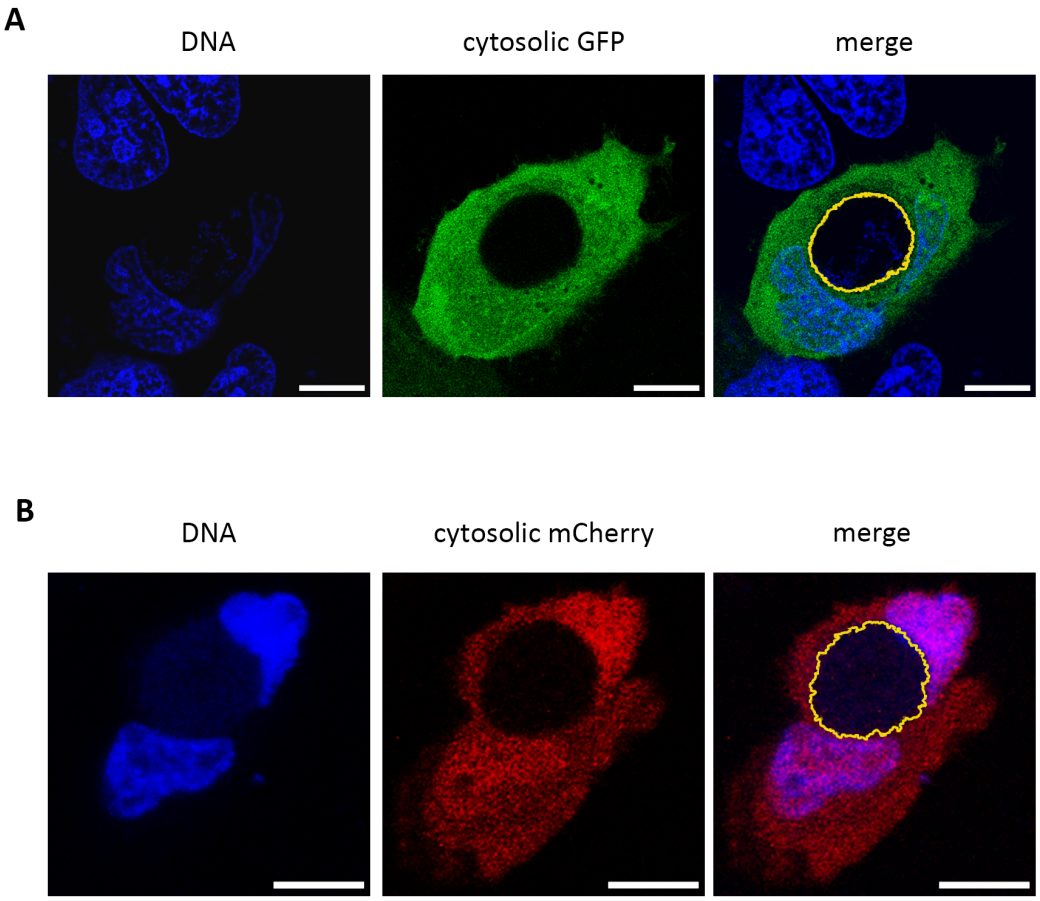
A
DNA
cytosolic GFP
merge
B
DNA
cytosolic mCherry
merge

Figure 4.10. *C.trachomatis* LGV2 inclusions exclude both GFP and mCherry 36hpi. Confocal xy-sections of *C.trachomatis* LGV2 infected HeLa cells (MOI=1) at 24hpi. (A) HeLa cells expressing cytosolic green fluorescent protein (GFP) (green) after infection incubation (0hpi). Following fixation at 30hpi cells were labelled with DRAQ-5 DNA stain (blue). Inclusion circled in yellow. Scale bars, 10μm. (B) HeLa cells expressing cytosolic mCherry fluorescent protein (mCherry) (red) after infection incubation (0hpi). Following fixation at 30hpi cells were labelled with Hoechst DNA stain (blue). Inclusion circled in yellow. Scale bars, 10μm.

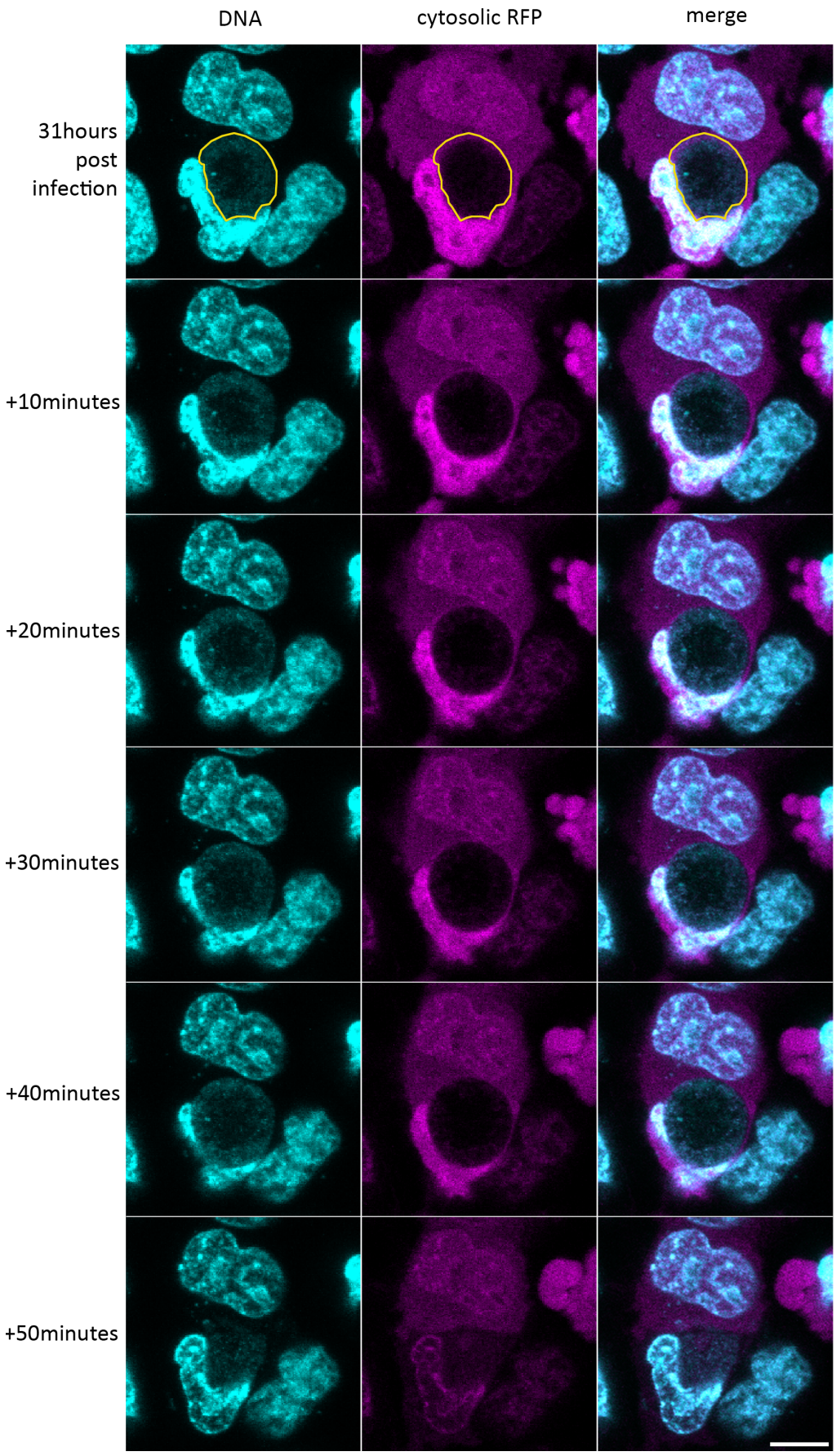
DNA
cytosolic RFP
merge
31hours post infection
+10minutes
+20minutes
+30minutes
+40minutes
+50minutes

Figure 4.11. *C.trachomatis* LGV2 inclusions become porous to mCherry. Live confocal xyz-projections of *C.trachomatis* LGV2 infected HeLa cells (MOI=1) expressing cytosolic mCherry (magenta) labelled using Hoechst DNA stain (cyan) from 31-32hpi. Inclusion outlined in yellow (31hpi panels). Scale bar, 10μm.

To observe the moment at which mCherry is no longer excluded from the inclusion in conjunction with changes in K^+ concentration, mean pixel intensities from ROIs from four inclusions within the FOV were compared (labelled 1-4 in **Figure 4.12 A**). *C.trachomatis* infections progress at slightly different rates from cell to cell, therefore within each FOV the inclusion expansion occurs in different cells at different times. To synchronise the moment of inclusion expansion the frames in which the inclusion expansion occurs was identified (for each inclusion {1-4} the frame immediately following inclusion membrane lysis is marked with * in **Figure 4.12B**). The ROI used to obtain mean pixel intensity for inclusion number 1 (**Figure 4.12A**) is illustrated in white in **Figures 4.13**. Similar to the cell observed in **Figure 4.11**, the cell shown in **Figure 4.13** shows a loss of K^+ from the inclusion from 30h 20m, leading up to permeabilisation of the inclusion membrane. Mean pixel intensity values for mCherry and APG-2 channels from ROIs from the four inclusions were corrected for background fluorescence and photobleaching, as described previously. DNA fluorescence intensity was corrected to account for any changes resulting from bacterial movements within the ROI. These data show that, for all the cells assayed, there was a peak in K^+ concentration 60 minutes before the inclusion became permeable to cytosolic mCherry (**Figure 4.14**). The loss of inclusion membrane integrity appears to correspond with the frame immediately after the lowest point in APG-2 fluorescence intensity. Although the inclusion membrane appears to have been compromised, the bacteria are still retained within the host cell at the end of image capture (**Figure 4.13** 110-140). This shows that, although the expansion event occurs asynchronously, all inclusions

A

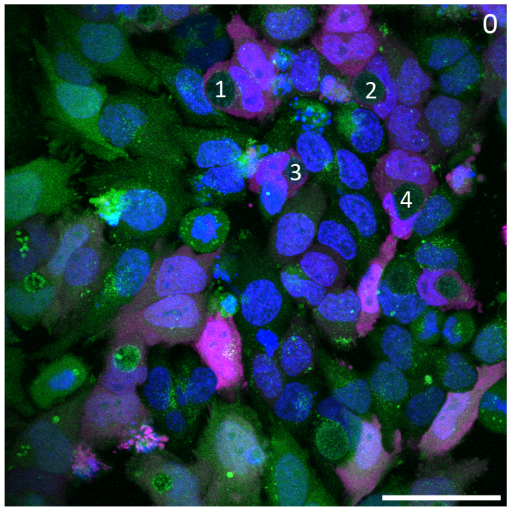

B

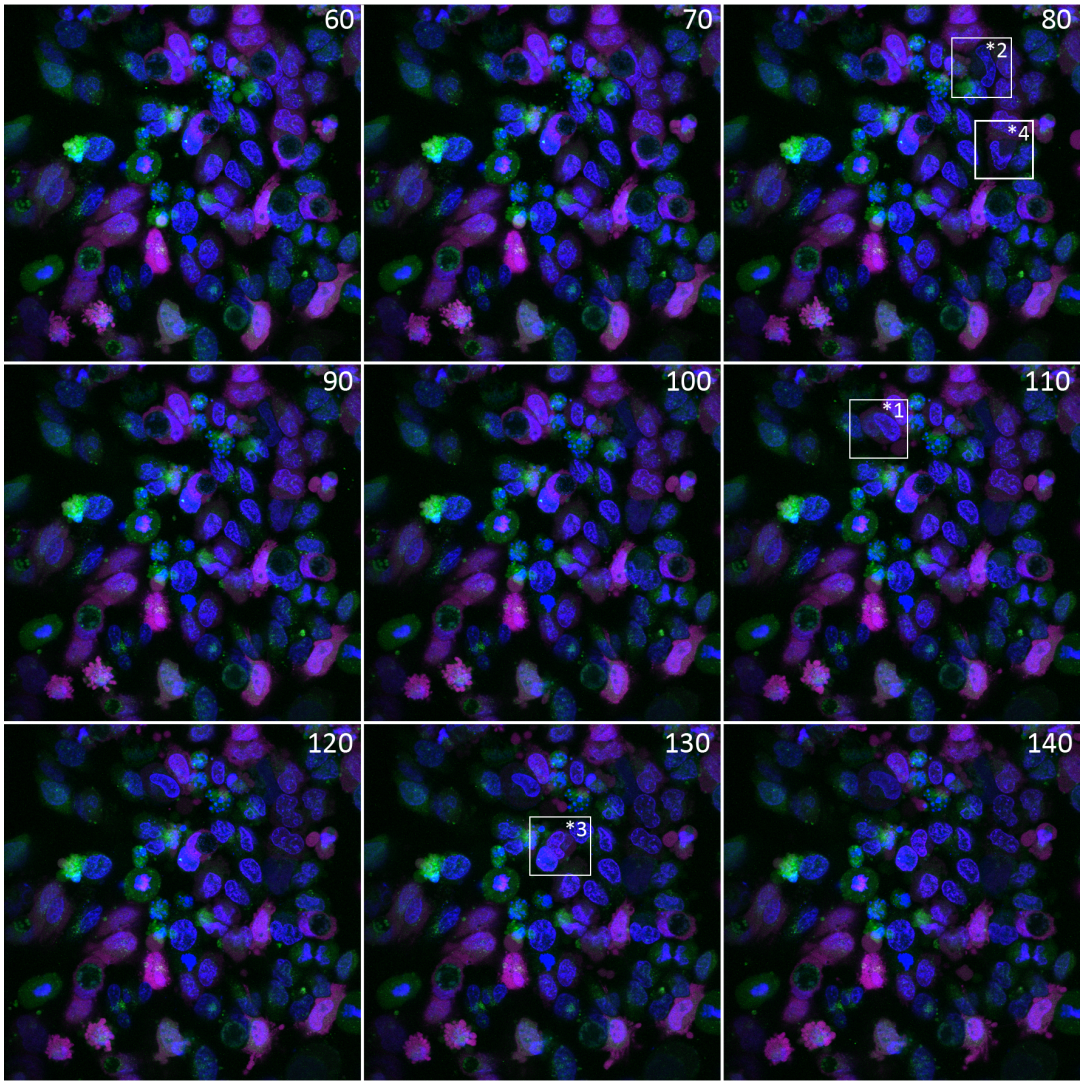

Figure 4.12. Inclusion membrane permeabilisation occurs in different frames for each inclusion within a 50 minute window. (A) Live confocal xyz-projection of HeLa cells infected with *C.trachomatis* LGV2 (MOI=1) expressing cytosolic mCherry fluorescent protein (magenta). Cells were labelled at 30hpi using APG-2 K^+ probe (green) and Hoechst DNA stain (blue). Confocal xyz-stacks were obtained every 10 minutes from 30h to 32h 20m post infection (0-140 minutes after the beginning of image capture). Numbers indicate inclusions assayed for fluorescence intensity throughout the timecourse. Scale bar, 50μm. (B) To observe fluorescence intensity changes throughout the timecourse, the frame immediately following the expansion were synchronised. The frames immediately after inclusion permeabilisation are indicated by an asterisk (*) for each inclusion.

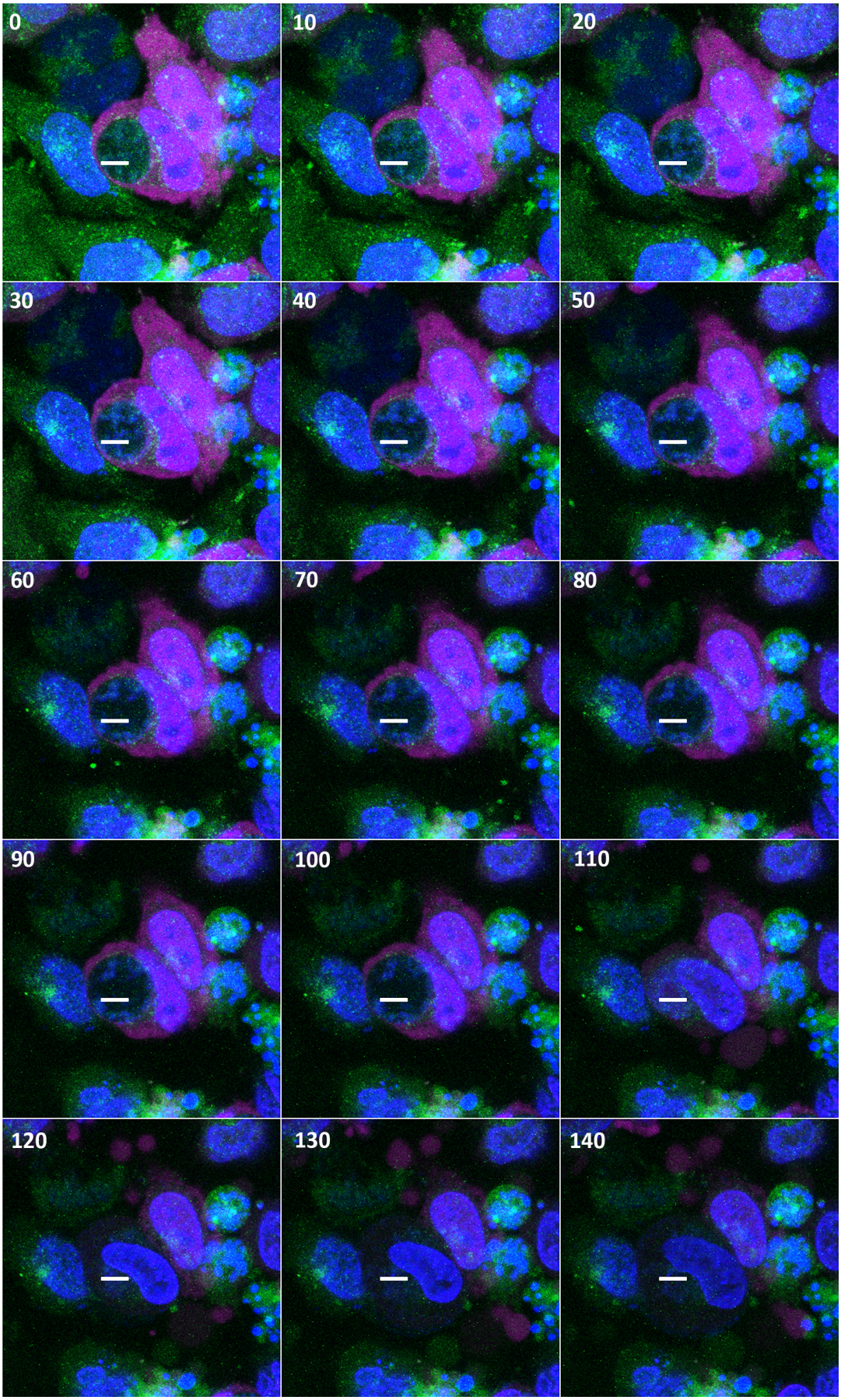
0
10
20
30
40
50
60
70
80
90
100
110
120
130
140

Figure 4.13. *C.trachomatis* LGV2 inclusion permeabilisation coincides with lowest APG-2 fluorescence intensity. Live confocal xyz-projections of *C.trachomatis* LGV2 infected HeLa cells (MOI=1) expressing cytosolic mCherry (magenta) labelled at 30hpi with APG-2 K^+ probe (green) and Hoechst DNA stain (blue). Confocal xyz-stacks were obtained every 10 minutes from 30h to 32h 20m post infection (0-140 minutes after the beginning of image capture). White line indicates the ROI analysed for this inclusion (**Figure 4.12** inclusion 1). Scale bar (shown in red), 10μm. (Also see **Supplementary movie S1**)

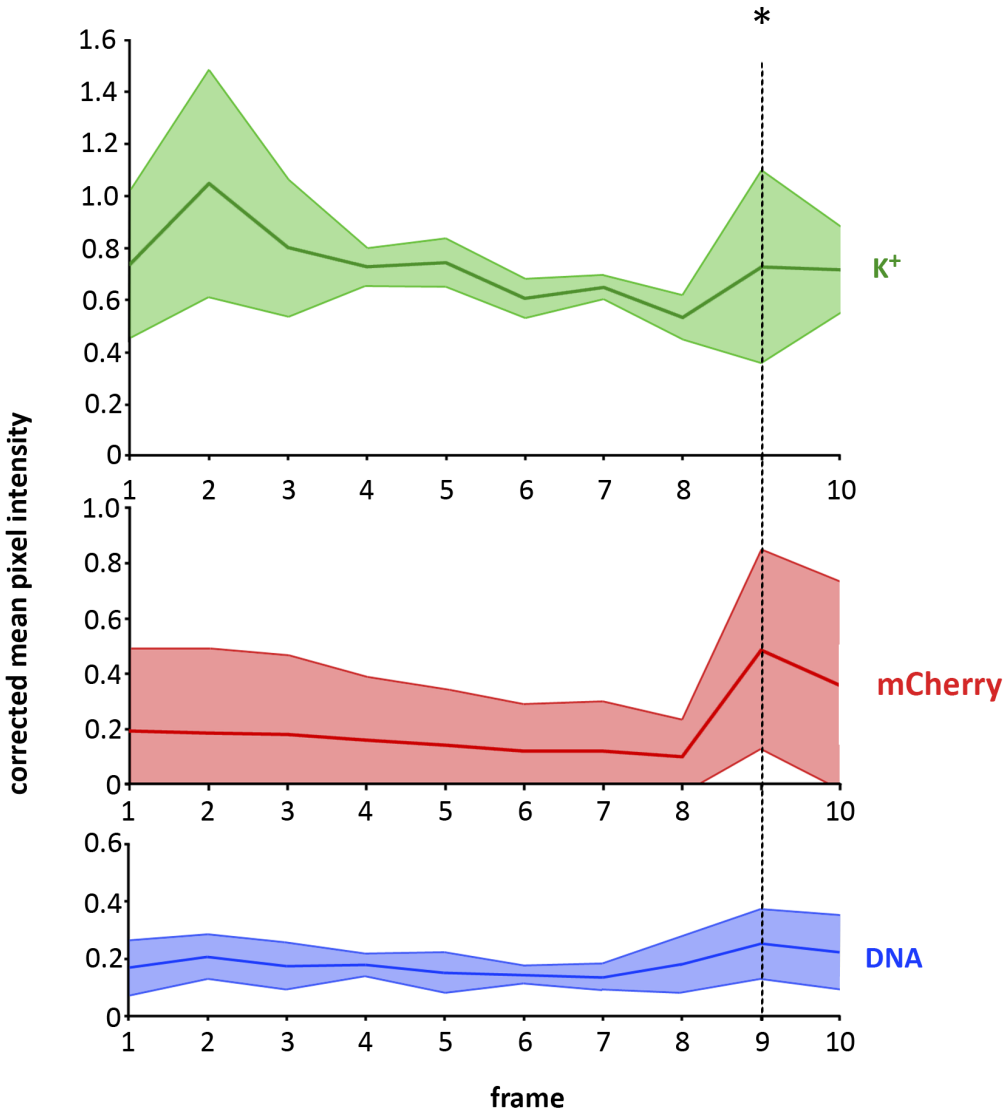
*
1.6
1.4
1.2
1.0
0.8
0.6
0.4
0.2
0
K+
1.0
0.8
0.6
0.4
0.2
0
mCherry
0.6
0.4
0.2
0
DNA
1 2 3 4 5 6 7 8 9 10
corrected mean pixel intensity
frame

Figure 4.14. Inclusion permeabilisation coincides with lowest intracellular K^+ concentration. *C.trachomatis* infected HeLa cells (MOI=1) expressing cytosolic mCherry and labelled using Hoechst DNA stain and APG-2 K^+ at 30hpi underwent confocal time-lapse imaging from 30-36hpi. Confocal xyz-projections were compiled and analysed to observe the frames in which each inclusion became permeable to mCherry (**Figure 4.12**). Mean fluorescence intensity measurements, corrected for photobleaching and background fluorescence, for the synchronised frames over the time-course were assayed in the mCherry, DNA and K^+ channels and averaged for four inclusions in the FOV (ROI for the first inclusion illustrated in **Figure 4.13**). Asterisk (*) indicates frame immediately after permeabilisation (As shown in **Figure 4.12B**). Shaded area indicates standard deviation.

observed in this field of view exhibit the same pattern of K^+ loss followed by inclusion permeabilisation.

These data demonstrate that the inclusion membrane becomes permeable when the K^+ concentration reaches its lowest ebb, however it is insufficient to establish whether the membrane lyses or simply becomes porous to larger molecules. To observe changes to the inclusion membrane following K^+ loss by bacteria, HeLa cells were fixed and embedded for EM sectioning 32h after infection with *C.trachomatis* LGV2. Contrast was enhanced using malachite green and the sample was negatively stained using uranyl acetate. Ultra thin sections were then observed at low magnification using an electron microscope. At 32hpi the monolayer contained a mixed population of cells containing intact inclusions (**Figure 4.15A**), inclusions with apparently intact membranes with less distinction between the lumen and the host cell cytosol (**Figure 4.15B**), cells that appeared to contain cytosolic bacteria (**Figure 4.15C**), and cells that had lysed to release the bacteria (**Figure 4.15D**). These images would seem to corroborate the previous observation that bacteria release is a two-stage process, as suggested by Hybiske and Stephens (2007).

The pattern of K^+ fluctuations exhibited by the cells observed in these assays, *i.e.* a peak in K^+ concentration followed by a gradual efflux for 60-80 minutes before lysis of the inclusion membrane at the lowest K^+ concentration, could indicate a role for K^+ in the late stages of the *C.trachomatis* infection cycle. The observation that the bacterial K^+ concentration is lowest immediately before inclusion membrane lysis would suggest that the efflux is involved in the bacterial release mechanism. To elucidate any role for

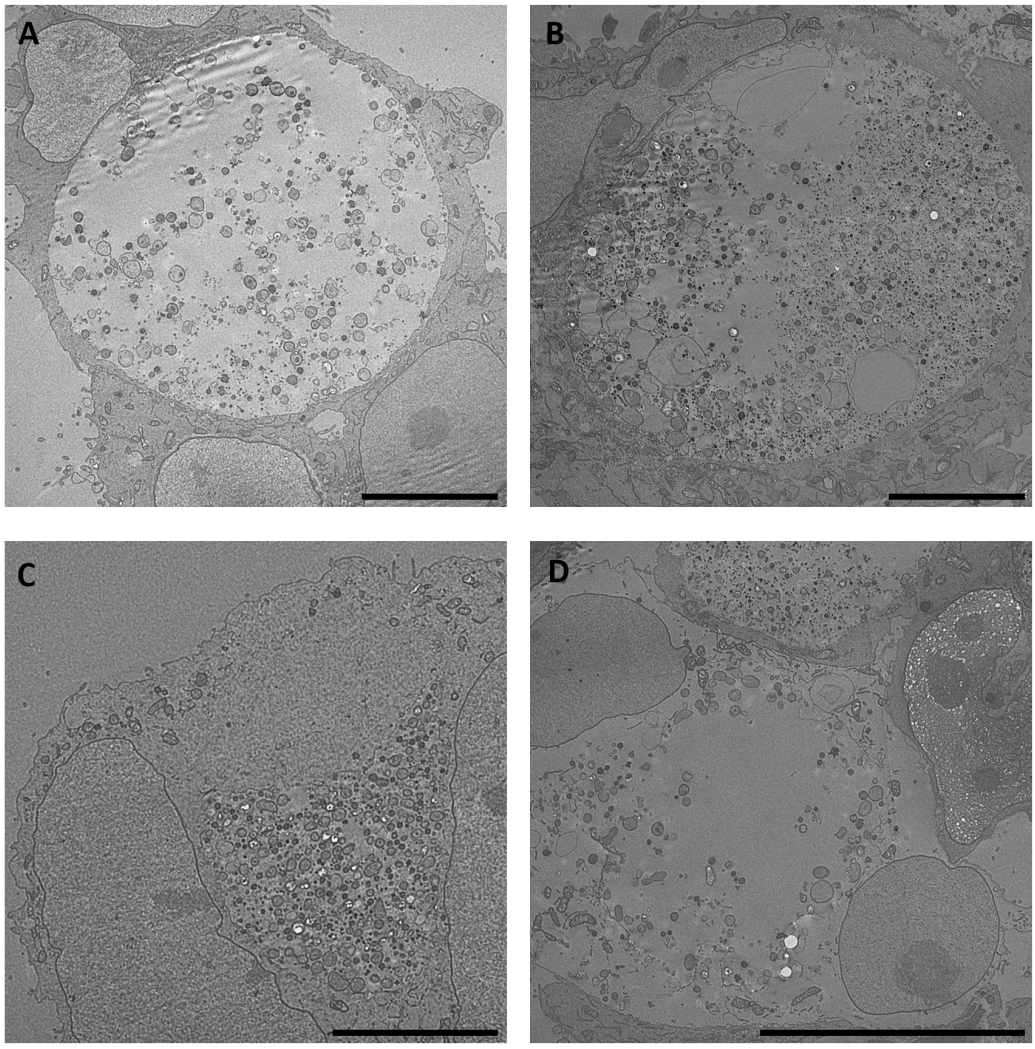
A
B
C
D

Figure 4.15. Ultrastructural analysis of *C.trachomatis* LGV2 shows cytosolic bacteria prior to host cell lysis. Transmission electron micrographs of HeLa cells infected with *C.trachomatis* LGV2 (MOI=1) were gluteraldehyde fixed at 32hpi with malachite green and negative stained using uranyl acetate prior to embedding and sectioning. Scale bars, 50μm.

a K^+ efflux in bacterial exit from host cells, the effect of inducing a K^+ efflux late in the infection cycle on inclusions within a population of cells was observed.

4.7 An induced K^+ efflux induces chlamydial extrusion in favour of lysis

Inclusion membrane permeabilisation and subsequent lysis appears to occur coincidentally with the loss of K^+ from bacteria. Previous experiments have shown that inducing an efflux of K^+ after RB-EB differentiation does not significantly influence bacterial infectivity (**Section 4.2**). However, any effect of nigericin treatment on inclusion morphology and integrity at this timepoint was not assayed. To ascertain if an induced K^+ efflux affects bacterial exit from the host cell, the number of inclusions following nigericin treatment later in the infection cycle was quantified.

HeLa cells infected with *C.trachomatis* LGV2 were treated with nigericin at 30hpi. Samples were fixed at 32hpi and co-labelled using an anti-*Chlamydia* spp. antibody and DAPI DNA stain. Bacteria could be observed within inclusions, which appear similar in morphology to those seen under control conditions. However, there were noticeably fewer inclusions in nigericin treated cells than under control conditions (**Figure 4.16A**). The average number of mature inclusions and cells, counted in 10 random FOVs at 63x magnification, after either 30m or 2h of nigericin treatment at 30hpi were then compared to equivalent control coverslips (**Figure 4.16B**). After 30m nigericin treated coverslips had more cells remaining, but half the number of inclusions when compared to control conditions. It would appear that, no matter the duration of nigericin

A

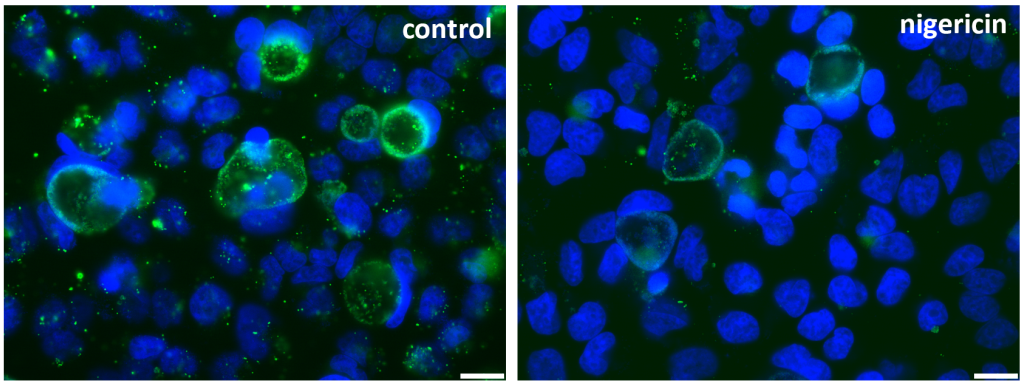
control
nigericin

B

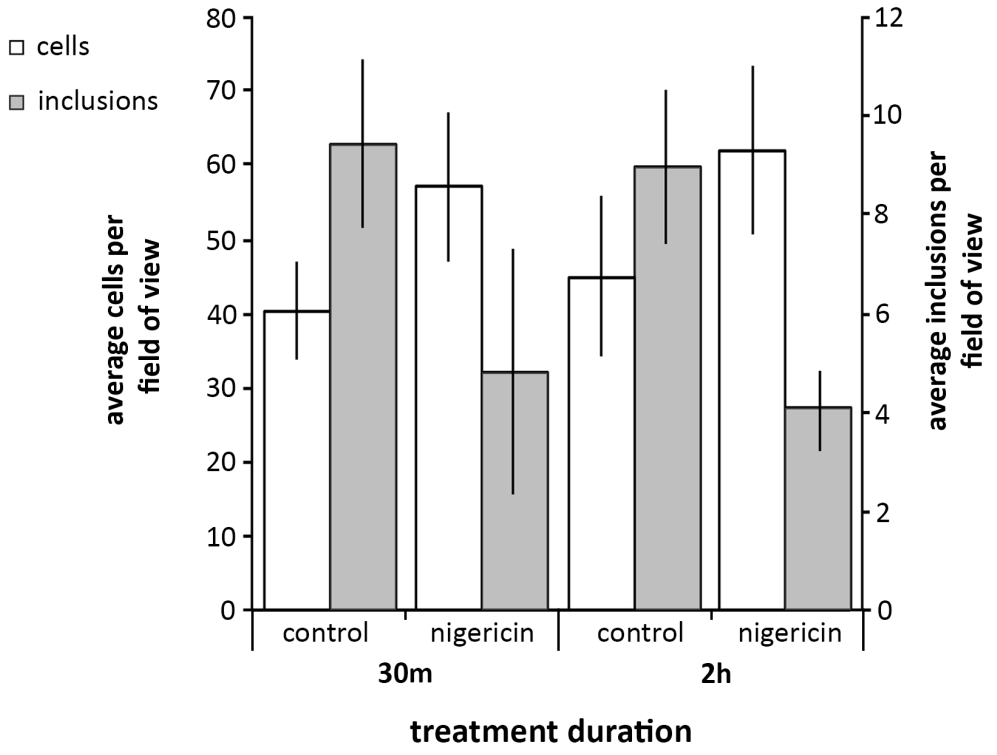
cells
inclusions
average cells per field of view
average inclusions per field of view
80
70
60
50
40
30
20
10
0
12
10
8
6
4
2
0
control
nigericin
control
nigericin
30m
2h
treatment duration

Figure 4.16. Ionophore-induced K^+ efflux 30hpi reduces the number of *C.trachomatis* LGV2 inclusions but not the number of HeLa cells. (A) Fluorescence micrographs of *C.trachomatis* LGV2 infected HeLa cells (MOI=1), either untreated (control) or treated at 30hpi with 1μM nigericin (nigericin). Cells were fixed after 30 minutes of treatment and labelled using DAPI DNA stain (blue) and FITC-conjugated *Chlamydia* spp. MOMP/LPS specific antibody (green). Scale bars, 7.5μm. (B) The average number of cells and inclusions for 10 random FOVs were counted at 63x magnification for each condition after either 30 minutes or 2 hours of treatment.

treatment, there are considerably fewer inclusions when compared to control conditions. Interestingly, nigericin treated coverslips have consistently more cells remaining on the coverslip than the equivalent control conditions. This would suggest that a greater number of bacteria have been egressed via host cell lysis in control conditions, and demonstrates that cells that have undergone a nigericin-induced K^+ efflux 30hpi are more likely to survive a *C.trachomatis* LGV2 infection. This would suggest that a greater number of bacteria were egressed from nigericin treated cells, as opposed to equal numbers egressed and lysed as observed in *C.trachomatis* LGV2 infection of HeLa cells by Hybiske and Stevens (2007). This would indicate that the speed of K^+ loss has an impact on the method of bacterial egress from host cells, *i.e.* a rapid decrease, such as the efflux induced by nigericin treatment, will result in bacterial extrusion whereas a gradual loss, as observed by live imaging (**Figures 4.7** and **4.14**), will result in host cell lysis.

To observe host cell exit by *C.trachomatis* after treatment at 30hpi with nigericin, Hoechst labelled HeLa cells were imaged every 10 minutes for 4 hours. Fifty minutes after nigericin treatment a number of bacteria were seen exiting the host cell (**Figure 4.17** panel 50* and **4.18** panel 50) however the host cell appeared to remain intact. Surprisingly, a considerable number of bacteria could still be seen constrained within the host cell cytosol. The host cell nucleus then began to expand indicating a reduction in the pressure exerted on the nucleus following the release of some of the bacteria (**Figure 4.17** panel 80-120). Two hundred minutes after nigericin addition another burst of bacteria was released from the host cell (**Figure 4.17** panel 200* and **4.18** panel 200), but a large number of bacteria remained within the host cell (**Figure 4.17**

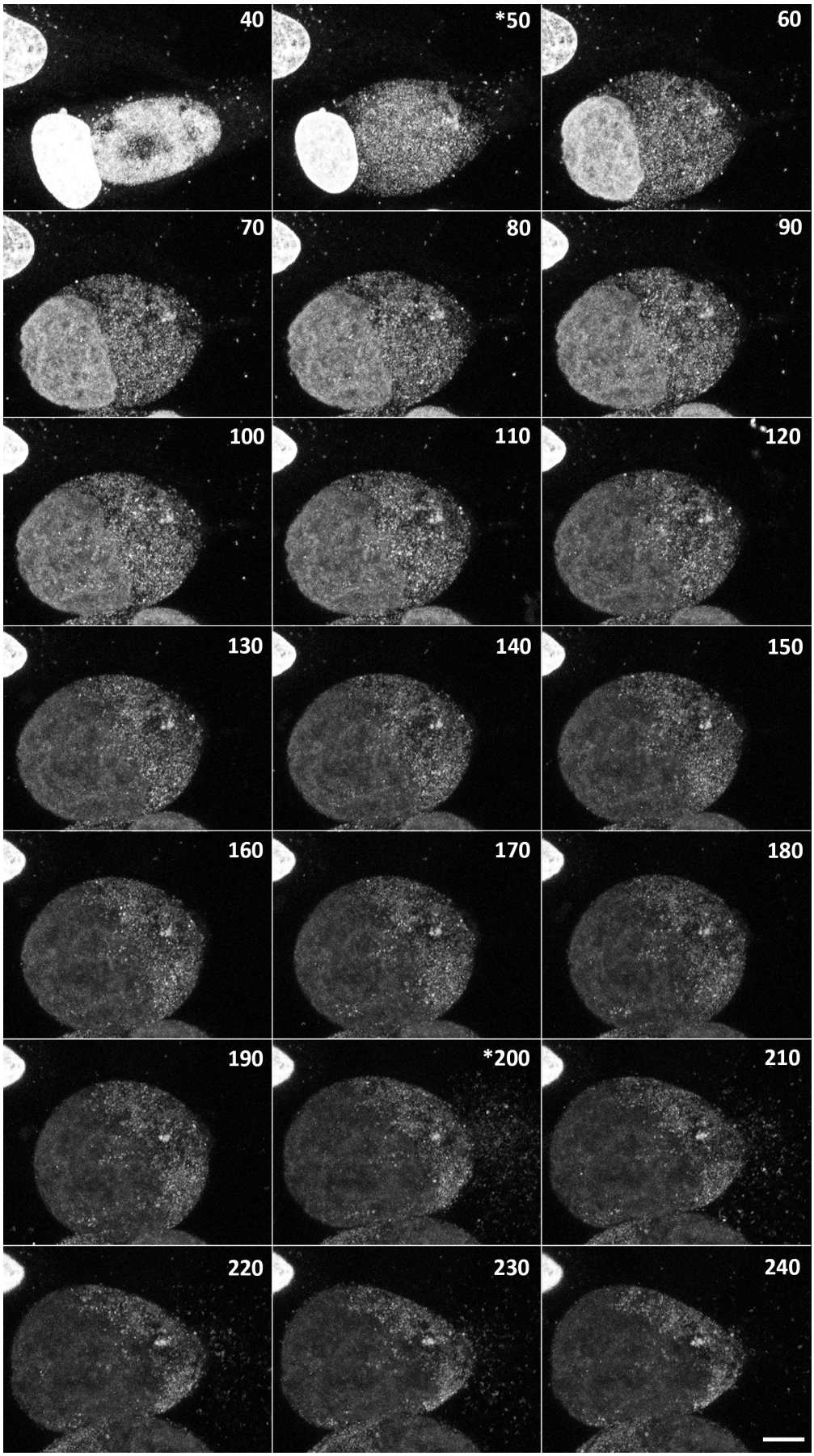
40
*50
60
70
80
90
100
110
120
130
140
150
160
170
180
190
*200
210
220
230
240

Figure 4.17. Treatment of *C.trachomatis* LGV2 infected HeLa cells with nigericin 30hpi causes bacterial egress in distinct bursts. Live confocal xyz-projections of *C.trachomatis* LGV2 infected HeLa cells (MOI=1) labelled with Hoechst DNA stain treated at 30hpi with 1μM nigericin. Asterisk (*) Indicates frames where bursts of bacteria can be seen exiting the host cell. Scale bar, 10μm. (Also see **Supplementary movie S2**)

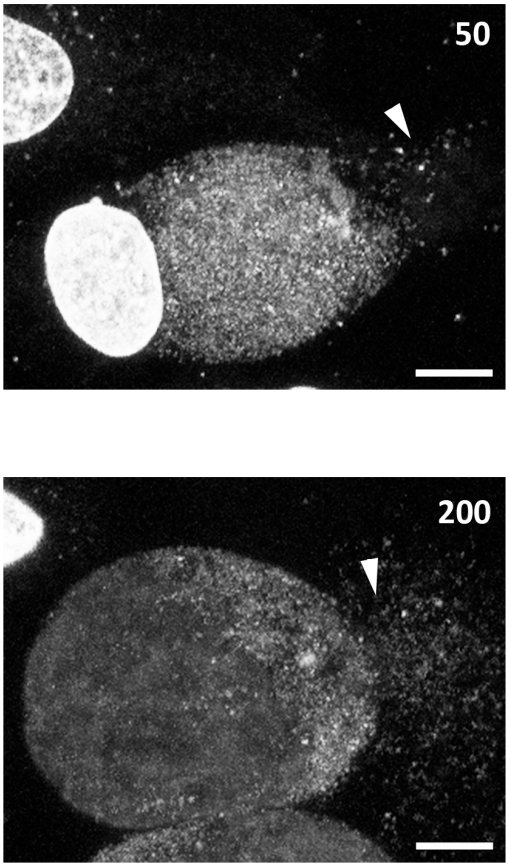
50
200

Figure 4.18. Bacteria egress nigericin treated cells in bursts, leaving the host cell membrane intact. Live confocal xyz-projections of HeLa cells infected with *C.trachomatis* LGV2 (MOI=1) and treated with 1μM nigericin at 30hpi. Cells were labelled with Hoechst DNA stain and imaged from 30h 40m-36hpi. First burst of bacteria (50, indicated by white arrow) leaving the cell 50 minutes after nigericin treatment. Second burst of bacteria (200, indicated by white arrow) leaving the cell 200 minutes after nigericin treatment. Scale bars, 10μm.

panels 210-240). The bursts of bacteria being released from the host cell are best illustrated in the supplementary movie **S2**.

These observations are distinct from previously described extrusion mechanisms (Todd and Caldwell, 1985; Hybiske and Stephens, 2007; Lutter *et al.,* 2013), whereby packages of bacteria, either the entire contents of the inclusion or part thereof, are extruded from the host cell. Classical extrusion is inhibited by blebbistatin, a cell permeable myosin II specific inhibitor. Blebbistatin reduces interactions between myosin motors and actin, which is necessary for chlamydial extrusion (Kovács *et al.,* 2004; Hybiske and Stephens 2007). Using blebbistatin to suppress extrusion activity during nigericin treatment will determine whether nigericin-induced bacterial release is myosin dependent, and therefore implicate K^+ efflux in chlamydial extrusion.

HeLa cells infected with *C.trachomatis* LGV2 were treated 30hpi with either nigericin, blebbistatin, a combination of both nigericin and blebbistatin, or left untreated. After 6h of treatment the average number of cells and mature inclusions from 10 random FOVs, at 63x magnification, were scored for each condition. As shown previously, nigericin treatment reduced the average number of inclusions dramatically, when compared to control conditions, however there was no significant change in the number of cells on the coverslip (**Figure 4.19**). Blebbistatin treated conditions had a greater number of mature inclusions per FOV than control conditions, and a comparable number of cells to both control and nigericin conditions. These data suggest that, by 36hpi, a large number of inclusions would have been extruded under normal circumstances, but nigericin treatment induces extrusion in a greater

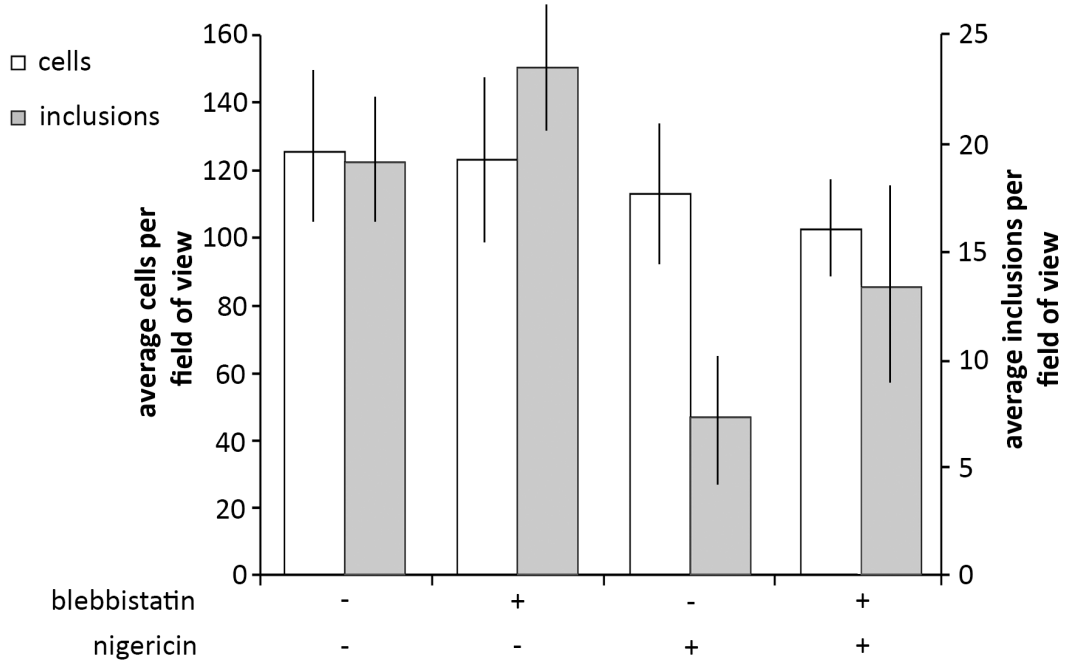
cells
inclusions
average cells per field of view
average inclusions per field of view
160
140
120
100
80
60
40
20
0
25
20
15
10
5
0
blebbistatin
nigericin
-
+
-
+
-
-
+
+

Figure 4.19. Treatment with blebbistatin decreases K+ efflux-induced extrusion from *C.trachomatis* LGV2 infected HeLa cells. HeLa cells were infected with *C.trachomatis* LGV2 (MOI-1) and either left untreated, treated 30hpi with 1μM nigericin, treated 30hpi with 50μM blebbistatin, or 30hpi with a combination of both 1μM nigericin and 50μM blebbistatin. Cells were fixed at 36hpi and labelled using DAPI DNA stain and FITC-conjugated *Chlamydia* spp. MOMP/LPS specific antibody. The number of cells and inclusions from 10 random FOVs at 63x magnification were then counted. Error bars indicate standard deviation.

proportion of cells. Treatment with both blebbistatin, to inhibit extrusion, and nigericin, which seems to induce extrusion, caused a decrease in both the number of cells and the number of inclusions. Fewer inclusion were lost in conditions treated with both nigericin and blebbistatin than in conditions treated with nigericin alone (**Figure 4.19**).

Taken together these data indicate that a K^+ efflux induces bacterial release from cells. In addition, inducing a rapid K^+ efflux from infected cells appears to increase the number of inclusions released from host cells via a myosin II dependent egress mechanism.

4.8 Discussion

The data presented in this chapter illustrate a novel K^+ cycle during chlamydial development. Replicating *Chlamydiae* require K^+, and starvation during the RB phase of the infection cycle induces persistence (**Chapter 3**). To further understand the role that K^+ fulfils during the chlamydial infection cycle, time course experiments restricting K^+ availability to bacteria at different phases of the infection cycle was undertaken. Surprisingly, restricting K^+ at timepoints after RB-EB differentiation had progressively less of an impact on bacterial infectivity the later in the infection cycle the K^+ efflux occurred (**Figure 4.1**). Equivalent timecourse experiments inducing a K^+ efflux at similar phases of the infection cycle (**Table 4.1**) using other *Chlamydiae*-host combinations revealed that, irrespective of bacterial strain or host cell, a K^+ efflux once EBs are

present in the inclusion has less of an impact on the infectivity of *Chlamydiae* (**Figure 4.3**). For all combinations assayed, the greater the number of EBs present at the time of the induced K^+ efflux, the more infectivity was recovered at the end of the infection cycle. This indicates that RBs and EBs have differing requirements for K^+.

To observe K^+ during the *C.trachomatis* infection cycle, APG-2 a K^+ sensitive fluorescent probe was used in live cells. HeLa cells contain diffuse cytosolic K^+ with a higher concentration in the mitochondria (**Figures 4.4A** and **4.5A**). At 12hpi, RBs contained a high concentration of APG-2, which corresponds to a high K^+ concentration (**Figure 4.5**). Interestingly, as bacterial replication progresses, cytosolic and mitochondrial K^+ concentrations decrease, which suggests that the bacteria are acquiring K^+ from the host cell (**Figure 4.5**). This was supported by FRAP analysis of the bacteria, which showed that K^+ was continually acquired by RBs (**Figure 4.6**).

Late in the infection cycle, once bacteria had differentiated into EBs (as shown in section **3.2**, **Figure 3.2**), bacteria exhibited significantly less APG-2 concentration, and therefore potentially contained less K^+ (**Figure 4.5**). This would suggest that the K^+ accumulated during bacterial replication is lost at some point during the transition from RB-EB. This is consistent with the observations made by Chang and Moulder (1978), which showed that there was a substantial decrease in total K^+ concentration from HeLa cells with physiological titres of *C.psittaci* at 48hpi.

These observations prompted live confocal microscopy of HeLa cells infected with *C.trachomatis* LGV2 during the period associated with RB-EB differentiation (as per **Figure 3.2**), from 30-36hpi. These experiments showed a peak in K^+ concentration 30h

30m after infection (**Figures 4.7/4.14**) followed by a striking loss of K^+ over a period of 60-80 minutes. When the K^+ concentration reached its lowest concentration, approximately 32hpi, inclusion size increased dramatically (**Figure 4.9**, **Supplementary movie S1**). This increase in the size of the inclusion coincides with the inclusion membrane becoming permeable to mCherry, which is excluded from the inclusion prior to this point (**Figures 4.11** and **4.14**). Electron microscopy of *C.trachomatis* LGV2 infected HeLa cells 32hpi revealed cells containing cytosolic bacteria (**Figure 4.15**), demonstrating that the inclusion membrane ruptures before the host cell membrane, as briefly described by Hybiske and Stephens (2007).

Nigericin-induced efflux of K^+ later in the infection cycle, at 30hpi, was shown to induce extrusion of inclusions in a large proportion of cells (**Figure 4.16**). Interestingly, nigericin induced K^+ efflux induces egress of *Toxoplasma gondii* from human foreskin fibroblasts in a calcium dependent manner (Fruth and Arrizabalaga, 2007). Unlike the chlamydial extrusion mechanism described by Hybiske and Stephens (2007), the inclusion did not appear to be extruded in its entirety, instead the bacteria were released in bursts (**Figure 4.17**, **Supplementary movie S2**). Inhibition of classical myosin II-dependent chlamydial extrusion mechanisms reduced bacterial extrusion following K^+ ionophore treatment (**Figure 4.17**). These observations suggest that rapid K^+ efflux, such as the K^+ decrease following ionophore treatment, induces a myosin II dependent extrusion mechanism.

Taken together, these data suggest that a chlamydial K^+ efflux at the end of the infection cycle plays a role in bacterial exit from the host cell, with a rapid efflux

inducing an egress type mechanism and a slower K^+ loss resulting in lysis of the host cell. This efflux would appear to be the result of K^+ loss from bacteria during the transition from RB back to EB, and could potentially provide the motivation for RB scavenging of host K^+ during replication.

Chapter 5 – Discussion

The results described in this thesis present compelling evidence for a potassium ion (K^+) cycle throughout intracellular *Chlamydiae* development. During replication the bacteria actively accumulate K^+ from the host, and in the majority of cells, this requires the activation of glibenclamide-sensitive inwardly rectifying potassium (K_{ir}) channels. At timepoints that correlate with RB-EB differentiation K^+ is gradually lost from the bacteria until a basal level is reached (**Figure 5.1A**). This K^+ loss corresponds with inclusion membrane permeabilisation and lysis, resulting in the release of bacteria from the inclusion into the host cell cytosol, an event observed by live imaging and electron microscopy of fixed cells. Rapidly depleting K^+, using a specific K^+ ionophore at late stages of the infection cycle induces myosin II-dependent extrusion, implicating a functional role for K^+ in release of pathogens from the infected cell (**Figure 5.1B**).

These data raise a number of interesting questions about the methods involved in K^+ acquisition, accumulation and storage, and the mechanisms by which the bacteria utilise these ions to trigger their exit from the host cell.

K^+ uptake and loss by bacteria demonstrates a need for ion transport systems in both the inclusion and bacterial membranes. Previous studies have identified three major potassium specific transport systems in Gram-negative bacteria; Trk, a rapid low affinity transport system active at alkaline or neutral pH (Epstein, 2003; Su *et al.,* 2009; Liu, 2013); Kup, which has a similar K^+ affinity to the Trk system but is active under acidic conditions (Trchounian and Kobayashi, 1999; Epstein, 2003; Liu, 2013); and Kdp, a highly specific system induced by low K^+ conditions (5mM or less) (Frymier *et al.,* 1997; Epstein, 2003; Xue *et al.,* 2011). Although no homologous systems have so far

been identified among the hypothetical*Chlamydiaceae*, CT440 has been shown to localize to the *C.trachomatis* inclusion membrane from 12hpi (Li *et al.* 2008; 2011) and has predicted structure-based homology to a neurotransmitter-gated ion-channel transmembrane pore (Oliver, Nobeli, and Hayward; personal communication).

Following on from the observation that inhibiting the SUR domains of K_{ir} channels using glibenclamide induced AB development in host cells infected with *C.trachomatis* at 12hpi (**Figure 3.9**), we sought to determine the location from which the glibenclamide acts in infected cells. Experiments using fluorescently labelled bodipy-Texas red-glibenclamide, revealed that the drug localises to the plasma membrane and endoplasmic reticulum (ER) in infected HeLa cells, and was also dispersed throughout the *C.trachomatis* LGV2 inclusion 24hpi (**Figure 5.2**). This suggests that either glibenclamide is retained within the inclusion, or glibenclamide-sensitive channels exist within the inclusion. This could have interesting implications when considered with the observation by Dumoux *et al* (2012) that the rER is transiently recruited to the chlamydial inclusion. ER is recruited during bacterial invasion, following which *Chlamydia*-ER interactions decrease until the bacteria have established an inclusion. When HeLa cells were infected with *C.trachomatis* LGV2, proteins from the ER were recruited to, and translocated into, the chlamydial inclusion at 24hpi (Dumoux *et al.,* 2012), which coincides with the period of K^+ accumulation we have described (**Figures 4.1** and **4.6**).

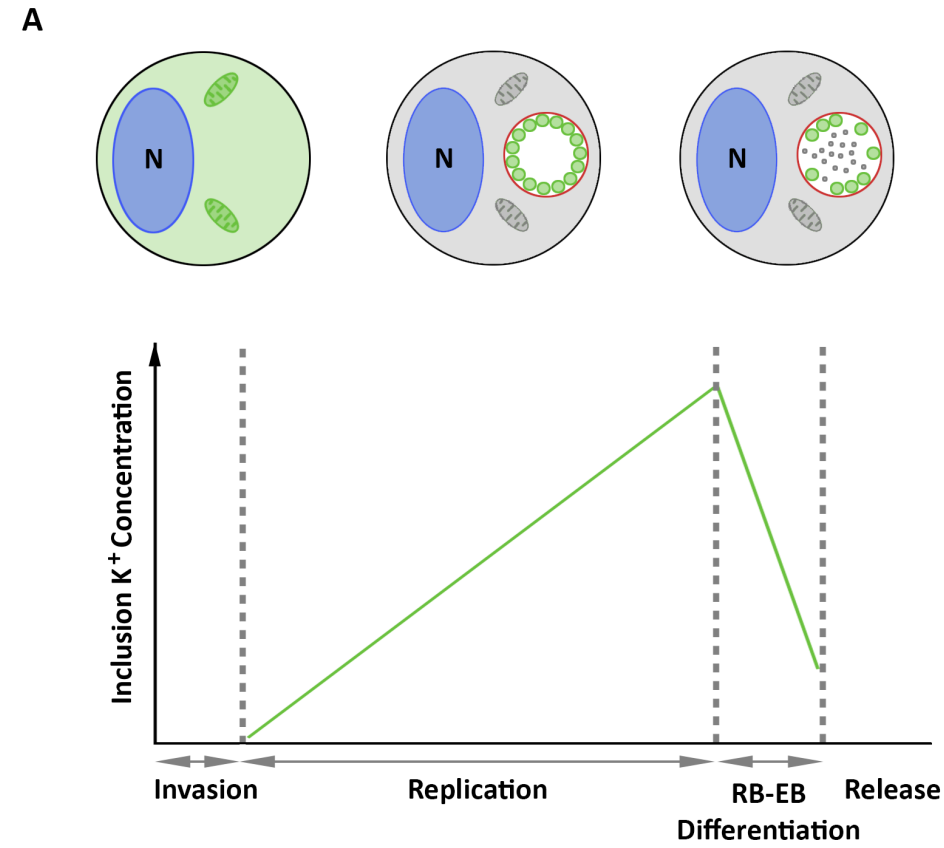
A
N
N
N
Inclusion K+ Concentration
Invasion
Replication
RB-EB
Differentiation
Release

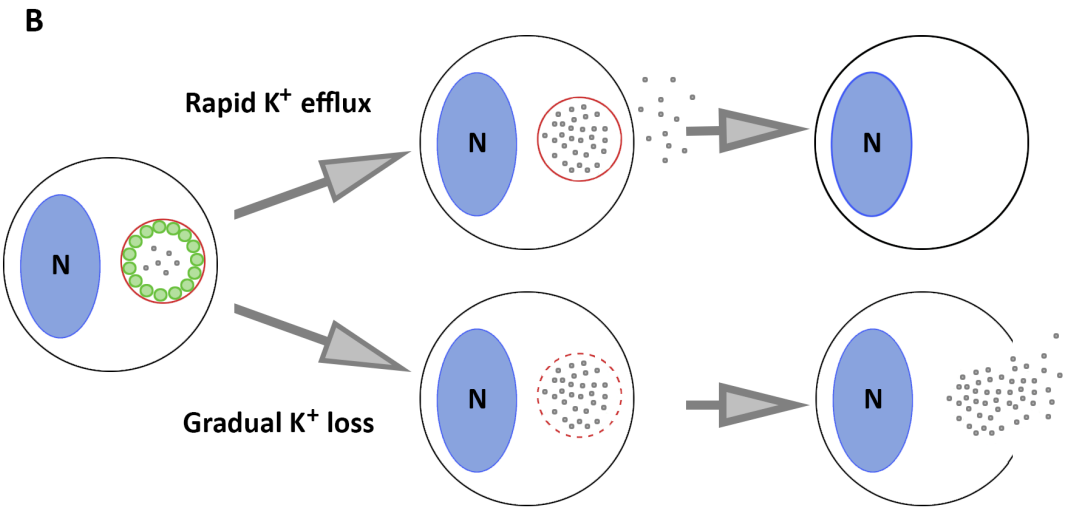
B
Rapid K+ efflux
N
N
N
Gradual K+ loss
N
N

Figure 5.1. *Chlamydiae* acquire K^+ from the host cell and via inwardly rectifying K^+ channels (K_{ir}) during replication, and nature of K^+ efflux at the end of the infection cycle influences exit mechanism. Schematic representation of the proposed K^+ cycle during intracellular *Chlamydiae* development. (A) Prior to infection epithelial cells have high mitochondrial and cytosolic K^+ (green). Following EB-RB differentiation replicating bacteria acquire K^+, scavenged from the host and requiring K_{ir} activity. As bacteria differentiate K^+ is lost from the inclusion. (B) The speed of K^+ exit influences the method of bacterial exit from the host cell. Rapid K^+ efflux results in modular egress of bacteria leaving the host cell intact. Gradual loss of K+ results in inclusion membrane permeabilisation followed by bacterial release via lysis.

Identifying the function of K^+ during RB replication could further our understanding of *Chlamydiae*-host interactions. For example, previous studies have shown that pathogens such as *Pseudomonas aeruginosa* and *Salmonella typhimurium* induce a K^+ efflux from host cells to activate NLRC4 (Lindestam-Arlehamn *et al.,* 2010) and NLRP3 (Franchi *et al.,* 2007; Lindestam-Arlehamn *et al.,* 2010) inflammasome assemblies respectively, and consequently induce caspase-1 production followed by IL-1β and IL-18 processing. Caspase-1 activation is increased during *C.trachomatis* infection (Abdul-Sater *et al.,* 2009; 2010a; 2010b) specifically from 36-48hpi (Lu *et al.,* 2000), which coincides with our observations that K^+ is accumulated prior to RB-EB differentiation but lost from 32hpi onwards (**Figures 4.6** and **4.7**). This could indicate that bacteria scavenge K^+ from the host in order to control inflammasome activation, or even evade detection by the host. We have observed that caspase-1 is enriched within inclusions containing ionophore-induced ABs (**Figure 5.3**), suggesting that inducing a K^+ efflux during RB replication impacts the inflammatory response to bacteria. We have demonstrated that K^+ is lost from bacteria towards the end of the infection cycle in HeLa cells (**Figure 4.7**), and that an ionophore-induced K^+ efflux at 30hpi causes extrusion of bacteria (**Figures 4.16** and **4.17**), which could potentially implicate a role for either caspase-1 or downstream processes in the final stages of the intracellular chlamydial infection cycle. These observations warrant further investigation into the direct effects of K^+ efflux on inflammasome activity and the importance of cytokines during the final stages of the chlamydial infection cycle.

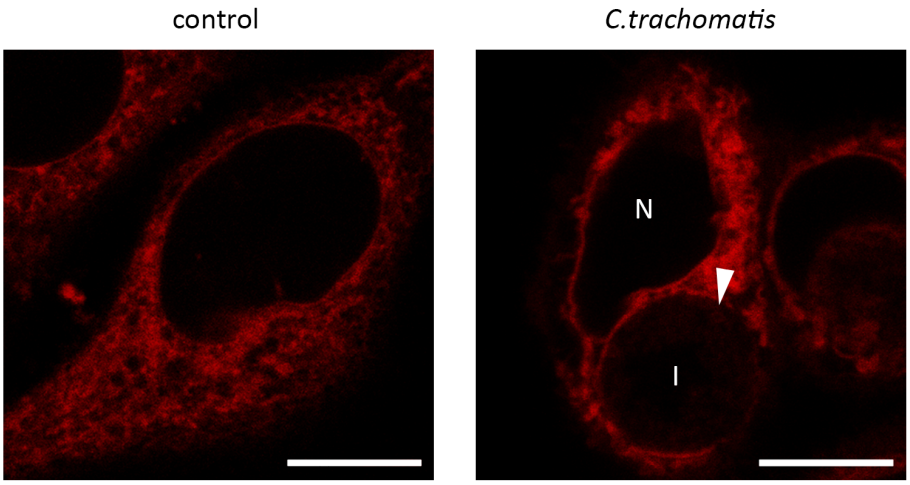
control
C.trachomatis
N
I

Figure 5.2. Fluorescently labelled glibenclamide can be seen within chlamydial inclusions. Live confocal xy-sections of HeLa cells (control) or HeLa cells infected with *C.trachomatis* LGV2 (MOI=1) (*C.*trachomatis) were labelled at 24hpi with BODIPY TexasRed Glibenclamide. N indicates nucleus, I indicates inclusion, and white arrow indicated labelling within the chlamydial inclusion. Scale bars, 10μm.

RBs may have a nutritional need for K^+ during replication. One interesting observation during this project was that even slight fluctuations in K^+ concentration, such as those caused by monensin treatment (**Figures 3.4-3.6**) were sufficient to induce persistence. This suggests that K^+ concentrations must be very carefully controlled by the bacteria to allow the infection cycle to occur. These observations further reinforce the essential role of K^+ during chlamydial development.

The involvement of K^+ efflux in bacterial release from the host cell (**Figure 4.13**) could indicate that the bacteria accumulate K^+ during replication to facilitate exit from the inclusion, either via lysis or extrusion. The efflux appears to occur as bacteria differentiate from RBs to EBs (**Figure 4.4**), however we currently have no direct evidence that this is the case. It would be useful to ascertain where in the RB-EB transition, and indeed how, K^+ is lost from the bacteria. For example, K^+ loss during bacterial reorganisation could simply be the result of reduced bacterial membrane integrity, equally, accumulated K^+ could be released by the bacteria as a signal or trigger to induce the RB-EB transition. Determining the specific role of K^+, as a signal for, or a co-factor in, bacterial reorganisation would enhance our understanding of the mechanisms involved in RB-EB redifferentiation.

Interestingly, in each experiment where K^+ concentrations were monitored in live cells we observed an increase in K^+ concentrations after the inclusion membrane ruptured (**Figures 4.7** and **4.14**). This could suggest that the bacteria utilise a similar K^+-dependent mechanism to lyse the host cell membrane as was used to lyse the

inclusion membrane. Further investigation of these events could help determine how bacteria are released at the end of the infection cycle.

Blebbistatin inhibition of nigericin-induced chlamydial extrusion (**Figure 4.17**) would indicate a myosin II dependent mechanism. Extrusion has previously been observed to require actin rearrangement in cells infected with *C.trachomatis* (Hybiske and Stephens, 2007; Lutter, 2013), therefore observing changes to the actin cytoskeleton following nigericin-induced K^+ efflux could further our understanding of the mechanisms of bacterial extrusion.

We have also shown that an induced K^+ efflux at the beginning of the infection cycle, 1hpi, disrupts inclusion biogenesis (**Figure 4.2**). Bacteria remain intracellular following nigericin-induced K^+ efflux, however it is unclear whether the bacteria are contained in entry vesicles or have become cytosolic (**Figure 4.2B**). There also appears to be less replication following a K^+ efflux early in the infection cycle. This could indicate that K^+ gradients are important during the initial stages of *C.trachomatis* infection, or even during EB-RB differentiation. Indeed, it has been hypothesised that one of the primary functions of the chlamydial biphasic development cycle is to enable the bacteria to adapt to differing environmental conditions from the extracellular milieu to the host cell cytosol (Liu *et al*., 2010). Further investigation into the role of K^+ at the beginning of the infection cycle could provide insight into inclusion biogenesis and bacterial adaptation to the intracellular environment.

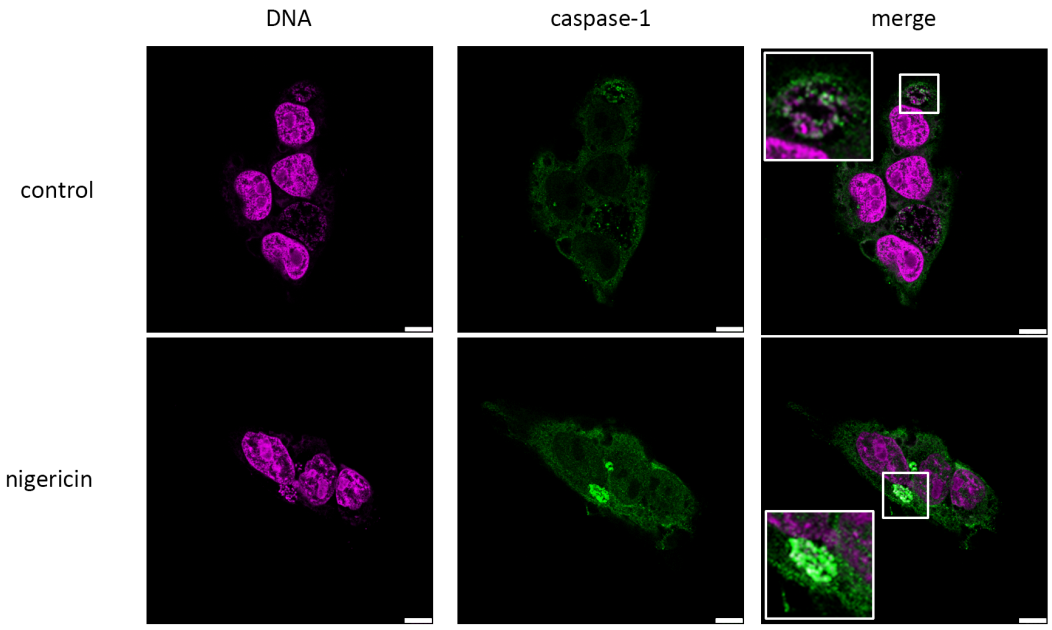
DNA
caspase-1
merge
control
nigericin

Figure 5.3. Caspase-1 is enriched within nigericin-induced persistent inclusions. Confocal xy-sections of HeLa cells infected with *C.trachomatis* LGV2 (MOI=1), either untreated (control) or treated at 12hpi with 1μm nigericin, and fixed at 24hpi. Cells were then labelled using DRAQ-5 DNA stain (magenta) and anti-caspase-1 primary antibody followed by AlexaFluor®488 conjugated secondary antibody (green). Scale bars, 10μm. Insets show indicated areas at higher magnification.

The data presented in this thesis show that *Chlamydiae* require K^+ for successful replication, and demonstrate a novel role for K^+ during bacterial exit from host cells, suggesting that the rate of K^+ loss from bacteria influences the mode of bacterial egress from cells.

Appendices

Appendix 1 – Primer sequences

		Sequence	Amplicon size
Mycoplasma	Forward	5'-ACTCCTACGGGAGGCAGCAGTA	712bp
Mycoplasma	Reverse	5'-TGCACCATCTGTCACTCTGTTAACCTC	
Eukaryotic 18S	Forward	5'-ATGGCCGTTCTTAGTTGGTG	217bp
Eukaryotic 18S	Reverse	5'-CGCTGAGCCAGTCAGTGTAG	
C.trachomatis 16S	Forward	5'-CGCCTGAGGAGTACACTCGC	207bp
C.trachomatis 16S	Reverse	5'-CCAACACCTCACGGCACGAC	

Appendix 2 – Ionophore structures

Chloride Ionophore I

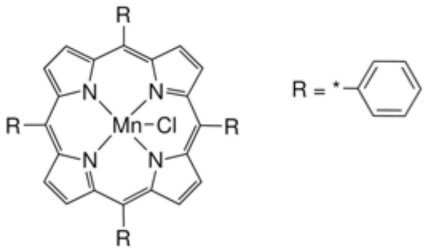

Ionomycin

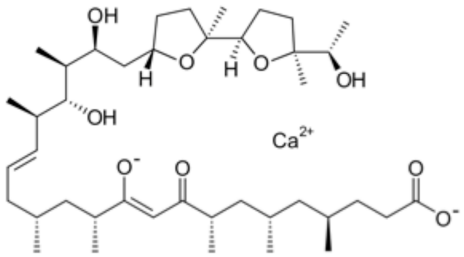

Monensin

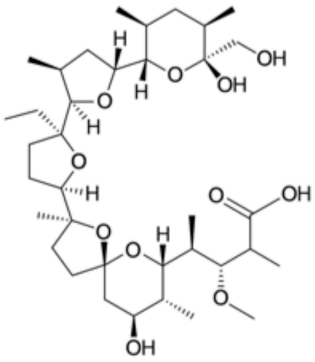

Nigericin

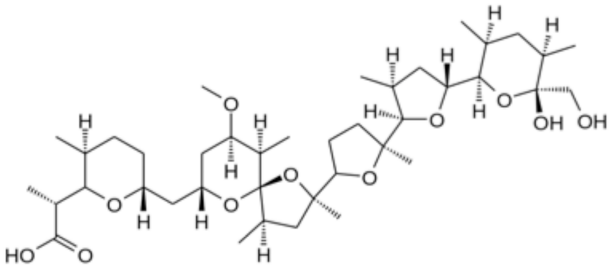

Valinomycin

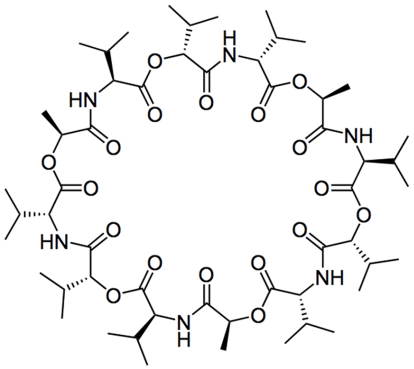

Appendix 3 – Plasmids

Plasmid	Product	Size	Bacterial Resistance
pEGFP-C2	GFP-X	4735bp	kanamycin
pCherry-C3	Cherry-X	711bp	kanamycin

Appendix 4 – ImageJ fluorescent image series mean pixel intensity macro

```
ListeImages=newArray(nImages);
for (i=1; i<=nImages; i++)
{selectImage(i);
ListeImages [i-1]=getTitle;}
Dialog.create("Measure");
Dialog.addChoice("Image", ListeImages);
Dialog.show();
monStack=Dialog.getChoice();
selectImage(monStack);
z=nSlices;
for (i=1; i<=z; i++ )
{selectImage(monStack);
setSlice(i);
run("Measure");}
```

Appendix 5 – FRAP wizard settings

	number of frames	interval (seconds)
pre-bleach	3	7.8*
bleach	2	7.8*
post-bleach 1	10	7.8*
post-bleach 2	20	20

* indicates minimised interval between frames

Appendix 6 – Mann-Whitney critical *U* values for 0.05 significance level

N_1	N_2					
	5	**6**	**7**	**8**	**9**	**10**
5	2	3	5	6	7	9
6	3	5	6	8	10	11
7	6	6	8	10	12	14
8	6	8	10	13	15	17
9	7	10	12	15	17	20
10	8	11	14	17	20	23

Bibliography

Abdelsamed, H., Peters, J., and G.I. Byrne. 2013. Genetic variation in *Chlamydia trachomatis* and their hosts: impact on disease severity and tissue tropism, *Future Microbiol.* 8:1129-46.

Abdul-Sater, A.A., Koo, E., Häcker, G., and D.M. Ojcius. 2009. Inflammasome-dependent caspase-1 activation in cervical epithelial cells stimulates growth of the intracellular pathogen *Chlamydia trachomatis*. *J. Biol. Chem.* 284:26789-96.

Abdul-Sater, A.A., Saïd-Sadier, N., Padilla, E.V., and D.M. Ojcius. 2010a. Chlamydial infection of monocytes stimulates IL-1β secretion through activation of the NLRP3 inflammasome. *Microbes and Infection*. 12:652-61.

Abdul-Sater, A.A., Saïd-Sadier, N., Lam, V.M., Singh, B., Pettengill, M.A., Soares, F., Tattoli, I., Lipinsky, S., Girardin, S.E., Rosentiel, P., and D.M. Ojcius. 2010b. Enhancement of reactive oxygen species production and chlamydial infection by the mitochondrial nod-like family member NLRX1. *J. Biol. Chem.* 285: 41637-45.

Abrami, L., Fivaz, M., Glauser, P., Parton, R.G., and F.G. van der Goot. 1998. A pore-forming toxin interacts with a GPI-anchored protein and causes vacuolation of the endoplasmic reticulum. *J. Cell Biol.* 140: 525-40.

Allan, I., and J.H. Pearce. 1983. Amino acid requirements of strains of *Chlamydia trachomatis* and *C.psittaci* growing in McCoy cells: relationship with clinical syndrome and host origin. *J. Gen. Microbiol.* 129: 2001-7.

Azenabor, A.A., Kennedy, P., and S. Balistreri. 2007. *Chlamydia trachomatis* infection of human trophoblast alters estrogen and progesterone biosynthesis: an insight into role of infection in pregnancy Sequelae. *Int. J. Med. Sci.* 4: 223-31.

Backowski, M.A., Braun, V., and J.H. Brumell. 2008. *Salmonella*-containing vacuoles: directing traffic and nesting to grow. *Traffic.* 9:2022-31.

Bannantine, J.P., Griffiths, R.S., Viratyosin, W., Brown, W. J., and D.D. Rockey. 2000. A secondary structure motif predictive of protein localisation to the chlamydial inclusion membrane. *Cellular Microbiology*. 2:35-47.

Barron, A.L., White, H.J., Rank, R.G., Soloff, B.L., and E.B. Moses. 1981. A new animal model for the study of *Chlamydia trachomatis* genital infections: infection of mice with the agent of mouse pneumonitis. *J. Infect. Dis.* 143:63-6.

Bauler, L.D., and T. Hackstadt. 2014. Expression and targeting of secreted proteins from *Chlamydia trachomatis. J. Bacteriol.* doi: 10.1128/JB.

Beatty, W.L. 2006. Trafficking from CD63-positive late endocytic multivesicular bodies is essential for intracellular development of *Chlamydia trachomatis. J. Cell Science.* 119: 350-9.

Beatty, W.L. 2008. Late endocytic multivesicular bodies intersect the chlamydial inclusion in the absence of CD63. *Infect. Immun.* 76:2872-81.

Bers, D.M., Barry, W.H., and S. Despa. 2003. Intracellular Na^+ regulation in cardiac monocytes. *Cardiovascular Research.* 57:897-912.

Betts, H.J., Wolf, K., and K.A. Fields. 2009. Effector protein modulation of host cells:examples on the *Chlamydia* spp. arsenal. *Curr. Opin. Microbiol.* 12:81-87.

Betts-Hampikian, H.J., and K.A. Fields. 2010. The chlamydial type III secretion mechanism: revealing cracks in a tough nut. *Frontiers in Microbiology.* 1: 1-13.

Brondersen, D.E., Clemons, W.M., Carter, A.P., Morgan-Warren, R.J., Wimberly, B.T., and V. Ramakrishnan. 2000. The structural basis for the action of the antibiotics tetracycline, pactamycin, and hygromycin B on the 30S ribosomal subunit. *Cell.* 103: 1143-54.

Bryan, J., and L. Aguilar-Bryan. 1999. Sulfonylurea receptors: ABC transporters that regulate ATP-sensitive K^+ channels. *Biochimica et Biophysica Acta.* 1461: 285-303.

Bush, R.M., and K.D.E. Everett. 2001. Molecular evolution of the *Chlamydiaceae. Int. J. Syst. Evol. Microbiol.* 51: 203-220.

Büttner, D. 2012. Protein export according to schedule: architecture, assembly, and regulation of type III secretion systems from plant- and animal-pathogenic bacteria. *Microbiol. Mol. Biol. Rev.* 76: 262-310.

Caldwell, H.D., Kromhout, J., and J. Schachter. 1981. Purification and partial characterisation of the major outer membrane protein of *Chlamydia trachomatis. Infect. Immun.* 31: 1161-76.

Carabeo, R.A., and T. Hackstadt. 2001. Isolation and characterisation of a mutant Chinese hamster ovary cell line that is resistant to *Chlamydia trachomatis* infection and a novel step in the attachment process. *Infect. Immun.* 69: 5899-904.

Carabeo, R.A., Grieshaber, S.S., Fischer, E., and T. Hackstadt. 2002. *Chlamydia trachomatis* induces remodelling of the actin cytoskeleton during attachment and entry into HeLa cells. *Infect. Immun.* 70: 3793-803.

Carabeo, R.A., Mead, D.J., and T. Hackstadt. 2003. Golgi-dependent transport of cholesterol to the *Chlamydia trachomatis* inclusion. *PNAS.* 100: 6771-6.

Carabeo, R.A., Grieshaber, S.S., Hasenkrug, A., Dooley, C., and T. Hackstadt. 2004. Requirement for the Rac GTPase in *Chlamydia trachomatis* invasion of non-phagocytic cells. *Traffic.* 5: 418-25.

Carabeo, R.A., Dooley, C., Grieshaber, S.S., and T. Hackstadt. 2007. Rac interacts with Abi-1 and WAVE2 to promote an Arp2/3-dependent actin recruitment during chlamydial invasion. *Cellular Microbiology.* 9: 2278-88.

Carter, J.D., Gerard, H.C., Whittum-Hudson, J.A., and P. Hudson. 2012. The molecular basis for disease phenotype in chronic *Chlamydia*-induced arthritis. *Int. J. Clin. Rheumatol.* 7: 627-40.

Chang, G.T., and J.W. Moulder. 1978. Loss of inorganic ions from host cells infected with *Chlamydia psittaci*, *Infect. Immun.* 19: 827-32.

Chellas-Géry, B., Linton, C.N., and K. A. Fields. 2007. Human GCIP interacts with CT847, a novel *Chlamydia trachomatis* type III secretion substrate, and is degraded in a tissue-culture infection model. *Cellualar Microbiology.* 9: 2417-30.

Chen, A.L., Johnson, K.A., Lee, J.K., Sütterlin, C., and M. Tan. 2012. CPAF: a chlamydial protease in search of an authentic substrate. *PLoS Pathogens.* 8: e1002842.

Chen, D., Lei, L., Lu, C., Flores, R., DeLisa, M.P., Roberts, T.C., Romsberg, F.E., and G. Zhong. 2010. Secretion of the chlamydial virulence factor CPAF requires the Sec-dependent pathway. *Microbiology.* 156: 3031-40.

Cheng, W., Shivshankar, P., Li, Z., Chen, L., Yeh, I., and G. Zhong. 2008. Caspase-1 contributes to *Chlamydia trachomatis*-induced upper urogenital tract inflammatory pathologies without affecting the course of course of infection. *Infect. Immun.* 76: 515-22.

Chiappino, M.L., Dawson, C., Schachter, J., and B.A. Nichols. 1995. Cytochemical localisation of glycogen in *Chlamydia trachomatis* inclusions. *J. Bacteriol.* 177: 5358-63.

Clausen, J.D., Christiansen, G., Holst, H.U., and S. Birkelund. 1997. *Chlamydia trachomatis* utilises the host cell microtubule network during early events of infection. *Mol. Microbiol.* 25: 441-49.

Clemens, D.L., and M.A. Horwitz. 1996. The *Mycobacterium tuberculosis* phagosome interacts with early endosomes and is accessible to exogenously administered transferrin. *J. Exp. Med.* 184: 1349-55.

Cocchiaro, J.L., Kumar, Y., Fischer, E.R., Hackstadt, T., and R.H. Valdivia. 2008. Cytoplasmic lipid droplets are translocated into the lumen of the *Chlamydia trachomatis* parasitophorous vacuole. *PNAS.* 105: 9379-84.

Coles, A.M., Reynolds, D.J., Harper, A., Devitt, A., and J.H. Pearce. 1993. Low-nutrient induction of abnormal chlamydial development: a novel component of chlamydial pathogenesis? *FEMS Microbiology Letters.* 106: 193-200.

Corsaro, D., Valassina, M., and D. Venditti. 2003. Increasing diversity within *Chlamydiae*. *Critical Reviews in Microbiology.* 29: 37-78.

Dautry-Varsat, A., Subtil, A., and T. Hackstadt. 2005. Recent insights into the mechanisms of *Chlamydia* entry. *Cellular Microbiology.* 7: 1714-22.

Delevoye, C., Nilges, M., Dehoux, P., Paumet, F., Perrinet, S., Dautry-Varsat, A., and A. Subtil. 2008. SNARE protein mimicry by an intracellular bacterium. *PLoS Pathogens.* 4: e1000022.

Derré, I., Swiss, R., and H. Agaisse. 2011. The lipid transfer protein CERT interacts with the *Chlamydia* inclusion protein IncD and participates to ER- *Chlamydia* inclusion membrane contact sites. *PLoS Pathogens.* 7: e1002092.

Ding, H., Gong, S., Tian, Y., Yang, Z., Brunham, R., and G. Zhong. 2013. Transformation of sexually transmitted infection-causing serovars of *Chlamydia trachomatis* using blasticidin for selection. *PLoS One.* 8: e80534.

Dugan, J., Rockey, D.D., Jones, L., and A.A. Andresen. 2004. Tetracycline resistance in *Chlamydia suis* mediated by genomic islands inserted into the chlamydial *Inv*-like gene. *Antimicrob. Agents Chemother.* 48: 3989-95.

Dumoux, M., Clare, D.K., Saibil, H.R., and R.D. Hayward. 2012. *Chlamydiae* assemble a pathogen synapse to hijack the host endoplasmic reticulum. *Traffic*. 13: 1612-27.

Egan, A.J., and W. Vollmer. 2013. The physiology of bacterial cell division. *Ann. N.Y. Acad. Sci.* 1277: 8-28.

Eley, A. 2003. *Chlamydia trachomatis* is bad for your sperm! *Microbiology Today.* 30: 61-2.

Eley, A., Hosseinzadeh, S., Geary, I., and A.A. Pacey. 2005. Apoptosis of ejaculated human sperm is induced by co-incubation with *Chlamydia trachomatis* lipopolysaccharide. *Human Reproduction.* 20: 2601-7.

Epstein, W. 2003. The roles and regulation of potassium in bacteria. *Prog. Nucleic Acid Res. Mol. Biol.* 75: 293-320.

Escalante-Ochoa, C., Ducatelle, R., and F. Haesebrouck. 1998. The intracellular life of *Chlamydia psittaci*: how do the bacteria interact with the host cell? *FEMS Microbiology Reviews.* 22: 65-78.

Everett, K.D.E., Bush, R.M., and A.A. Andersen. 1999. Emended description of the order *Chlamydiales*, proposal of *Parachlamydiaceae* fam. Nov., each containing one monotypic genus, revised taxonomy of the family *Chlamydiaceae*, including a new genus and five new species, and standards for the identification of organisms. *Int. J. Syst. Bacteriol.* 49: 415-40.

Fields, K.A., Mead, D.J., Dooley, C.A., and T. Hackstadt. 2003. *Chlamydia trachomatis* type III secretion: evidence for a functional apparatus during early-cycle development. *Mol. Microbiol.* 48: 671-83.

Franchi, L., Kanneganti, T., Dubyak, G.R., and G. Núñez. 2007. Differential requirement of P2X7 receptor and intracellular K^+ for caspase-1 activation induced by intracellular and extracellular bacteria. *J. Biol. Chem.* 282: 18810-8.

Franchi, L., Muñoz-Planillo, R., and G. Núñez. 2012. Sensing and reacting to microbes through the inflammasomes. *Nature Immunology.* 13: 325-32.

Friis, R. 1972. Interaction of L-cells and *Chlamydia psittaci*: entry of the parasite and host response to its development. *J. Bacteriol.* 110: 706-21.

Fruth, I.A., and G. Arrizabalaga. 2007. *Toxoplasma gondii*: induction of egress by the potassium ionophore nigericin. *Int. J. Parasitol.* 37: 1559-67.

Frymier, J.S., Reed, T.D., Fletcher, S.A., and L. N. Csonka. 1997. Characterization and transcriptional regulation of the hdp operon of *Salmonella typhimurium*. *J. Bacteriol.* 179: 3061-3.

Galán, J.E., and A. Collmer. 1999. Type III secretion machines: bacterial devices for protein delivery into host cells. *Science*. 284: 1322-8.

Galle, M., Schotte, P., Haegman, M., Wullaert, A., Yang, H.J., Jin, S., and R. Beyaert. 2008. The *Pseudomonas aeruginosa* type III secretion system plays a dual role in the regulation of caspase-1 mediated IL-1β maturation. *J. Cell. Mol. Med.* 12: 1767-76.

Garber, S.S., Messerli, M.A., Hubert, M., Lewis, R., Hammar, K., Indyk, E., and P.J.S. Smith. 2005. Monitoring Cl^- movements in single cells exposed to hypotonic solution. *J. Membrane Biol.* 203: 101-10.

Geisler, W.M., Suchland, R.J., Rockey, D.D., and W.E. Stamm. 2001. Epidemiology and clinical manifestations of unique *Chlamydia trachomatis* isolates that occupy non-fusogenic inclusions. *J. Infect. Dis.* 184: 879-84.

Gerrits, M.M., de Zoete, M.R., Arents, N.L.A., Kuipers, E.J., and J.G. Kusters. 2002. 16S rRNA mutation-mediated tetracycline resistence in *Helicobacter pylori. Antimicrob. Agents Chemother.* 46: 2996-3000.

Gervassi, A., Alderson, M.R., Suchland, R., Maisonneuve, J.F., Grabstein, K.H., and P. Probst. 2004. Differential regulation of inflammatory cytokine secretion by human dendritic cells upon *Chlamydia trachomatis* infection. *Infect. Immun.* 72: 7231-9.

Ghuysen, J., and C. Goffin. 1999. Lack of cell wall peptidoglycan versus penicillin sensitivity: new insights into the chlamydial anomaly. *Antimicrob. Agents Chemother.* 43:2339-44.

Gordon, F.B., and A.L. Quan. 1965. Occurrence of glycogen in inclusions of the psittacosis-lymphogranuloma venereum-trachoma agents. *J. Infect. Dis.* 115: 186-96.

Gottlieb, S.L., Martin, D.M., Xu, F., Byrne, G.F., and R.C. Brunham. 2010. Summary: the natural history and immunobiology of *Chlamydia trachomatis* genital infection and implications for chlamydial control. *J. Infect. Dis.* 201: S190-204.

Grieshaber, S., Swanson, J.A., and T. Hackstadt. 2002. Determination of the physical environment within the *Chlamydia trachomatis* inclusion using ion-selective ratiometric probes. *Cellular Microbiology.* 4: 273-83.

Grieshaber, S.S., Grieshaber, N.A., and T. Hackstadt. 2003. *Chlamydia trachomatis* uses host dynein to traffic to the microtubule-organising centre in a p50 dynamitin-independent process. *J. Cell Sci.* 116: 3793-802.

Grieshaber, S.S., Grieshaber, N.A., Miller, N., and T. Hackstadt. 2006. *Chlamydia trachomatis* causes centrosomal defects resulting in chromosomal segregation abnormalities. *Traffic.* 7: 940-9.

Groisman, E.A., and H. Ochman. 1996. Pathogenicity islands: bacterial evolution in quantum leaps. *Cell.* 87: 791-4.

Guseva, N.V., Knight, S.T., Whittmore, J.D., and P.B. Wyrick. 2003. Primary cultures of female swine genital epithelial cells *in vitro*: a new approach for the study of hormonal modulation of chlamydial infection. *Infect. Immun.* 71: 4700-10.

Hackstadt, T., Rockey, D.D., Heinzen, R.A., and M.A. Scidmore. 1996. *Chlamydia trachomatis* interrupts an exocytic pathway to acquire endogenously synthesised sphingomyelin in transit from the Golgi apparatus to the plasma membrane. *EMBO J.* 15: 964-77.

Hackstadt, T., Scidmore-Carlson, M.A., Shaw, E.I., and E.R. Fischer. 1999. The *Chlamydia trachomatis* IncA protein is required for homotypic vesicle fusion. *Cellular Microbiology.* 1: 119-30.

Halaas, Ø., Steigedal, M., Haug, M., Awuh, J.A., Ryan, L., Brech, A., Sato, S., Husebye, H., Cangelosi, G.A., Akira, S., Strong, R.K., Espevik, T., and T.H. Flo. 2010. Intracellular *Mycobacterium avium* intersect transferrin in the $Rab11^{+}$ recycling endocytic pathway and avoid lipocalin 2 trafficking to the lysosomal pathway. *J. Infect. Dis.* 201: 783-92.

Harris, S.R., Clarke, I.N., Seth-Smith, H.M.B., Solomon, A.W., Cutcliffe, L.T., Marsh, P., Skilton, R.J., Holland, M.J., Mabey, D., Peeling, R.W., Lewis, D.A., Spratt, B.G., Unemo, M., Persson, K., Bjartling, C., Brunham, R., de Vries, H.J.C., Morré, S.A., Speksnijder, A., Bébéar, C.M., Clerc, M., de Barbeyrac, B., Parkhill, J., and N. R. Thomson. 2012. Whole-genome analysis of diverse *Chlamydia trachomatis* strains identifies phylogenetic relationships masked by current clinical typing. *Nature genetics.* 44: 413-20.

Hatch, T.P. 1996. Disulphide cross-linked envelope proteins: functional equivalent of peptidoglycan in *Chlamydiae*? *J. Bacteriol.* 78: 1-5.

Heinzen, R.A., Scidmore, M.A., Rockey, D.D., and T. Hackstadt. 1996. Differential integration with endocytic and exocytic pathways distinguish parasitophorous vacuoles of *Coxiella burnetii* and *Chlamydia trachomatis. Infect. Immun.* 64: 796-809.

Heisey, R.M., and A.R. Putnam. 1986. Herbicidal effects of geldanamycin and nigericin, antibiotics from *Streptomyces hygroscopicus. J. Nat. Prod.* 49: 859-65.

Heuer, D., Lipsinki, A.R., Machuy, N., Karlas, A., Wehrens, A., Siedler, F., Brinkman, V., and T.F. Meyer. 2009. *Chlamydia* causes fragmentation of the Golgi compartment to ensure reproduction. *Nature Letters.* 457: 731-5.

Higashi, N. 1965. Electron microscopic studies on the mode of reproduction of trachoma virus and psittacosis virus in cell culture. *Exp. Mol. Pathol.* 4: 24-39.

Hille, B., Armsrtong, C.M., and R. MacKinnon. 1999. Ion channels: from idea to reality. *Nature Medicine.* 5: 1105-9.

Hogan, R.J., Mathews, S.A., Mukhopadyay, S., Summersgill, J.T., and P. Timms. 2004. Chlamydial persistence: beyond the biphasic paradigm. *Infect. Immun.* 72: 1843-55.

Honarmand, H. 2013. Atherosclerosis induced by *Chlamydophila pneumonia*: a controversial theory. *Interdisciplinary Perspectives on Infectious Diseases.* 2013: ID941392.

Howie, S.E.M., Horner, P.J., Horne, A.W., and G. Entrician. 2011. Immunity and vaccines against sexually transmitted *Chlamydia trachomatis* infection. *Curr. Opin. Infect. Dis.* 24: 56-61.

Hsia, R., Pannekoek, Y., Ingerowski, E., and P.M. Bavoil. 1997. Type III secretion genes identify a putative virulence locus of *Chlamydia. Mol. Microbiol.* 25: 351-9.

Hu, V.H., Harding-Esch, E.M., Burton, M.J., Bailey, R.L., Kadimpeul, J., and D.C.W. Mabey. 2010. Epidemiology and control of trachoma: systematic review. *Tropical Medicine and International Health.* 15: 673-91.

Hueck, C.J. 1998. Type III secretion systems in bacterial pathogens of animals and plants. *Microbiology and Molecular Biology Reviews.* 62: 379-433.

Huser, M., Morf, W.E., Fluri, K., Seller, K., Schulthess, P., and W. Simon. 1990. Transport properties of anion-selective membranes based on cobyrinates and metalloporphyrin complexes as ionophores. *Helvetica Chemica Acta.* 73: 1481-96.

Hybiske, K., and R.S. Stephens. 2007. Mechanisms of host cell exit by the intracellular bacterium *Chlamydia. PNAS.* 104: 11430-35.

Jalal, H., Stephen, H., Alexander, S., Carne, C., and C. Sonnex. 2007. Development of real-time PCT assays for genotyping of *Chlamydia trachomatis. J. Clin. Microbiol.* 45: 2649-53.

Jamil, M.S., Hocking, J.S., Bauer, H.M., Ali, H., Wand, H., Smith, K., Walker, J., Donovan, B., Kaldor, J.M., and R.J. Guy. 2013. Home-based chlamydia and gonorrhoea screening: a systematic review of strategies and outcomes. *BMC Public Health.* 13: 189-200.

Jewett, T.J., Fischer, E.R., Mead, D.J., and T. Hackstadt. 2006. *Chlamydial* TARP is a bacterial nucleator of actin. *PNAS*. 103: 15599-604.

Jewett, T.J., Miller, N.J., Dooley, C.A., and T. Hackstadt. 2010. The conserved TARP actin binding domain is important for chlamydial invasion. *PLoS Pathogens.* 6: e1000997.

Jutras, I., Abrami, L., and A. Dautry-Varsat. 2003. Entry of the lymphogranuloma venereum strain of *Chlamydia trachomatis* into host cells involves cholesterol-rich membrane domains. *Infect. Immun.* 71: 260-6.

Kahane, S., and M.G. Friedman. 1992. Reversibility of heat shock in *Chlamydia trachomatis. FEMS Microbiology Letters.* 97: 25-30.

Kalman, S., Mitchell, W., Marathe, R., Lammel, C., Fan, J., Hyman, R.W., Olinger, L., Grimwood, J., Davis, R.W., and R.S. Stephens. 1999, Comparative genomics of *Chlamydia pneumoniae* and *C.trachomatis. Nature Genetics.* 21: 385-9.

Kari, L., Goheen, M.M., Randall, L.B., Taylor, L.D., Carlson, J.H., Whitmire, W.M., Virok, D., Rajaram, K., Endresz, V., McClarty, G., Nelson, D.E., and H.D.Caldwell. 2011. Generation of targeted *Chlamydia trachomatis* null mutants. *PNAS.* 108: 7189-93.

Kaul, R., Hoang, A., Yau, P., Bradbury, E.M., and M.W. Wenman. 1997. The chlamydial EUO gene encodes a histone H1-specific protease. *J. Bacteriol.* 179: 5928-34.

Knowlton, A.E., Brown, H.M., Richards, T.S., Andreolas, L.A., Patel, R.K., and S.S. Grieshaber. 2011. *Chlamydia trachomatis* infection causes mitotic spindle pole defects independently from its effects on centrosome amplification. *Traffic*. 12: 854-66.

Kozoriz, M.G., Church, J., Ozog, M.A., Naus, C.C., and C. Krebs. 2010. Temporary sequestration of potassium by mitochondria in astrocytes. *J. Biol. Chem.* 285:31107-19.

Kubori, T., Matsushima, Y., Nakamura, D., Uralil, J., Lara-Tajero, M., Sukhan, A., Galán, J.E., and S. Aizawa. 1998. Supramolecuar structure of the *Salmonella typhimurium* type III protein secretion system. *Science.* 280: 602-5.

Kumar, K.A., Garcia, C.R.S., Chandran, V.R., Van Rooijen, N., Zhou, Y., Winzeler, E., and V. Nussenzweig. 2007. Exposure of *Plasmodium* sporozoites to the intracellular concentration of potassium enhances infectivity and reduces cell passage activity. *Mol. Biochem. Parasit.* 156: 32-40.

Kumar, Y., and R.H. Valdivia. 2008a. Actin and intermediate filaments stabilise the *Chlamydia trachomatis* vacuole by forming dynamic structural scaffolds. *Cell Host and Microbe.* 4: 159-69.

Kumar, Y., and R.H. Valdivia. 2008b. Reorganisation of the host cytoskeleton by the intracellular pathogen *Chlamydia trachomatis. Communicative and Integrative Biology.* 1: 175-77.

Lad, S.P., Li, J., de Silva Correia, J., Pan, Q., Gadwal, S., Ulevitch, R.J., and E. Li. 2007. Cleavage of p65/RelA of the NF-κB pathway by *Chlamydia. PNAS.* 104: 2933-8.

Li, Z., Chen, C., Chen, D., Wu, Y., Zhong, Y., and G. Zhong. 2008. Characterisation of fifty putative inclusion membrane proteins encoded in the *Chlamydia trachomatis* genome. *Infect. Immun.* 76: 2746-57.

Li, Z., Huang, Q., Su, S., Zhou, Z., Chen, C., Zhong, G., and Y. Wu. 2011. Localisation and characterisation of the hypothetical protein CT440 in *Chlamydia trachomatis*-infected cells. *Sci.e China Life Sci.* 54: 1048-54.

Liechti, G.W., Kuru, E., Hall, E., Kalinda, A., Brun, Y.V., VanNieuwenhze, M., and A.T. Maurelli. 2013. A new metabolic cell-wall labelling method reveals peptidoglycan in *Chlamydia trachomatis. Nature.* doi: 10.1038/nature

Lindestam Arlehamn, C.S., Pétrilli, V., Gross, O., Tschopp, J., and T.J. Evans. 2010. The role of potassium in inflammasome activation by bacteria. *J. Biol. Chem.* 285: 10508-18.

Liu, C., and T.E. Hermann. 1978. Characterisation of ionomycin as a calcium ionophore. *J. Biol. Chem.* 253: 5892-4.

Liu, X., Afrane, M., Clemmer, D.E., Zhong, G., and D.E. Nelson. 2010. Identification of *Chlamydia trachomatis* outer membrane complex proteins by differential proteomics. *J. Bacteriol.* 192: 2852-60.

Liu, Y., Ho, K.K., Su, J., Gong, H., Chang, A.C., and S. Lu. 2013. Potassium transport of Salmonella is important for type III secretion and pathogenesis. *Microbiology.* 159: 1705-19

Longbottom, D. 2003. Chlamydial vaccine development. *J. Med. Microbiol.* 52: 537-40.

Lu, H., Shen, C., and R.C. Brunham. 2000. *Chlamydia trachomatis* infection of epithelial cells induces the activation of caspase-1 and release of mature IL-18. *J. Immunol.* 165: 1463-69.

Lutter, E., Martens, C., and T.Hachstadt. 2012. Evolution and conservation of predicted inclusion membrane proteins in *Chlamydiae*. *Comparative and Functional Genomics.* 2012: ID 362104.

Lutter, E.I., Barger, A.C., Nair, V., and T. Hackstadt. 2013. *Chlamydia trachomatis* inclusion membrane protein CT228 recruits elements of the myosin phosphatase pathway to regulate release mechanisms. *Cell Reports.* 3: 1921-31.

Malhotra, M., Sood, S., Mukherjee, A., Muralidhar, S., and M. Bala. 2013. Genital *Chlamydia trachomatis*: an update. *Indian J. Med. Res.* 138: 303-16.

Matsumoto, A. 1981. Isolation and electron microscopic observations of intracytoplasmic inclusions containing *Chlamydia psittaci. J. Bacteriol.* 145: 605-12.

Matsumoto, A., Bessho, H., Uehira, K., and T. Suda. 1991. Morphological studies of the association of mitochondria with chlamydial inclusion and fusion of chlamydial inclusions. *J. Electron Microsc.* 40: 356-63.

Misaghi, S., Belsara, Z.R., Catic, A., Spooner, E., Ploegh, H.L., and M.N. Starnbach. 2006. *Chlamydia trachomatis*-derived deubiquitinating enzymes in mammalian cells during infection. *Mol. Microbiol.* 61: 142-50.

Mital, J., Miller, N.J., Dorward, D.W., Dooley, C.A., and T. Hackstadt. 2013. Role for chlamydial inclusion proteins in inclusion membrane structure and biogenesis. *PLoS One.* 8: e63426.

Mollenhauer, H.H., Morré, D.J., and L.D. Rowe. 1990. Alteration of intracellular traffic by monensin; mechanism, specificity and relationship to toxicity.

Molinari, M., Eriksson, K.K., Clanca, V., Galli, C., Cresswell, P., Michalak, M., and A. Helenlus. 2004. Contrasting functions of calreticulin and calnexin in glycoprotein folding and ER quality control. *Molecular cell.* 13: 125-35.

Moroney, J.F., Guevara, R., Iverson, C., Chen, F.M., Skelton, S.K., Messmer, T.O., Plikaytis, B., Williams, P.O., Blake, P., and J.C. Butler. 1998. Detection of chlamydiosis in a shipment of pet birds, leading to recognition of an outbreak of clinically mild psittacosis in humans. *Clin. Infect. Dis.* 26: 1425-9.

Moulder, J.W. 1966. The relation of the psittacosis group (*Chlamydiae*) to bacteria and viruses. *Annu. Rev. Microbiol.* 20: 107-30.

Moulder, J.W., 1991. Interaction of *Chlamydiae* and host cells *in vitro. Microbiological Reviews.* 55: 143-90.

Mueller, K.E., Plano, G.V., and K.A. Fields. 2014. New frontiers in type III secretion biology: the *Chlamydia* perspective. *Infect. Immun.* 82:2-9.

Mueller, P., and D.O. Rudin. 1967. Development of K^+-Na^+ discrimination in experimental biomolecular lipid membranes by macrocyclic antibiotics. *Biochemical and Biophysical Research Communications.* 26: 398-404.

Muñoz-Planillo, R., Kuffa, P., Martinez-Colón, G., Smith, B.L., Rajendiran, T.M., and G. Núñez. 2013. K^+ efflux is the common trigger of NLRP3 inflammasome activation by bacterial toxins and particulate matter. *Immunity.* 38: 1142-53.

Nguyen, B.D., and R.H. Valdivia. 2012. Virulence detreminants in the obligate intracellular pathogen *Chlamydia trachomatis* revealed by forward genetic approaches. *PNAS.* 109: 1263-8.

Nguyen, B.D., and R.H. Valdivia. 2013. Forward genetic approaches in *Chlamydia trachomatis. J. Vis. Exp.* 80: e5066.

Nicholls, D.G. 2006. Simultaneous monitoring of ionophore- and inhibitor-mediated plasma and mitochondrial membrane potential changes in cultured neurons. *J,Biol. Chem.* 281:14864-74.

Numazaki, K., Wainberg, M.A., and J. McDonald. 1989. *Chlamydia trachomatis* infections in infants. *CMAJ.* 140: 615-22.

Oliver, Nobeli, and Hayward. Personal communication.

O'Neill, C.E., Seth-Smith, H.M.B., Van Der Pol, B., Harris, S.R., Thomson, N.R., Cutcliffe, L.T., and I.N. Clarke. 2013. *Chlamydia trachomatis* clinical isolates identified as tetracycline resistant do not exhibit resistance *in vitro*: whole-genome sequencing reveals a mutation in *PorB* but no evidence for tetracycline resistance genes. *Microbiology*. 159: 748-56.

Oriel, J.D. 1992. Male genital *Chlamydia trachomatis* infections. *Journal of Infection.* 25: 35-7

Ouellette, S.P., Dorsey, F.C., Moshiach, S., Cleveland, J.L., and R.A. Carabeo. 2011. *Chlamydia* species-dependent differences in the growth requirement for lysosomes.

Pantoja, L.G., Miller, R.D., Ramirez, J.A., Molestina, R.E., and J.T. Summersgill. 2001. Characterisation of *Chlamydia pneumoniae* persistence in Hep-2 cells treated with gamma interferon. *Infect. Immun.* 69: 7927-32.

Patin, D., Bostock, J., Chopra, I., Mengin-Lecreulx, D., and D. Blanot. 2012. Biochemical characterisation of the chlamydial MurF ligase, and possible sequence of chlamydial peptidoglycan pentapeptide stem. *Arch. Micobiol.* 194: 505-12.

Perfettini, J., Hospital, V., Stahl, L., Jungas, T., Verbeke, P., and D.M.Ojcius. 2003. Cell death and inflammation during infection with the obligate intracellular pathogen, *Chlamydia. Biochimie.* 85: 763-9.

Peterson, E.M., and L.M. de la Maza. 1988. *Chlamydia* parasitism: ultrastructural characterisation of the interaction between the chlamydial cell envelope and the host cell. *J. Bacteriol.* 170: 1389-92.

Pétrilli, V., Papin, S., Dostert, C., Mayor, A., Martinon, F., ans J. Tschopp. 2007. Activation of the NLRP3 inflammasome is triggred by low intracellular potassium concentration. *Cell Death and Differentiation.* 14: 1583-9.

Pirbhai, M., Dong, F., Zhong, Y., Pan, K.Z., and G. Zhong. 2006. The secreted protease factor CPAF is responsible for degrading pro-apoptotic BH3-only proteins in *Chlamydia trachomatis* infected cells. *J. Biol. Chem.* 281: 31495-501.

Pressman, B.C. 1976. Biological applications of ionophores. *Annu. Rev. Biochem.* 45: 501-30.

Raulston, J.E. 1997. Response of *Chlamydia trachomatis* serovar E to iron restriction *in vitro* and evidence for iron-regulated chlamydial proteins. *Infect. Immun.* 65: 4539-47.

Ristow, H, Salnikow, J., and H. Kleinkauf. 1974. Biosynthesis of valinomycin. *FEBS Letters.* 42: 127-30.

Rosqvist, R., Håkansson, S., Forsberg, Å., and H. Wolf-Watz. 1995. Functional conservation of the secretion and translocation machinery for virulence proteins of *Yersiniae, Salmonellae,* and *Shigellae. EMBO J.* 14: 4187-95.

Roulis, E., Polkinghorne, A., and P. Timms. 2013. *Chlamydia pneumoniae*: modern insights into an ancient pathogen. *Trends in Microbiology.* 21: 120-8.

Rzomp, K.A., Scholtes, L.D., Briggs, B.J., Whittaker, G.R., and M.A. Scidmore. 2003. Rab GTPases are recruited to chlamydial inclusions in both a species-dependent and species independent manner. *Infect. Immun.* 71: 5855-70.

Rzomp, K.A., Moorhead, A.R., and M.A. Scidmore. 2006. The GTPase Rab4 interacts with *Chlamydia trachomatis* inclusion protein CT229. *Infect. Immun.* 74: 5362-73.

Schotte, P., Denecker, G., Van Den Broeke, A., Vandenabeele, P., Cornelis, G.R., and R. Beyaert. 2004. Targeting Rac1 by the *Yersinia* effector protein YopE inhibits caspase-1-mediated maturation and release of interleukin-1β. *J. Biol. Chem.* 279: 25134-42.

Schwab, J.C., Beckers, C.J.M., and K.A. Joiner. 1994. The parasitophorous vacuole membrane surrounding intracellular *Toxoplasma gondii* functions as a molecular sieve. *Proc. Natl. Acad. Sci.* 91:509-13.

Scidmore-Carlson, M.A., Shaw, E.I., Dooley, C.A., Fischer, E.R., and T. Hackstadt. 1999. Identification and characterisation of a *Chlamydia trachomatis* early operon encoding four novel inclusion membrane proteins. *Mol. Microbiol.* 33: 753-65.

Scidmore-Carlson, M.A., Fischer, E.R., and T. Hackstadt. 2003. Restricted fusion of *Chlamydia trachomatis* vesicles with endocytic compartments during the initial stages of infection. *Infect. Immun.* 71: 973-84.

Schoborg, R.V. 2011. *Chlamydia* persistence – a tool to dissect *Chlamydia*-host interactions. *Microbes and Infection.* 13: 649-62.

Senn, L., Hammershlag, M.R., and G.Greub. 2005. Therapeutic approaches to *Chlamydia* infections. *Expert Opin. Pharmacother.* 6: 2281-90.

Shi, N., Ye, B., and J.C. Makielski. 2005. Function and distribution of the SUR isoforms and splice variants. *J. Mol. Cell. Cardiology.* 39: 51-60.

Skwor, T., Kandel, R.P., Basravi, S., Khan, A., Sharma, B., and D. Dean. 2010.Characterisatio of humoral immune responses to chlamydial HSP60, CPAF, and CT795 in inflammatory and severe trachoma. *Invest. Opthalmol. Vis. Sci.* 51: 5128-36.

Smith, R.V., and M.A. Nessen. 1971. Atomic absorption analysis of sodium, potassium, and calcium in Ringer's solution. *J. Pharm. Sci.* 60: 907-8.

Sönnichsen, B., Lowe, M., Levine, T., Jämsä, E., Dirac-Svejstrup, B., and G. Warren. 1998. A role for giantin indocking COPI vesicles to Golgi membranes. *J. Cell. Biol.* 140: 1013-21.

Stamm, W.E. 1999, *Chlamydia trachomatis* infections: progress and problems. *J. Infect. Dis.* 179: S380-3.

Stephens, R.S., Kalman, S., Lammel, C., Fan, J., Marathe, R., Aravind, L., Mitchell, W., Olinger, L., Tatusov, R.L., Zhao, Q., Koonin, E.V., and R.W. Davis. 1998. Genome sequence of an obligate intracellular pathogen of humans: *Chlamydia trachomatis. Science.* 282: 754-59.

Stephens, R.S. 2003. The cellular paradigm of chlamydial pathogenesis. *TRENDS in Microbiology.* 11:44-51.

Stephens, R.S., Myers, G., Eppinger, M., and P.M. Bavoil. 2009. Divergence without difference: phylogeneticsand taxonomy of *Chlamydia* resolved. *FEMS Immunol. Med. Microbiol.* 55: 115-119.

Stern, P.H. 1977. Ionophores. Chemistry, physiology and potential applications to bone biology. *Clin. Orthop. Relat. Res.* 122: 273-98.

Stone, C.B., Johnson, D.L., Bulir, D.C., Gilchrist, J.D., and J.B. Mahoney. 2008. Characterisation of the putative type III secretion ATPase CdsN (Cpn0707) of *Chlamydia pneumoniae. J. Bacteriol.* 190: 6580-8.

Su, H., Watkins, N.G., Zhang, Y., and H.D. Caldwell. 1990. *Chlamydia trachomatis*-host cell interactions: role of the chlamydial major outer membrane protein as an adhesin. *Infect. Immun.* 58: 1017-25.

Su, H., Raymond, L., Rockey, D.D., Fischer, E., Hackstadt, T., and H.D. Caldwell. 1996. A recombinant *Chlamydia trachomatis* major outer membrane protein binds to heparin sulphate receptors on epithelial cells. *Proc. Natl. Acad. Sci. USA.* 93: 11143-8.

Su, J., Gong, H., Lai, J., Main, A., and S. Lu. 2009. The potassium transporter Trk and external potassium modulate *Salmonella enterica* protein secretion and virulence. *Infect. Immun.* 77: 667-75.

Subtil, A., Wyplosz, B., Balañá, M.E., and A. Dautry-Varsat. 2004. Analysis of *Chlamydia caviae* entry sites and involvement of Cdc-42 and Rac activity. *J. Cell Sci.* 117: 3923-33.

Suchland, R.J., Rockey, D.D., Bannantine, J.P., and W.E. Stamm. 2000. Isolates of *Chlamydia trachomatis* that occupy non-fusogenic inclusions lack IncA, a protein localised to the inclusion membrane. *Infect. Immun.* 68: 360-7.

Szabò, I., Leanza, L., Gulbins, E., and M. Zoratti. 2012. Physiology of potassium channels in the inner membrane of mitochondria. *Pflugers Arch. – Eur. J. Physiol.* 463: 231-46.

Taylor, B.D., Darville, T., Tan, C., Bavoil, P.M., Ness, R.B., and C.L. Haggerty. 2011. The role of *Chlamydia trachomatis* polymorphic membrane proteins in inflammatory sequelae among women with pelvic inflammatory disease. *Infect. Dis. Obstet. Gynecol.* 2011: ID 989762.

Thalmann, J., Jankin, K., May, M., Sommer, K., Ebeling, J., Hofmann, F., Genth, H., and A. Klos. 2010. Actin reorganisation induced by *Chlamydia trachomatis* serovar D – evidence for a critical role of the effector protein CT166 targeting Rac. *PLoS One.* 5: e9887.

Todd, W.J., and H.D. Caldwell. 1985. The interaction of *Chlamydia trachomatis* with host cells: ultrastructural studies of the mechanism of release of a biovar II strain from HeLa 229 cells. *J. Infect. Dis.* 151: 1037-44.

Trchounian, A., and H. Kobayashi. 1999. Kup is the major K^+ uptake system in *Escherichia coli* upon hyper-osmotic stress at low pH. *FEBS Letters.* 447: 144-8.

Tseng, T., Tyler, B.M., and J.C. Setubal. 2009. Protein secretion systems in bacterial-host associations, and their descriptions in gene oncology. *BMC Microbiology.* 9: S2.

Tse, S.M.L., Mason, D., Botelho, R.J., Chiu, B., Reyland, M., Hanada, K., Inman, R.D., and S. Grinstein. 2005. Accumulation of diacylglycerol in the *Chlamydia* inclusion vacuole. *J. Biol. Chem.* 280: 25210-5.

Valdivia, R.H. 2008. *Chlamydia* effector proteins and new insights into chlamydial cellular microbiology. *Curr. Opin. Microbiol.* 11: 53-9.

Van Ooij, C., Homola, E., Kincaid, E., and J. Engel. 1998, Fusion of *Chlamydia trachomatis*-containing inclusions is inhibited at low temperatures and requires bacterial protein synthesis. *Infect. Immun.* 66: 5364-71.

Verbeke, P., Welter-Stahl, L., Ying, S., Hansen, J., Häcker, G., Darville, T., and D.M. Ojcius. 2006. Recruitment of BAD by the *Chlamydia trachomatis* vacuole correlates with host-cell survival. *PLoS Pathogens.* 2: e45.

Wang, Y., Kahane, S., Cutcliffe, L.T., Skilton, R.J., Lambden, P.R., and I.N. Clarke. 2011. Development of a transformation system for *Chlamydia trachomatis*: restoration of glycogen biosynthesis by acquisition of a plasmid shuttle vector. *PLoS Pathogens.* 7: e1002258.

Way, D.L., Grosso, D.S., Davis, J.R., Surwit, E.A., and C.D. Christian. 1983. Characterisation of a new human endometrial carcinoma (RL95-2) established in tissue culture. *In Vitro.* 19: 147-58.

White, J.A. 2009. Manifestations and management of lymphogranuloma venereum. *Curr. Opin. Infect. Dis.* 22: 57-66.

WHO. 2011. Prevalence and incidence of sexually transmitted infections. ISBN: 978 92 4 150245 0

WHO. 2012. Trachoma: situation and trends.

Wilson, D.P., Whittum-Hudson, J.A., Timms, P., and P.M. Bavoil. 2009. Kinematics of intracellular *Chlamydiae* provide evidence for contact-dependent development. *J. Bacteriol.* 191: 5734-42.

Xue, T., You, Y., Hong, D., Sun, H., and B. Sun. 2011. The *Staphylococcus aureus* KdpDE two-component system couples extracellular K^+ sensing and Agr signaling to infection programming. *Infect. Immun.* 79: 2154-2167.

Zhang, J.P., and R.S. Stephens. 1992. Mechanism of *C.trachomatis* attachment to eukaryotic host cells. *Cell.* 69: 861-9.